# NEW EXPERIMENTAL SETUP FOR 3D CHARACTERIZATION OF GRANULAR SHAPE AND ASSOCIATED MORPHOLOGICAL QUANTIFIERS

by

Samad Kazemi Khosrowshahi

B.S., Civil Engineering, Azad University of Shabestar, 2007

M.S., Geotechnical Engineering, Istanbul Technical University, 2014

Submitted to the Institute for Graduate Studies in
Science and Engineering in partial fulfillment of
the requirements for the degree of
Doctor of Philosophy

Graduate Program in Civil Engineering

Boğaziçi University

2024

# ACKNOWLEDGEMENTS

I would like to express my deepest gratitude to my supervisor, Prof. Özer Çinicioğlu, and co-supervisor, Assist. Prof. İrem Zeynep Yıldırım for their unwavering support, immense knowledge, and encouragement throughout this journey. Their expertise, patience, and constructive feedback have been invaluable in shaping this thesis. It would not be possible to finish this work without their valuable understanding and support.

I extend my heartfelt appreciation to Prof. Erol Güler, who made a great contribution to my academic life. I was lucky to have a chance to learn from his outstanding knowledge and personality.

I am also grateful to Prof. Nilüfer Özyurt Zihnioğlu, Prof. Hilmi Luş, Prof. Ilgın Yaşar, Assist Prof. Berrak Teymür, and Prof. Pelin Özener for their insightful comments and encouragement, but also for the vital guidance that encouraged me to widen my research from various perspectives.

I am indebted to my friends and colleagues for their encouragement, discussions, and moral support, which have made this endeavor a fulfilling experience.

Special thanks to my family for their unconditional love, encouragement, and understanding during the ups and downs of this doctoral journey. I want to dedicate this thesis to my beloved mother, for all the years we were away from each other, and for her endless love and to my brother with his non-ending support, he has made me stronger and better than I could have ever imagined.

This work is partially supported by the Scientific Research Projects (BAP) of Boğaziçi University, Grant No: 17521.

# ABSTRACT

## NEW EXPERIMENTAL SETUP FOR 3D CHARACTERIZATION OF GRANULAR SHAPE AND ASSOCIATED MORPHOLOGICAL QUANTIFIERS

Mechanical response and behavior of granular materials are affected by particle shape parameters. However, the determination of a three-dimensional shape is complicated and requires advanced equipment and techniques which limits its feasibility. Accordingly, this study proposes a practical and economical setup for three-dimensional shape characterization. With the proposed setup, images captured by a regular camera can be used for three-dimensional quantification of granular shapes. The method involves using multiple images of grains and enhancement of several two-dimensional descriptors for three dimensions. The details of the proposed setup are outlined and descriptors that express three-dimensional shapes from two-dimensional images are presented. An open-source image processing program ImageJ is used to process the obtained digital images from the developed system for creating binary images and measurement of related parameters to be used in shape analysis and determination of particle shape descriptors. Seven different sand samples with various gradations and properties are investigated. Further, a series of laboratory tests aimed to focus on the effect of particle shape on the mechanical properties of granular materials including stress-strain and stress-dilatancy behavior. The results of laboratory tests revealed a meaningful relation between particle shape and mechanical properties. The developed imaging system is capable of two and three-dimensional shape characterization of granular materials. Accordingly, the proposed shape descriptors successfully indicate the shape parameters of a particle.

# ÖZET

## GRANÜL ŞEKİL VE İLİŞKİLİ MORFOLOJİK NİCELİK GÖSTERGELERİNİN ÜÇ BOYUTLU KARAKTERİZASYONU İÇİN YENİ DENEYSEL KURULUM

Granüler malzemelerin mekanik tepkisi ve davranışı dane şeklinden etkilenir. Ancak üç boyutlu dane şeklinin belirlenmesi kolay değildir, bunun yapılması gelişmiş donanım ve tekniklerin gerekliliği nedeniyle genellikle fizibil olmamaktadır. Bu çalışmada üç boyutlu şekil karakterizasyonu için pratik ve ekonomik bir deney kurulumu önerilmektedir. Önerilen deney kurulumunu kullanarak, basit bir fotoğraf makinası ile çekilen görüntüler, dane şeklinin üç boyutta belirlenmesi için kullanılabilir. Yöntem, bir danenin birden fazla görüntüsünü kullanarak üç boyut için dane şekil tanımlayıcılarının geliştirilmesini içerir. Ayrıca elde edilen iki boyutlu görüntüler kullanılarak üç boyutlu şekil için yeni şekil tanımlayıcıları sunulmaktadır. İlgili dane parametrelerin ölçümü için geliştirilen deney düzeneğinden elde edilen dijital görüntülerin işlenmesi amacıyla açık kaynaklı bir görüntü işleme programı olan ImageJ kullanılmıştır. İşlenen görüntülerden elde edilen sonuçlar kullanılarak yeni üç boyutlu şekil tanımlayıcıları belirlenmesi hedeflenmiştir. Bunun için çeşitli gradasyon ve mühendislik özelliklerine sahip yedi farklı kum numunesi incelenmiştir. Ayrıca, bu kum örnekleri üzerinde bir dizi laboratuvar deneyi yapılarak stres-gerinim ve stres-genişleme davranışı da dahil olmak üzere granüler malzemelerin mekanik özellikleri üzerindeki dane şekli etkisinin belirlenmesine odaklanılmıştır. Geliştirilen görüntüleme sistemi granüler malzemelerin iki ve üç boyutlu şekil karakterizasyonunu yapabilmektedir. Önerilen üç boyutlu şekil tanımlayıcıları bir parçacığın şekil parametrelerini başarıyla göstermektedir.

# TABLE OF CONTENTS

ACKNOWLEDGEMENTS . . . iii
ABSTRACT . . . iv
ÖZET . . . v
LIST OF FIGURES . . . ix
LIST OF TABLES . . . xiii
LIST OF SYMBOLS . . . xvii
LIST OF ACRONYMS/ABBREVIATIONS . . . xix
1. INTRODUCTION . . . 1
1.1. Motivation . . . 1
1.2. Objectives and Scope . . . 1
1.3. Thesis Outline . . . 2
2. BACKGROUND AND LITERATURE REVIEW . . . 3
2.1. Particle Shape . . . 3
2.1.1. Particle Shape of Granular Materials . . . 3
2.2. Particle Shape Effects on Engineering Properties . . . 4
2.2.1. Crushing . . . 4
2.2.2. Void Ratio and Compressibility . . . 4
2.2.3. Internal Friction Angle and Dilatancy . . . 5
2.2.4. Dynamic Properties . . . 6
2.2.5. Thermal Conductivity . . . 7
2.3. Particle Shape Characterization . . . 8
3. MATERIALS AND METHODS . . . 14
3.1. Materials . . . 14
3.2. 3D Imaging Setup . . . 17
3.2.1. Sample Selection for Imaging . . . 20
3.2.2. Mirrors Specifications . . . 20
3.2.3. Distance Correction Factor . . . 21
3.2.4. Shape Descriptors . . . 24

3.2.5. Determination of 2D Shape Descriptors . . . 26
3.2.6. Proposed 3D Shape Descriptors . . . 27
3.2.7. Minimum Number of Required Particles for Shape Analysis . . 28
4. LABORATORY TESTING PROGRAM . . . 30
4.1. Laboratory Tests . . . 30
4.1.1. Angle of Repose . . . 30
4.1.2. Santamarina's Critical State Friction Angle . . . 31
4.1.3. Specimen Preparation for Triaxial Tests . . . 33
4.1.4. Initialization Phase . . . 34
4.1.5. Saturation Phase . . . 35
4.1.6. Consolidation Phase . . . 35
4.1.7. Shear Phase . . . 37
5. RESULTS AND DISCUSSION . . . 38
5.1. Results of Image Analysis . . . 38
5.1.1. Particle Shape Analysis . . . 38
5.1.2. Results of 2D Shape Analysis . . . 39
5.1.3. Comparison of the Determined 2D and 3D Shape Descriptors . 47
5.1.4. Size Effect on Shape Descriptors . . . 52
5.2. Particle Shape Classification Based on 3D Shape Analysis . . . 54
5.3. Image-Based Particle Size Distribution . . . 55
5.4. Laboratory Tests . . . 58
5.4.1. Results of One-Dimensional Oedometer Tests . . . 58
5.4.2. Results of CD Triaxial Tests . . . 60
6. CONCLUSION . . . 67
7. FUTURE WORKS . . . 69
REFERENCES . . . 70
APPENDIX A: DETERMINED 2D AND 3D SHAPE DESCRIPTORS . . . 85
A.1. Determined 2D And 3D Shape Descriptors of GB . . . 85
A.2. 2D and 3D Shape Descriptors of Sand A . . . 86
A.3. 2D and 3D Shape Descriptors of Sand B . . . 89
A.4. 2D and 3D Shape Descriptors of Sand C . . . 94

A.5. 2D and 3D Shape Descriptors of Sand D . . . . . 101
A.6. 2D and 3D Shape Descriptors of Sand E . . . . . 106
A.7. 2D and 3D Shape Descriptors of Sand F . . . . . 108
A.8. Copyright Details . . . . . 113

# LIST OF FIGURES

Figure 2.1. Particle shape classification based on roundness and sphericity. . . 11

Figure 3.1. Scaled photos of the investigated materials in this study. From left to right, sand samples are sorted in ascending order of $D_{50}$. . . . . 14

Figure 3.2. Particle size distribution of the investigated materials. . . . . 15

Figure 3.3. Determination of void ratio thresholds using shaking table. . . . . 16

Figure 3.4. Different views of an arbitrary created particle. . . . . 18

Figure 3.5. Binary images of particle outlines from different views. Sides from top to down. . . . . 18

Figure 3.6. Schematic of the developed 3D imaging setup. . . . . 19

Figure 3.7. The developed 3D imaging setup. . . . . 19

Figure 3.8. Flowchart for 2D and 3D particle shape analysis of each material based on the developed 3D imaging system. . . . . 20

Figure 3.9. Effect of the reflective surface on the reflection. . . . . 21

Figure 3.10. (a) Particle #40 – 8 of sand F on the developed 3D imaging setup, (b) Schematic illustration of the imaging setup including binary images of the dominant face and two projected images on the mirrors, reference scale, and the reflection of side scale on the mirrors. . . . 22

Figure 3.11. 3D imaging system. . . . . 23

Figure 3.12. Photo of Sand A grains taken by the digital camera with a mounted macro lens. . . . . 24

Figure 3.13. Shape describing sub-quantities. . . . . 24

Figure 3.14. Particles of a random green-colored sample in the sand size range. 25

Figure 3.15. Illustration of notations for projected particle outline in 2D analysis. 26

Figure 3.16. Illustration of notations for 3D shape analysis of all faces. . . . . 28

Figure 3.17. (a) changes on cumulative average values of shape descriptors by the number of analyzed particles of Sand C. (b) shape value changes for a number of particles from 25 to 30. (c) shape value changes for a number of particles from 45 to 50. . . . . 29

Figure 4.1. Angle of repose for the investigated samples. . . . . 31

Figure 4.2. Santamarina's method. . . . . 31

Figure 4.3. Santamarina's method to determine the critical state friction angles of the investigated materials. . . . . 32

Figure 4.4. Triaxial test setup, soil mechanics laboratory of Boğaziçi University (2023). . . . . 32

Figure 4.5. Setup of sample preparation for triaxial test. . . . . 34

Figure 4.6. Skempton's B value in the saturation phase of a $Co_2$-injected sample. 35

Figure 4.7. Consolidation phase of a CD triaxial test of Sample B with relative density of $I_d$= 63 % under consolidation pressure of $\sigma'_c$= 200 kPa. (a) time - $\varepsilon_1$, (b) e- $\varepsilon_1$ relationship. . . . . 36

Figure 4.8. Shear phase of a CD triaxial test of Sample B with a relative density of $I_d$= 63 % under consolidation pressure of $\sigma'_c$= 200 kPa. . . . . 37

Figure 5.1. Weighted average values of the determined 2D shape descriptors. . 42

Figure 5.2. Relation between the determined 2D shape descriptors for all particles. . . . . 42

Figure 5.3. Weighted average values of the determined 3D shape descriptors. . 46

Figure 5.4. Relation between the determined 3D shape descriptors for all particles. . . . . 46

Figure 5.5. Relation between weighted average of the determined 2D and 3D particle shape descriptors for the studied six sand samples. . . . . 48

Figure 5.6. Relation between the determined 2D and 3D shape descriptors for all particles. . . . . 49

Figure 5.7. Relation between the determined 2D and 3D shape descriptors based on each face. . . . . 50

Figure 5.8. Frequency of shape descriptors for all samples. . . . . 51

Figure 5.9. Sample images of particles with various size ranges. . . . . 52

Figure 5.10. Effect of particle size on roundness. . . . . 53

Figure 5.11. Effect of particle size on sphericity. . . . . 54

Figure 5.12. Particle shape classification based on 3D roundness and sphericity. 55

Figure 5.13. Schematic of particles passing sieve opening. . . . . 56

Figure 5.14. Flowchart for determination of particle size based on digital images. 57

Figure 5.15. Particle size distribution of Sand B based on sieve analysis and digital imaging. . . . . 58

Figure 5.16. Particle size distribution of Sand B based on sieve analysis and digital imaging Time-$e$ relationship for one-dimensional oedometer tests. . . . . 59

Figure 5.17. Relation between sphericity and compression index. . . . . 60

Figure 5.18. Effect of relative density on stress-strain and volumetric behavior of Sand A under consolidation pressure of 100 kPa. . . . . 63

Figure 5.19. Effect of consolidation pressure on stress-strain and volumetric behavior of loose-medium samples of Sand B. . . . . 64

Figure 5.20. $\phi'_p$ - $\psi'_p$ relationship for CD triaxial tests. . . . . 65

Figure 5.21. Relation between sphericity and peak friction angle for the six samples. . . . . 65

Figure 5.22. Relation between sphericity and critical state friction angle for the sand samples. . . . . 66

# LIST OF TABLES

Table 2.1. Alternative roundness classification based on the measurement. . . 10

Table 2.2. Sphericity based on measurement of three perpendicular axes. . . . 12

Table 3.1. Properties of the investigated materials. . . . . 17

Table 5.1. Results of 2D shape analysis. . . . . 39

Table 5.2. Results of 3D shape analysis. . . . . 43

Table 5.3. Data sources. . . . . 60

Table A.1. Determined 2D and 3D shape descriptors of GB particles retained on sieve #40, PR = 100, PSR = 0.250 – 0.850 mm. . . . . 85

Table A.2. Determined 2D and 3D shape descriptors of Sand A particles retained on sieve #40, PR = 0.80, PSR = 0.425 – 0.850 mm. . . . . 86

Table A.3. Determined 2D and 3D shape descriptors of Sand A grains retained on sieve #60, PR = 12.38, PSR = 0.250 – 0.425 mm. . . . . 87

Table A.4. Determined 2D and 3D shape descriptors of Sand A grains retained on sieve #100, PR = 86.82, PSR = 0.150 – 0.250 mm. . . . . 88

Table A.5. Determined 2D and 3D shape descriptors of Sand B grains retained on sieve #20, PR = 16.90, PSR = 0.850 – 2.00 mm. . . . . 89

Table A.6. Determined 2D and 3D shape descriptors of Sand B grains retained on sieve #40, PR = 35.42, PSR = 0.425 – 0.850 mm. . . . . 90

Table A.7. Determined 2D and 3D shape descriptors of Sand B grains retained on sieve #60, PR = 22.01, PSR = 0.250 – 0.425 mm. . . . . 91

Table A.8. Determined 2D and 3D shape descriptors of Sand B grains retained on sieve #100, PR = 20.07, PSR = 0.150 – 0.250 mm. . . . . 92

Table A.9. Determined 2D and 3D shape descriptors of Sand B grains retained on sieve #140, PR = 5.60, PSR = 0.106 – 0.150 mm. . . . . 93

Table A.10. Determined 2D and 3D shape descriptors of Sand. . . . . 94

Table A.11. Determined 2D and 3D particle shape descriptors of Sand C retained on sieve #20, PR = 36.75, PSR = 0.850 – 2.00 mm. . . . . 96

Table A.12. Determined 2D and 3D shape descriptors of Sand C particles retained on sieve #40, PR = 21.17, PSR = 0.425 – 0.850 mm. . . . . 97

Table A.13. Determined 2D and 3D particle shape descriptors of Sand C retained on sieve #60, PR = 12.32, PSR = 0.250 – 0.425 mm. . . . . 98

Table A.14. Determined 2D and 3D particle shape descriptors of Sand C retained on sieve #100, PR = 11.00, PSR = 0.150 – 0.250 mm. . . . 99

Table A.15. Determined 2D and 3D particle shape descriptors of Sand C retained on sieve #140, PR = 3.78, PSR = 0.106 – 0.150 mm. . . . . 100

Table A.16. Determined 2D and 3D particle shape descriptors of Sand D retained on sieve #10, PR = 36.61, PSR = 2.00 – 2.74 mm. . . . . 101

Table A.17. Determined 2D and 3D particle shape descriptors of Sand D retained on sieve #20, PR = 36.31, PSR = 0.850 – 2.00 mm. . . . . 102

Table A.18. Determined 2D and 3D particle shape descriptors of Sand D retained on sieve #60. PR=7.10, PSR=0.250-0.425 mm. . . . . 103

Table A.19. Determined 2D and 3D particle shape descriptors of Sand D retained on sieve #100, PR = 4.97, PSR = 0.150 – 0.250 mm. . . . . 104

Table A.20. Determined 2D and 3D particle shape descriptors of Sand D retained on sieve #140, PR = 2.22, PSR = 0.106 – 0.150 mm. . . . . 105

Table A.21. Determined 2D and 3D particle shape descriptors of Sand E retained on sieve #10, PR = 66.43, PSR = 2.00 - 4.75 mm. . . . . 106

Table A.22. Determined 2D and 3D particle shape descriptors of Sand E retained on sieve #20, PR = 33.57, PSR = 0.850 – 2.00 mm. . . . . 107

Table A.23. Determined 2D and 3D particle shape descriptors of Sand F retained on sieve #10, PR = 90.70, PSR = 2.00 - 4.75 mm. . . . . 108

Table A.24. Determined 2D and 3D shape descriptors of Sand F grains retained on sieve #20, PR = 8.20, PSR = 0.850 – 2.00 mm. . . . . 109

Table A.25. Determined 2D and 3D particle shape descriptors of Sand F retained on sieve #40, PR = 0.34, PSR = 0.425 – 0.850 mm. . . . . 110

Table A.26. Determined 2D and 3D particle shape descriptors of Sand F retained on sieve #60, PR = 0.70, PSR = 0.250 – 0.425 mm. . . . . 111

Table A.27. Determined 2D and 3D particle shape descriptors of Sand F retained on sieve #100, PR = 0.06, PSR = 0.150 – 0.250 mm. . . . . 112

# LIST OF SYMBOLS

| | |
|---|---|
| $A$ | Area of projected particle outline |
| $A_c$ | Area of the convex hull of the projected particle outline |
| $AR_{2D}$ | Two-dimensional aspect ratio |
| $AR_{3D}$ | Three-dimensional aspect ratio |
| $B$ | Skempton's degree of saturation |
| $C_c$ | Coefficient of gradation |
| $C_d$ | Distance correction factor for reflected images on the mirrors |
| $C_u$ | Coefficient of uniformity |
| $CX_{2D}$ | Two-dimensional convexity |
| $CX_{3D}$ | Three-dimensional convexity |
| $d_{Fmax}$ | Maximum Feret's diameter |
| $dFmin$ | Minimum Feret's diameter |
| $D_{50}$ | Mean particle size |
| $e$ | Void ratio |
| $e_{max}$ | Maximum void ratio |
| $e_{min}$ | Minimum void ratio |
| $f$ | Frequency of shape descriptors |
| $F_1$ | The face of the particle outline reflected on mirror one |
| $F_2$ | The face of the particle outline reflected on mirror two |
| $F_D$ | Dominant face of the projected particle outline |
| $G$ | Secant shear modulus |
| $G_o$ | Small strain shear modulus |
| $G_s$ | Specific gravity |
| $H$ | Height of sample drop in air pluviation method |
| $I_d$ | Relative density |
| $MAXd_{Fmax}$ | The largest maximum Feret's diameter of all faces |
| $MAXr_{cir}$ | The largest radius of circumscribed circle among all faces |
| $MINd_{Fmin}$ | The smallest minimum Feret's diameter of all faces |

| | |
|---|---|
| $MINr_{ins}$ | The smallest radius of the inscribed circle among all faces |
| $P'_p$ | Peak mean effective stress |
| $P$ | Perimeter of the projected particle outline |
| $q'$ | Effective derivative stress |
| $q'_p$ | Peak effective derivative stress |
| $r_{cir}$ | Radius of the circumscribed circle surrounding particle outline |
| $r_{ins}$ | Radius of the inscribed circle fitted inside of particle outline |
| $R_{2D}$ | Two-dimensional roundness |
| $R_{3D}$ | Three-dimensional roundness |
| $S_{2D}$ | Two-dimensional sphericity |
| $S_{3D}$ | Three-dimensional sphericity |
| $SP$ | Poorly graded sand |
| $SW$ | Well graded sand |
| | |
| $\alpha$ | Reference scale |
| $\beta$ | Reflected scale |
| $\varepsilon_1$ | Axial strain |
| $\varepsilon_v$ | Volumetric strain |
| $\mu m$ | Micro millimeter |
| $\nu$ | Poison's ratio |
| $\theta_i$ | Angle of incident light |
| $\theta_r$ | Angle of reflected light |
| $\psi$ | Dilation angle |
| $\psi'_p$ | Peak drained dilation angle |
| $\sigma_c$ | Consolidation pressure |
| $\phi_{cr}$ | Critical state friction angle |
| $\phi_{cr-S}$ | Critical state friction angle by Santamarina's method |
| $\phi_{cr-T}$ | Critical state friction angle obtained by triaxial tests |
| $\phi'_p$ | Peak effective friction angle |

# LIST OF ACRONYMS/ABBREVIATIONS

| | |
|---|---|
| 2D | Two Dimensional |
| 3D | Three Dimensional |
| AC | Axial Compression |
| CT | Computed Tomography |
| DEM | Discrete Element Modeling |
| GB | Glass Beads |
| ISO | Isotropic |
| PR | Percent Retained |
| PSR | Particle Size Range |
| SMT | Synchrotron Micro Tomography |
| TDR | Time Domain Reflectometry |
| USCS | Unified Soil Classification System |

# 1. INTRODUCTION

## 1.1. Motivation

Morphology, shape, and size of particles have a crucial role on engineering behavior of granular materials. In soil mechanics and geotechnical engineering, sandy soils are known coarse-grained soils. Hence, a precise and realistic shape characterization of coarse materials and sand grains is a predominant step for understanding engineering properties of granular materials. In particle shape analysis, sand grains tend to be placed on their most stable side which is usually the wider surface of the particle. So, two-dimensional particle shape analysis is not capable of giving a complete idea of a real grain shape. In contrast, three-dimensional study considers all three dimensions (3D) and provides more accurate and realistic ideas. As mentioned before, 3D studies are based on advanced and expensive technologies which may not be available or affordable in practice. In this study, a cost-efficient and practical imaging system, which makes it possible to have an accurate evaluation of the particle shape, was developed. The main research idea is based on developing an imaging setup for obtaining 3D shape descriptors from three two-dimensional (2D) images in three orthogonal surfaces. It consists of a digital camera, and an imaging setup involving two optic mirrors. The particle shape is represented by three 2D images from three perpendicular surfaces, two reflected images on the mirrors and one image directly captured by the camera. This is a simple and practical approach for a precise understanding of the morphology and shape parameters of particles in a three-dimensional system.

## 1.2. Objectives and Scope

The objective of this study to provide a new, simplified, and practical setup and technique for 3D characterization of particles shape. It is based on developing a new imaging system which makes it possible to conduct 3D shape analysis of a grain from its 2D images. Consequently, this work aims to investigate the effect of particle shape on

engineering properties and macro scale behavior of sand. It involves a comprehensive experimental program consisting of digital image processing and laboratory tests.

### 1.3. Thesis Outline

This study involves six main sections. Firstly, the importance of particle shape and size on mechanical behavior of granular materials is described. Chapter 1 presents the aim of the study and the general outline.

Chapter 2 presents a literature review concerning the evaluation of particle shapes. This part explains different techniques utilized for characterizing the shapes of grains in both two and three dimensions. Moreover, it explores the impact of particle shape on the engineering properties of granular materials.

In Chapter 3 the studied materials and their properties are presented. Then the developed imaging setup and their related proposed shape descriptor for 3D shape characterization is explained. In one next step in section 4, the laboratory experimental programs consisting of a series of triaxial tests for determining the stress-strain and volumetric behavior of the investigated materials are presented.

In Chapter 5 the results of particle shape analysis, and experimental tests are presented and discussed. This section explains how the proposed method for 3D particle shape assessment results in more accurate and realistic evaluation comparing with conventional 2D techniques. In Chapter 6 the conclusions are summarized.

# 2. BACKGROUND AND LITERATURE REVIEW

## 2.1. Particle Shape

### 2.1.1. Particle Shape of Granular Materials

Formation history, mineralogy, size, and shape of particles have a remarkable effect on engineering properties and mechanical behavior of soil [1–9]. particle shape and size of granular materials are considered as an effective factor on macroscale behavior of soil mass. In the case of cohesive soils and fine materials like clay, engineering behavior and structural bonds are highly dependent on the forces between the clay particles and minerals. Theses can be mentioned as chemical, ion-electrostatic, molecular, and magnetic forces [10]. However, in the case of cohesionless and granular materials, there are no remarkable bonds between particles. Besides the stress conditions such as confining pressure and loading type, the strength and mechanical properties of a granular media is based on particle size and shape parameters, void ratio, and also the crushing strength of each single grain. Several researchers conclude that particle shape influence on mechanical properties of soil material and unbound aggregates [11–28]. Many researches reveal that mechanical behavior of granular materials are affected by their particle shape parameters. The main engineering properties affected by grain shape can be mentioned as grain crushing strength and pattern [28–31], packing density and void ratio [32–36], internal friction angle [37–40], thermal [41] and hydraulic conductivity [42–46], liquefaction susceptibility [47–51], volume change, and stress-dilatancy parameters [52–56]. Furthermore, the latest advances in computational geotechnics and discrete element modeling (DEM) techniques reveal a significant involvement of descriptors representing particle shape-size properties [57–63].

## 2.2. Particle Shape Effects on Engineering Properties

### 2.2.1. Crushing

Crushing mechanism and strength of a particle have been a point of interest for many researchers. These studies considered various aspects such as various shape parameters like roundness, sphericity, convexity, elongation or aspect ratio, also packing homogeneity, and loading condition. In 2022, Meng et al. [29] studied the effect of particle morphology on crushing strength conducting a series of single-particle crushing tests. The study considered main morphological parameters particularly sphericity, aspect ratio, and convexity of the investigated samples. The study shows that grain shape characteristics has a remarkable role on crushing process and strength of granular materials. In 2024, Karimipetanlar et al. [30] investigated the influence of particle shape on crushing pattern and energy dissipation on sand grains by use of DEM. The concluded that particles with higher values of sphericity, roundness and convexity have larger crushing strength. Zhao et al. [31] investigated the crushing of quarts sands under one-dimensional compression. They used in situ X-ray tomography and X-ray scan technologies to monitor the failure patterns. The study revealed the importance of particle size and scale-dependent evolution on crushing pattern.

### 2.2.2. Void Ratio and Compressibility

Void ratio limits have an important role on compressibility and mechanical parameters such as shear strength, hydraulic conductivity, and liquefaction susceptibility [64–67]. In addition to the effect of fine contents and particle size distribution, several researches studied the effect of shape and size effects on relative density and void ratio of cohesionless soils. Maroof [68] in 2022 studied effect of roundness and sphericity of five different morphological granular materials with nine various gradations on the maximum and minimum void ratios. The measured shape parameters by micro-CT images. The results showed that for the samples with higher roundness and sphericity, the limit void ratios decrease. Analyzing four types of sand, Zhaoyang Xu [69]

found that increasing irregularity of particle shape results in larger void ratio, and consequently higher values of minimum void ratio.

### 2.2.3. Internal Friction Angle and Dilatancy

Internal friction angle and dilation characteristics are intrinsic properties which directly related to the stress-strain behavior of cohesionless and granular materials. The impact of grain shape on shear strength and stress-dilatancy have been documented by many researches [70–76]. In 2021, Arda and Çinicioğlu [78], investigated grain shape on stress-dilatancy parameters by conducting 2D image analysis and a series of triaxial tests with various stress paths. The results showed that increasing sphericity and roundness results in higher values of dilatancy. Cho et al (2006) [79] studies impact of particle shape of crushed sands on stiffness and strength parameters. They found that critical state friction angle ($\varphi_{cr}$) increases by increasing of grain shape irregularity. They emphasized on importance of particle shape on soil index properties which demands proper characterization, particularly for clean sands and gravels. Alshibli and Cil (2018) [80] studied grain shape influence on friction and dilatancy of sand. They conducted triaxial comparison tests under various confining pressures, and quantified shape parameters 3D high-resolution SMT images. They concluded that shear strength parameters (peak friction angle, critical state friction angle, and dilation angle) increase as roundness and sphericity (form) decrease. Based on another research on natural sands by Altuhafi (2016) [81], it was showed that convexity as an overall shape parameter has no clear impact on friction angle. It was also concluded that surface texture and particle roughness have no remarkable effect on any parameters while shape affects most aspects of sand behavior. Amirpour Harehdasht et al. (2017) [82], investigated particle shape and gradation effect on stress-dilatancy by conducting a series of drained triaxial compression tests. The results revealed that stress-dilatancy behavior of the studied materials was significantly affected by variation of the median particle size ($D_{50}$). In summary, the previous researches obviously show a robust connection between particle shape parameters and mechanical properties of granular materials.

### 2.2.4. Dynamic Properties

Cyclic behavior and dynamic properties of cohesionless soils is another key factor which are affected by grain shape. Several studies have aimed to understand the impact of particle shape and morphology on dynamic behavior such as wave propagation, and liquefaction susceptibility. In 1998, Santamarina and Cascante [83] studied impact of surface roughness on wave propagation parameters. They conducted an experimental program and image analysis on particles, by use of scanning electron microscope (SEM). They concluded that by increasing surface roughness, shear wave velocity decreases, indicating lower stiffness. It was also mentioned that as surface roughness increases, damping becomes independent from applied stress. In addition, for small-strains stiffness decreases with surface roughness, while it increases in the case of large-strains. Ham et al. (2012) [84] performed a 2D image analysis, and conducted a series of resonant column tests to understand the relation between particle shape descriptors and microscopic damping in clean sands. It was found that comparing with sphericity, roundness and roughness are more effective on damping behavior of the studied samples. Payan et al. (2016) [85] investigated gradation and particle grain shape effect on small-strain Young's modulus (E) and Poisson's ratio () of sand. They proposed a new model for prediction of the E and V based on gradation and shape parameters. In an experimental and numerical study by Kumari and Sitharam (2010) [86] particle shape effect on liquefaction resistance was investigated. The results showed that the models simulated by spherical particles underestimate the cyclic resistance and result in liquefaction in lower load cycles. Using Discrete Element Method (DEM), Ashmawy et al. (2003) [87] evaluated grain shape effect on liquefaction behavior of different types of sand. The used two-dimensional projection of particle shapes for simulation of the investigated materials. As a results of the simulated cyclic shear tests, it was understood that particle morphology has a significant role on liquefaction resistance of the samples with same void ratios. The findings also showed that in the case of large void ratios, particle shape has no effect on liquefaction susceptibility. In another DEM study, Hu et al. (2023) [88] simulated a series of cyclic undrained triaxial tests to evaluate influence of particle shape parameters including roundness and sphericity

on dynamic properties of granular materials. They found that particle shape has no remarkable effect on shear modulus ratio $G/G_0$; however, damping ratio significantly is affected at lager strains due to dilatancy. In addition, the results showed that the samples consisting of angular grains generally have higher secant shear modulus G than the specimens with rounded particles.

### 2.2.5. Thermal Conductivity

Particle shape and morphological characterization can be beneficial for appropriate approaches in the field of Geo-energy and geothermal systems as carbon-free and sustainable applications in geotechnical engineering. As a part of evaluation and optimization of geothermal systems, researches focused on the role of shape characteristics on thermal conductivity of granular media. Lee et al. (2017) [89] investigated grain shape effect of nine different sands on thermal conductivity quantifying four shape parameters of sphericity, convexity, elongation, and slenderness. A thermal needle probe was used for measurement of heat transfer rate. As a results, they mentioned that rounded particles have larger interparticle contact surface and consequently higher thermal conductivity. It was also indicated that stress-induced thermal conductivity is governed by interparticle contact area and initial packing density. Effect of particle size on granular mixtures was investigated by Lee et al. (2015) [90]. They concluded that the relative size ratio of the main granular material in a mixture is the dominant effective factor on heat conduction. Zhang et al. (2019) [91] investigated influence of particle size and fines content on thermal conductivity of quarts sands in dry and wet conditions. They developed a new thermo-time domain reflectometry (thermo-TDR) probe to simultaneously measure thermal properties and moisture content of the samples. Results showed that for uniform sands by reduction of particle size thermal conductivity decreases, but increases for nonuniform sands as sand pores are filled by fine particles. Comparing dry and wet samples, it was found that thermal conductivity was increased with moisture content. Fei et al. (2019) [92] investigated effect of three-dimensional roundness and sphericity on heat conduction of granular materials. For a reliable quantification of 3D shape descriptors, they developed a method based on re-

construction of particles from micro-computed tomographic (CT) images. Using finite element simulation, they concluded that thermal conductivity decreases with porosity. Considering the governing role of interparticle contact area on thermal conductivity, it was observed that the rate of heat transfer in granular materials increases with roundness and sphericity. performing a series of thermal needle tests, Xiao et al. (2020) [93] studied effect of sphericity, aspect ratio, and convexity on thermal conductivity of five granular soil mixtures with the same mineral composition. As an effect of grain shape, thermal conductivity of the samples with the same relative density increased with increasing average sphericity and roundness.

## 2.3. Particle Shape Characterization

The topics mentioned above, clearly indicate the crucial and significant role of morphology and particle shape characteristics on different engineering and mechanical properties of granular materials. This important role is not limited only in soil mechanics and is considered in a wide range of various fields such as pharmacology, filtration materials, coffee beans products, granular material deposition systems, and cosmetic products. Hence, appropriate evaluation of particle shape parameters is a key factor to understand behavior of granular materials. Particle shape descriptors can be classified as qualitative and quantitative. Shape quality of a particle describes its shape in term of words such as spherical, elongated, angular, round, and etc. Quantitative descriptors are related to measurement of particle shape parameters. In engineering applications, compared with qualitative descriptors, quantitative ones are more important because of reproducibility. Different terminologies such as form, sphericity, circularity, roundness, irregularity, angularity, slenderness, elongation, flakiness, surface texture, roughness aspect ratio, and convexity were used by researchers during the historical development of particle shape descriptors; however, all these represent similar shape quantities for a corresponded shape parameter. According to the literature, these particle shape descriptors are generally categorized in three main groups of sphericity, roundness, and roughness. These are scale-dependent shape descriptors from large to small scale respectively where sphericity describes overall form, roundness is about particle's corners

and indicates grain shape irregularity, and roughness defines the texture of a particle's surface. Researchers proposed various methods for particle shape characterization and morphology measurement methods. Since the earliest 1900's, Pentland [95], Wadell [96], Riley [97], and some other authors developed their own techniques to define and quantify the form and morphology of particles. These methods range from conventional techniques such as sieve analysis, manual measurement, and visual charts to recently developed technologies like digital imaging. Sive analysis is a common traditional method which mostly is used to determine particle size distribution. Researches show that passing of particles is not only depended on size, but also affected by shape of particles. Persson in 1988 [persson] mentioned that sieving can be used to measure elongation index for certain size ranges of particles. Manual measurement of particles is a time-consuming procedure, so visual charts were developed for a quick and practical grain shape evaluation. New technologies and advanced imaging systems have made it possible to measure and obtain shape properties both in 2D and 3D. X-ray CT imaging method is known as a common technique for particle imaging in the last three decades. A new and more accurate method as synchrotron X-ray micro-tomography (SMT) is also was used for particle shape imaging [97-101]. Thanks to development of advanced and commercial devices, many researchers have investigated particle shape effect on granular soil behavior. However, most of these studies are based on 2D analysis. Some researchers have conducted 3D analysis which demand expensive and advanced imaging systems.

Considering many numbers of studies on particle shape characterizations, it is understood that researchers have accepted sphericity, roundness, and roughness as appropriate parameters to describe a particle shape and morphology. Wadell 1932 [102], Krumbein (1941) [103], and Powers (1953) [104] proposed dimensionless definitions for particle shape parameters. Sphericity (circularity in 2D) is considered as a large-scale parameter which is related to overall form of the particle and indicates similarity of a particle shape to a sphere (circle in 2D). Roundness (Angularity) as a medium-scale shape quantifies ratio of the average radii of corners' curvature to the radius of maximum inscribed sphere (inscribed circle in 2D) in the particle. Roughness (smoothness)

is a small-scale parameter which defines particle surface texture related to radius of the particle. Some studies classified particle roundness based on the method of measurement proposed by Wadell in 1932. Table 2.1 shows these classifications which categorized roundness mainly in six groups. For average values, Russel and Taylor (1937) [105] used arithmetic mid-point values while Pettijohn (1949) [106], Powers (1953) [104], and Blott and Pye (2008) [107] defined mean values based on geometric mid-points. Geometric mean is the average value of finite set of data related to the product of them.

Table 2.1. Alternative roundness classification based on the measurement.

| Classification | Russell and Taylor -1937 | | Pettijohn -1949 | | Powers -1953 | | Blott and Pye -2008 | |
|---|---|---|---|---|---|---|---|---|
| | Class limits | Arithmetic mid-point | Class limits | Geometric mid-point | Class limits | Geometric mid-point | Class limits | Geometric mid-point |
| Very angular | - | - | - | - | 0.12 - 0.17 | 0.14 | - | - |
| Angular | 0.00 - 0.15 | 0.075 | 0.00 - 0.15 | 0.125 | 0.17 - 0.25 | 0.21 | 0 - 0.13 | 0.09 |
| Sub-angular | 0.15 - 30 | 0.225 | 0.15 - 0.25 | 0.200 | 0.25 - 0.35 | 0.30 | 0.13 - 0.25 | 0.18 |
| Sub-rounded | 0.30 - 0.50 | 0.400 | 0.25 - 0.40 | 0.315 | 0.35 - 0.49 | 0.41 | 0.25 - 0.50 | 0.35 |
| Rounded | 0.50 - 0.70 | 0.600 | 0.40 - 0.60 | 0.500 | 0.49 - 0.70 | 0.59 | 0.50 - 1.00 | 0.71 |
| Well rounded | 0.70 - 1.00 | 0.850 | 0.60 - 1.00 | 0.800 | 0.70 - 1.00 | 0.84 | - | - |

Irregularity of a particle shape is an indicator of overall regularity which represents a particle with straight sides or those having continues curvature to outside. Blott and Pye (2008) [107] indicated that measurements of form, sphericity, and roundness is generally sufficient to characterize a particle regularity. Shape classification charts are beneficial tools for a quick and suitable understanding of general particle shape. Figure 1 shows a developed chart by Cho et al. in 2006 [79] based on the sphericity and roundness definitions proposed by Wadell in 1932. It represents qualification and quantification classes of the mentioned shape descriptors. It reveals that sphericity as a form indicator is independent from roundness as a medium-scale shape descriptor.

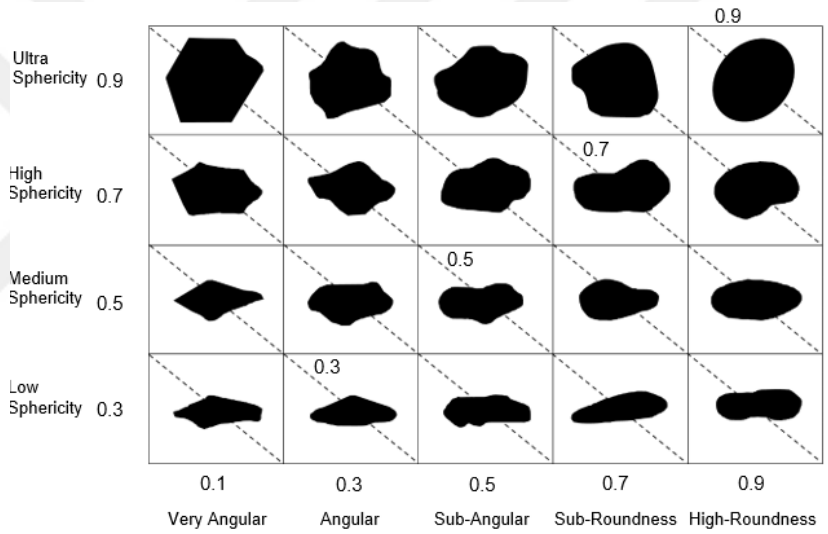



Figure 2.1. Particle shape classification based on roundness and sphericity (Modified after Cho et al., 2006). Dash lines represent consistent irregularity.

Roughness is a small-scale shape parameter which describes surface texture of a particle. According to literature, effect of roughness on a grain shape irregularity and engineering properties is not as crucial as roundness and sphericity. In 1998, Janoo [108] defined roughness as the ratio of particle outline perimeter and convex perimeter. Later in 1988 Kuo et al. [109] described roughness as the ratio of perimeter and average diameter of a particle outline. Convexity ratio is used by Mora and Kwan (2000) [110] for quantification of particle surface texture. Since particle roughness is a small-scale shape descriptor, its appropriate quantification is depended on accurate measurement of surface. Thus, advanced imaging systems and high-resolution images

would be beneficial for a reliable evaluation of surface texture.

Table 2.2. Sphericity based on measurement of three perpendicular axes.

| **Descriptor Name** | **Relationship** | **Reference** |
|---|---|---|
| Flatness index | $S = \frac{(a+b)}{2c}, a \gg b \gg c$ | Wentworth 1922a [111] |
| Pebble sphericity | $S = \sqrt[3]{\frac{b-c}{a^2}}$ | Pye and Pye 1943 [112] |
| Working sphericity | $S = \frac{12.8\times\sqrt[3]{(\frac{c}{b})^2}\times(\frac{b}{a})}{1+(\frac{c}{b})(1+(\frac{b}{a})+6\times\sqrt{1+(\frac{c}{b})^2 1+(\frac{b}{a})^2)}}$ | Ashenbrenner 1956 [112] |
| Shape factor | $S = \frac{ac}{b^2}$ | Ashenbrenner 1956 [112] |
| Maximum projection sphericity | $S = \sqrt[3]{\frac{c^2}{a-b}}$ | Sneed & Folk 1958 [113] |
| Williams shape factor | $S = 1 - \frac{ac}{b^2} when b^2 > ac$ $S = \frac{b^2}{ac} - when b^{2\leq} ac$ | Williams[2] 1965 [114] |
| Janke form factor | $S = \frac{c}{\sqrt{\frac{a^2+b^2+c^2}{3}}}$ | Janke[2] 1966 [115] |
| Oblate-prolate index | $S = \frac{10(\frac{a-b}{a-c}-0.5)}{\frac{c}{a}}$ | Dobkins & Folk 1970 [116] |
| a, b, and c are measured lengths of three axes perpendicular to each other ($a \gg b \geq c$). $S$ represents particle sphericity. | | |

Many of the studies about particle shape characterization provide shape parameters based on two-dimensional form. Wentworth (1922) [111] was one of the earliest researchers who measured particle dimensions in three perpendicular axes to quantify sphericity. The lengths of axes were identified as a, b, and c representing the longest, medium, and shortest measured lengths consequently. Based on the ratio of these measurements, Krumbein (1941) [103], provided a chart for quick determination of sphericity. Similarly, some other researchers defined particle sphericity getting advantage of the measurement method proposed by Wentworth. Some of these definitions are presented in Table **??**.

According to the literature, many methods and shape descriptors have been developed during the historical studies on morphology and particle shape characterization. These range from simple and traditional methods to recently developed advanced systems. Many 2D and 3D shape descriptors have been defined; however, the determination of shape descriptors requires appropriate measurement of shape parameters. For 2D forms, based on the definition of a descriptor, some of these shape parameters can be mentioned as area, perimeter, diameter, inscribed circles, minimum circumscribed circle, and convex hull area. In the case of 3D evaluation, surface area, volume, inscribed spheres, minimum circumscribed sphere, and convex hull volume are some of the parameters that may need to be measured. So, for a proper particle shape characterization, it should be mentioned that measurement of a shape parameter is as important as definition of a shape descriptor. Hence, this study introduces a simple and practical system for 3D shape evaluation, by proposing new shape descriptors and development of a practical measurement setup for determination of shape parameters.

# 3. MATERIALS AND METHODS

## 3.1. Materials

For particle shape characterization and laboratory experimental testing program, seven different granular materials were selected including a wide range of size-shape parameters from very rounded manufactured material to angular particles of a crushed stone. Figure 3.1 shows scald photos of the materials were used in this study consisting of glass beads and six various sand samples. Glass beads which were identified as GB, have the most rounded and spherical shape, and considered as a reference material for comparison with the other investigated samples. They are manufactured materials and have diameters ranging from 425 $\mu$m – 600 $\mu$m. The other six materials are sand samples obtained from different locations in Turkey. The sand samples were labeled based on their mean sizes ($D_{50}$) in ascending order.

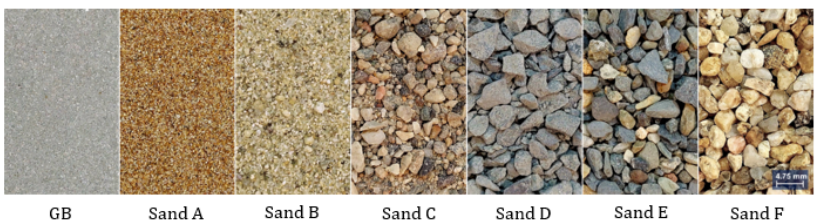



Figure 3.1. Scaled photos of the investigated materials in this study. From left to right, sand samples are sorted in ascending order of $D_{50}$.

Sample A is yellow color quartz sand of predominantly sandstone origin. It was obtained from the Kilyos, a coastline of the Black Sea on the European side of Istanbul. Sample B is light grey-greenish colored sand with dominant quartz minerals. It was also gathered from the Black Sea coast in Çerkezköy. Another sample named Sand C, is a brown-colored sand which has a complete quart's mineralogy. It was gathered from the Asian side of the Black Sea coast in Istanbul. It is classified as a well-graded sample involving a wide range of particle sizes. A crushed sandstone named Sand D, is another used material which was provided from a concrete batching plant in Istanbul.

It is a gray-colored sand with angular and irregular grain shapes. This type of material is commonly used as aggregate for road construction and making concrete products. Material E is a grey-yellowish colored coarse sand obtained from a riverbed in a region in the middle of Turkey named Akpinar. Same as sample D, this one is also useful in construction applications. The final material named Sand F, is a light yellow colored coarse sand prepared in a certain gradation in the purpose of drainage and filtration applications. It has quartz-silica minerals and was provided from an aggregate factory in Istanbul.

Gradation and essential index parameters of the samples were determined by conducting the relative laboratory tests. Before the tests, all sand samples were washed to clean them from dust and impure components. Then they were dried in an oven for 24 hours at 180 $^oC$. To determine particle size distribution sieve analysis were conducted by the standard of ASTM D6913 [117]. The utilized sieve numbers were 4, 10, 20, 40, 60, 100, 120, and 200 with sieve opening sizes ranging from 4.75 mm to 0.075 mm. Figure 3.2 shows size distribution curves for the studied materials.

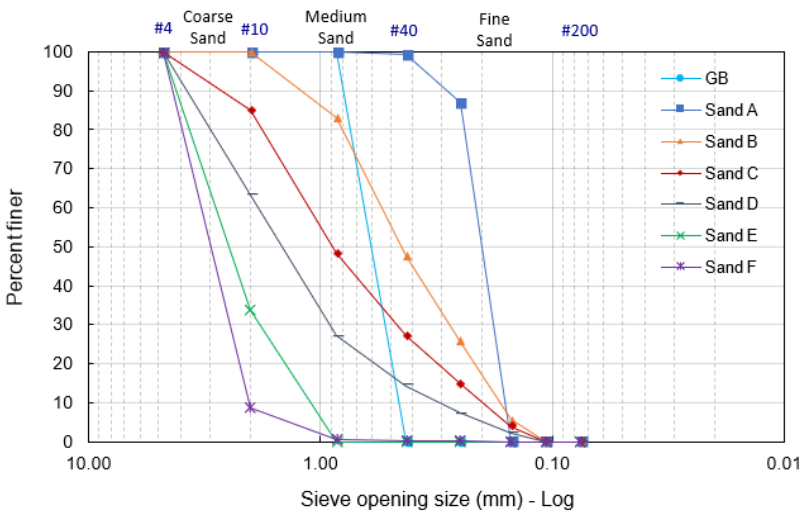



Figure 3.2. Particle size distribution of the investigated materials.

Consequently, median particle size ($D_{50}$), uniformity coefficient ($C_u$), and coefficient of curvature ($C_c$) were obtained. According to the results, sand samples C and D were classified as well-graded sand while all the other ones were identified as poorly-

graded sand. Size gradation of Glass beads (GB) shows very small variation of grain sizes ranging in the middle of the size distribution bound for all samples. The size of the samples obviously covers all the gradation regions involving fine, medium, and coarse sands. The values of $D_{50}$ varies from 0.20 mm to 2.95 mm. This wide size range reveals a promising size distribution of the selected materials to explore the size of particles.

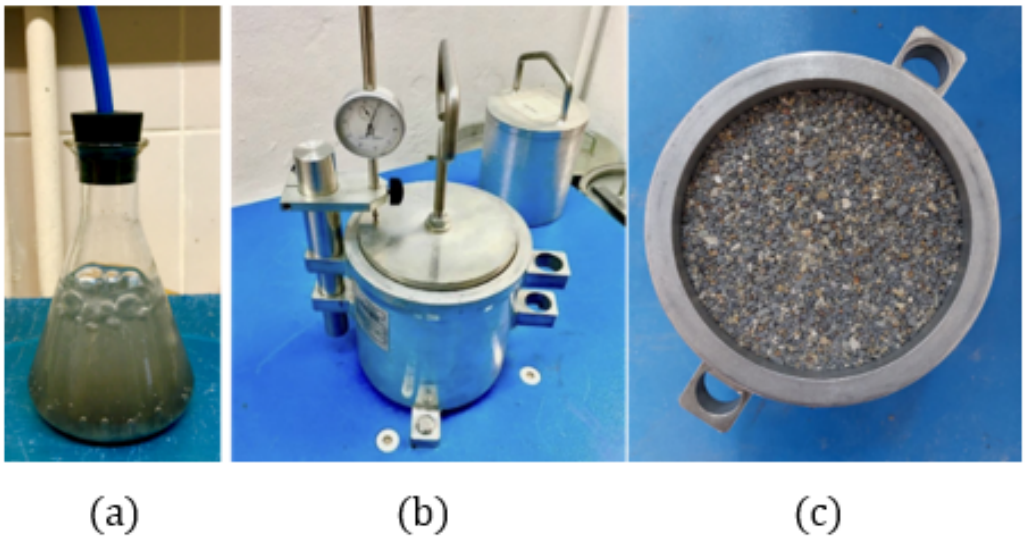



Figure 3.3. Determination of void ratio thresholds using shaking table. (a) vacuum application during specific gravity test (b) setup preparation before applying vibration, (c) Sand E densified due to vibration at the end of the test.

Specific gravity ($G_s$) of the materials were obtained by pycnometer method in accordance to ASTM D854-14 [118].To determine the maximum and minimum void ratios, shaking table method was used based on ASTM-D4253 [119]. Figure 3.4 shows samples from the mentioned tests. The properties of the investigated materials are presented in Table 3.1.

Table 3.1. Properties of the investigated materials.

| Property | GB | Sand A | Sand B | Sand C | Sand D | Sand E | Sand F |
|---|---|---|---|---|---|---|---|
| Classification | *SP* | *SP* | *SP* | *SW* | *SW* | *SP* | *SP* |
| $D_{50}$ (mm) | 0.60 | 0.20 | 0.45 | 0.89 | 1.46 | 2.48 | 2.95 |
| $C_u$ | 1.41 | 1.27 | 3.26 | 5.98 | 7.76 | 2.57 | 1.62 |
| $C_c$ | 0.93 | 0.88 | 0.86 | 1.05 | 1.90 | 1.09 | 0.91 |
| $G_s$ | 2.45 | 2.66 | 2.63 | 2.62 | 2.71 | 2.69 | 2.67 |
| $e_{max}$ | 0.66 | 0.76 | 0.78 | 0.67 | 0.78 | 0.93 | 0.82 |
| $e_{min}$ | 0.35 | 0.49 | 0.48 | 0.33 | 0.36 | 0.58 | 0.59 |

According to the density index values, sand C with minimum void ratio ($e_{min}$) of 0.33, has densified more than the other samples while Sand E with maximum void ratio ($e_{max}$) of 0.93 has the largest void ratio.

## 3.2. 3D Imaging Setup

It was aimed to develop a practical and cost-efficient setup for three-dimensional particle shape characterization of granular materials mainly in the sand size range. In two-dimensional space, the outline of an object varies based on changing the view directions. Figure 3.4 shows a random particle created by Rock Generator, an open-source software for generating rock shapes. As it is shown, the particle has completely different shape in various views. This implies that 2D shape analysis may not be sufficient for a proper shape characterization Six views of the particle are presented, and for each of them, a different particle shape appears. However, as it is shown in Figure 3.5, each pair of top-bottom, left-right, and front-back sides gives the same particle outline for the corresponding direction.

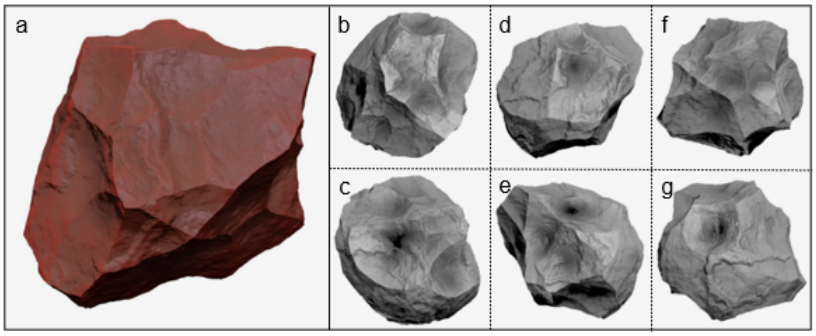



Figure 3.4. Different views of an arbitrary created particle. (a) perspective, (b) top, (c) bottom, (d) left, (e) right, (f) front, (g) back.

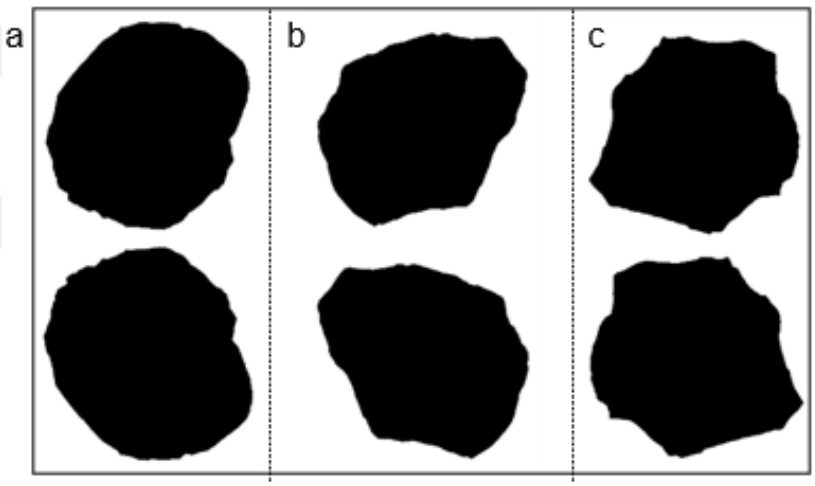



Figure 3.5. Binary images of particle outlines from different views. Sides from top to down: (a) top – down, (b) left – right, (c) front – back.

The 3D imaging setup was designed based on use of three 2D images obtained from three perpendicular planes. Among these images, one image is captured directly by the camera and the other ones are the side images of a grain projected on the mirrors installed in the imaging platform setup. The mirrors are positioned at an angle of 45 degrees to the horizontal surface to reflect the side views of the placed particle on the platform. Figure 3.6 shows a schematic of the developed imaging setup.

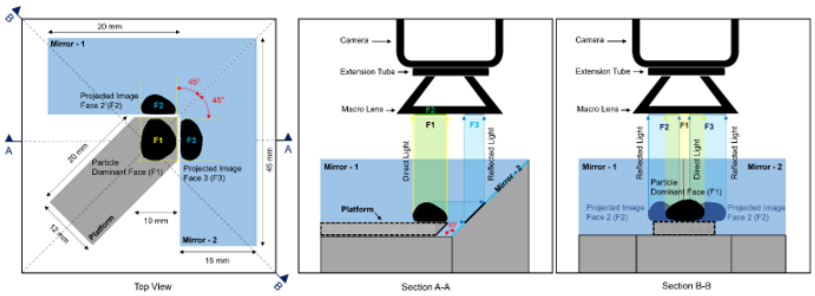



Figure 3.6. Schematic of the developed 3D imaging setup.

The developed 3D imaging setup consists of two main parts: a digital camera and lighting system, and a platform for placing particles. The system can cover all sand particle sizes defined in the Unified Soil Classification System (USCS) ranging from 0.075 mm to 4.75mm. However, the higher size is not limited to 4.75 mm and the particles with sizes up to 15.00 mm can be evaluated.

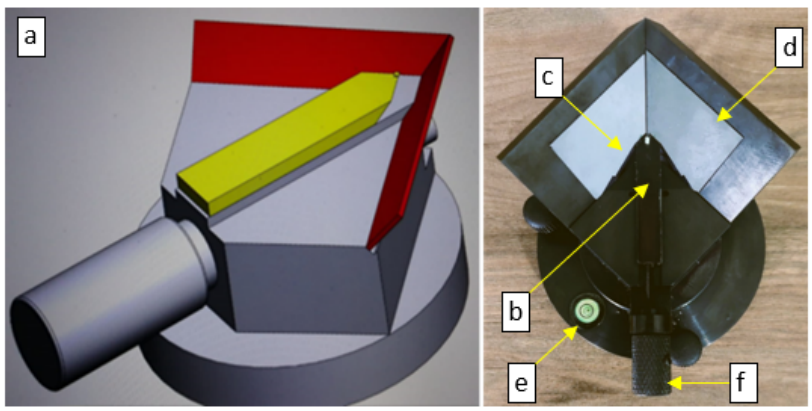



Figure 3.7. The developed 3D imaging setup. (a) conceptual illustration, (b) mobile platform, (c) Aluminum-coated mirror-1, (d) Aluminum-coated mirror-2, (e) level, (f) adjustment valve for horizontal movement of the platform.

To conduct the experiments, dogbone specimens are fixed in a tensile rig (Kamm-rath and Weiss) with maximum 10KN load capacity which is a screw-driven mechanism operated by control unit. The load frame itself is assembled on a positioning stage with 3 translational degrees of freedom (x, y, z) which is controlled by computer to address any 3D position in space inside its ranges. Figure 3.7 shows the test setup schematically.

### 3.2.1. Sample Selection for Imaging

Particle selection for the imaging analysis was performed based on the size gradation for each sample. During the sieve analysis, sample particles for image analysis were obtained from the remaining part of the samples on each sieve. Figure 3.8 shows the procedure of 2D and 3D particle shape characterization in this study.

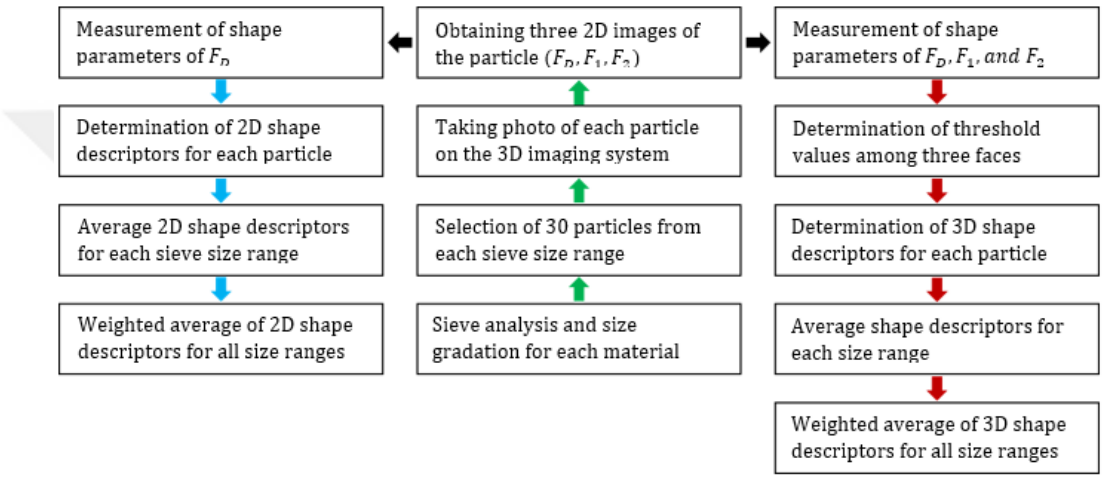



Figure 3.8. Flowchart for 2D and 3D particle shape analysis of each material based on the developed 3D imaging system.

### 3.2.2. Mirrors Specifications

Based on the location of reflection surface, there are two main types of mirrors consisting of household mirrors and optical mirrors. The main difference between them is the location of the coating material which is applied on the back surface for usual mirrors while for optical applications the coating layer is placed on the front surface. Figure 3.9 illustrates the coating surfaces of different types of mirrors.

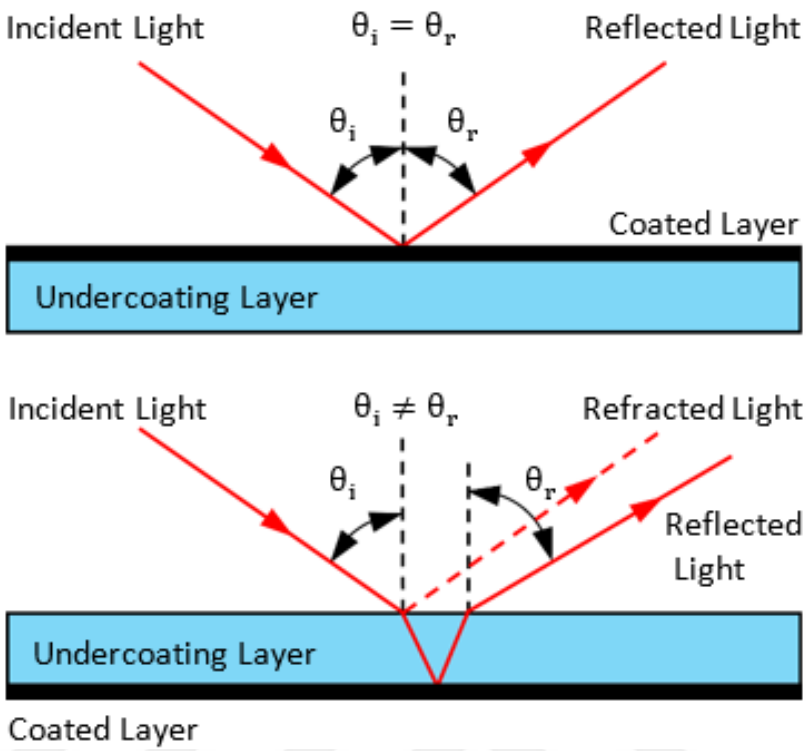



Figure 3.9. Effect of the reflective surface on the reflection.

In the back-surface coated mirror, the incident light passes through the base material which causes refraction. Meanwhile, in the front-surface coated mirror, the incident light is directly reflected from the surface symmetrically. Here, again the thickness of the coating layer is critical to minimize any light refraction. As a reflective material, aluminum can reflect 90 percent of light which is in the acceptable range for use in this study. The mirrors were created in the Physics Science Laboratory of Boğaziçi University. An aluminum layer of 125 nm thickness was coated on the 1 mm thick industrial wafer.

### 3.2.3. Distance Correction Factor

As a reference, a physical scale was installed on the surface of the platform which was used for placing the measuring objects. It is crucial that the scales of all images to be identical. However, the distance between the placed particles on the platform and the mirrors varies depending on the size of the measuring sample. This distance

causes a reduction in the size of the projected images. To correct this deviation, as it is shown in Figure 3.10, additional scales were placed on the two sides of the platform.

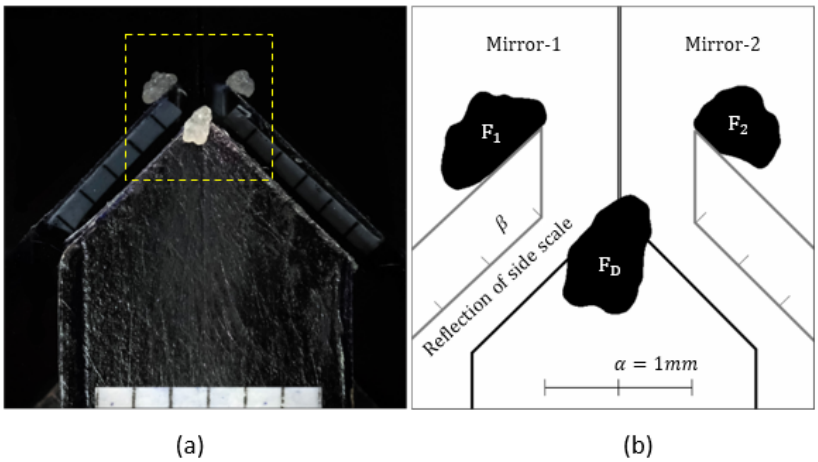



Figure 3.10. (a) Particle #40 – 8 of sand F on the developed 3D imaging setup, (b) Schematic illustration of the imaging setup including binary images of the dominant face and two projected images on the mirrors, reference scale, and the reflection of side scale on the mirrors.

The distance correction factor was determined by the difference between the corresponding distances on the side and reference scales. For most of the captured samples, this value was around 1.020408 which means the size of the projected images was approximately 2.04 percent less than the main scale. Subsequently, measured values of the projected outlines were modified multiplying by the correction factor.

3D imaging system is a compound of three main parts consisting of digital camera, imaging setup, and LED light. Each part has been developed and selected to provide the required specifications for obtaining desired images. Figure 6 shows the details and clarifies how these separate parts work together. A Fujifilm X-T4 camera body with an image sensor size of 23.5 mm × 15.60 mm was selected. Considering the size of the target objects for image capturing, a Fujifilm automatic X F80 mm lens was mounted for macro photography. Furthermore, a 16 mm extension tube macro tube was also added to the system. Mounting an extension tube between a lens and a camera body

increases the distance between the lens elements and the sensor enabling users to focus closer than the normal minimum focus distance of the object. This is beneficial to set the camera closer to the objects, especially in the case of grains with the size of below 0.425 mm. A Lightening LED with 1020 LUX of brightness provided enough suitable light to avoid shadows and obtain clear images.

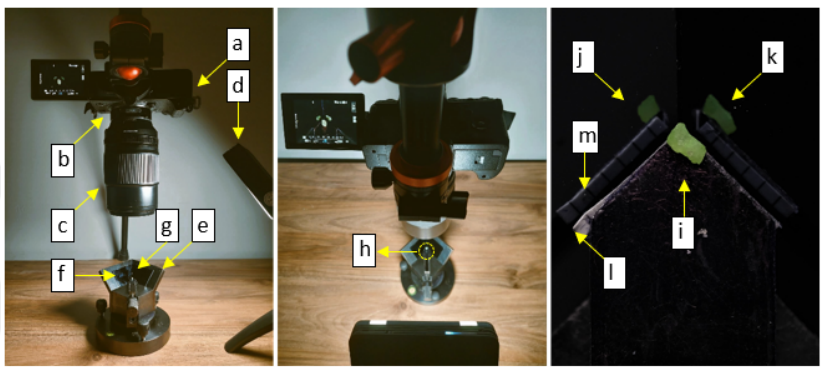



Figure 3.11. 3D imaging system; (a) Fujifilm X-T4 digital camera, (b) extension tube, (c) XF80 mm F2.8 macro lens, (d) LED light, (e) imaging setup, (f) mirror-1, (g) mirror-2, (h) particle placed on the platform of the imaging setup, (i) face of the particle directly captured by the camera, (j) side face of the particle reflected on the mirror-1, (k) side face of the particle reflected on the mirror-2, (l) side scale, (m) reflection of side scale on the mirror-1.

The developed system preciously reveals the side faces of particles on the installed mirrors. This provides three 2D images of a particle in three perpendicular faces to be taken in image processing for creating binary images and consequently scaling and related measurements for shape analysis.




Figure 3.12. Photo of Sand A grains taken by the digital camera with a mounted macro lens.

### 3.2.4. Shape Descriptors

Particle shape descriptors can be classified into two main groups as qualitative and quantitative. Qualitative descriptors are related to the shape of the particle while quantitative ones are related to the measured dimensions. In the engineering field, the quantitative description of the particle is more important due to the reproducibility. In the field of geotechnical engineering, there is no distinct standard for particle shape identification. Many studies define particle shape parameters within three main groups of small, intermediate, and large scales. As it is shown in Figure 3.13, small scale corresponds to the texture and surface parameters of a particle while the intermediate and large scales are defining shape and form of a grain. Various shape descriptors for each scaling class have been proposed by several researchers; however, many of them are limited to two-dimensional measurements.

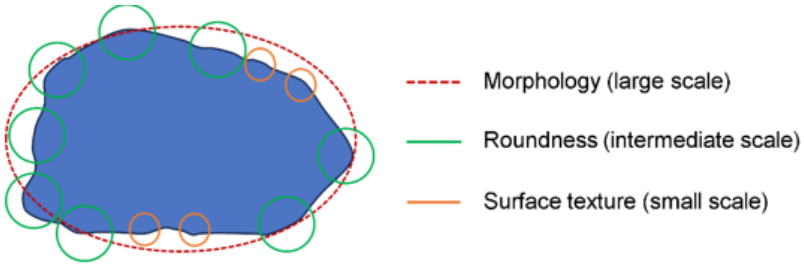



Figure 3.13. Shape describing sub-quantities (Modified after Mitchell and Soga, 2005).

This work uses two-dimensional definitions from literature and proposes three-dimensional shape descriptors based on the developed 3D imaging setup. The effect of the shape and form of a particle on the engineering properties of sand has been approved by several researchers. Hence, this research focuses on intermediate, and macro-scale particle shape parameters. Roundness, sphericity, aspect ratio, and convexity are four main parameters which have been evaluated in two and three-dimensional approaches. Roundness ($R$) is an intermediate scaled indicator of particle outline irregularity which is a vital parameter of granular materials and directly related to internal and critical friction angles, and subsequently to the shear strength and volumetric behavior of a granular material. Sphericity ($S$) describes the overall form of a grain and shows how a particle form is like a circle in 2D or a sphere in 3D. Aspect ratio ($AR$) is also a form indicator which is the ratio of minimum to maximum Feret's diameters. $AR$ is a good parameter to evaluate how a particle has an elongated shape. Convexity ($Cx$) defines the convex hall of a particle outline. $Cx$ can be considered as irregularity of the overall form of a particle. Convex hulls can have a remarkable role in the interlocking mechanism of a packed granular media.

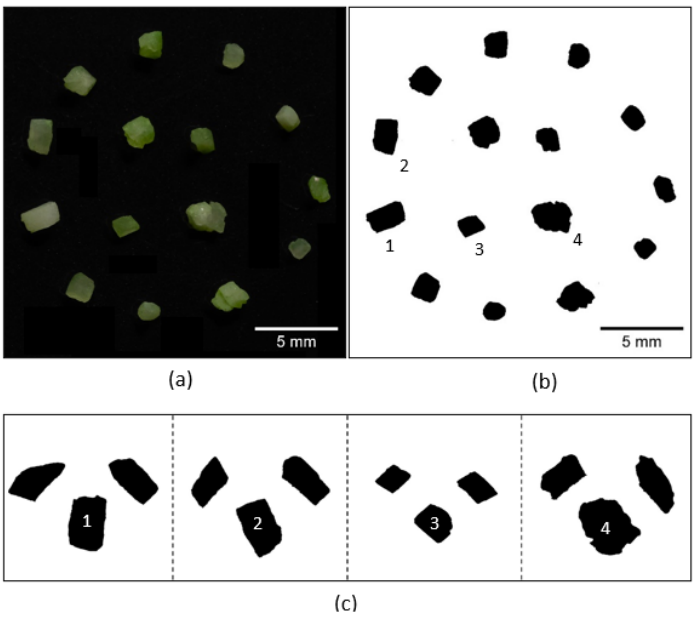



Figure 3.14. Particles of a random green-colored sample in the sand size range. (a) 2D digital image, (b) Processed binary images from the digital image, (c) 3D images obtained from the developed imaging setup.

### 3.2.5. Determination of 2D Shape Descriptors

2D Shape analysis was conducted based on the proposed definitions in the literature listed in Table 2.1. For 2D roundness ($R_{2D}$), the well-known Wadell's relation was used. In 1932 Wadell defined roundness as the ratio of average radii of corner circles ($r_i$) to the radius of the inscribed circle ($r_{ins}$) of a particle outline. In 1963, Krumbein and Sloss defined sphericity ($S_{2D}$) as the radius ratio of the inscribed circle ($r_{ins}$) to the circumscribed circle ($r_{cir}$). Mora and Kwan in 2000, proposed aspect ratio ($AR_{2D}$) as the ratio of minimum Feret's diameter ($d_{Fmin}$) to maximum Frets's diameter ($d_{Fmax}$). Feret's diameters are the longest and shortest distances between any two elongations of a particle outline. The notations of a particle outline are presented in Figure 3.15. 2D convexity ($Cx_{2D}$) is described as the ratio of particle area to the sum of particle area and convex hull.

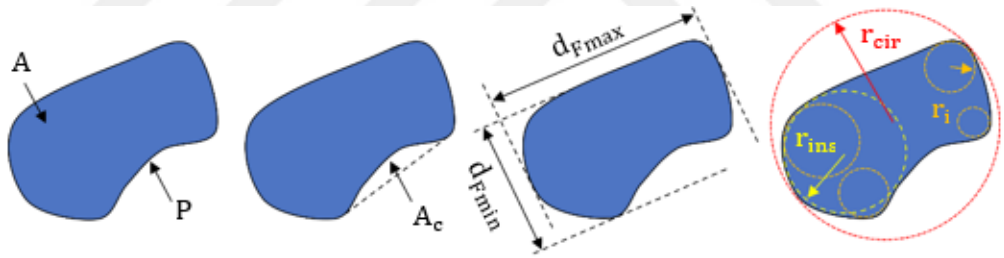



Figure 3.15. Illustration of notations for projected particle outline in 2D analysis.

In this stage, the projected images on the mirrors were neglected and the shape analysis was conducted considering only the particle face which is obtained from the image directly captured by the camera. This face was named the dominant face ($F_D$) and is the most stable face of a particle which usually has larger outline values compared with the other faces. Using ImageJ, the required parameters for each shape descriptor were obtained from the binary image of each $F_1$, and then 2D shape descriptors were calculated

$$R_{2D} = (\Sigma r_i/N)/r_{ins}, \tag{3.1}$$

$$S_{2D} = r_{ins}/r_{cir}, \tag{3.2}$$

$$AR_{2D} = d_{Fmin}/d_{Fmax}, \tag{3.3}$$

$$Cx_{2D} = A/(A + A_c). \tag{3.4}$$

### 3.2.6. Proposed 3D Shape Descriptors

3D particle shape analysis was conducted considering all three faces of any placed particle in the imaging setup and proposing four new shape descriptors. Keeping the basic concept of the shape descriptors for 2D analysis, this part introduces the three-dimensional version of the mentioned shape descriptors consisting of 3D roundness ($R_{3D}$), 3D sphericity ($S_{3D}$), 3D aspect ratio ($AR_{3D}$), and 3D convexity ($Cx_{3D}$), Table **??** describes the proposed three-dimensional shape descriptors in this study.

Since the radii of a sphere and its corresponding circle are identical, the radius of circles was used as size indicators of the spheres. Radii for corner spheres ($r_i$), minimum inscribed sphere ($MINr_{ins}$), maximum circumscribed sphere ($MAXr_{max}$), and smallest Feret's diameter ($MINd_{Fmin}$), and largest Feret's diameter ($MAXd_{Fmax}$) are the terms used for 3D evaluation.

$r_{i3}$ is the radius of any circle that can be placed in the corners of particle faces. Minimum and maximum of the parameters above represent their smallest and largest values among the three projected faces. Figure 3.16 illustrates the notation of the mentioned parameters

$$R_{3D} = (\Sigma r_{i3}/N)/(MINr_{ins}) \; for \; r_{i3} \leq MINr_{ins}, \tag{3.5}$$

$$S_{3D} = MINr_{ins}/MAXd_{cir}, \tag{3.6}$$

$$AR_{3D} = MINd_{Fmin}/MAXd_{Fmax}, \tag{3.7}$$

$$Cx_{3D} = \sum_{i=1}^{3} A_i/(A_i + A_{ci}). \tag{3.8}$$

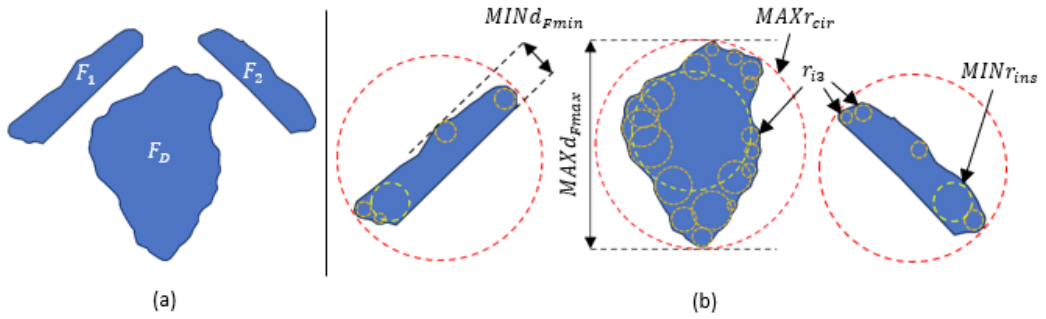



Figure 3.16. Illustration of notations for 3D shape analysis of all faces. (a) outlines of the dominant face and two projected faces on mirrors. (b) measurements among the outlines of all faces.

$R_{3D}$ indicates irregularity of particle surface by examining its faces in three orthogonal axes. It was defined as the ratio of the average radii of the corner spheres to the radius of the minimum inscribed circle ($MINr_{ins}$) among three faces. For this, it is essential to check that the radius of any corner sphere should be equal to or less than the $MINr_{ins}$. Otherwise, especially in the case of flat particles a corner sphere for one face can be larger than $MINr_{ins}$ which conflicts with overall 3D integration of the grain shape. As a shape form indicator, $S_{3D}$ describes how a grain shape is related to a sphere and was defined as the radius ratio of the smallest inscribed sphere to the largest circumscribed sphere among three faces. $AR_{3D}$ shows the degree of particle elongation considering the ratio of Feret's diameters. $Cx_{3D}$ was defined as the ratio of the faces' areas and the corresponding convex hulls.

### 3.2.7. Minimum Number of Required Particles for Shape Analysis

The number of analyzed particles is an important factor for accurate evaluation of the shape parameters. The minimum number of required particles was estimated based on the variation of cumulative average values of the determined 3D shape descriptors. Figure 3.17 shows effect of the number of analyzed particles on the determined 3D shape descriptors of Sand C.

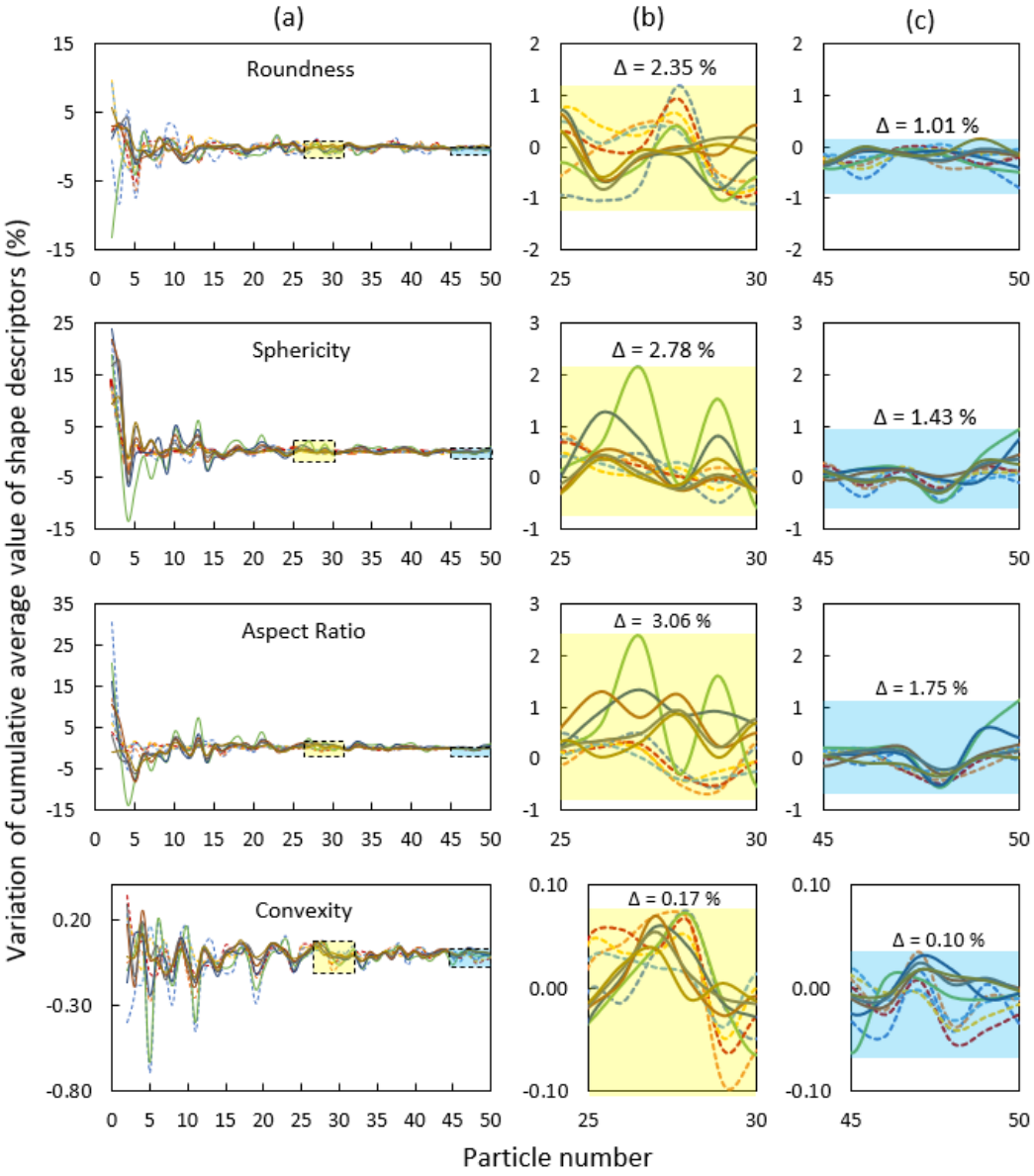



Figure 3.17. (a) changes on cumulative average values of shape descriptors by the number of analyzed particles of Sand C. (b) shape value changes for a number of particles from 25 to 30. (c) shape value changes for a number of particles from 45 to 50.

It shows how increasing the number of particles leads to a remarkable reduction in the cumulative average values of the shape descriptors. For 30 number of particles, the maximum change is about 3% while it drops to 1.75% for 50 particles. In this study, accepting an approximate maximum error of 3%, 30 particles were considered as the minimum number of particles for shape analysis.

# 4. LABORATORY TESTING PROGRAM

## 4.1. Laboratory Tests

The laboratory testing programs aim to investigate particle shape effects on the engineering and mechanical properties of the investigated materials in this study. As the main part of the experimental program, several Consolidated Drained (CD) triaxial tests were conducted. With the series of CD triaxial tests, stress-strain and stress-dilatancy parameters of sand and their relationship with average grain shape parameters are investigated. A series of tests was conducted on all samples prepared in various densities and applying three different consolidation pressures of 100, 200, and 300 kPa. The tests were conducted at the Soil Mechanics Laboratory of Boğaziçi University using Goecomp triaxial testing system shown in Figure 4.1.

### 4.1.1. Angle of Repose

Besides shape analysis, to have a good evaluation of shape effect on engineering properties, it is important to also investigate mechanical properties which internal friction angle is one of them. The angle of repose is a simple method to get an idea about the friction angle of the materials.

It is the steepest angle of descent or dip relative to the horizontal plane to which a material can be piled without slumping. So, before starting the main experimental program, as is shown in Figure 4.1, the angle of repose was obtained for the studied materials. GB as the most rounded and sphere sample has the smallest angle of 23 degrees while Sand D as the most irregular studied material has the steepest repose angle of 39 degrees.

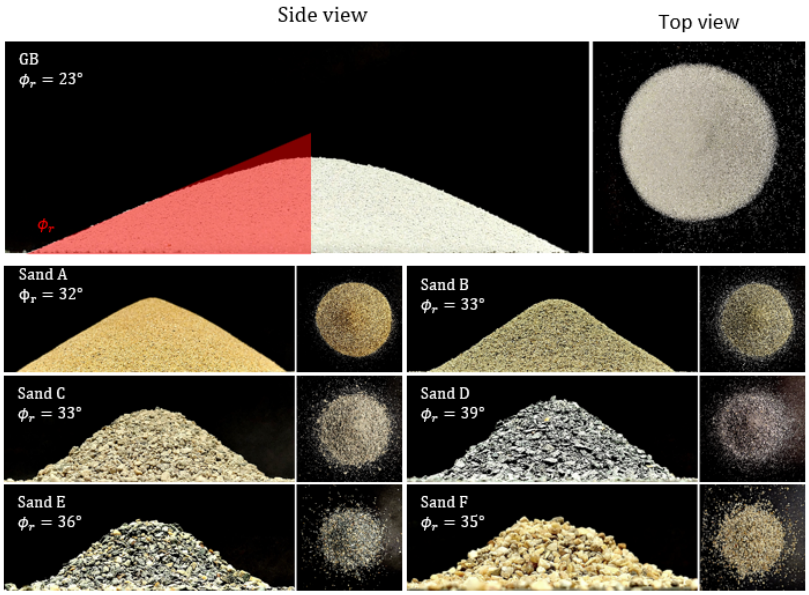



Figure 4.1. Angle of repose for the investigated samples.

### 4.1.2. Santamarina's Critical State Friction Angle

As another initial test, a simplified method proposed by Santamarina (2001) [120] was used to get an approximate evaluation of critical state friction angles for the studied materials. As it is shown in Figure 4.2, firstly a pure sample is putted in 1000 mL of de-aired water in a cylinder, and then the cylinder is slowly rotated 60 degrees and is brought back to the first position. The angle between the horizontal line and the creatd inclined line in the middle of cylinder represents the critical state friction angle.

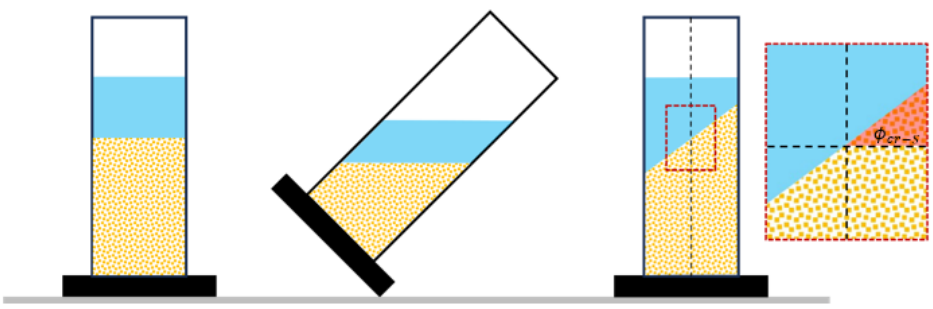


Figure 4.2. Santamarina's method.

Figure 4.3 shows the determined critical friction angles based on Santamarina's method. The Sand D with the lowest sphericity has the largest value while GB as the most rounded and sphere sample has the smallest $\phi_{cr-S}$. This means that samples with irregular particle shapes have a higher tendency of particles to interlock and consequently larger shear strength.

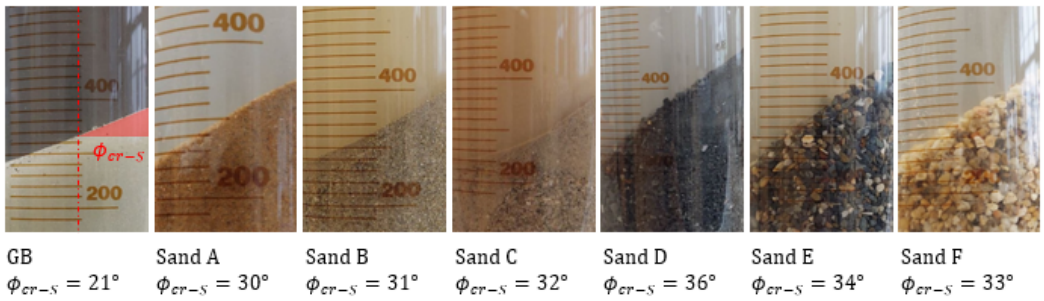



Figure 4.3. Santamarina's method to determine the critical state friction angles of the investigated materials.




Figure 4.4. Triaxial test setup, soil mechanics laboratory of Boğaziçi University (2023). (a) LoadTrac for applying axial load, (b) FlowTrac - 1 for applying cell pressure around the specimen, (c) FlowTrac - 2 for applying pore water pressure inside the sample, (d) Load cell to measure applied load, (e) Cell containing water, (f) De-aired water supply tank, (g) A sheared sample.

It is a fully automated triaxial setup with three main parts consisting of LoadTrac for applying axial loads, and two FlowTrac-II s to provide desired cell and sample pressure on the specimen. The LoadTrac-II is capable of applying axial load up to 45 kN while each FlowTrac-II has a volume capacity of 250 cc and can apply pore pressure up to 1400 kPa. Strain controlled tests were performed to follow small strains for accurate evaluation on the stress-strain behavior and volumetric strains of the tested samples. Each test has four main steps consisting of initialization, saturation, consolidation, and shear phases. The test data are recorded during all phases and at the end of the tests are collected for analysis and consequently to determine the desired mechanical properties of the samples.

Consequently, a series of oedometer tests were conducted to evaluate the relationship between compressibility and shape parameters of granular materials.

### 4.1.3. Specimen Preparation for Triaxial Tests

To evaluate the samples in various conditions, the samples with different relative densities were prepared mainly in loose, medium, and dense classes. Initially, sand samples were dried in an oven at 50° for 24 hours, then for preparing medium, dens, and very dense specimens, the air pluviation method proposed by Al-Shibli et al. was used. Dry sand flow down of a funnel and spread out through four sets of USCS No.4 sieves. The desired densities were achieved by changing the height of the drop ($H$) shown in Figure 4.5. This method was used to prepare specimens for samples of GB, Sand A, and Sand B having $D_{50}$ less than 0.60 mm. In the case of preparing loose specimens, and for samples of Sand C, Sand D, Sand E, and Sand F with higher values of $D_{50}$ ranging between 0.89 mm and 2.95 mm, specimens were prepared by holding a funnel with a spout diameter of 13 mm according to the procedure of D4254 (ASTM 2016b) [121]. Several specimens were prepared to determine the appropriate height of drop for each desired relative density. The specimens were prepared in approximate diameters of 50 mm and height of 10 - 12 mm.

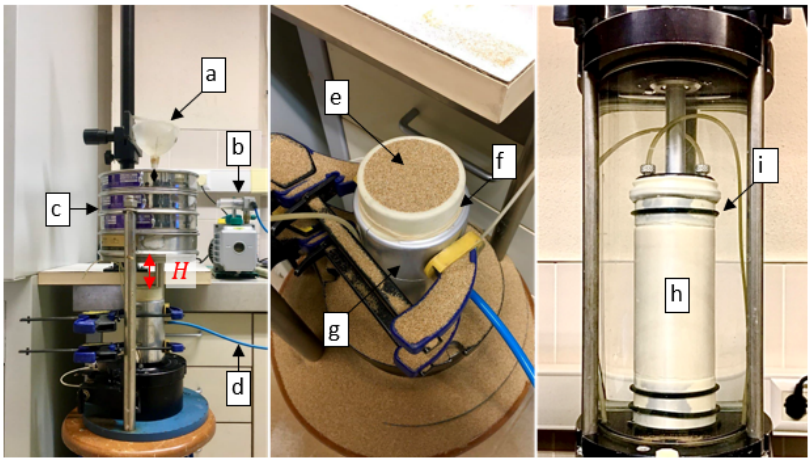



Figure 4.5. Setup of sample preparation for triaxial test. (a) Funnel, (b) Vacuum pump, (c) four sets of No. 4 sieves, (d) Vacuum line connected to the mold, (e) Sand A placed by air pluviation method, (f) Membrane, (g) Sample preparation mold, (h) prepared sample ready for test, (j) plastic rubber.

### 4.1.4. Initialization Phase

After preparation of specimen, it is placed in the Geocomp triaxial test setup. At this step, the specimen data such as initial values of diameter, height, mass, and specific gravity are imported to the system software. The aim of this phase is setting up the test phases and parameters, calibration of load and displacement sensors, and troubleshooting any probable problems such as network connection problems or leakage in the pore water and cell pressure lines. Subsequently, the test begins according to the defined settings in the system. The tests were started by applying identical vertical and horizontal stress of 30 kPa as cell pressure, and 15 kPa as sample pressure by stress rate of 30 kPa/min.

In the case of dense specimens, Co2 gas was injected into the samples before starting the test. This replaces air inside the sample voids with Co2 gas which can be dissolved in the imported pore water in the sample and accelerates the process of sample saturation.

### 4.1.5. Saturation Phase

Specimen saturation was performed by applying pore water pressure inside the sample and filling voids with pore water. The degree of saturation was measured using Skempton's coefficient presented in the equation below

$$B = \frac{\Delta u}{\Delta \sigma'}, \tag{4.1}$$

where B is Skempton's coefficient of saturation, $\Delta u$ is changes in pore water pressure, and $\Delta \sigma$ is changes in cell or confining pressure. The specimen is considered saturated when $B$ value becomes equal or greater than 95 percent. Figure 4.6 shows the saturation phase of a medium-dense specimen of Sand $B$. For this Sample $Co_2$ gas was injected to accelerate the saturation and it is obvious that saturation of such a relatively dense sample is completed perfectly within a short time in 79 minutes.

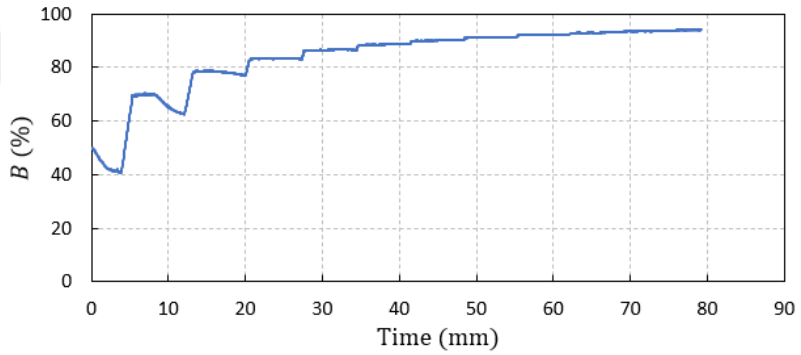



Figure 4.6. Skempton's B value in the saturation phase of a $Co_2$-injected sample. CD - ISO triaxial test of Sample B with relative density of $I_d$= 63% under consolidation pressure of $\sigma'_c$= 200 kPa.

### 4.1.6. Consolidation Phase

The tests were performed under three different consolidation pressures of 100, 200, and 300 kPa. By increasing cell pressure at a stress rate of 5 kPa/min, the pore water inside the sample is drained gradually. This small stress rate was applied intentionally to avoid shearing the specimen during the consolidation phase. The cell pressure rises until the applied effective stress around the specimen reaches the desired consolidation

pressure. Then the system performs a real-time check continuously to keep the pressure constant. Figure 4.7 shows the process of applying 200 kPa of consolidation pressure on the specimen of Sand B.

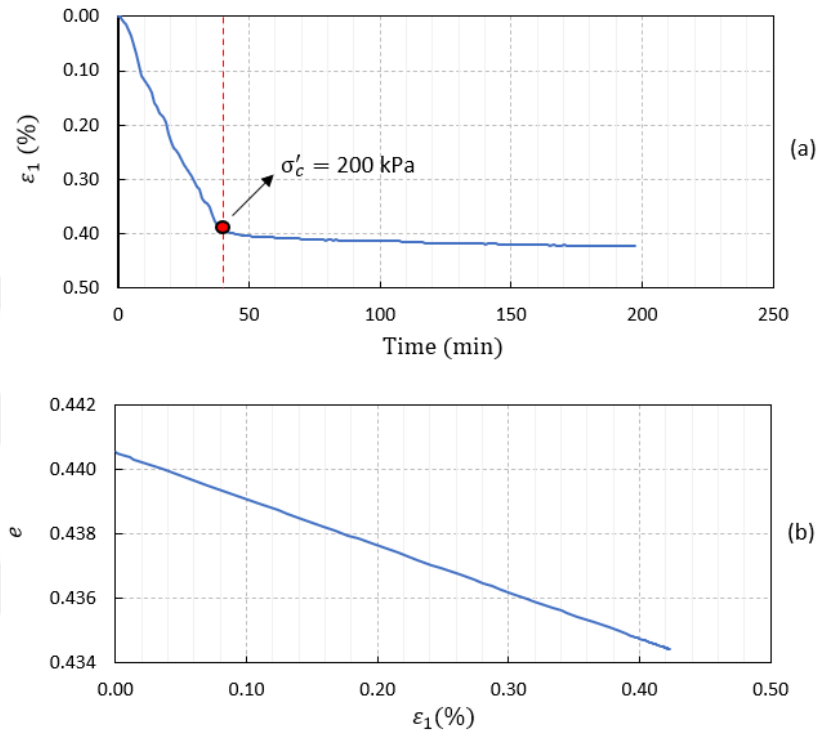



Figure 4.7. Consolidation phase of a CD triaxial test of Sample B with relative density of $I_d$= 63 % under consolidation pressure of $\sigma'_c$= 200 kPa. (a) time - $\varepsilon_1$, (b) e-$\varepsilon_1$ relationship.

As shown in Figure 4.7- (a), increasing the consolidation pressure with a stress rate of 5 kPa/min causes larger axial strain for 40 minutes, the point at which consolidation pressure of 200 kPa is reached when $\sigma'_c$= 200 kPa. Then, the system continues keeping stress constant and the strain changes become minimal. Similarly, Figure 4.7-(b) indicates the reduction of the void ratio by increasing the consolidation pressure. The phase continues according to according to the square root of time method proposed by Taylor.

### 4.1.7. Shear Phase

Following the previous step, the shear phase begins by applying an isotropic axial compression stress path under drained conditions. While the confining pressure is kept at 200 kPa, LoadTrac-II starts applying axial compression load on the specimen.

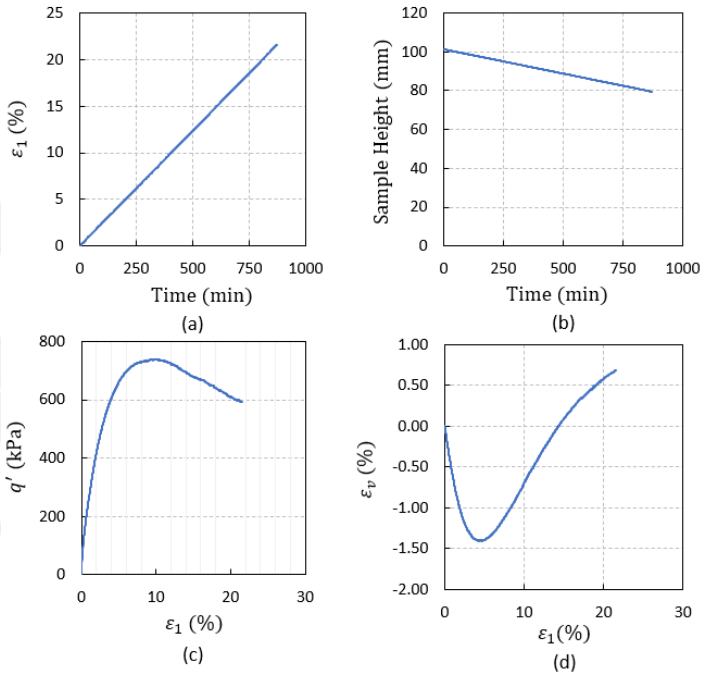



Figure 4.8. Shear phase of a CD triaxial test of Sample B with a relative density of $I_d$= 63 % under consolidation pressure of $\sigma'_c$= 200 kPa. (a) Time - $\varepsilon_1$ , (b) Time - Sample height, (c) $q'$- $\varepsilon_1$ , (d) $\varepsilon_1$- $\varepsilon_v$ relationship AC stress path.

Figure 4.8 shows the shear phase of a medium-dense sample of Sand B under a confining pressure of 200 kPa. By applying axial compression load and increasing axial strain the height of the specimen decreases. The sample shears at about 6 percent of axial strain where derivative stress reaches its maximum value of 754 kPa. In the $\varepsilon_1$- $\varepsilon_v$ graph, compression is defined by a negative sign, so by the initiation of the shear phase the specimen is compressed and then as it is expected for dense cohesionless materials, due to the mobility of densified particles, volume extension of the specimen occurs at the approximate axial strain of 4.2 percent.

# 5. RESULTS AND DISCUSSION

## 5.1. Results of Image Analysis

According to the results of shape analysis, there is a remarkable difference between 2D and 3D shape descriptors, except for convexity. For instance, a particle which is quantified as very spherical in 2D yields very low sphericity in 3D when the other two orthogonal faces are considered. This shows how a 3D approach can lead to more accurate and realistic results compared to a 2D approach.

### 5.1.1. Particle Shape Analysis

The results of particle shape analysis are presented in Table 5.1. For each sample, it shows particles size ranges (PSR), average shape values for each range, and the determined shape descriptors based on the weighted average values. Seven different materials were studied based on 2D and 3D particle shape characterization. According to USCS, the size of the investigated samples remains within the sand class. Studying a total number of 860 particles including 2,580 projected grain faces resulted in 6,880 calculated shape descriptors in 2D and 3D. The obtained shape descriptors were calculated using 15,480 measured shape parameters. 2D analysis is based on only the dominant face (F1) of each particle while in 3D analysis all three faces are taken in account including F1, F2, and F3. To consider the effect of gradation and particle size ranges, the final values of shape descriptors for each analyzed sample are calculated using weighted average method. First, the arithmetic mean value is determined for each particle size range, then considering the content of sample in each range, the weighted average is obtained.

### 5.1.2. Results of 2D Shape Analysis

The determined 2D Shape parameters are presented in Table 5.1. It shows the average values based on the particle size range of each sample and the weighted average data obtained according to the percentage of retained material on each sieve size range.

Table 5.1. Results of 2D shape analysis.

| Material | Sieve # | Percent Retained | PRC (mm) | Range average | | | | Weighted average | | | |
|---|---|---|---|---|---|---|---|---|---|---|---|
| | | | | | $S_{2D}$ | $AR_{2D}$ | $Cx_{2D}$ | $R_{2D}$ | $S_{2D}$ | $AR_{2D}$ | $Cx_{2D}$ |
| GB | 40 | 100 | 0.425 - 0.850 | 1.00 | 1.00 | 1.00 | 1.00 | 1.00 | 1.00 | 0.85 | 1.00 |
| Sand A | 40 | 0.80 | 0.425 - 0.850 | 0.45 | 0.69 | 0.75 | 0.96 | 0.59 | 0.70 | 0.72 | 0.96 |
| | 60 | 12.38 | 0.250 - 0.425 | 0.55 | 0.68 | 0.72 | 0.96 | | | | |
| | 100 | 86.82 | 0.150 - 0.250 | 0.60 | 0.71 | 0.73 | 0.96 | | | | |
| Sand B | 20 | 16.90 | 0.850 - 2.00 | 0.46 | 0.64 | 0.69 | 0.96 | 0.49 | 0.67 | 0.71 | 0.96 |
| | 40 | 35.42 | 0.425 - 0.850 | 0.45 | 0.68 | 0.72 | 0.96 | | | | |
| | 60 | 22.01 | 0.250 - 0.425 | 0.49 | 0.70 | 0.75 | 0.96 | | | | |
| | 100 | 20.07 | 0.150 - 0.250 | 0.56 | 0.64 | 0.67 | 0.96 | | | | |
| | 140 | 5.60 | 0.106 - 0.150 | 0.60 | 0.68 | 0.70 | 0.95 | | | | |

Table 5.1 Results of 2D shape analysis. (cont.)

| Material | Sieve # | Percent Retained | PRC (mm) | Range average | | | | Weighted average | | | |
|---|---|---|---|---|---|---|---|---|---|---|---|
| | | | | | $S_{2D}$ | $AR_{2D}$ | $Cx_{2D}$ | $R_{2D}$ | $S_{2D}$ | $AR_{2D}$ | $Cx_{2D}$ |
| Sand C | 10 | 14.98 | 2.00 - 4.75 | 0.50 | 0.67 | 0.74 | 0.97 | 0.50 | 0.64 | 0.69 | 0.96 |
| | 20 | 36.75 | 0.850 - 2.00 | 0.51 | 0.64 | 0.69 | 0.97 | | | | |
| | 40 | 21.17 | 0.425 - 0.850 | 0.46 | 0.61 | 0.65 | 0.95 | | | | |
| | 60 | 12.32 | 0.250 - 0.425 | 0.49 | 0.63 | 0.68 | 0.96 | | | | |
| | 100 | 11.00 | 0.150 - 0.250 | 0.56 | 0.68 | 0.71 | 0.96 | | | | |
| | 140 | 3.78 | 0.106 - 0.150 | 0.55 | 0.60 | 0.63 | 0.95 | | | | |
| Sand D | 10 | 36.61 | 2.00 - 4.75 | 0.45 | 0.58 | 0.64 | 0.95 | 0.47 | 0.59 | 0.65 | 0.95 |
| | 20 | 36.31 | 0.850 - 2.00 | 0.45 | 0.59 | 0.65 | 0.95 | | | | |
| | 40 | 12.79 | 0.425 - 0.850 | 0.47 | 0.63 | 0.67 | 0.96 | | | | |
| | 60 | 7.10 | 0.250 - 0.425 | 0.54 | 0.60 | 0.63 | 0.96 | | | | |
| | 100 | 4.97 | 0.150 - 0.250 | 0.59 | 0.67 | 0.69 | 0.95 | | | | |
| | 140 | 2.22 | 0.106 - 0.150 | 0.59 | 0.64 | 0.66 | 0.94 | | | | |

Table 5.1 Results of 2D shape analysis. (cont.)

| Material | Sieve # | Percent Retained | PRC (mm) | Range average | | | | Weighted average | | | |
|---|---|---|---|---|---|---|---|---|---|---|---|
| | | | | | $S_{2D}$ | $AR_{2D}$ | $Cx_{2D}$ | $R_{2D}$ | $S_{2D}$ | $AR_{2D}$ | $Cx_{2D}$ |
| Sand E | 10 | 66.43 | 2.00 - 4.75 | 0.51 | 0.61 | 0.66 | 0.97 | 0.52 | 0.62 | 0.66 | 0.97 |
| | 20 | 33.57 | 0.850 - 2.00 | 0.54 | 0.63 | 0.67 | 0.97 | | | | |
| Sand F | 10 | 90.70 | 2.00 - 4.75 | 0.52 | 0.70 | 0.74 | 0.98 | 0.52 | 0.70 | 0.73 | 0.98 |
| | 20 | 8.20 | 0.850 - 2.00 | 0.53 | 0.67 | 0.71 | 0.97 | | | | |
| | 40 | 0.34 | 0.425 - 0.850 | 0.45 | 0.65 | 0.72 | 0.96 | | | | |
| | 60 | 0.70 | 0.250 - 0.425 | 0.49 | 0.65 | 0.69 | 0.95 | | | | |
| | 100 | 0.06 | 0.150 - 0.250 | 0.53 | 0.65 | 0.69 | 0.94 | | | | |

Four 2D shape descriptors including roundness, sphericity, aspect ratio, and convexity were determined based on shape analysis on the dominant faces of seven different samples. Figure 5.1 shows the weighted average values for each sample. As a reference material, the obtained shape descriptors for GB were 1.00 which is not included in the graph. Except for convexity which ranges between 0.95 and 1.00, there are remarkable changes of other shape values among different samples. Sand A as a beach sand has the most rounded particles while Sand D which is a crushed sand sample had the most angular ones. Similarly, Sand D also has the lowest sphericity and aspect ratio values that indicates irregular shape of particles.

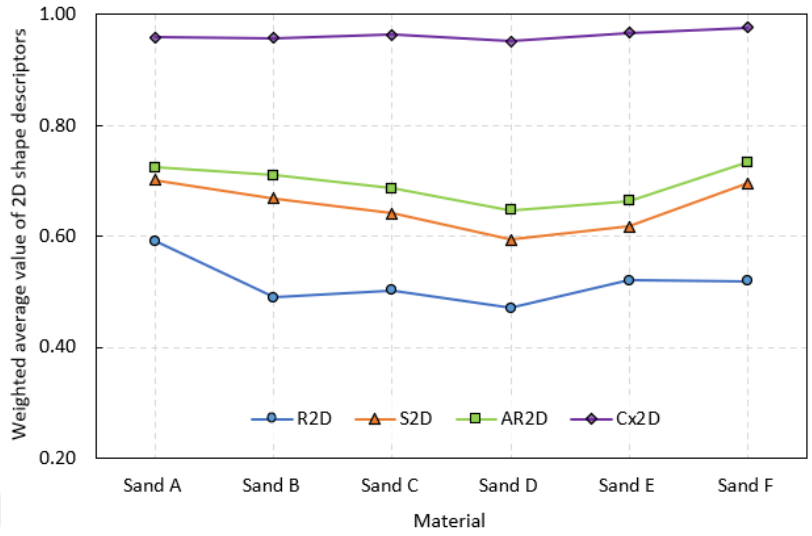



Figure 5.1. Weighted average values of the determined 2D shape descriptors.

According to Figure 5.1, Convexity has the larger values while the roundness moves in the lowest band. Values of sphericity and aspect ratio change in the same way, slightly higher for aspect ratio.

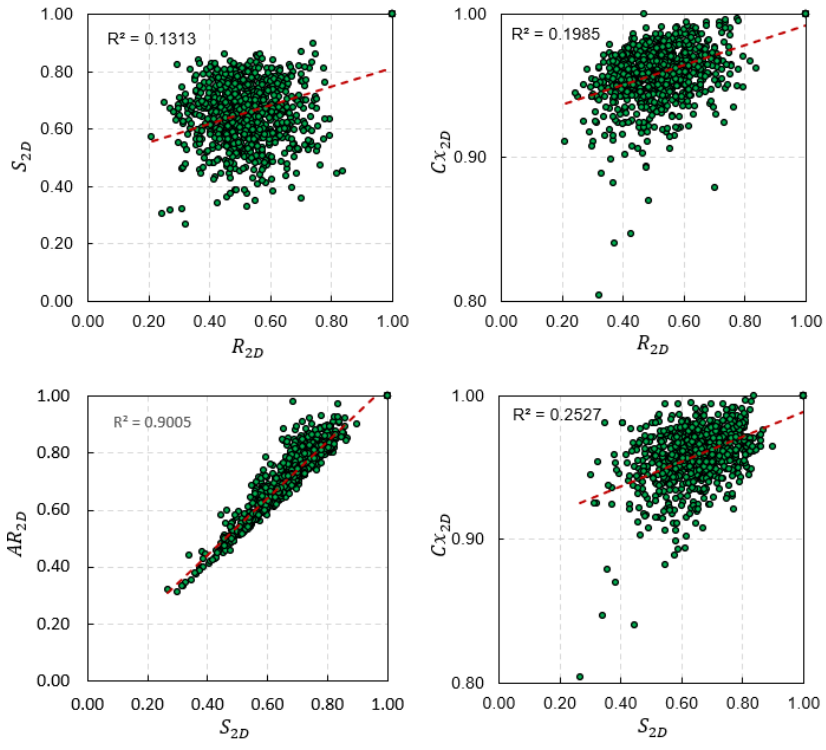



Figure 5.2. Relation between the determined 2D shape descriptors for all particles.

The results of the two-dimensional analysis explain the relationship between shape descriptors. Figure 5.2 reveals the relation between the determined 2D shape descriptors for all particles of the seven studied materials. It is clear that $S_{2D}$ and $AR_{2D}$ are in a good alignment with each other. It can be explained that both of these shape parameters are related to medium-scale of particle shape describing the overall form. In contrast, there is no meaningful connection between other shape descriptors. Roundness indicates the surface irregularity and to somehow texture of a grain in small scale, while convexity is medium scale parameter which is related to convex hulls of overall shape. Hence, these two shape descriptors are independent of each other.

Table 5.2. Results of 3D shape analysis.

| Material | Sieve # | Percent Retained | PRC (mm) | Range average | | | | Weighted average | | | |
|---|---|---|---|---|---|---|---|---|---|---|---|
| | | | | | $S_{2D}$ | $AR_{2D}$ | $Cx_{2D}$ | $R_{2D}$ | $S_{2D}$ | $AR_{2D}$ | $Cx_{2D}$ |
| GB | 40 | 100 | 0.425 - 0.850 | 1.00 | 1.00 | 1.00 | 1.00 | 1.00 | 1.00 | 1.00 | 1.00 |
| Sand A | 40 | 0.80 | 0.425 - 0.850 | 0.52 | 0.45 | 0.47 | 0.96 | 0.60 | 0.47 | 0.49 | 0.95 |
| | 60 | 12.38 | 0.250 - 0.425 | 0.61 | 0.43 | 0.45 | 0.95 | | | | |
| | 100 | 86.82 | 0.150 - 0.250 | 0.60 | 0.47 | 0.50 | 0.95 | | | | |
| Sand B | 20 | 16.90 | 0.850 - 2.00 | 0.53 | 0.47 | 0.49 | 0.96 | 0.55 | 0.49 | 0.52 | 0.96 |
| | 40 | 35.42 | 0.425 - 0.850 | 0.52 | 0.52 | 0.56 | 0.96 | | | | |
| | 60 | 22.01 | 0.250 - 0.425 | 0.57 | 0.48 | 0.51 | 0.95 | | | | |
| | 100 | 20.07 | 0.150 - 0.250 | 0.60 | 0.47 | 0.49 | 0.95 | | | | |
| | 140 | 5.60 | 0.106 - 0.150 | 0.63 | 0.49 | 0.50 | 0.95 | | | | |

Table 5.2 Results of 3D shape analysis. (cont.)

| Material | Sieve # | Percent Retained | PRC (mm) | Range average | | | | Weighted average | | | |
|---|---|---|---|---|---|---|---|---|---|---|---|
| | | | | | $S_{2D}$ | $AR_{2D}$ | $Cx_{2D}$ | $R_{2D}$ | $S_{2D}$ | $AR_{2D}$ | $Cx_{2D}$ |
| Sand C | 10 | 14.98 | 2.00 - 4.75 | 0.52 | 0.44 | 0.47 | 0.97 | 0.53 | 0.44 | 0.47 | 0.96 |
| | 20 | 36.75 | 0.850 - 2.00 | 0.52 | 0.47 | 0.50 | 0.97 | | | | |
| | 40 | 21.17 | 0.425 - 0.850 | 0.50 | 0.39 | 0.41 | 0.96 | | | | |
| | 60 | 12.32 | 0.250 - 0.425 | 0.54 | 0.42 | 0.44 | 0.96 | | | | |
| | 100 | 11.00 | 0.150 - 0.250 | 0.58 | 0.46 | 0.48 | 0.96 | | | | |
| | 140 | 3.78 | 0.106 - 0.150 | 0.60 | 0.45 | 0.48 | 0.94 | | | | |
| Sand D | 10 | 36.61 | 2.00 - 4.75 | 0.52 | 0.33 | 0.35 | 0.96 | 0.51 | 0.34 | 0.36 | 0.95 |
| | 20 | 36.31 | 0.850 - 2.00 | 0.50 | 0.33 | 0.36 | 0.95 | | | | |
| | 40 | 12.79 | 0.425 - 0.850 | 0.50 | 0.39 | 0.40 | 0.95 | | | | |
| | 60 | 7.10 | 0.250 - 0.425 | 0.53 | 0.35 | 0.36 | 0.94 | | | | |
| | 100 | 4.97 | 0.150 - 0.250 | 0.60 | 0.40 | 0.42 | 0.94 | | | | |
| | 140 | 2.22 | 0.106 - 0.150 | 0.60 | 0.41 | 0.43 | 0.94 | | | | |

Table 5.2 Results of 3D shape analysis. (cont.)

| Material | Sieve # | Percent Retained | PRC (mm) | Range average | | | | Weighted average | | | |
|---|---|---|---|---|---|---|---|---|---|---|---|
| | | | | | $S_{2D}$ | $AR_{2D}$ | $Cx_{2D}$ | $R_{2D}$ | $S_{2D}$ | $AR_{2D}$ | $Cx_{2D}$ |
| Sand E | 10 | 66.43 | 2.00 - 4.75 | 0.55 | 0.43 | 0.46 | 0.97 | 0.55 | 0.43 | 0.46 | 0.97 |
| | 20 | 33.57 | 0.850 - 2.00 | 0.56 | 0.44 | 0.46 | 0.97 | | | | |
| Sand F | 10 | 90.70 | 2.00 - 4.75 | 0.56 | 0.51 | 0.53 | 0.98 | 0.56 | 0.51 | 0.53 | 0.98 |
| | 20 | 8.20 | 0.850 - 2.00 | 0.54 | 0.54 | 0.57 | 0.97 | | | | |
| | 40 | 0.34 | 0.425 - 0.850 | 0.51 | 0.53 | 0.57 | 0.96 | | | | |
| | 60 | 0.70 | 0.250 - 0.425 | 0.51 | 0.52 | 0.56 | 0.95 | | | | |
| | 100 | 0.06 | 0.150 - 0.250 | 0.57 | 0.51 | 0.54 | 0.94 | | | | |

In three-dimensional analysis, 3D particle shape descriptors including roundness, sphericity, aspect ratio, and convexity were determined based on the faces of particles in three orthogonal planes. Figure 5.3 shows the weighted average values for each sample. As a reference material, likewise the 2D analysis, the obtained shape descriptors for GB were 1.00 which is not included in the graph.

Convexity ranges between 0.95 and 1.00 while the other shape parameters change significantly for each sample. Same as 2D analysis, the 3D results remark Sand A as the most rounded sample against Sand D with the lowest roundness.

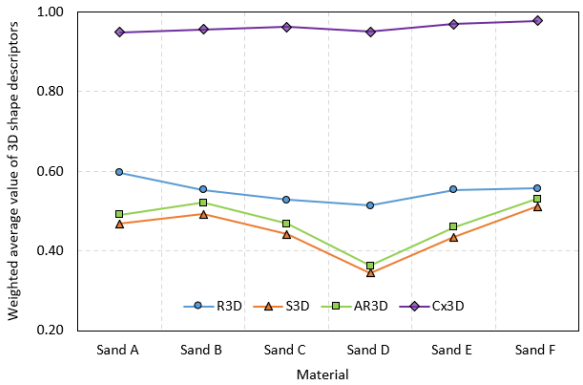



Figure 5.3. Weighted average values of the determined 3D shape descriptors.

Same as for 2D results, the larger values belong to the convexity with no remarkable changes for different materials. Sphericity and aspect ratio again change in the same manner as 2D analysis. However, there is a remarkable change in $R_{3D}$ and it gets values higher than $S_{3D}$ and $R_{3D}$. It varies in a band ranging from 0.50 to 0.60 which is higher than the corresponding zone for $R_{2D}$. 2D analysis is based on the dominant face of a particle which has the most stable side and generally has larger outline compared to side faces reflected on the mirrors. Meanwhile, the 3D analysis also considers side faces with smaller outlines beside the dominant face. Referring to the roundness definition, a smaller radius of inscribed circles in the side faces results in $R_{3D}$ larger than $R_{2D}$.

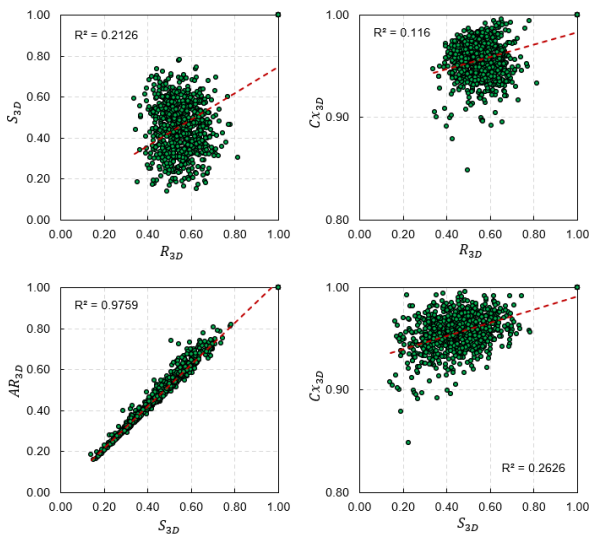



Figure 5.4. Relation between the determined 3D shape descriptors for all particles.

According to Figure 5.4, the three-dimensional aspect ratio and sphericity values are perfectly aligned with each other. It should be mentioned that $S-AR$ alignment of 3D analysis with an R-squared value of 0.97 is higher than 2D one with an R-squared value of 0.90.

### 5.1.3. Comparison of the Determined 2D and 3D Shape Descriptors

Considering the results of the particle shape analysis in the previous sections, the three-dimensional approach results in a realistic and more reliable evaluation of a grain shape. For a quick estimation of particle shape characteristics, it would be beneficial if a correlation could be achieved for a transition from 2D to 3D shape descriptors. This section attempts to investigate the determined shape parameters to understand whether there is any logical relation between 2D and 3D shape parameters. Figure 5.5 shows the relation between the weighted average of shape descriptors for the six investigated sand samples in this study. Since there is a big data gap between shape parameters for sand samples and GB, to avoid this data gap, the shape parameters of GB were not plotted. The plotted values shows that there is no remarkable different between 2D and 3D values of convexity. Also, relatively there is a good alignment for 2D - 3D relationship of roundness with value of 0.83 for $R^2$. The relations the between determined 2D and 3D shape descriptors are presented below. Accordingly, the following equations suggest a correlation for conversion of 2D to 3D shape descriptors for the studied sand samples

$$R_{3D} = 0.6216R_{2D} + 0.2296, \tag{5.1}$$

$$S_{3D} = 1.1787S_{2D} - 0.3214, \tag{5.2}$$

$$AR_{3D} = 1.6284AR_{2D} - 0.6564, \tag{5.3}$$

$$Cx_{3D} = 1.2695Cx_{2D} - 0.2614. \tag{5.4}$$

It must be mentioned that the proposed correlations are based on shape analysis of particle faces of six different sand materials in this study and cannot be generalized for all granular materials. For a more precious and reliable approach, it is required

to study further different samples with various shape characteristics. For a better estimation, it is essential to fill the mentioned data gap between six sand materials and GB. In addition, material origin and gradation, and sample preparation for imaging are some other factors which should be considered to make a reliable connection between 2D and 3D shape parameter of a particle.

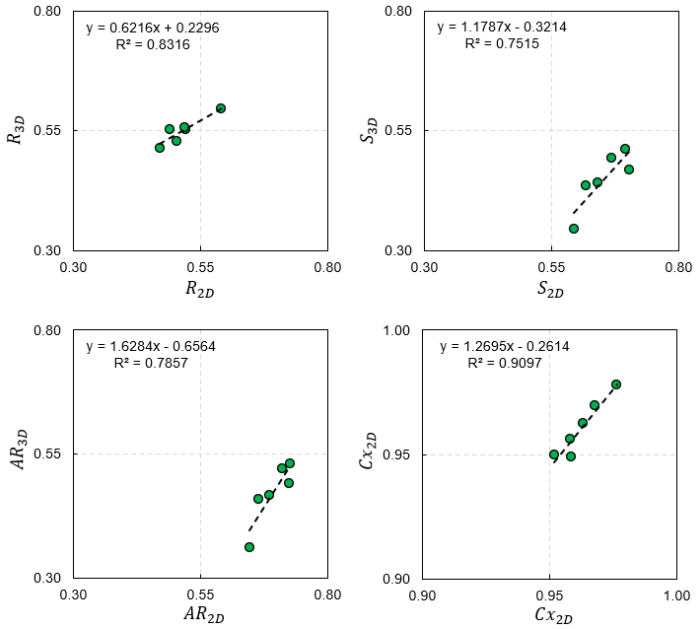



Figure 5.5. Relation between weighted average of the determined 2D and 3D particle shape descriptors for the studied six sand samples.

Additionally, the shape parameters for all particles of the sand samples including all particle size ranges are plotted. As mentioned before, there is no significant difference between 2D and 3D values of convexity. However, there is no distinct 2D - 3D relation for the shape parameters of the particles from various samples. As shown in Figure 5.5, this relation is more meaningful for the particle from the same sample.

As a result, with R-square values of higher than 0.95, there is a good agreement between the 2D and 3D values of four main shape descriptors. $R_{2D}$ and $R_{3D}$ are in the best alignment with R-square of 0.83 for the weighted average values.

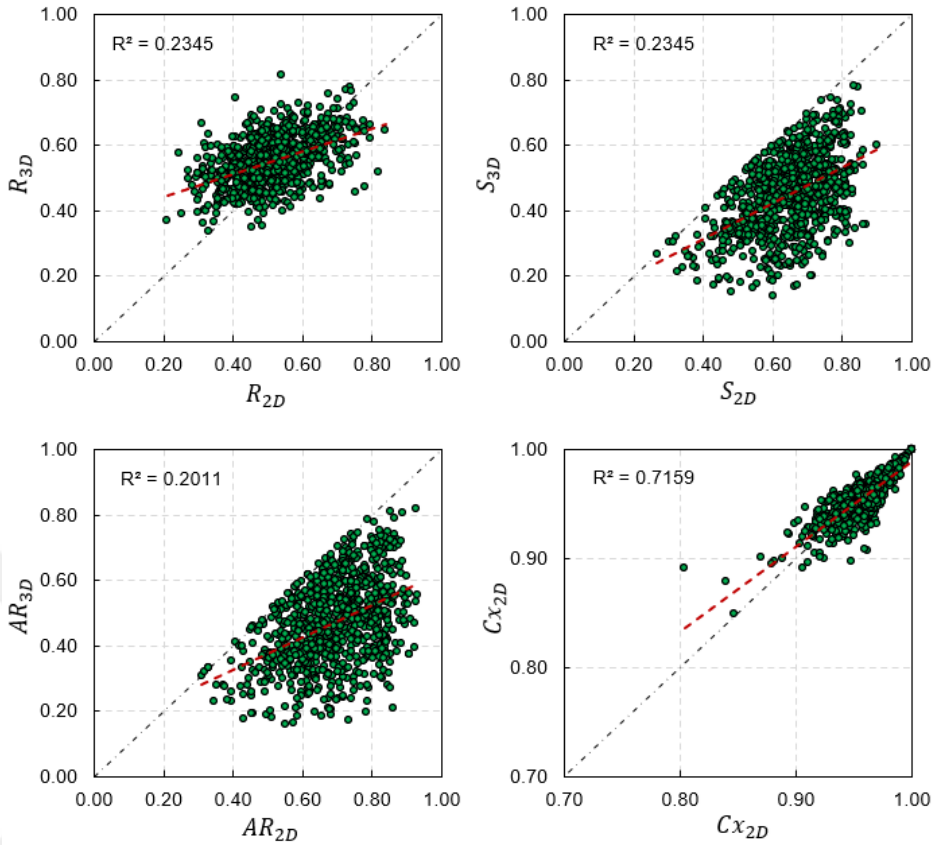



Figure 5.6. Relation between the determined 2D and 3D shape descriptors for all particles.

The plotted results on the graphs of Figure 5.6 reveal a surprising connection between 2D - 3D relation for sphericity and aspect ratio. As mentioned before, these two descriptors change similarly as indicators of the general form of a particle shape. In the $S_{2D}$-$S_{3D}$ and $AR_{2D}$-$AR_{3D}$ graphs, the plotted data remain under the middle line. It means that according to the proposed shape descriptors, the 3D values of S and $AR$ are always less than the 2D ones. This implies the role of two projected faces included in three-dimensional evaluation.

Figure 5.7 shows the relation between the determined 2D and 3D shape descriptors based on different faces of all particles. Face 2 and Face 3 are representing the reflected side image of a particle on the mirrors.

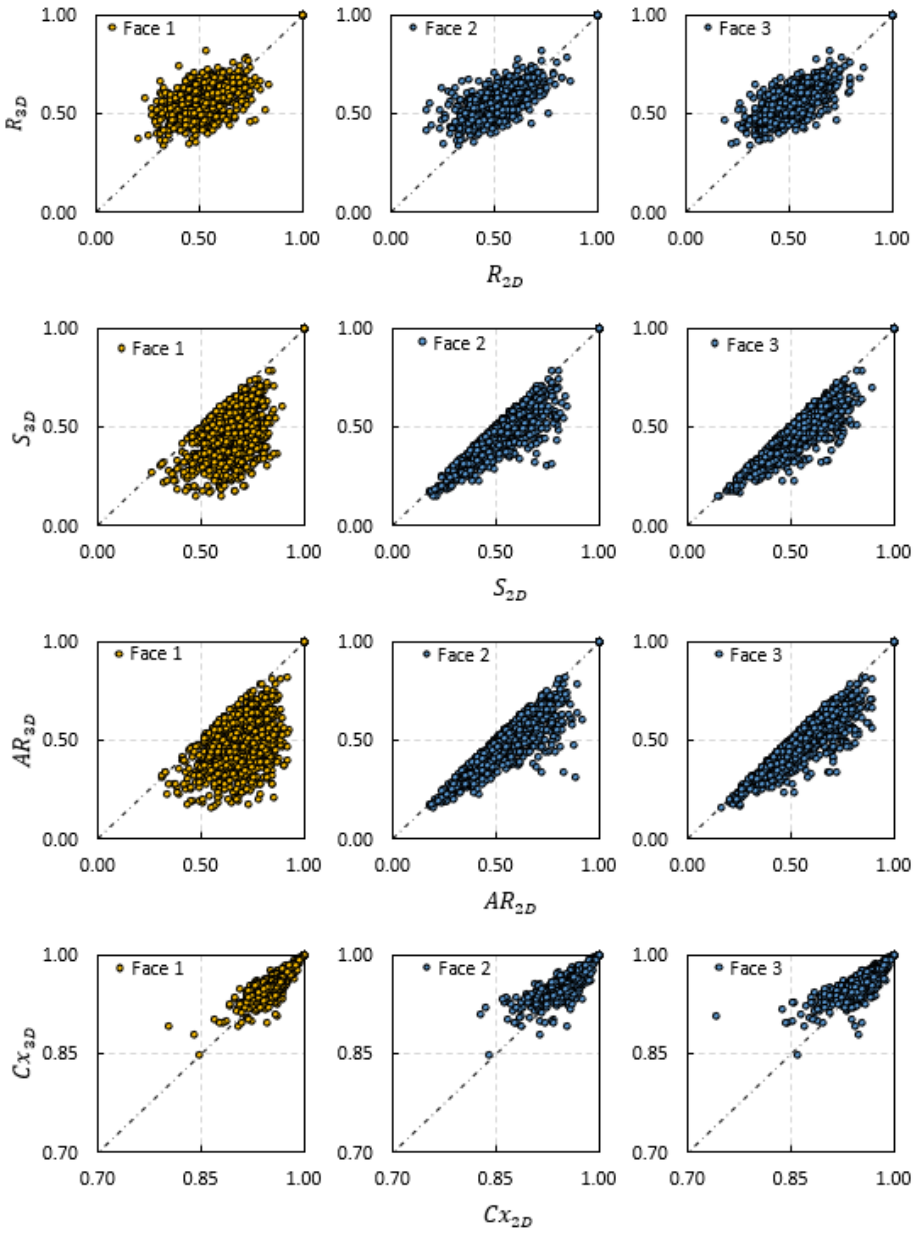



Figure 5.7. Relation between the determined 2D and 3D shape descriptors based on each face.

Figure 5.8 shows the value frequency of shape descriptors for all analyzed particles. Results show that 2D roundness gives smaller values of 3D analysis. In the case of sphericity, 2D values are higher than 2D ones. Results of aspect ratio reveal higher 2D values compared with 3D ones; however, both analysis types result in the same number of particles for the corresponding peak aspect ratios. For convexity, there is no remarkable difference between the obtained 2D and 3D particle shape indicators.

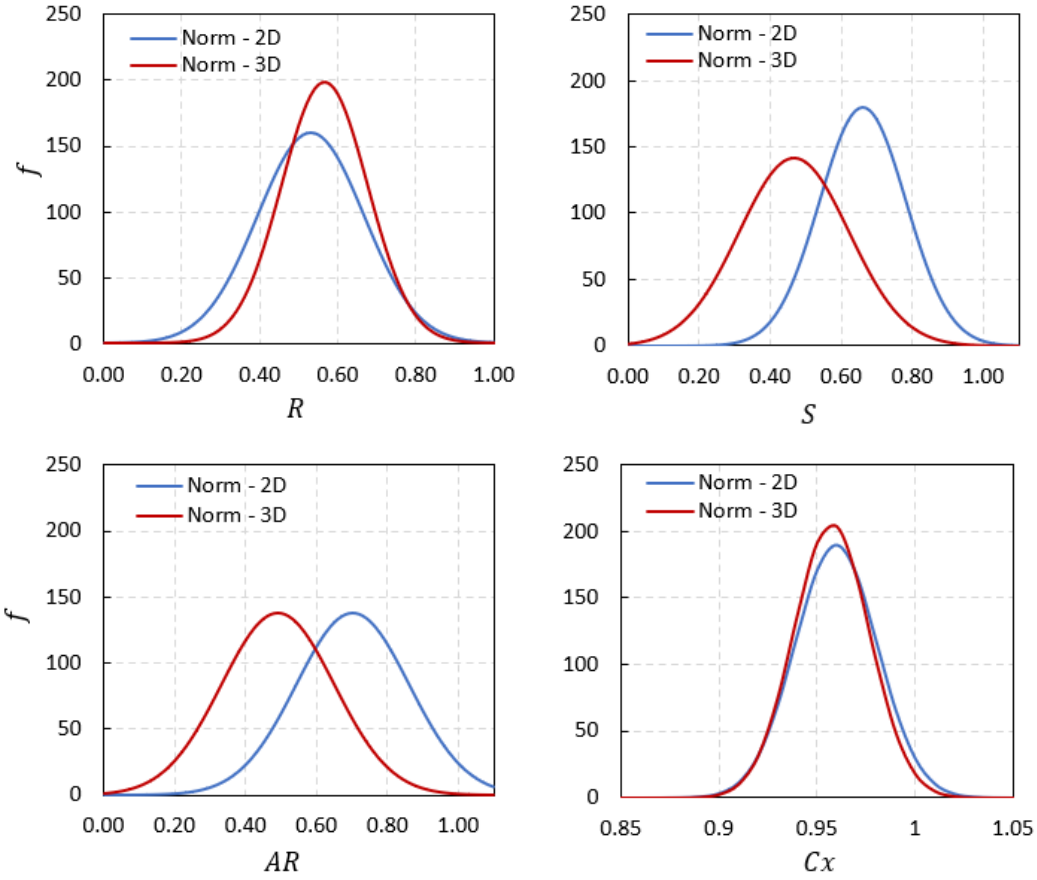



Figure 5.8. Frequency of shape descriptors for all samples.

3D shape analysis successfully reveals how a particle shape could be different from various sides. Figure 5.9 shows a series of obtained photos and the corresponding binary images from different samples and size ranges. This approves the capability of imaging setup for providing desired particle photos with a size range between 0.106 mm and to 4.75 mm.

The created binary images accurately represent the outlines of a particle in three dimensions. The developed imaging setup leads to a realistic evaluation of particle shape considering various projected sides of a grain on three orthogonal surfaces.

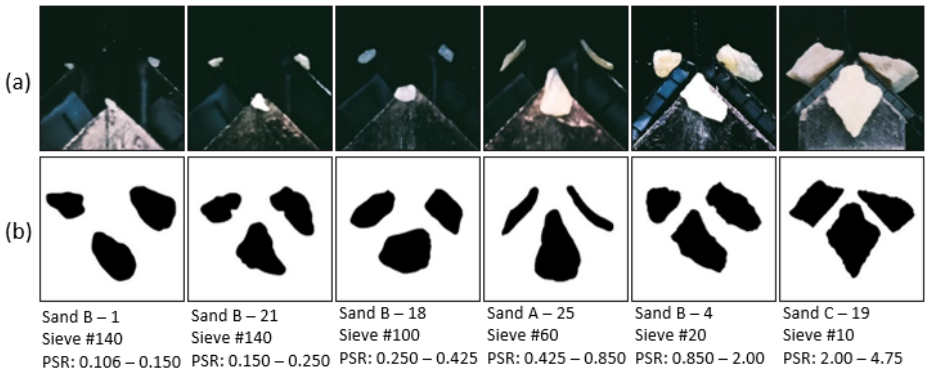



Figure 5.9. Sample images of particles with various size ranges. (a) digital images obtained from the developed imaging setup, (b) corresponding produced binary images. PSR is in mm. The binary images are not in scale.

### 5.1.4. Size Effect on Shape Descriptors

Besides shape and form, the size of a particle is another important property of a granular material. This section studies the effect of particle size on the determined shape descriptors. For this, the average shape value for each particle size range is compared with the corresponding sieve size on which samples are retained. Figure 5.10 shows size-roundness relation of six studied sand samples. It should be mentioned that since all shape descriptors for GB are identical and equal to 1.00, this sample is not included in the figure. Results show a general reduction in roundness by increasing the particle size. However, sand E has a different behavior. Also, the $R_{3D}$ values are less than $R_{2D}$ for all cases except Sand E. Sand A, Sand B, and Sand C are natural beach sands. These samples have been exposed to weathering and erosion for a long time.

Shape analysis results of sphericity, aspect ratio, and convexity of the studied materials in this study indicate that there is no remarkable relation between the size of a grain and its mentioned shape parameters. For instance, as shown in Figure 5.11, sphericity varies in a range by changing the size of a grain.

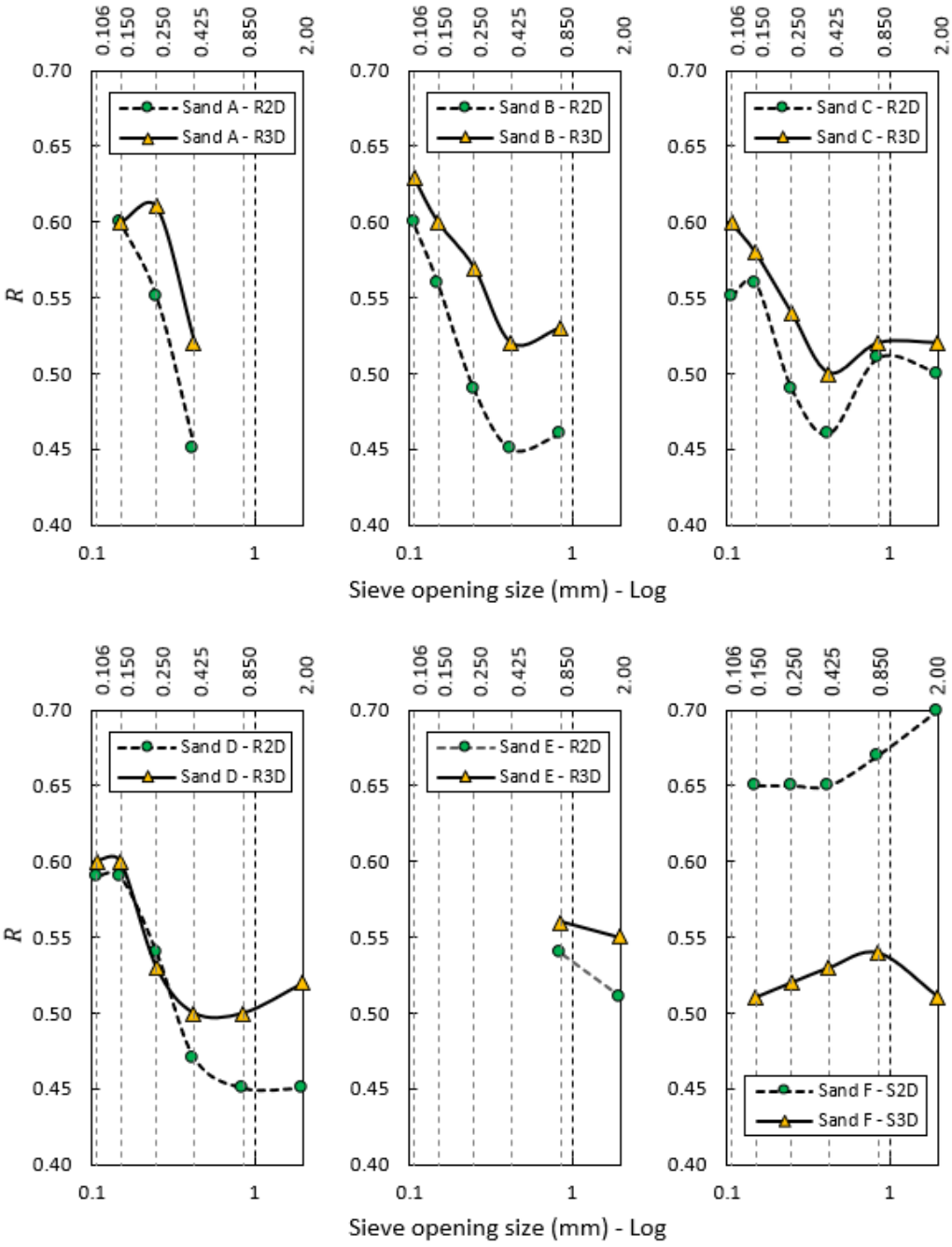



Figure 5.10. Effect of particle size on roundness.

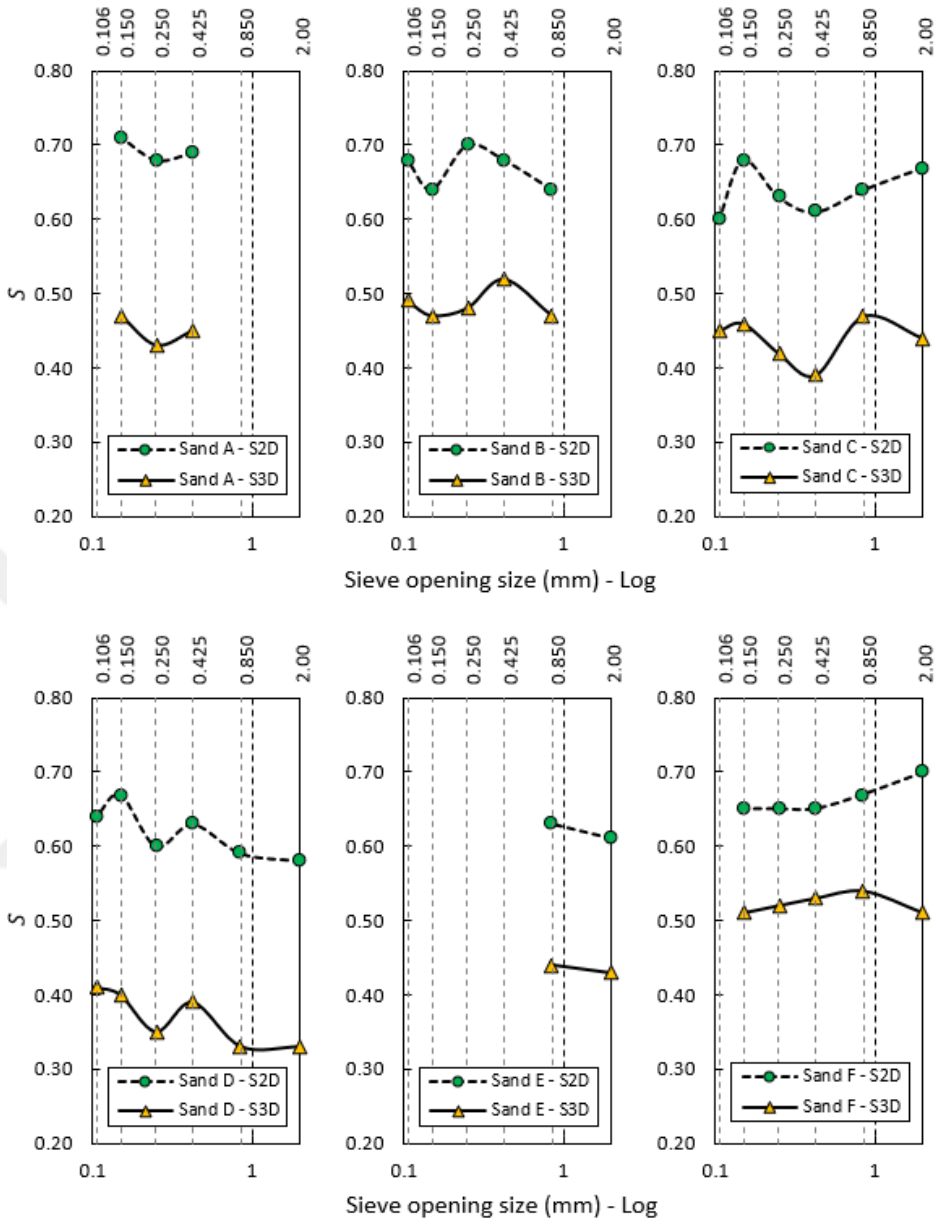



Figure 5.11. Effect of particle size on sphericity.

## 5.2. Particle Shape Classification Based on 3D Shape Analysis

There are some classifications in literature based on 2D shape descriptors; however, they consider only one side of a particle shape which is defined as the dominant face ($F_D$) in this study. This study introduces a classification chart based on the proposed 3D roundness and sphericity. As is shown in Figure 5.12, considering the three faces of a particle results in a more realistic shape evaluation. The chart reveals that a

very high sphere particle has very high sphere outlines in all three faces. For instance, particle #1 shows the faces of GB in this study which has an ideal rounded sphere shape. In the case of particle # 2, the dominant face has a high sphere outline, but considering two other faces in 3D analysis, it is classified as a medium sphere. Similarly for roundness, higher roundness in all three faces defines realistic roundness particles. roundness as a medium-scale indicator was quantified in five groups while sphericity as an indicator of overall form was classified in four categories.

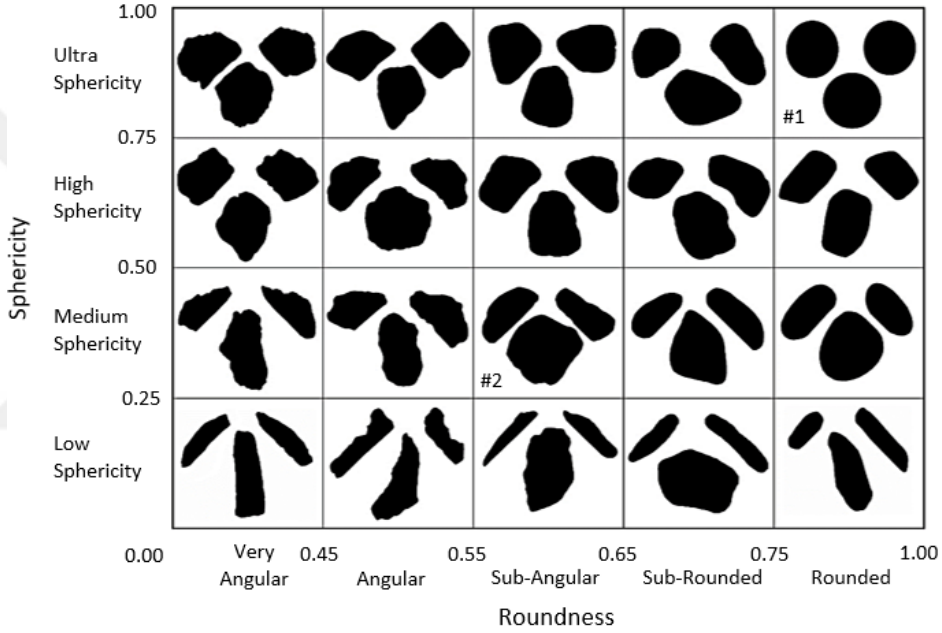



Figure 5.12. Particle shape classification based on 3D roundness and sphericity.

## 5.3. Image-Based Particle Size Distribution

Gradation and size distribution are key factors affecting the mechanical behavior of granular materials. As a conventional method, sieve analysis is known as the most common technique to determine size distribution. In this method, the size identification is based on the percent of passing particles from different sizes of sieves' openings. Square-meshed sieves are used in soil mechanics and many other sectors for particle size analysis. The sieves are classified based on their opening sides which is the length of a square. Figure 5.13 shows a schematic of sieve openings in various conditions in which a particle passes through the sieve opening. Sample 1 represents a particle

with a medium-sphere shape. In the parallel direction, the size of particle is larger than the sieve opening size and it remains on the sieve. In a diagonal position, the same particle passes through the sieve opening, because the diagonal of a square is longer than its side. By 90 degrees rotating the particle, it passes again. Sample 2 illustrates an elongated particle with low sphericity. Unlike sample-1, this particle does not pass the sieve even in a diagonal direction, but similar to sample-1, passes the sieve by 90 degrees rotation. Hence, conventional sieving methods in some cases may not reflect the real particle size, particularly in the case of the particles having very flat or elongated shapes.

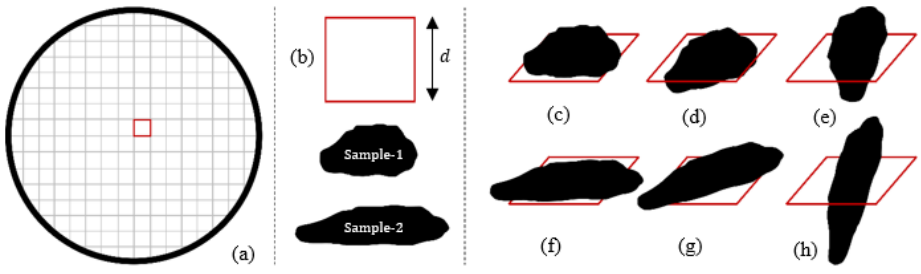



Figure 5.13. Schematic of particles passing sieve opening. (a) top view of a sieve mesh, (b) sieve opening, (c) Sample-1 in parallel direction remains on the sieve, (d) Sample-1 in diagonal direction passes the sieve, (e) Sample-1 in rotated direction passes the sieve, (f) Sample-2 in parallel direction remains on sieve, (g) Sample-2 in diagonal direction remains on the sieve, (h) Sample-2 in rotated direction passes the sieve. d is sieve opening size.

A method based on the developed 3D imaging setup shows a good agreement with the results obtained from the conventional sieve analysis. As mentioned before, the minimum Frets's diameter ($dF_{min}$) represents the smallest diameter of a particle outline. In this method, the particle size is defined as the largest $dF_{min}$ of a particle among three 2D images obtained from the developed setup. Similar to the sieving concept, the determined particle size is compared with any desired size, $S_i$ (opening size in sieve analysis). Figure 5.14 shows the steps for the recognition of particle size based on the suggested method.

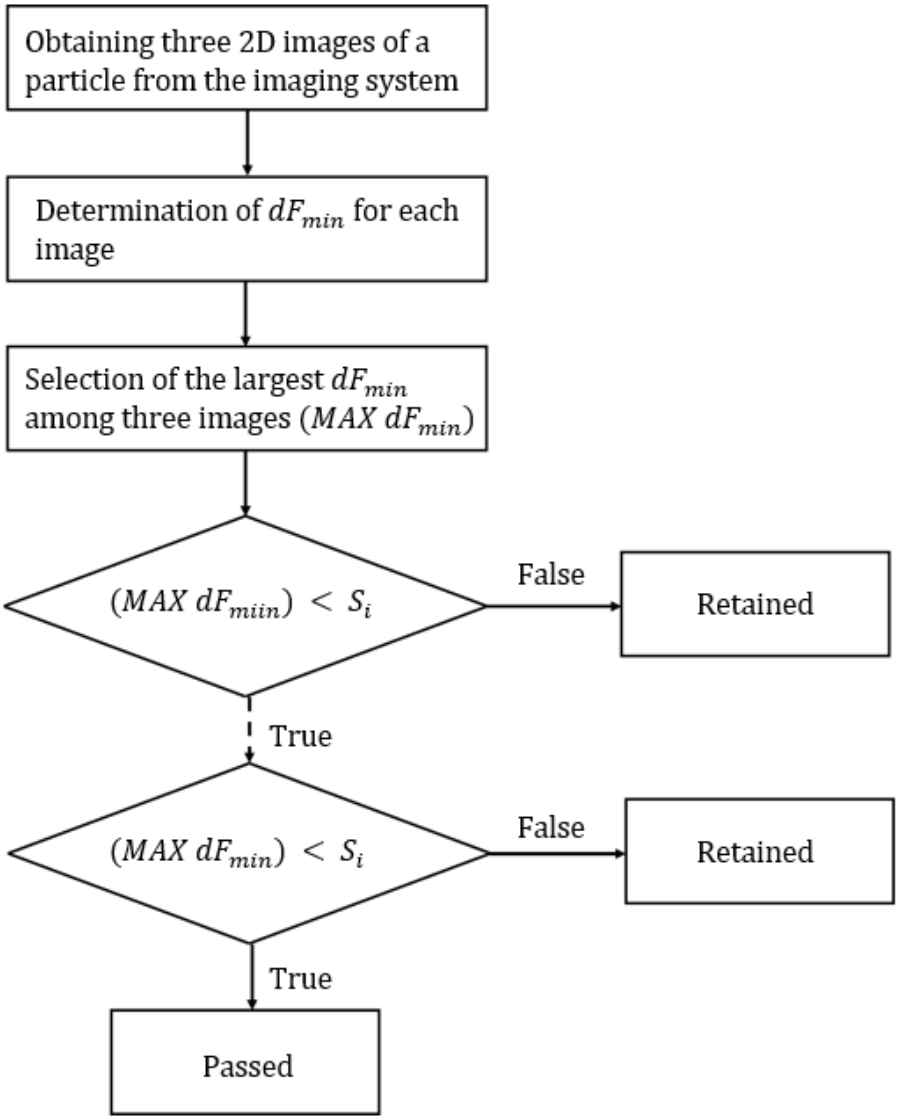



Figure 5.14. Flowchart for determination of particle size based on digital images.

Following the process showed in Figure 40, there number of retained particles for each corresponded sieve size is determined. Considering the number of all explored particles, similar to sieve analysis, the relevant percentages of passing particles were obtained. Figure 5.15 shows particle size distribution of Sand B according to conational sieve analysis, and two image-based size evaluation methods based on 8 and 32 sieves.

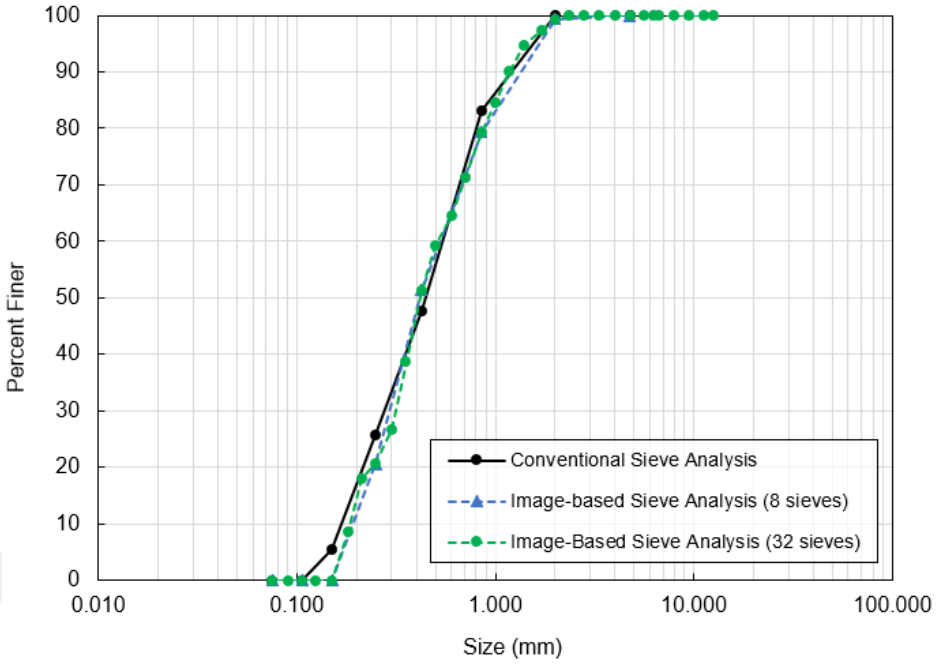



Figure 5.15. Particle size distribution of Sand B based on sieve analysis and digital imaging.

For image-based sieving, 150 particles were selected randomly. Then their determined 3D shape values were used to draw particle size distribution curves. It was observed that the image-based curves are similar to the one obtained from conventional saving method with an approximate offset of 0.15 mm. This technique can be considered a non-destructive method for size analysis of sensitive granular materials in some sectors like pharmacology. In addition, the number of size ranges can be modified to any size from 0.075 to 4.75 mm.

## 5.4. Laboratory Tests

### 5.4.1. Results of One-Dimensional Oedometer Tests

To investigate the particle shape parameters on compressibility of granular materials, a series of one-dimensional oedometer tests following ASTM D2435-04 [121] were conducted for the studied materials. Figure 5.16 shows changes of void ratio by time for the investigated materials.

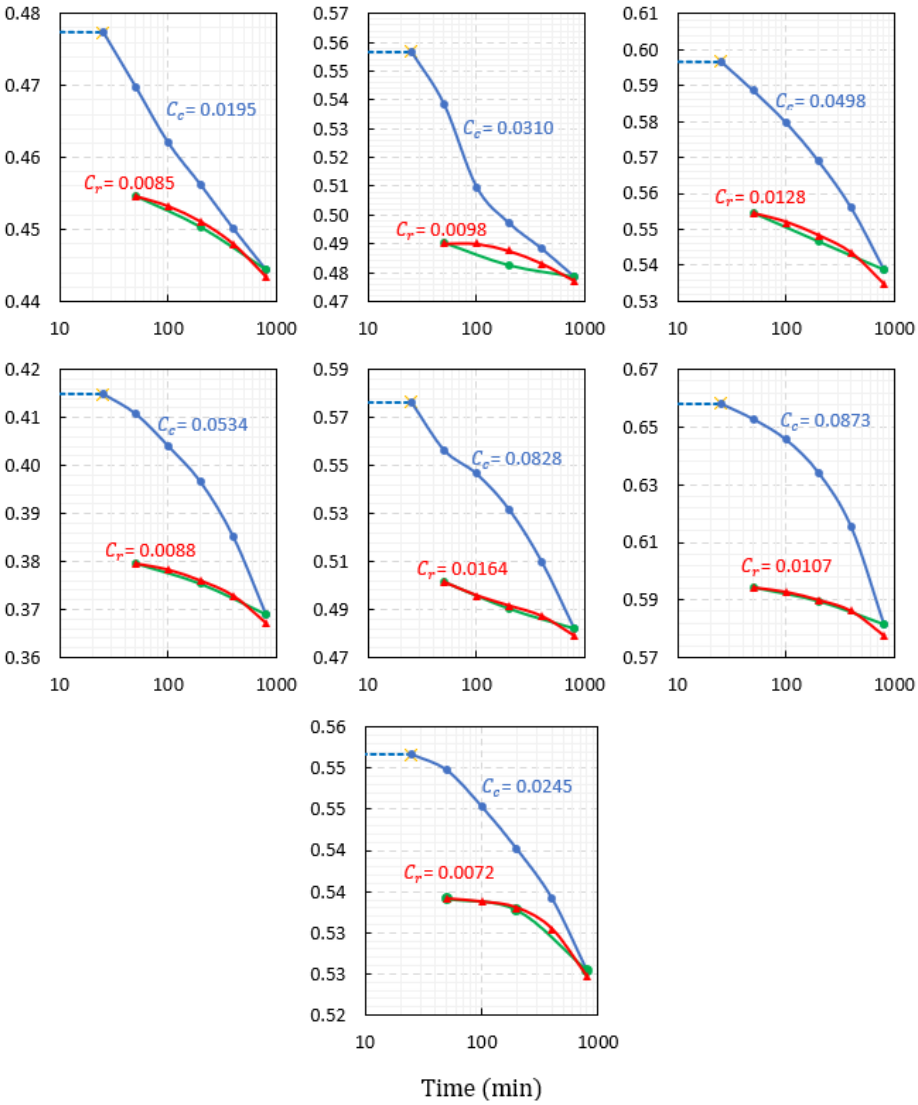



Figure 5.16. Particle size distribution of Sand B based on sieve analysis and digital imaging Time-$e$ relationship for one-dimensional oedometer tests.

The samples were prepared at relative densities ranging from 66 to 77 percent. As shown in Figure 5.17 shows that compression index (Cc) decreases by increasing sphericity. This means that samples with spherical particle shapes have low tendency to compression. In the case of the other shape descriptors, no meaningful relation was observed.

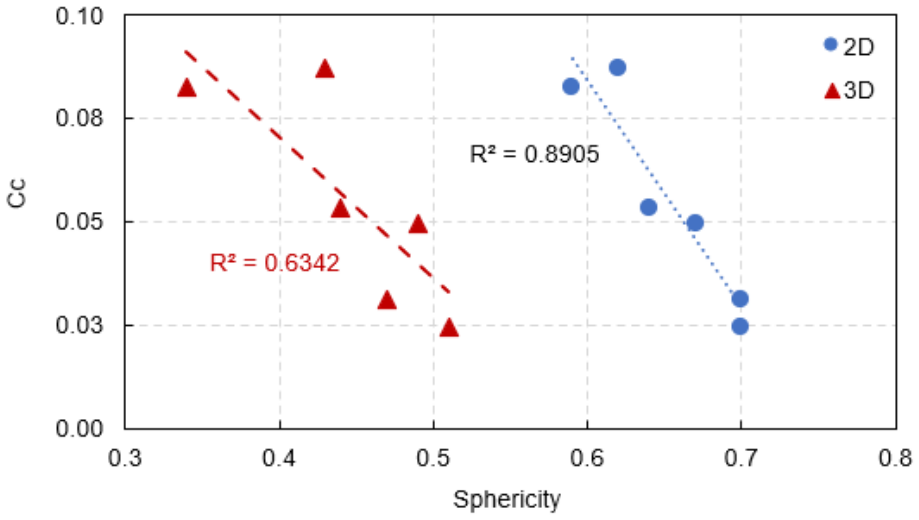



Figure 5.17. Relation between sphericity and compression index.

### 5.4.2. Results of CD Triaxial Tests

The results of CD triaxial tests on seven investigated materials are presented in Table 5.3. It includes stress-strain and volumetric parameters consisting of mean effective and derivative stresses, peak and critical state friction angles, rate of dilation, peak dilation angle, and corresponding axial strains for points of failure and peak dilation angle.

Table 5.3. Data sources.

| Material | Stress Type | $\sigma'_c$ (kPa) | $I_d$ (%) | $p'_p$ (kPa) | $q'_p$ (kPa) | $\phi'_p$ (deg) | $\phi'_{cr}$ (deg) | $\psi'_p$ (deg) | $\varepsilon_{a-p}$ (%) | $\varepsilon_{a-\psi}$ (%) |
|---|---|---|---|---|---|---|---|---|---|---|
| GB | AC-ISO | 100 | 48.34 | 188 | 265 | 34.70 | 22.04 | 16.00 | 1.61 | 2.15 |
| | | 100 | 49.53 | 186 | 259 | 34.29 | 22.94 | 14.41 | 2.00 | 0.02 |
| | | 200 | 28.24 | 331 | 393 | 29.70 | 22.57 | 10.14 | 1.37 | 0.30 |
| | | 200 | 39.84 | 352 | 455 | 32.14 | 21.24 | 12.50 | 1.91 | 2.70 |
| | | 300 | 29.06 | 488 | 562 | 28.96 | 27.83 | 10.89 | 2.03 | 1.61 |
| | | 300 | 36.63 | 528 | 682 | 32.16 | 20.64 | 13.70 | 1.26 | 0.73 |
| Sand A | AC-ISO | 100 | 25.03 | 203 | 309 | 37.35 | 30.28 | 8.41 | 2.89 | 3.34 |
| | | 100 | 41.49 | 208 | 323 | 38.17 | 28.83 | 8.53 | 3.39 | 4.25 |
| | | 100 | 56.79 | 233 | 399 | 41.82 | 33.04 | 15.74 | 3.73 | 4.48 |

Table 5.3 Data sources. (cont.)

| Material | Stress Type | $\sigma'_c$ (kPa) | $I_d$ (%) | $p'_p$ (kPa) | $q'_p$ (kPa) | $\phi'_p$ (deg) | $\phi'_{cr}$ (deg) | $\psi'_p$ (deg) | $\varepsilon_{a-p}$ (%) | $\varepsilon_{a-\psi}$ (%) |
|---|---|---|---|---|---|---|---|---|---|---|
| | | 100 | 87.40 | 262 | 481 | 44.83 | 37.21 | 18.80 | 3.94 | 3.24 |
| | | 200 | 27.71 | 378 | 533 | 34.84 | 27.44 | 6.67 | 4.52 | 4.95 |
| | | 200 | 48.79 | 422 | 667 | 38.68 | 30.45 | 10.19 | 4.39 | 4.16 |
| | | 200 | 83.91 | 478 | 833 | 42.51 | 31.98 | 16.69 | 3.46 | 4.17 |
| | | 300 | 40.14 | 576 | 827 | 35.42 | 26.07 | 8.25 | 4.38 | 5.19 |
| | | 300 | 56.34 | 699 | 1196 | 41.76 | 31.74 | 16.71 | 3.96 | 4.85 |
| | | 300 | 82.60 | 644 | 1032 | 39.21 | 31.78 | 15.14 | 3.34 | 4.09 |
| Sand B | AC-ISO | 100 | 39.52 | 196 | 288 | 36.20 | 30.81 | 5.89 | 6.07 | 5.81 |
| | | 100 | 46.54 | 188 | 263 | 34.64 | 30.23 | 3.30 | 7.50 | 7.16 |
| | | 100 | 66.96 | 230 | 391 | 41.44 | 33.02 | 12.24 | 6.56 | 8.79 |
| | | 100 | 86.05 | 222 | 366 | 40.26 | 32.25 | 11.64 | 4.42 | 5.15 |
| | | 200 | 29.80 | 369 | 506 | 33.95 | 28.14 | 1.40 | 11.19 | 10.46 |
| | | 200 | 54.33 | 389 | 566 | 35.89 | 34.93 | 4.54 | 7.18 | 6.03 |
| | | 200 | 62.71 | 452 | 754 | 40.83 | 30.65 | 10.88 | 5.41 | 6.27 |
| | | 300 | 39.47 | 554 | 763 | 34.12 | 29.58 | 1.20 | 9.94 | 10.01 |
| | | 300 | 75.41 | 617 | 950 | 37.80 | 29.69 | 7.29 | 6.64 | 7.44 |
| | | 300 | 81.88 | 619 | 957 | 38.00 | 33.75 | 6.47 | 7.23 | 8.11 |
| Sand C | AC-ISO | 100 | 28 | 209 | 328 | 38.40 | 30.11 | 4.47 | 9.71 | 10.37 |
| | | 100 | 36 | 211 | 334 | 38.70 | 32.13 | 5.65 | 9.33 | 9.77 |
| | | 100 | 85 | 264 | 493 | 45.33 | 32.89 | 19.82 | 5.14 | 6.33 |
| | | 200 | 23 | 398 | 593 | 36.67 | 34.32 | 2.06 | 12.32 | 14.46 |
| | | 200 | 69 | 447 | 740 | 40.49 | 36.63 | 5.62 | 10.06 | 9.82 |
| | | 300 | 58 | 617 | 951 | 37.84 | 34.69 | 2.33 | 5.10 | 14.78 |
| | | 300 | 90 | 729 | 1286 | 43.00 | 42.33 | 11.04 | 8.34 | 10.28 |
| Sand D | AC-ISO | 100 | 37.94 | 221 | 362 | 40.17 | 39.26 | 2.01 | 12.63 | 14.95 |
| | | 100 | 38.03 | 223 | 368 | 40.38 | 37.06 | 1.40 | 17.18 | 19.38 |
| | | 100 | 56.87 | 233 | 400 | 41.81 | 39.47 | 3.17 | 12.12 | 15.47 |
| | | 200 | 80.68 | 494 | 881 | 43.44 | 39.18 | 5.57 | 10.89 | 14.36 |
| | | 200 | 40.35 | 414 | 641 | 38.03 | 37.98 | 0.00 | 15.83 | 16.98 |
| | | 200 | 55.40 | 439 | 716 | 39.92 | 35.98 | 1.52 | 14.82 | 19.55 |
| | | 300 | 82.44 | 702 | 1205 | 41.90 | 36.86 | 3.83 | 11.83 | 14.73 |
| | | 300 | 60.04 | 627 | 980 | 38.34 | 37.46 | 0.09 | 14.14 | 18.24 |
| | | 300 | 43.25 | 605 | 916 | 37.18 | 37.17 | 0.00 | 18.32 | 20.04 |

Table 5.3 Data sources. (cont.)

| Material | Stress Type | $\sigma'_c$ (kPa) | $I_d$ (%) | $p'_p$ (kPa) | $q'_p$ (kPa) | $\phi'_p$ (deg) | $\phi'_{cr}$ (deg) | $\psi'_p$ (deg) | $\varepsilon_{a-p}$ (%) | $\varepsilon_{a-\psi}$ (%) |
|---|---|---|---|---|---|---|---|---|---|---|
| Sand E | AC-ISO | 100 | 29.46 | 192 | 277 | 35.50 | 35.35 | 0.00 | 9.63 | 8.41 |
| | | 100 | 41.03 | 198 | 293 | 36.49 | 32.50 | 0.77 | 11.03 | 20.14 |
| | | 100 | 85.70 | 229 | 387 | 41.36 | 36.12 | 7.28 | 5.50 | 10.27 |
| | | 200 | 48.27 | 374 | 522 | 34.51 | 34.49 | 0.00 | 11.06 | 10.36 |
| | | 200 | 72.33 | 387 | 562 | 35.76 | 35.76 | 0.00 | 10.36 | 13.05 |
| | | 200 | 78.98 | 403 | 609 | 37.13 | 34.76 | 0.54 | 12.49 | 15.31 |
| | | 300 | 85.32 | 570 | 814 | 35.16 | 34.03 | 0.00 | 14.11 | 19.78 |
| Sand F | AC-ISO | 100 | 24.90 | 199 | 297 | 36.68 | 33.90 | 7.19 | 4.18 | 3.18 |
| | | 100 | 60.96 | 207 | 322 | 38.06 | 34.18 | 8.39 | 4.48 | 4.48 |
| | | 100 | 82.60 | 226 | 377 | 40.86 | 30.79 | 13.13 | 4.63 | 4.29 |
| | | 100 | 83.82 | 234 | 401 | 41.82 | 37.74 | 14.44 | 2.91 | 2.94 |
| | | 200 | 83.33 | 425 | 676 | 38.90 | 34.23 | 10.08 | 3.21 | 3.36 |
| | | 300 | 88.25 | 613 | 939 | 37.61 | 37.41 | 6.98 | 5.76 | 5.80 |

The relationship between mean effective stress ($p'$) versus deviator stress ($q'$), axial strain ($\varepsilon_1$) versus deviator stress ($q'$), axial strain ($\varepsilon_1$) versus volumetric strain ($\varepsilon_v$), and axial strain ($\varepsilon_1$) versus the rate of dilation ($d\varepsilon_v/d\varepsilon_1$ ) are plotted using the data obtained from the shear phase of the tests. According to Schanz, T., Vermeer, P.A. [122], peak dilatancy angles were determined based on the maximum rate of dilation

$$\psi_p = sin^{-1}\left(-\frac{\left(\frac{d\varepsilon_v}{d\varepsilon_1}\right)_p}{2-\left(\frac{d\varepsilon_e}{d\varepsilon_1}\right)_p}\right). \tag{5.5}$$

According to the results obtained from shear phase, it is understood that for a constant consolidation pressure, the relative density of specimen affects engineering properties of the studied materials. For instance, the mechanical behavior of loose, medium, and dense samples of Sand A under constant consolidation pressure ($\sigma'_c$) of 100 kPa is plotted in Figure 5.18 shows the effect of relative density ($I_d$) on mean effective stress ($p'$), deviator stress ($q'$), volumetric strain ($\varepsilon_v$), and rate of dilation ($d\varepsilon_v/d\varepsilon_1$). For the same confining pressure, the peak friction angle ($\phi'_p$) for the loose, medium, and dense samples are $37.35^o$, $41.82^o$, and $44.83^o$ respectively. Similarly, in the case of critical stat friction angle ($\phi'_{cr}$), these values are $30.28^o$, $33.04^o$, and $37.21^o$.

This means that denser samples have larger shear strength parameters which causes sample failure at higher shear stresses.

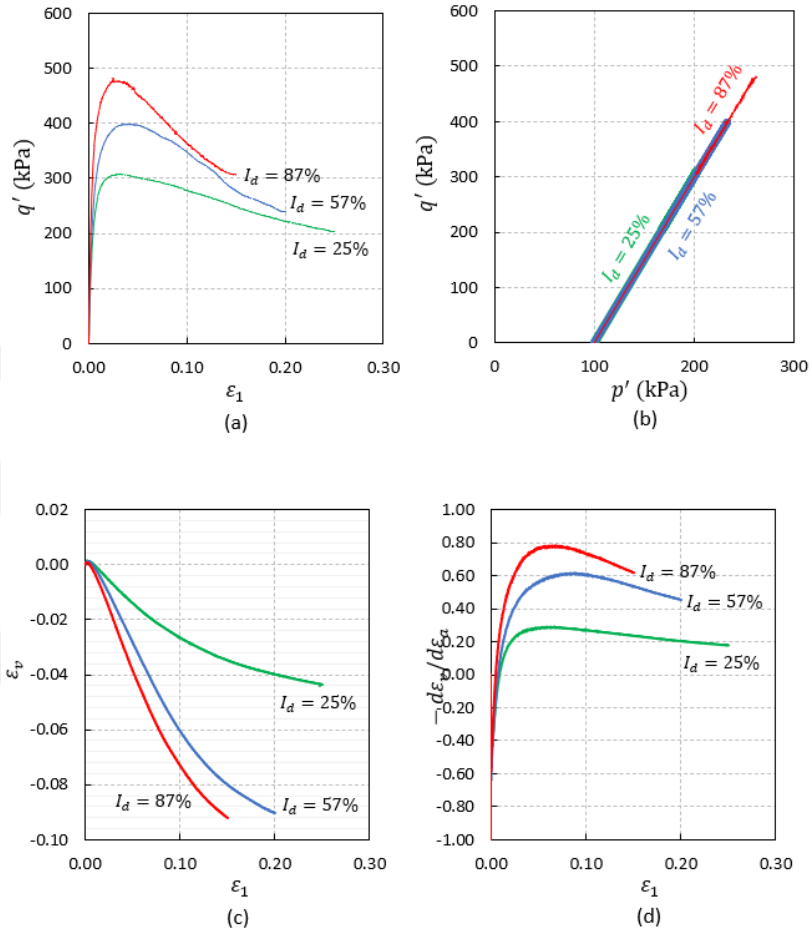



Figure 5.18. Effect of relative density on stress-strain and volumetric behavior of Sand A under consolidation pressure of 100 kPa. (a) $q'$- $\varepsilon_1$, (b) $p'$- $q'$, (c) $\varepsilon_1$- $\varepsilon_v$, (d) rate of axial strain to volumetric relationship.

For an identical confining pressure, $p'$- $q'$ relationship shows that except for the maximum values which are dependent on the relative densities ($I_d$) of samples, the stress paths for sample with various densities match each other. In the case of volume change during the shear phase, at the very beginning samples tend to compress slightly, and then by mobilization of grains, a remarkable volume expansion of the specimens is obvious. It should be mentioned that positive signs are defined for volumetric compression. Denser samples are exposed to a larger volumetric strain ($\varepsilon_v$), the corresponding $\varepsilon_v$ at 10 percent of axial strain for the mentioned loose, medium, and dense

specimens are 2.8, 6.00, and 7.2 percent. $\varepsilon_1$ - $(d\varepsilon_v/d\varepsilon_1)$ relationship shows the rate of dilation based on axial strain. From loose to dense relative densities, the samples with a higher rate of dilation have the peak dilation angles $(\psi_p)$ of $8.41^o$, $15.74^o$, and $18.80^o$ respectively.

Furthermore, the effect of different consolidation pressures $(\sigma_c')$ on the samples having similar relative densities investigated. In Figure 5.19, the shear phase results of the samples of Sand B with medium relative densities under three different $\sigma_c'$ of 100, 200, and 300 kPa are plotted. It can be derived from $\varepsilon_1$- $q'$ relationship that higher $\sigma_c'$ results in a larger shear strength. $p'$- $q'$ relationship shows the same direction of the stress path with offsets of start points equal to the difference among applied consolidation pressures.

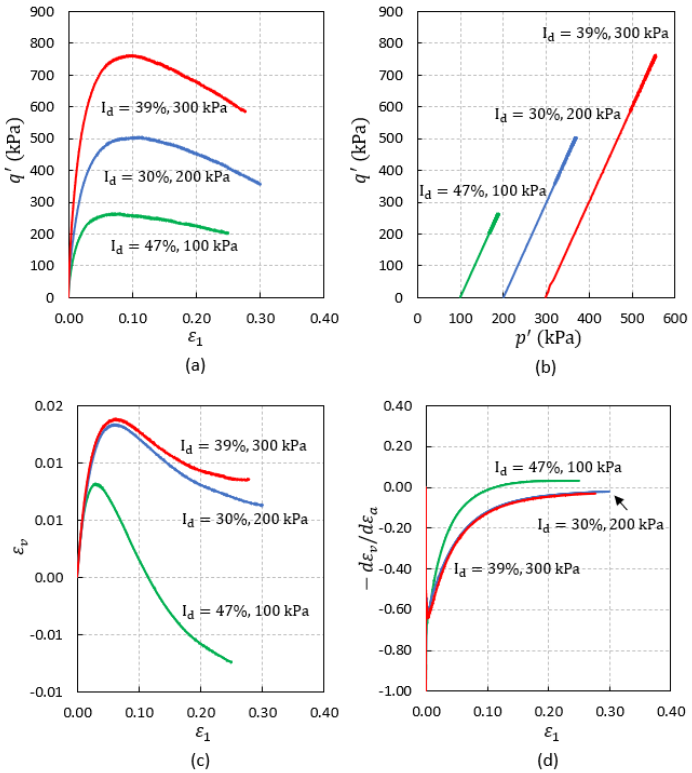



Figure 5.19. Effect of consolidation pressure on stress-strain and volumetric behavior of loose-medium samples of Sand B. (a) $q'$- $\varepsilon_1$, (b) $p'$- $q'$, (c) $\varepsilon_1$- $\varepsilon_v$, (d) rate of axial strain to volumetric relationship.

According to the results of triaxial CD tests on the studied materials, the peak effective dilation angle ($\psi'_p$) increases by increasing of the peak effective friction angle ($\phi'_p$). In addition, as it is shown in Figure 5.2, the materials with higher values of roundness and sphericity dilate at lower $\phi'_p$. For instance, For GB which have the maximum value of 1.00 for shape descriptors, the $\phi'_p$-$\psi'_p$ relation is in the lowest band while it is located the highest band for Sand D having the smallest roundness, sphericity, and aspect ratio compared with the other materials.

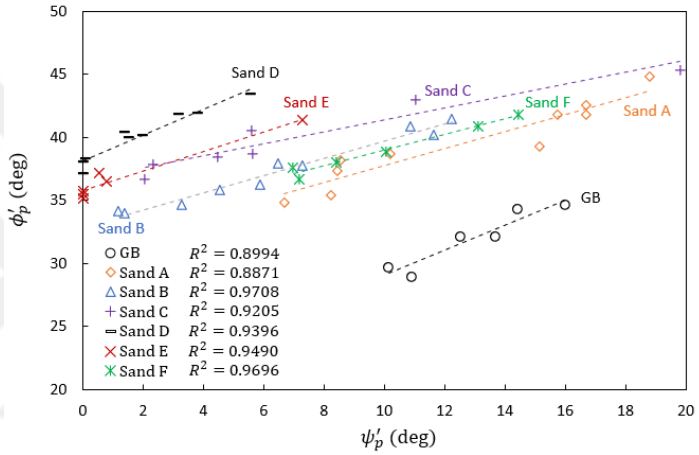



Figure 5.20. $\phi'_p$ - $\psi'_p$ relationship for CD triaxial tests.

Figure 5.21 shows the relation between sphericity and peak friction angle of the studied sand materials. It shows that more sphere materials have smaller peak friction angle and consequently lower shear strength. Comparing 2D and 3D cases reveals that the changes rate is higher for 2D analysis.

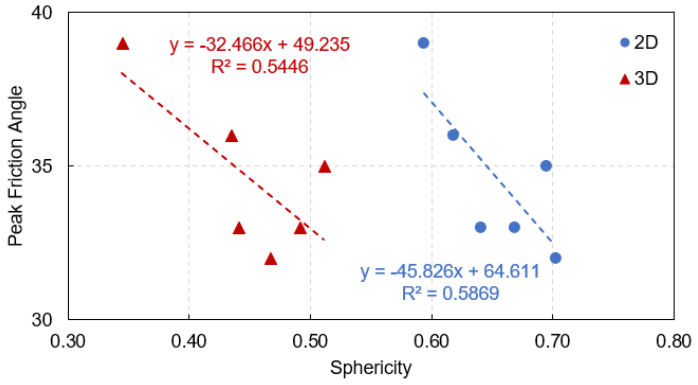



Figure 5.21. Relation between sphericity and peak friction angle for the six samples.

Figure 5.22 shows relation between sphericity and critical state friction angle. Similar to the case of peak friction angle, critical stated friction angle reduces by increasing sphericity. Again, 2D analysis gives higher rate of change for S- $\Phi'_{cr}$ relationship.

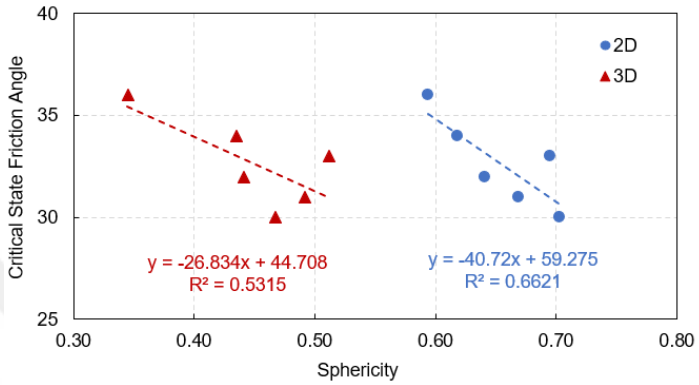



Figure 5.22. Relation between sphericity and critical state friction angle for the sand samples.

# 6. CONCLUSION

Particle shape effect on mechanical behavior of cohesionless soil are emphasized by several researchers; however, most of them are based on 2D evaluation or experimental laboratory tests with no distinct idea about realistic shape parameters. This research aims to investigate the 3D shape parameters of granular materials based on three 2D projected particle images on three orthogonal surfaces. The system consists of a digital camera with a mounted macro lens, an extension tube, and the developed imaging platform with two installed aluminum-coated mirrors. In addition, four 3D shape descriptors were proposed for the developed imaging setup. These indicators are roundness, sphericity, aspect ratio, and convexity which gives a comprehensive and clear idea about intermediate-scale and large-scale shape parameters of the investigated materials. Seven different granular materials were analyzed in 2D and 3D. Particle selection for each sample material was performed considering the size gradation according to USCS. A total number of 860 particles involving 2,580 projected grain faces resulted in 6,880 calculated shape descriptors in 2D and 3D. For the determination of shape descriptors 15,480 shape parameters were measured. The final shape indicators were obtained by calculating weighted average values from particle size ranges for each material. The study was involved of three main sections consisting of developing a cost-effective and practical 3D imaging setup, proposing new 3D shape descriptors based on the developed setup, and investigating particle shape effect on the mechanical behavior of the studied materials. The study is concluded by presenting the following results:

The developed 3D imaging setup was able to successfully characterize a particle shape in three morphological scales of small, medium, and large sizes represented by roundness, sphericity and aspect ratio (form), and convexity. The theoretical maximum value of proposed shape descriptors is 1.00 representing the most regular, rounded, and sphere grain shape. Glass beads were identified as the most regularly shaped particle while Sand D (crushed sand) has the most irregular particle shape. As large-scale

shape descriptors, there is a meaningful between sphericity and aspect ratio while no remarkable link was observed among the other pair combinations of the determined indicators.

The determined shape indicators for the seven studied materials show a meaningful relation between 2D and 3D analysis. Accordingly, equations relating 2D and 3D shape parameters were proposed. However, these may be used cautiously just for an approximate estimation. Defining reliable relations must be done investigation a large number of samples with different size and shape parameters.

Compared with 2D, 3D shape analysis results in lower sphericity and aspect ratio while slightly higher values for roundness. Both analyses give almost the same values of convexity ranging from 0.95 to 1.00.

A particle shape classification chart was introduced based on the 3D sphericity and roundness. Compared with the related 2D classifications in literature, this is a more reliable approach considering the various sides of a particle.

# 7. FUTURE WORKS

The results show that the developed 3D imaging system and the corresponding proposed shape descriptors can properly characterize a particle shape. The most time-consuming step was analyzing the obtained 2D images captured by the digital camera. This briefly was including creation of binary images, measurement of various shape parameters from the binary images, and finally calculating the shape descriptors. In the measurement, to evaluate some parameters such as $MAXd_{Fmax}$, $MINd_{Fmin}$, $MAXr_{cir}$, and $MINr_{ins}$, it was also required to make a comparison among the values obtained from the three faces of a particle. Developing a computer code automate this process from making binary images to calculation of shape descriptors can reduce the analyze time significantly and make the system even more quick and practical. Furthermore, it will make it possible to analyze larger numbers of particles for each sample quickly and minimize the tolerance of errors for the calculated shape indicators.

Studying glass beads and six sand samples showed the important role of particle shape parameters on their mechanical properties like friction angles and stress-dilatancy behavior. However, because of the limited number of the studied samples, there are remarkable data gaps among the evaluated values, especially between the data of sand samples and glass beads. So, analyzing a larger number of different samples can cover the mentioned data gaps and better evaluation particle shape effect on mechanical properties.

In the proposed method for particle size distribution based on the developed 3D imaging setup, selection of particles and their randomization is a crucial factor that should be considered. Developing a proper technique for particle selection is a must for applicability of the proposed method.

# REFERENCES


1. Seed, H.B., R.J. Woodward Jr and R. Lundgren, "Clay Mineralogical Aspects of the Atterberg Limits", *Journal of the Soil Mechanics and Foundations Division*, Vol. 90, No. 4, pp. 107-131, 1964.

2. Beroya, M.A.A., A. Aydin and R. Katzenbach, "Insight into the Effects of Clay Mineralogy on the Cyclic Behavior of Silt-Clay Mixtures", *Engineering Geology*, Vol. 106, No. 3-4, pp. 154-162, 2009.

3. Geremew, A.M. and E.K Yanful, "Dynamic Properties and Influence of Clay Mineralogy Types on the Cyclic Strength of Mine Tailings", *International Journal of Geomechanics*, Vol. 13, No. 4, pp. 441-453, 2013.

4. Lupogo, K., "Effect of Fines Mineralogy on the Oedometric Compressional Behavior of Sandy Soils", *Journal of Civil Engineering and Construction Technology*, Vol. 4, No. 7, pp. 232-238, 2013.

5. Khosrowshahi, S., A. Şenol and H. Yıldırım, "Improvement of Expansive Soils Using Fiber Materials", *In the 11th International Congress on Advances in Civil Engineering*, Istanbul, Turkey, 2014.

6. Tiwari, B., M. Principe and M. Biabani, "Influence of Activity and Mineralogy in Compaction and Shear Strength Characteristics of Clays", *In Geo-Congress 2014: Geo-characterization and Modeling for Sustainability*, Vol. 1, No. 1, pp. 1357-1366, 2014.

7. Mehta, B. and A. Sachan, "Effect of Mineralogical Properties of Expansive Soil on its Mechanical Behavior", *Geotechnical and Geological Engineering*, Vol. 35, No. 6, pp. 2923-2934, 2017.

8. Akgün, H.A.G., A.A. Türkmenoğlu, K. Kelam, Yousefi-Bavil, G. Öner and M. K.

Koçkar, "Assessment of the Effect of Mineralogy on the Geotechnical Parameters of Clayey Soils", *A Case Study for the Orta County*, Vol. 164, No. 1, pp. 44-53, 2018.

9. Chittoori, B. C., A.J. Puppala and A. Pedarla, "Addressing Clay Mineralogy Effects on Performance of Chemically Stabilized Expansive Soils Subjected to Seasonal Wetting and Drying", *Journal of Geotechnical and Geoenvironmental Engineering*, Vol. 144, No. 1, pp. 04017097-04017120. 2018.

10. Osipov, V., "Structural Bonds and the Properties of Clays", *Bulletin of Engineering Geology and the Environment*, Vol. 12, No. 1, 1975.

11. Holubec, I. and E. D'appolonia, Effect of Particle Shape on the Engineering Properties of Granular Soils, ASTM STP, Vol. 523, No. 1, pp. 304-318, 1973.

12. Mair, K., K. M. Frye and C. Marone, "Influence of Grain Characteristics on the Friction of Granular Shear Zones", *Journal of Geophysical Research, Solid Earth*, Vol. 107, pp. 10, pp. ECV-4- ECV-10, 2002.

13. Yasin, S.J.M. and A.M.M. Safiullah, "Effect of Particle Characteristics on the Strength and Volume Change Behaviour of Sand", *Journal Civil Engineering 3*, Vol. 3, No. 2, pp. 127-148, 2003.

14. Cho, G.C., J. Dodds and J.C. Santamarina, "Closure to "Particle Shape Effects on Packing Density", Stiffness and Strength: Natural and Crushed Sands" By Gye-Chun Cho, Jake Dodds and J. Carlos Santamarina, *Journal of Geotechnical and Geoenvironmental Engineering*, Vol. 133, No. 11, pp. 1474-1474, 2007.

15. Peña Olarte, A. A., "Influence of Particle Shape on the Global Mechanical Response of Granular Packings", *Micromechanical Investigation of the Critical State in Soil Mechanics, Mitteilung Des Instituts Für Geotechnik*, Vol.1, No. 1, pp. 79, 2008.

16. Tsomokos, A. and V.N. Georgiannou, "Effect of Grain Shape and Angularity on the Undrained Response of Fine Sands", *Canadian Geotechnical Journal*, Vol. 47, No. 5, pp. 539-551, 2010.

17. Lim, M. S., D. C. Wijeyesekera, A. Zainorabidin and I. Bakar, "The Effects of Particle Morphology (Shape and Sizes) Characteristics on its Engineering Behaviour and Sustainable Engineering Performance of Sand", *International Journal of Integrated Engineering*, Vol. 4, No. 4, pp. 120-140, 2012.

18. Li, Y., "Effects of Particle Shape and Size Distribution on the Shear Strength Behavior of Composite Soils Bulletin of Engineering", *Geology and the Environment*, Vol. 72, No. 3, pp. 371-381, 2013.

19. Rodriguez, J., *Importance of the Particle Shape on Mechanical Properties of Soil Materials*, Ph.D. Thesis, Luleå Tekniska Universitet, 2013.

20. Yang, J. and X. D. Luo, "Exploring the Relationship Between Critical State and Particle Shape for Granular Materials", *Journal of the Mechanics and Physics of Solids*, Vol. 84, No. 1, pp. 196-213, 2015.

21. Altuhafi, F.N., M.R. Coop and V.N. Georgiannou, "Effect of Particle Shape on the Mechanical Behavior of Natural Sands", *Journal of Geotechnical and Geoenvironmental Engineering*, Vol. 142, No. 12, pp. 04016071-0401690, 2016.

22. Payan, M., A. Khoshghalb, K. Senetakis and N. Khalili, "Effect of particle shape and validity of Gmax models for sand", *A critical review and a new expression, Computers and Geotechnics*, Vol. 72, No. 1, pp. 28-41, 2016.

23. Dai, B.B., J. Yang and C.Y. Zhou, "Observed Effects of Interparticle Friction and Particle Size on Shear Behavior of Granular Materials", *International Journal of Geomechanics*, Vol. 16, No. 1, pp. 04015011-04015025, 2016.

24. Kandasami, R.K. and T.G. Murthy, "Manifestation of Particle Morphology on the

Mechanical Behaviour of Granular Ensembles", *Granular Matter*, Vol. 19, No. 2, pp. 1-13, 2017.

25. Giang, P.H. H., P.O. Van Impe, W.F. Van Impe, P. Menge and W. Haegeman, "Small-Strain Shear Modulus of Calcareous Sand and Its Dependence on Particle Characteristics and Gradation", *Soil Dynamics and Earthquake Engineering*, Vol. 100, No. 1, pp. 371-379, 2017.

26. Mahawish, A., A. Bouazza and W.P. Gates, "Effect of Particle Size Distribution on the Bio-Cementation of Coarse Aggregates", *Acta Geotechnica*, Vol. 13, No. 4, pp. 1019-1025. 2018.

27. Lu, Z., A. Yao, A. Su, X. Ren, Q. Liu and S. Dong, "Re-Recognizing the Impact of Particle Shape on Physical and Mechanical Properties of Sandy Soils, A Numerical Study", *Engineering Geology*, Vol. 253, No. 1, pp. 36-46, 2019.

28. Xiao, Y., M.Q. Meng, A. Daouadjie, Q.S. Chen, Z.J. Wu and X. Jiang, "Effects of Particle Size on Crushing and Deformation Behaviors of Rockfill Materials", *Geosci Front*, Vol. 11, No. 2, pp. 375 -388, 2020.

29. Meng, M., Y. Xiao, X. Duan, Z. Sun, L. Du, H. Fan and H. Liu, "Crushing Strength of Artificial Single-Particle Considering the Effect of Particle Morphology", *Acta Geotechnica*, Vol. 17, No. 9, pp. 3909-3926, 2022.

30. Karimipetanlar, M., U. El Shamy, K.N. Kalfas and N. Makris, "The Influence of Particle Shape on Crushing Pattern and Energy Dissipation Within A Pressurized Sand Damper", *Computers and Geotechnics*, Vol. 166, No. 1, pp. 106020-106035, 2024.

31. Zhao, B., J. Wang and E. ò,G. Viggiani and M.R. Coop, "Investigation of Particle Breakage Under One-Dimensional Compression of Sand Using X-Ray Microtomography", *Canadian Geotechnical Journal*, Vol. 57, No. 5, PP. 754-762, 2020.

32. Cubrinovski, M. and K. Ishihara, "Maximum and Minimum Void Ratio Characteristics of Sands", *Soils and Foundations*, Vol. 42, No. 6, pp. 65-78, 2002.

33. Rousé, P.C., R.J. Fannin and D. A. Shuttle, "Influence of Roundness on the Void Ratio and Strength of Uniform Sand", *Géotechnique*, Vol. 58, No. 3, pp. 227-231, 2008.

34. Abbireddy, C.O.R. and C.R.I. Clayton, "The Impact of Particle Form on the Packing and Shear Behaviour of Some Granular Materials, An Experimental Study", Granular Matter, Vol. 17, No. 4, pp. 427-438, 2015.

35. Pino, L.F.M. and B.A. Baudet, "The Effect of The Particle Size Distribution on the Mechanics of Fibre-Reinforced Sands Under One-Dimensional Compression", *Geotextiles and Geomembranes*, Vol. 43, No. 3, pp. 250-258, 2015.

36. Suh, H.S., K.Y. Kim, J. Lee and T.S. Yun, "Quantification of Bulk Form and Angularity of Particle with Correlation of Shear Strength and Packing Density in Sands", *Engineering Geology*, Vol. 220, No. 1, pp. 256-265, 2017.

37. Frossard, E., "Effect of Sand Grain Shape on Interparticle Friction, Indirect Measurements by Rowe's Stress Dilatancy Theory", *Géotechnique*, Vol. 29, No. 3, pp. 341-350, 1979.

38. Shinohara, K., M. Oida and B. Golman, "Effect of Particle Shape on Angle of Internal Friction by Triaxial Compression Test", *Powder Technology*, Vol. 107, No. 1-2, pp. 131-136, 2000.

39. Alshibli, K.A. and M.B. Cil, "Influence of Particle Morphology on the Friction and Dilatancy of Sand", *Geoenviron Engineering*, Vol. 144, No. 3, pp. 04017118-04017128, 2018.

40. Yang, J. and X.D. Luo, "The Critical State Friction Angle of Granular Materials", *Does It Depend on Grading, Acta Geotechnica*, Vol. 13, No. 3, pp. 535-547, 2018.

41. Lee, C., H.S. Suh, B. Yoon and T.S. Yun, "Particle Shape Effect on Thermal Conductivity and Shear Wave Velocity in Sands", *Acta Geotechnica*, Vol. 12, No. 3, pp. 615-625, 2017.

42. Cabalar, A.F. and N. Akbulut, "Effects of the Particle Shape and Size of Sands on the Hydraulic Conductivity", *Acta Geotechnica Slovenica*, Vol. 13, No. 2, pp. 83-93, 2016.

43. Zieba, Z., "Influence of Soil Particle Shape on Saturated Hydraulic Conductivity", *Journal of Hydrology and Hydromechanics*, Vol. 65, No. 1, pp. 80, 2017.

44. Nguyen, T.T. and B. Indraratna, "The Role of Particle Shape on Hydraulic Conductivity of Granular Soils Captured Through Kozeny -Carman Approach", *Géotechnique Letters*, Vol. 10, No. 3, pp. 398-40, 2020.

45. Zheng, W., X. Hu, D.D. Tannant and B. Zhou, "Quantifying the Influence of Grain Morphology on Sand Hydraulic Conductivity", *A Detailed Pore-Scale Study. Computers and Geotechnics*, Vol. 135, No. 1, pp. 104147, 2021.

46. Rezaei, E., K. Zeinalzadeh and B. Ghanbarian, "Experimental Study of Hydraulic Properties in Grain Packs, Effects of Particle Shape and Size Distribution", *Journal of Contaminant Hydrology*, Vol. 243, No. 1, pp. 103918, 2021.

47. Sd, A.K.T.G. and A. Sitharam, "Liquefaction and Post Liquefaction Behaviour of Granular Materials, Particle Shape Effect", *Indian Geotechnical Journal*, Vol. 41, No. 4, pp. 186-195, 2011.

48. Wei, L.M. J. and Yang, "On the Role of Grain Shape in Static Liquefaction of Sand -Fines Mixtures", *Géotechnique*, Vol. 64, No. 9, pp. 740-745, 2014.

49. Keramatikerman, M. and A. Chegenizadeh, "Effect of Particle Shape on Monotonic Liquefaction, Natural and Crushed Sand", *Experimental Mechanics*, Vol. 57, No. 8, pp. 1341-1348, 2017.

50. Rui, S., Z. Guo, T. Si and Y. Li, "Effect of Particle Shape on the Liquefaction Resistance of Calcareous Sands", *Soil Dynamics and Earthquake Engineering*, Vol. 137, No. 1, pp. 106302, 2020.

51. Wei, X., J. Yang, Y.G. Zhou and Y. Chen, "Influence of Particle-Size Disparity on Cyclic Liquefaction Resistance of Silty Sands", *Géotechnique Letters*, Vol. 10, No. 2, pp. 155-161, 2020.

52. Cox, M.R.B., *The Influence of Grain Shape on Dilatancy*, The University of Arizona, 2008.

53. Amirpour Harehdasht, S., M. Karray, M. N. Hussien and M. Chekired, "Influence of Particle Size and Gradation on the Stress-Dilatancy Behavior of Granular Materials During Drained Triaxial Compression", *International Journal of Geomechanics*, Vol. 17, No. 9, pp. 04017077-04017095, 2017.

54. Amirpour Harehdasht, S., M. N. Hussien, M. Karray, V. Roubtsova and M. Chekired, "Influence of Particle Size and Gradationon Shear Strength-Dilation Relation of Granular Materials", *Canadian Geotechnical Journal*, Vol. 56, No. 2, pp. 208-227, 2019.

55. Xiao, Y., L. Long, T. Matthew Evans, H. Zhou, H. Liu and A. W. Stuedlein, "Effect of Particle Shape on Stress-Dilatancy Responses of Medium-Dense Sands", *Journal of Geotechnical and Geoenvironmental Engineering*, Vol. 145, No. 2, pp. 04018105-04018125, 2019.

56. Arda, C.O. and Ö. Cinicioglu, "Influence of Grain Shape on Stress-Dilatancy Parameters", *Granular Matter*, Vol. 23, No. 2, pp. 1-19, 2021.

57. Jensen, R.P., T.B. Edil, P.J. Bosscher, M.E. Plesha and N.B. Kahla, "Effect of Particle Shape on Interface Behavior Of DEM-Simulated Granular Materials", *International Journal of Geomechanics*, Vol. 1, No. 1, pp. 1-19, 2001.

58. Latha, G.M. and T.G. Sitharam, "Effect of Particle Size and Gradation on the Behaviour of Granular Materials Simulated Using DEM", *Indian Geotechnical Journal*, Vol. 38, No. 1, pp. 68-88, 2008.

59. Coetzee, C.J., "Calibration of the Discrete Element Method and the Effect of Particle Shape", *Powder Technology*, Vol. 297, No. 1, pp. 50-70, 2016.

60. Mollon, G., A. Quacquarelli, and E.O. and G. Viggiani, "Can Friction Replace Roughness in the Numerical Simulation of Granular Materials", *Granular Matter*, Vol. 22, No. 2, pp. 1-16, 2020.

61. Yin, Z.Y., P. Wang and F. Zhang, "Effect of Particle Shape on the Progressive Failure of Shield Tunnel Face in Granular Soils by Coupled FDM-DEM Method", *Tunnelling and Underground Space Technology*, Vol. 100, No. 1, pp.103394, 2020.

62. Nguyen, H.B.K., M.M. Rahman and A.B. Fourie, "How Particle Shape Affects the Critical State, Triggering of Instability and Dilatancy of Granular Materials-Results from A DEM Study", *Géotechnique*, Vol. 71, No. 9, pp. 749-764, 2021.

63. McDowell, G. and J. de Bono, "Relating Hydraulic Conductivity to Particle Size Using DEM", *International Journal of Geomechanics*, Vol. 21, No. 1, pp. 06020034-06020051, 2021.

64. Holubec, I. and E. D'appolonia, *Effect of Particle Shape on the Engineering Properties of Granular Soils, in Evaluation of Relative Density and Its Role in Geotechnical Projects, Involving Cohesionless Soils*, ASTM International, Canada, 1973.

65. Abbireddy, C.O.R. and C.R.I. Clayton, "The Impact of Particle Form on the Packing and Shear Behaviour of Some Granular Materials, an Experimental Study", *Granular Matter*, Vol. 17, No. 1, pp. 427-438, 2015.

66. Murphy, K.A., A.K. MacKeith, L.K. Roth and H.M. Jaeger, "The Intertwined Roles of Particle Shape and Surface Roughness in Controlling the Shear Strength

of a Granular Material", *Granular Matter*, Vol. 21, No. 3, pp. 72, 2019.

67. Maroof, M.A., A. Mahboubi and A. Noorzad, "Effects of Grain Morphology on Suffusion Susceptibility of Cohesionless Soils", *Granular Matter*, Vol. 23, No. 1, pp. 1-20, 2021.

68. Xu, Z., N. Xu and H. Wang, "Effects of Particle Shapes and Sizes on The Minimum Void Ratios of Sand", *Advanture Civil Engineering*, Vol. 1, No. 1, pp. 1 -12, 2019.

69. Mair, K., K.M. Frye and C. Marone, "Influence of Grain Characteristics on the Friction of Granular Shear Zones", *Journal of Geophysical Research: Solid Earth*, Vol. 107, No. B10, pp. ECV-4-ECV8, 2002.

70. Wegner, S., R. Stannarius, A. Boese, G. Rose, B. Szabo, E. Somfai and T. Börzsönyi, "Effects of Grain Shape on Packing and Dilatancy of Sheared Granular Materials", *Soft Matter*, Vol. 10, No. 28, pp. 5157-5167, 2014.

71. Xiao, Y., L. Long, T. Matthew Evans, H. Zhou, H. Liu and A.W. Stuedlein, "Effect of Particle Shape on Stress-Dilatancy Responses of Medium-Dense Sands", *Journal of Geotechnical and Geoenvironmental Engineering*, Vol. 145, No. 2, pp. 04018105-04018123, 2019.

72. Shinohara, K., M. Oida and B. Golman, "Effect of Particle Shape on Angle of Internal Friction by Triaxial Compression Test", *Powder Technology*, Vol. 107, No2, pp. 131-136, 2000.

73. Yang, Z.X., J. Yang and L.Z. Wang, "On the Influence of Inter-Particle Friction and Dilatancy in Granular Materials", *A Numerical Analysis. Granular Matter*, Vol. 14, No. 1, pp. 433-447, 2012.

74. Cox, M.R.B., *The Influence of Grain Shape on Dilatancy*, The University of Arizona, 2008.

75. Amirpour Harehdasht, S., M.N. Hussien, M. Karray, V. Roubtsova and M. Chekired, "Influence of Particle Size and Gradation on Shear Strength -Dilation Relation of Granular Materials", *Canadian Geotechnical Journal*, Vol. 56, No. 2, pp. 208-227, 2019.

76. Vangla, P. and G.M. Latha, "Influence of Particle Size on the Friction and Interfacial Shear Strength of Sands of Similar Morphology", *International Journal of Geosynthetics And Ground Engineering*, Vol. 1, No. 1, pp. 1-12, 2015.

77. Nguyen, H.B.K., M.M. Rahman and A.B. Fourie, "How Particle Shape Affects the Critical State, Triggering of Instability and Dilatancy of Granular Materials -Results from A DEM Study", *Géotechnique*, Vol. 71, No. 9, pp. 749-764, 2021.

78. Arda, Ç. and Ö. Çinicioğlu, "Influence of Grain Shape on Stress-Dilatancy Parameters", *Granular Matter*, Vol. 23, No. 1, pp. 1-19, 2021.

79. Cho, G.C., J. Dodds and C.J. Santamarina, "Particle Shape Effects on Packing Density, Stiffness and Strength, Natural and Crushed Sands", *Journal Geotech Geoenviron*, Vol. 132, No. 5, pp. 591 -602, 2006.

80. Alshibli, K.A. and M.B. Cil, "Influence of Particle Morphology on the Friction and Dilatancy of Sand", *Journal of Geotechnical and Geoenvironmental Engineering*, Vol. 144, No. 3, pp. 04017118-17130040, 2018.

81. Altuhafi, F.N., M.R. Coop and V.N. Georgiannou, "Effect of particle shape on the mechanical behavior of natural sands", *Journal of Geotechnical and Geoenvironmental Engineering*, Vol. 142, No. 12, pp. 04016071-0401690, 2016.

82. Amirpour Harehdasht, S., M. Karray, M.N. Hussien and M. Chekired, "Influence of Particle Size and Gradation on the Stress-Dilatancy Behavior of Granular Materials During Drained Triaxial Compression", *International Journal of Geomechanics*, Vol. 17, No. 9, pp. 04017077-04017094, 2017.

83. Santamarina, C. and G. Cascante, "Effect of Surface Roughness on Wave Propagation Parameters", *Geotechnique*, Vol. 48, No. 1, Pp. 129-136, 1998.

84. Ham, A., J.J.Wang and G. Stammer, "Relationships Between Particle Shape Characteristics and Macroscopic Damping in Dry Sands", *Journal of Geotechnical and Geoenvironmental Engineering*, Vol. 138, No. 8, pp. 1002-1011, 2012.

85. Payan, M., K. Senetakis, A. Khoshghalb and N. Khalili, "Effect of Gradation and Particle Shape on Small-Strain Young's Modulus and Poisson's Ratio of Sands", *International Journal of Geomechanics*, Vol. 17, No. 5, pp. 04016120-04016142, 2017.

86. Sitharam, S., *Effect of Particle Shape on the Cyclic Stress-Strain Behaviour of Granular Media*, ResearchGate, 2010.

87. Ashmawy, A.K., V.V. Hoang and B. Sukumaran, *Evaluating the Influence of Particle Shape on Liquefaction Behavior Using Discrete Element Modeling, in ISOPE International Ocean and Polar Engineering*, ResearchGate, 2003.

88. Hu, J., H. Wu, X. Gu and Q. Zhou, "Particle Shape Effects on Dynamic Properties of Granular Soils", *A DEM Study, Computers and Geotechnics*, Vol. 161, No. 1, pp. 105578-105599, 2023.

89. Lee, C., H.S., Suh, B. Yoon and T.S. Yun, "Particle Shape Effect on Thermal Conductivity and Shear Wave Velocity in Sands'", *Acta Geotechnica*, Vol. 12, No. 1, pp. 615-625, 2017.

90. Lee, J., T.S. Yun and S.U. Choi, "The Effect of Particle Size on Thermal Conduction in Granular Mixtures", *Materials*, Vol. 8, No. 7, pp. 3975-3991, 2015.

91. Zhang, N., X. Yu, A. Pradhan and A.J. Puppala, "Effects of Particle Size and Fines Content on Thermal Conductivity of Quartz Sands", *Transportation Research Record*, Vol. 2510, No. 1, pp. 36-43, 2015.

92. Fei, W., G.A. Narsilio and M.M. Disfani, "Impact of Three-Dimensional Sphericity and Roundness on Heat Transfer in Granular Materials", *Powder Technology*, Vol. 355, No. 1, pp. 770-781, 2019.

93. Xiao, Y., G. Ma, B. Nan and J.S. McCartney, "Thermal Conductivity of Granular Soil Mixtures with Contrasting Particle Shapes", *Journal of Geotechnical and Geoenvironmental Engineering*, Vol. 146, No. 5, pp. 06020004-06020024, 2020.

94. Pentland, A., "A Method of Measuring the Angularity of Sands. MAG. MN. AL Acta Eng. Dom.", *Transaction of the Royal Society of Canada*, Vol. 21, No. 3, pp. 43-65, 1927.

95. Wadell, H., "Volume, Shape and Roundness of Rock Particles", *The Journal of Geology*, Vol. 40, No. 5, pp. 443-451, 1932.

96. Riley, N.A., "Projection Sphericity", *Journal of Sedimentary Research*, Vol. 11, No. 2, pp. 94-95, 1941.

97. Wu, M., J. Lu, X. Li, S. Pan, J. Wang and Z. Yin, "Quantifying the Morphology of Crushed Sand Particles Using X-Ray Micro-Tomography", *Granular Matter*, Vol. 25, No. 4, pp. 80-97, 2023.

98. Venkatesh, A.M., D. Bouvard, P. Lhuissier and J. Villanova, "3D Analysis of Ceramic Powder Sintering by Synchrotron X-Ray Nano-Tomography", *Journal of the European Ceramic Society*, Vol. 43, No. 6, pp. 2553-2563, 2023.

99. Druckrey, A.M. and K.A. Alshibli, "3D Behavior of Sand Particles Using X-Ray Synchrotron Micro-Tomography", *In Geo-Congress 2014, Geo-Characterization and Modeling for Sustainability*, Vol. 1, No. 1, pp. 2814-2821, 2014.

100. Cheng, Z. and J. Wang, "An Investigation of the Breakage Behaviour Of A Pre-Crushed Carbonate Sand Under Shear Using X-Ray Micro-Tomography", *Engineering Geology*, Vol. 293, No. 1, pp. 106286-106299, 2021.

101. Cheng, Z. and J. Wang, "Experimental Investigation of Inter-Particle Contact Evolution of Sheared Granular Materials Using X-Ray Micro-Tomography", *Soils and Foundations*, Vol. 58, No. 6, pp. 1492-1510, 2018.

102. Wadell, H., "Volume, Shape, and Roundness of Rock Particles", *The Journal of Geology*, vol. 40, pp, 5, pp, 443-451, 1932.

103. Krumbein, W.C., "Measurement and Geological Significance of Shape and Roundness of Sedimentary Particles", *Journal of Sedimentary Research*, Vol. 11, No. 2, pp. 64-72, 1941.

104. Powers, M.C., "A New Roundness Scale for Sedimentary Particles", *Journal of Sedimentary Research*, Vol. 23, No. 2, pp. 117-119, 1953.

105. Russell, R.D. and R.E. Taylor, "Roundness and Shape of Mississippi Rivers", *The Journal of Geology*, Vol. 45, No. 3, pp. 225-267, 1937.

106. Pettijohn, F.J., *Sedimentary Rocks*, Harper and Row, New York, 1975.

107. Blott, S.J. and K. Pye, "Particle Shape: A Review and New Methods of Characterization and Classification", *Sedimentology*, Vol. 55, No. 1, pp. 31-632008.

108. Janoo, V.C., *Quantification of Shape, Angularity, and Surface Texture of Base Course Materials*, Crrel, Kingman, 1998.

109. Kubiak, K.J., T.G. Mathia, S. Fouvry, "Interface Roughness Effect on Friction Map under Fretting Contact Conditions", *Tribology International*, Vol. 43, No. 8, pp. 1500-1507, 2010.

110. Mora, C.F. and A.K.H. Kwan, "Sphericity, Shape Factor, and Convexity Measurement of Coarse Aggregate for Concrete Using Digital Image Processing", *Cement and concrete research*, Vol. 30, No. 3, pp. 351-358, 2000.

111. Wentworth, C.K., *The Shapes of Beach Pebbles*, US Government Printing Office, United States,1922.

112. Pye, W.D. and M.H. Pye, "Sphericity Determinations of Pebbles and Sand Grains", *Journal of Sedimentary Research*, Vol. 13, No. 1, pp. 28-34, 1943.

113. Sneed, E.D. and R.L. Folk, "Pebbles in the lower Colorado River, Texas a study in particle morphogenesis", *The Journal of Geology*, Vol. 66, No. 2, pp. 114-150, 1958.

114. Zeidan, M., X. Jia and R.A. Williams, "Errors Implicit in Digital Particle Characterisation", *Chemical Engineering Science*, Vol. 62, No. 7, pp. 1905-1914, 2007.

115. Janke, N.C., "Effect of Shape upon the Settling Velocity of Regular Convex Geometric Particles", *Journal of Sedimentary Research*, Vol. 36, No. 2, pp. 370-376, 1966.

116. Dobkins, J.E. and R.L. Folk, "Shape Development on Tahiti-Nui", *Journal of Sedimentary Research*, Vol. 40, No. 4, pp. 1167-1203, 1970.

117. American Society for Testing and Materials, D., *Standard Test Methods for Particle-Size Distribution (Gradation) of Soils Using Sieve Analysis*, American Society for Testing and Materials International: West Conshohocken, Pennsylvania, 2009.

118. American Society for Testing and Materials Committee D-18 on Soil and Rock, *Standard test Methods for Specific Gravity of Soil Solids by Water Pycnometer*, American Society for Testing and Materials International, Pennsylvania, 2006.

119. American Society for Testing and Materials Committee D-18 on Soil and Rock, *Standard test Methods for Maximum Index Density and Unit Weight of Soils Using A Vibratory Table*, American Society for Testing and Materials International, Pennsylvania, 2016.

120. Santamarina, J.C. and G.C. Cho, "Determination of Critical State Parameters in Sandy Soils-Simple Procedure", *Geotechnical Testing Journal*, Vol. 24, No. 2, pp. 185-192, 2001.

121. American Society for Testing and Materials Committee D-18 on Soil and Rock, *Standard test Methods for One-Dimensional Consolidation Properties of Soils Using Incremental Loading*, American Society for Testing and Materials International, Pennsylvania, 2004.

122. Schanz, T., P.A. Vermeer, "Angles of Friction and Dilatancy of Sand", *Geotechnique*, Vol. 46, No. 1, pp. 145-151, 1996.

# APPENDIX A: DETERMINED 2D AND 3D SHAPE DESCRIPTORS

## A.1. Determined 2D And 3D Shape Descriptors of GB

The values of the determined 2D and 3D shape descriptors of GB are presented in the following tables.

Table A.1. Determined 2D and 3D shape descriptors of GB particles retained on sieve #40, PR = 100, PSR = 0.250 – 0.850 mm.

| Part | $R_{2D}$ | | | $S_{2D}$ | | | $AR_{2D}$ | | | $CX_{2D}$ | | | | | | |
|---|---|---|---|---|---|---|---|---|---|---|---|---|---|---|---|---|
| No. | $F_D$ | $F_1$ | $F_2$ | $F_D$ | $F_1$ | $F_2$ | $F_D$ | $F_1$ | $F_2$ | $F_D$ | $F_1$ | $F_2$ | $R_{3D}$ | $S_{3D}$ | $AR_{3D}$ | $CX_{3D}$ |
| 1 | 1.00 | 1.00 | 1.00 | 1.00 | 1.00 | 1.00 | 1.00 | 1.00 | 1.00 | 1.00 | 1.00 | 1.00 | 1.00 | 1.00 | 1.00 | 1.00 |
| 2 | 1.00 | 1.00 | 1.00 | 1.00 | 1.00 | 1.00 | 1.00 | 1.00 | 1.00 | 1.00 | 1.00 | 1.00 | 1.00 | 1.00 | 1.00 | 1.00 |
| 3 | 1.00 | 1.00 | 1.00 | 1.00 | 1.00 | 1.00 | 1.00 | 1.00 | 1.00 | 1.00 | 1.00 | 1.00 | 1.00 | 1.00 | 1.00 | 1.00 |
| 4 | 1.00 | 1.00 | 1.00 | 1.00 | 1.00 | 1.00 | 1.00 | 1.00 | 1.00 | 1.00 | 1.00 | 1.00 | 1.00 | 1.00 | 1.00 | 1.00 |
| 5 | 1.00 | 1.00 | 1.00 | 1.00 | 1.00 | 1.00 | 1.00 | 1.00 | 1.00 | 1.00 | 1.00 | 1.00 | 1.00 | 1.00 | 1.00 | 1.00 |
| 6 | 1.00 | 1.00 | 1.00 | 1.00 | 1.00 | 1.00 | 1.00 | 1.00 | 1.00 | 1.00 | 1.00 | 1.00 | 1.00 | 1.00 | 1.00 | 1.00 |
| 7 | 1.00 | 1.00 | 1.00 | 1.00 | 1.00 | 1.00 | 1.00 | 1.00 | 1.00 | 1.00 | 1.00 | 1.00 | 1.00 | 1.00 | 1.00 | 1.00 |
| 8 | 1.00 | 1.00 | 1.00 | 1.00 | 1.00 | 1.00 | 1.00 | 1.00 | 1.00 | 1.00 | 1.00 | 1.00 | 1.00 | 1.00 | 1.00 | 1.00 |
| 9 | 1.00 | 1.00 | 1.00 | 1.00 | 1.00 | 1.00 | 1.00 | 1.00 | 1.00 | 1.00 | 1.00 | 1.00 | 1.00 | 1.00 | 1.00 | 1.00 |
| 10 | 1.00 | 1.00 | 1.00 | 1.00 | 1.00 | 1.00 | 1.00 | 1.00 | 1.00 | 1.00 | 1.00 | 1.00 | 1.00 | 1.00 | 1.00 | 1.00 |
| 11 | 1.00 | 1.00 | 1.00 | 1.00 | 1.00 | 1.00 | 1.00 | 1.00 | 1.00 | 1.00 | 1.00 | 1.00 | 1.00 | 1.00 | 1.00 | 1.00 |
| 12 | 1.00 | 1.00 | 1.00 | 1.00 | 1.00 | 1.00 | 1.00 | 1.00 | 1.00 | 1.00 | 1.00 | 1.00 | 1.00 | 1.00 | 1.00 | 1.00 |
| 13 | 1.00 | 1.00 | 1.00 | 1.00 | 1.00 | 1.00 | 1.00 | 1.00 | 1.00 | 1.00 | 1.00 | 1.00 | 1.00 | 1.00 | 1.00 | 1.00 |
| 14 | 1.00 | 1.00 | 1.00 | 1.00 | 1.00 | 1.00 | 1.00 | 1.00 | 1.00 | 1.00 | 1.00 | 1.00 | 1.00 | 1.00 | 1.00 | 1.00 |
| 15 | 1.00 | 1.00 | 1.00 | 1.00 | 1.00 | 1.00 | 1.00 | 1.00 | 1.00 | 1.00 | 1.00 | 1.00 | 1.00 | 1.00 | 1.00 | 1.00 |
| 16 | 1.00 | 1.00 | 1.00 | 1.00 | 1.00 | 1.00 | 1.00 | 1.00 | 1.00 | 1.00 | 1.00 | 1.00 | 1.00 | 1.00 | 1.00 | 1.00 |
| 17 | 1.00 | 1.00 | 1.00 | 1.00 | 1.00 | 1.00 | 1.00 | 1.00 | 1.00 | 1.00 | 1.00 | 1.00 | 1.00 | 1.00 | 1.00 | 1.00 |
| 18 | 1.00 | 1.00 | 1.00 | 1.00 | 1.00 | 1.00 | 1.00 | 1.00 | 1.00 | 1.00 | 1.00 | 1.00 | 1.00 | 1.00 | 1.00 | 1.00 |
| 19 | 1.00 | 1.00 | 1.00 | 1.00 | 1.00 | 1.00 | 1.00 | 1.00 | 1.00 | 1.00 | 1.00 | 1.00 | 1.00 | 1.00 | 1.00 | 1.00 |
| 20 | 1.00 | 1.00 | 1.00 | 1.00 | 1.00 | 1.00 | 1.00 | 1.00 | 1.00 | 1.00 | 1.00 | 1.00 | 1.00 | 1.00 | 1.00 | 1.00 |
| 21 | 1.00 | 1.00 | 1.00 | 1.00 | 1.00 | 1.00 | 1.00 | 1.00 | 1.00 | 1.00 | 1.00 | 1.00 | 1.00 | 1.00 | 1.00 | 1.00 |
| 22 | 1.00 | 1.00 | 1.00 | 1.00 | 1.00 | 1.00 | 1.00 | 1.00 | 1.00 | 1.00 | 1.00 | 1.00 | 1.00 | 1.00 | 1.00 | 1.00 |
| 23 | 1.00 | 1.00 | 1.00 | 1.00 | 1.00 | 1.00 | 1.00 | 1.00 | 1.00 | 1.00 | 1.00 | 1.00 | 1.00 | 1.00 | 1.00 | 1.00 |
| 24 | 1.00 | 1.00 | 1.00 | 1.00 | 1.00 | 1.00 | 1.00 | 1.00 | 1.00 | 1.00 | 1.00 | 1.00 | 1.00 | 1.00 | 1.00 | 1.00 |
| 25 | 1.00 | 1.00 | 1.00 | 1.00 | 1.00 | 1.00 | 1.00 | 1.00 | 1.00 | 1.00 | 1.00 | 1.00 | 1.00 | 1.00 | 1.00 | 1.00 |
| 26 | 1.00 | 1.00 | 1.00 | 1.00 | 1.00 | 1.00 | 1.00 | 1.00 | 1.00 | 1.00 | 1.00 | 1.00 | 1.00 | 1.00 | 1.00 | 1.00 |
| 27 | 1.00 | 1.00 | 1.00 | 1.00 | 1.00 | 1.00 | 1.00 | 1.00 | 1.00 | 1.00 | 1.00 | 1.00 | 1.00 | 1.00 | 1.00 | 1.00 |
| 28 | 1.00 | 1.00 | 1.00 | 1.00 | 1.00 | 1.00 | 1.00 | 1.00 | 1.00 | 1.00 | 1.00 | 1.00 | 1.00 | 1.00 | 1.00 | 1.00 |
| 29 | 1.00 | 1.00 | 1.00 | 1.00 | 1.00 | 1.00 | 1.00 | 1.00 | 1.00 | 1.00 | 1.00 | 1.00 | 1.00 | 1.00 | 1.00 | 1.00 |
| 30 | 1.00 | 1.00 | 1.00 | 1.00 | 1.00 | 1.00 | 1.00 | 1.00 | 1.00 | 1.00 | 1.00 | 1.00 | 1.00 | 1.00 | 1.00 | 1.00 |

## A.2. 2D and 3D Shape Descriptors of Sand A

The values of the determined 2D and 3D shape descriptors of Sand A are presented in the following tables. The results are presented for all particle size ranges of the sample.

Table A.2. Determined 2D and 3D shape descriptors of Sand A particles retained on sieve #40, PR = 0.80, PSR = 0.425 – 0.850 mm.

| Part | $R_{2D}$ | | | $S_{2D}$ | | | $AR_{2D}$ | | | $CX_{2D}$ | | | | | | |
|---|---|---|---|---|---|---|---|---|---|---|---|---|---|---|---|---|
| No. | $F_D$ | $F_1$ | $F_2$ | $F_D$ | $F_1$ | $F_2$ | $F_D$ | $F_1$ | $F_2$ | $F_D$ | $F_1$ | $F_2$ | $R_{3D}$ | $S_{3D}$ | $AR_{3D}$ | $CX_{3D}$ |
| z | 0.36 | 0.51 | 0.51 | 0.71 | 0.46 | 0.61 | 0.75 | 0.49 | 0.62 | 0.95 | 0.94 | 0.96 | 0.52 | 0.44 | 0.47 | 0.95 |
| 2 | 0.44 | 0.65 | 0.69 | 0.45 | 0.25 | 0.24 | 0.46 | 0.26 | 0.24 | 0.95 | 0.94 | 0.94 | 0.66 | 0.19 | 0.19 | 0.95 |
| 3 | 0.48 | 0.44 | 0.38 | 0.81 | 0.61 | 0.67 | 0.85 | 0.63 | 0.71 | 0.97 | 0.95 | 0.96 | 0.48 | 0.60 | 0.63 | 0.96 |
| 4 | 0.54 | 0.56 | 0.51 | 0.74 | 0.55 | 0.67 | 0.75 | 0.56 | 0.68 | 0.96 | 0.96 | 0.97 | 0.55 | 0.53 | 0.54 | 0.96 |
| 5 | 0.43 | 0.55 | 0.45 | 0.56 | 0.47 | 0.61 | 0.65 | 0.49 | 0.62 | 0.93 | 0.95 | 0.96 | 0.50 | 0.44 | 0.46 | 0.94 |
| 6 | 0.45 | 0.40 | 0.43 | 0.78 | 0.70 | 0.81 | 0.84 | 0.78 | 0.84 | 0.97 | 0.95 | 0.96 | 0.46 | 0.67 | 0.70 | 0.96 |
| 7 | 0.38 | 0.49 | 0.46 | 0.69 | 0.60 | 0.60 | 0.75 | 0.61 | 0.68 | 0.96 | 0.97 | 0.97 | 0.52 | 0.47 | 0.52 | 0.97 |
| 8 | 0.47 | 0.38 | 0.54 | 0.76 | 0.64 | 0.56 | 0.82 | 0.65 | 0.57 | 0.96 | 0.97 | 0.97 | 0.55 | 0.51 | 0.52 | 0.97 |
| 9 | 0.29 | 0.39 | 0.61 | 0.82 | 0.47 | 0.54 | 0.91 | 0.48 | 0.57 | 0.95 | 0.96 | 0.96 | 0.50 | 0.46 | 0.48 | 0.95 |
| 10 | 0.42 | 0.53 | 0.55 | 0.70 | 0.63 | 0.60 | 0.75 | 0.65 | 0.62 | 0.96 | 0.96 | 0.96 | 0.53 | 0.55 | 0.57 | 0.96 |
| 11 | 0.44 | 0.48 | 0.47 | 0.74 | 0.67 | 0.60 | 0.78 | 0.70 | 0.63 | 0.96 | 0.96 | 0.95 | 0.46 | 0.55 | 0.58 | 0.96 |
| 12 | 0.39 | 0.49 | 0.51 | 0.67 | 0.43 | 0.51 | 0.69 | 0.43 | 0.50 | 0.96 | 0.92 | 0.96 | 0.52 | 0.38 | 0.38 | 0.95 |
| 13 | 0.40 | 0.59 | 0.58 | 0.58 | 0.26 | 0.26 | 0.72 | 0.28 | 0.29 | 0.94 | 0.91 | 0.89 | 0.60 | 0.22 | 0.24 | 0.93 |
| 14 | 0.49 | 0.52 | 0.51 | 0.78 | 0.55 | 0.54 | 0.93 | 0.59 | 0.56 | 0.96 | 0.96 | 0.96 | 0.55 | 0.51 | 0.55 | 0.96 |
| 15 | 0.32 | 0.51 | 0.30 | 0.54 | 0.62 | 0.75 | 0.56 | 0.63 | 0.90 | 0.94 | 0.97 | 0.97 | 0.40 | 0.54 | 0.56 | 0.96 |
| 16 | 0.60 | 0.52 | 0.62 | 0.78 | 0.59 | 0.69 | 0.81 | 0.60 | 0.71 | 0.98 | 0.97 | 0.97 | 0.60 | 0.56 | 0.58 | 0.97 |
| 17 | 0.52 | 0.56 | 0.56 | 0.81 | 0.71 | 0.74 | 0.80 | 0.71 | 0.78 | 0.98 | 0.98 | 0.97 | 0.56 | 0.68 | 0.69 | 0.98 |
| 18 | 0.41 | 0.45 | 0.55 | 0.66 | 0.20 | 0.21 | 0.78 | 0.21 | 0.24 | 0.93 | 0.88 | 0.89 | 0.50 | 0.17 | 0.20 | 0.91 |
| 19 | 0.46 | 0.55 | 0.53 | 0.70 | 0.60 | 0.55 | 0.83 | 0.60 | 0.57 | 0.96 | 0.98 | 0.97 | 0.57 | 0.52 | 0.56 | 0.97 |
| 20 | 0.27 | 0.50 | 0.51 | 0.67 | 0.35 | 0.38 | 0.85 | 0.35 | 0.40 | 0.95 | 0.96 | 0.93 | 0.52 | 0.31 | 0.35 | 0.95 |
| 21 | 0.54 | 0.46 | 0.42 | 0.63 | 0.55 | 0.61 | 0.70 | 0.56 | 0.67 | 0.95 | 0.97 | 0.94 | 0.51 | 0.49 | 0.51 | 0.95 |
| 22 | 0.53 | 0.43 | 0.38 | 0.75 | 0.37 | 0.28 | 0.77 | 0.36 | 0.29 | 0.98 | 0.96 | 0.96 | 0.51 | 0.27 | 0.27 | 0.97 |
| 23 | 0.56 | 0.46 | 0.45 | 0.86 | 0.72 | 0.76 | 0.87 | 0.76 | 0.77 | 0.97 | 0.96 | 0.98 | 0.51 | 0.70 | 0.74 | 0.97 |
| 24 | 0.38 | 0.45 | 0.54 | 0.79 | 0.51 | 0.53 | 0.81 | 0.52 | 0.54 | 0.97 | 0.95 | 0.97 | 0.53 | 0.45 | 0.46 | 0.96 |
| 25 | 0.49 | 0.55 | 0.48 | 0.60 | 0.22 | 0.16 | 0.66 | 0.22 | 0.22 | 0.96 | 0.89 | 0.74 | 0.49 | 0.14 | 0.18 | 0.91 |
| 26 | 0.55 | 0.29 | 0.38 | 0.55 | 0.23 | 0.19 | 0.59 | 0.24 | 0.20 | 0.97 | 0.94 | 0.95 | 0.43 | 0.18 | 0.18 | 0.96 |
| 27 | 0.52 | 0.35 | 0.50 | 0.57 | 0.69 | 0.44 | 0.60 | 0.71 | 0.47 | 0.98 | 0.97 | 0.95 | 0.49 | 0.43 | 0.46 | 0.97 |
| 28 | 0.34 | 0.43 | 0.46 | 0.81 | 0.49 | 0.62 | 0.88 | 0.50 | 0.64 | 0.97 | 0.97 | 0.98 | 0.51 | 0.49 | 0.50 | 0.97 |
| 29 | 0.57 | 0.53 | 0.61 | 0.66 | 0.65 | 0.60 | 0.74 | 0.67 | 0.63 | 0.96 | 0.98 | 0.97 | 0.57 | 0.58 | 0.60 | 0.96 |
| 30 | 0.43 | 0.41 | 0.50 | 0.60 | 0.55 | 0.57 | 0.66 | 0.56 | 0.59 | 0.93 | 0.96 | 0.94 | 0.50 | 0.49 | 0.51 | 0.94 |

Table A.3. Determined 2D and 3D shape descriptors of Sand A grains retained on sieve #60, PR = 12.38, PSR = 0.250 – 0.425 mm.

| Part | $R_{2D}$ | | | $S_{2D}$ | | | $AR_{2D}$ | | | $CX_{2D}$ | | | | | | |
|---|---|---|---|---|---|---|---|---|---|---|---|---|---|---|---|---|
| No. | $F_D$ | $F_1$ | $F_2$ | $F_D$ | $F_1$ | $F_2$ | $F_D$ | $F_1$ | $F_2$ | $F_D$ | $F_1$ | $F_2$ | $R_{3D}$ | $S_{3D}$ | $AR_{3D}$ | $CX_{3D}$ |
| 1 | 0.50 | 0.51 | 0.57 | 0.68 | 0.29 | 0.24 | 0.70 | 0.29 | 0.25 | 0.97 | 0.93 | 0.88 | 0.52 | 0.23 | 0.24 | 0.94 |
| 2 | 0.49 | 0.54 | 0.48 | 0.72 | 0.57 | 0.71 | 0.74 | 0.62 | 0.74 | 0.94 | 0.92 | 0.97 | 0.55 | 0.57 | 0.62 | 0.94 |
| 3 | 0.62 | 0.61 | 0.69 | 0.75 | 0.73 | 0.60 | 0.78 | 0.74 | 0.61 | 0.97 | 0.96 | 0.97 | 0.65 | 0.60 | 0.61 | 0.97 |
| 4 | 0.51 | 0.59 | 0.59 | 0.62 | 0.28 | 0.34 | 0.68 | 0.28 | 0.34 | 0.97 | 0.95 | 0.95 | 0.62 | 0.23 | 0.24 | 0.96 |
| 5 | 0.50 | 0.56 | 0.63 | 0.56 | 0.70 | 0.73 | 0.58 | 0.79 | 0.76 | 0.94 | 0.95 | 0.96 | 0.59 | 0.56 | 0.58 | 0.95 |
| 6 | 0.56 | 0.72 | 0.58 | 0.72 | 0.45 | 0.37 | 0.83 | 0.46 | 0.38 | 0.95 | 0.96 | 0.96 | 0.65 | 0.36 | 0.38 | 0.95 |
| 7 | 0.32 | 0.45 | 0.79 | 0.69 | 0.28 | 0.27 | 0.79 | 0.27 | 0.29 | 0.95 | 0.93 | 0.92 | 0.60 | 0.25 | 0.27 | 0.94 |
| 8 | 0.48 | 0.65 | 0.60 | 0.56 | 0.46 | 0.35 | 0.57 | 0.49 | 0.35 | 0.96 | 0.95 | 0.95 | 0.57 | 0.30 | 0.32 | 0.95 |
| 9 | 0.56 | 0.74 | 0.63 | 0.63 | 0.34 | 0.40 | 0.70 | 0.37 | 0.42 | 0.96 | 0.93 | 0.94 | 0.71 | 0.32 | 0.35 | 0.95 |
| 10 | 0.60 | 0.69 | 0.63 | 0.75 | 0.56 | 0.54 | 0.86 | 0.56 | 0.56 | 0.96 | 0.97 | 0.95 | 0.64 | 0.51 | 0.53 | 0.96 |
| 11 | 0.45 | 0.48 | 0.44 | 0.74 | 0.45 | 0.52 | 0.81 | 0.44 | 0.53 | 0.95 | 0.96 | 0.96 | 0.51 | 0.45 | 0.44 | 0.96 |
| 12 | 0.58 | 0.55 | 0.52 | 0.73 | 0.71 | 0.69 | 0.86 | 0.80 | 0.77 | 0.97 | 0.95 | 0.95 | 0.58 | 0.60 | 0.70 | 0.95 |
| 13 | 0.53 | 0.66 | 0.58 | 0.52 | 0.35 | 0.44 | 0.55 | 0.36 | 0.45 | 0.95 | 0.95 | 0.95 | 0.63 | 0.32 | 0.34 | 0.95 |
| 14 | 0.57 | 0.62 | 0.61 | 0.73 | 0.62 | 0.60 | 0.74 | 0.60 | 0.62 | 0.96 | 0.97 | 0.97 | 0.63 | 0.57 | 0.59 | 0.97 |
| 15 | 0.55 | 0.62 | 0.57 | 0.51 | 0.21 | 0.24 | 0.51 | 0.21 | 0.25 | 0.96 | 0.94 | 0.94 | 0.67 | 0.18 | 0.18 | 0.95 |
| 16 | 0.46 | 0.56 | 0.47 | 0.67 | 0.53 | 0.46 | 0.71 | 0.54 | 0.53 | 0.94 | 0.89 | 0.91 | 0.50 | 0.43 | 0.50 | 0.92 |
| 17 | 0.68 | 0.56 | 0.66 | 0.80 | 0.74 | 0.60 | 0.81 | 0.78 | 0.60 | 0.98 | 0.96 | 0.97 | 0.63 | 0.60 | 0.60 | 0.97 |
| 18 | 0.56 | 0.70 | 0.60 | 0.78 | 0.67 | 0.53 | 0.84 | 0.68 | 0.58 | 0.98 | 0.97 | 0.95 | 0.67 | 0.53 | 0.58 | 0.96 |
| 19 | 0.58 | 0.61 | 0.53 | 0.65 | 0.61 | 0.71 | 0.67 | 0.63 | 0.77 | 0.96 | 0.95 | 0.96 | 0.58 | 0.58 | 0.62 | 0.96 |
| 20 | 0.55 | 0.51 | 0.63 | 0.72 | 0.39 | 0.43 | 0.72 | 0.39 | 0.45 | 0.96 | 0.94 | 0.93 | 0.59 | 0.36 | 0.37 | 0.94 |
| 21 | 0.46 | 0.57 | 0.56 | 0.56 | 0.34 | 0.46 | 0.58 | 0.34 | 0.47 | 0.97 | 0.95 | 0.93 | 0.55 | 0.30 | 0.31 | 0.96 |
| 22 | 0.61 | 0.49 | 0.59 | 0.69 | 0.60 | 0.50 | 0.72 | 0.60 | 0.51 | 0.95 | 0.97 | 0.97 | 0.52 | 0.49 | 0.49 | 0.96 |
| 23 | 0.52 | 0.70 | 0.67 | 0.81 | 0.50 | 0.54 | 0.88 | 0.50 | 0.54 | 0.95 | 0.96 | 0.96 | 0.61 | 0.47 | 0.48 | 0.95 |
| 24 | 0.65 | 0.68 | 0.70 | 0.62 | 0.45 | 0.59 | 0.62 | 0.47 | 0.59 | 0.97 | 0.96 | 0.95 | 0.67 | 0.40 | 0.42 | 0.96 |
| 25 | 0.55 | 0.35 | 0.80 | 0.71 | 0.29 | 0.33 | 0.75 | 0.30 | 0.33 | 0.97 | 0.91 | 0.92 | 0.66 | 0.29 | 0.30 | 0.95 |
| 26 | 0.63 | 0.59 | 0.58 | 0.79 | 0.58 | 0.56 | 0.80 | 0.59 | 0.59 | 0.98 | 0.97 | 0.95 | 0.66 | 0.49 | 0.51 | 0.97 |
| 27 | 0.58 | 0.59 | 0.57 | 0.66 | 0.44 | 0.32 | 0.68 | 0.43 | 0.32 | 0.96 | 0.96 | 0.94 | 0.56 | 0.31 | 0.31 | 0.95 |
| 28 | 0.48 | 0.69 | 0.67 | 0.53 | 0.38 | 0.35 | 0.58 | 0.38 | 0.35 | 0.94 | 0.95 | 0.95 | 0.71 | 0.31 | 0.32 | 0.94 |
| 29 | 0.55 | 0.60 | 0.56 | 0.66 | 0.71 | 0.76 | 0.73 | 0.76 | 0.80 | 0.95 | 0.96 | 0.97 | 0.59 | 0.65 | 0.68 | 0.96 |
| 30 | 0.70 | 0.79 | 0.65 | 0.77 | 0.64 | 0.76 | 0.77 | 0.64 | 0.76 | 0.98 | 0.97 | 0.97 | 0.71 | 0.63 | 0.63 | 0.97 |

Table A.4. Determined 2D and 3D shape descriptors of Sand A grains retained on sieve #100, PR = 86.82, PSR = 0.150 – 0.250 mm.

| Part | $R_{2D}$ | | | $S_{2D}$ | | | $AR_{2D}$ | | | $CX_{2D}$ | | | | | | |
|---|---|---|---|---|---|---|---|---|---|---|---|---|---|---|---|---|
| No. | $F_D$ | $F_1$ | $F_2$ | $F_D$ | $F_1$ | $F_2$ | $F_D$ | $F_1$ | $F_2$ | $F_D$ | $F_1$ | $F_2$ | $R_{3D}$ | $S_{3D}$ | $AR_{3D}$ | $CX_{3D}$ |
| 1 | 0.55 | 0.54 | 0.57 | 0.69 | 0.72 | 0.73 | 0.70 | 0.72 | 0.78 | 0.97 | 0.96 | 0.94 | 0.61 | 0.59 | 0.63 | 0.96 |
| 2 | 0.66 | 0.58 | 0.58 | 0.82 | 0.59 | 0.60 | 0.82 | 0.59 | 0.59 | 0.97 | 0.96 | 0.95 | 0.60 | 0.54 | 0.55 | 0.96 |
| 3 | 0.56 | 0.56 | 0.47 | 0.85 | 0.65 | 0.61 | 0.87 | 0.65 | 0.71 | 0.97 | 0.96 | 0.91 | 0.55 | 0.57 | 0.65 | 0.95 |
| 4 | 0.47 | 0.51 | 0.72 | 0.66 | 0.69 | 0.83 | 0.79 | 0.72 | 0.84 | 0.93 | 0.96 | 0.96 | 0.59 | 0.62 | 0.64 | 0.95 |
| 5 | 0.61 | 0.55 | 0.38 | 0.84 | 0.42 | 0.39 | 0.91 | 0.44 | 0.40 | 0.96 | 0.87 | 0.88 | 0.55 | 0.34 | 0.37 | 0.92 |
| 6 | 0.47 | 0.61 | 0.54 | 0.71 | 0.37 | 0.41 | 0.84 | 0.37 | 0.42 | 0.96 | 0.93 | 0.94 | 0.63 | 0.31 | 0.32 | 0.95 |
| 7 | 0.80 | 0.57 | 0.58 | 0.64 | 0.39 | 0.43 | 0.64 | 0.39 | 0.45 | 0.97 | 0.94 | 0.92 | 0.62 | 0.33 | 0.35 | 0.95 |
| 8 | 0.52 | 0.55 | 0.48 | 0.63 | 0.51 | 0.74 | 0.65 | 0.51 | 0.76 | 0.96 | 0.95 | 0.95 | 0.56 | 0.50 | 0.51 | 0.95 |
| 9 | 0.47 | 0.34 | 0.41 | 0.68 | 0.58 | 0.54 | 0.71 | 0.68 | 0.58 | 0.96 | 0.94 | 0.94 | 0.37 | 0.50 | 0.56 | 0.95 |
| 10 | 0.57 | 0.55 | 0.47 | 0.52 | 0.58 | 0.73 | 0.53 | 0.64 | 0.76 | 0.92 | 0.90 | 0.94 | 0.56 | 0.52 | 0.53 | 0.92 |
| 11 | 0.60 | 0.37 | 0.57 | 0.60 | 0.52 | 0.61 | 0.60 | 0.56 | 0.64 | 0.96 | 0.95 | 0.96 | 0.60 | 0.46 | 0.50 | 0.96 |
| 12 | 0.53 | 0.58 | 0.47 | 0.71 | 0.62 | 0.63 | 0.69 | 0.63 | 0.69 | 0.96 | 0.93 | 0.93 | 0.56 | 0.57 | 0.58 | 0.94 |
| 13 | 0.67 | 0.60 | 0.68 | 0.64 | 0.60 | 0.73 | 0.63 | 0.60 | 0.73 | 0.96 | 0.96 | 0.95 | 0.66 | 0.57 | 0.57 | 0.96 |
| 14 | 0.70 | 0.61 | 0.78 | 0.87 | 0.41 | 0.37 | 0.85 | 0.41 | 0.39 | 0.98 | 0.95 | 0.93 | 0.74 | 0.36 | 0.37 | 0.96 |
| 15 | 0.75 | 0.65 | 0.87 | 0.86 | 0.54 | 0.61 | 0.84 | 0.55 | 0.62 | 0.97 | 0.95 | 0.91 | 0.73 | 0.54 | 0.55 | 0.95 |
| 16 | 0.68 | 0.40 | 0.64 | 0.70 | 0.58 | 0.58 | 0.70 | 0.58 | 0.62 | 0.96 | 0.95 | 0.86 | 0.61 | 0.50 | 0.50 | 0.93 |
| 17 | 0.51 | 0.61 | 0.60 | 0.76 | 0.41 | 0.52 | 0.75 | 0.43 | 0.57 | 0.97 | 0.91 | 0.92 | 0.68 | 0.40 | 0.42 | 0.94 |
| 18 | 0.42 | 0.66 | 0.48 | 0.70 | 0.79 | 0.80 | 0.73 | 0.78 | 0.83 | 0.96 | 0.96 | 0.96 | 0.53 | 0.63 | 0.66 | 0.96 |
| 19 | 0.62 | 0.59 | 0.58 | 0.68 | 0.60 | 0.59 | 0.69 | 0.62 | 0.60 | 0.96 | 0.94 | 0.95 | 0.65 | 0.44 | 0.46 | 0.95 |
| 20 | 0.56 | 0.56 | 0.64 | 0.67 | 0.56 | 0.48 | 0.67 | 0.57 | 0.48 | 0.97 | 0.95 | 0.95 | 0.67 | 0.40 | 0.41 | 0.96 |
| 21 | 0.54 | 0.44 | 0.62 | 0.57 | 0.60 | 0.50 | 0.61 | 0.58 | 0.53 | 0.92 | 0.96 | 0.94 | 0.57 | 0.45 | 0.47 | 0.94 |
| 22 | 0.69 | 0.57 | 0.70 | 0.82 | 0.46 | 0.42 | 0.80 | 0.46 | 0.41 | 0.97 | 0.94 | 0.96 | 0.67 | 0.40 | 0.39 | 0.96 |
| 23 | 0.73 | 0.52 | 0.75 | 0.81 | 0.62 | 0.61 | 0.86 | 0.63 | 0.61 | 0.97 | 0.95 | 0.96 | 0.68 | 0.52 | 0.53 | 0.96 |
| 24 | 0.41 | 0.38 | 0.47 | 0.83 | 0.54 | 0.61 | 0.86 | 0.58 | 0.66 | 0.95 | 0.94 | 0.94 | 0.42 | 0.54 | 0.58 | 0.94 |
| 25 | 0.65 | 0.60 | 0.43 | 0.76 | 0.84 | 0.54 | 0.78 | 0.88 | 0.61 | 0.96 | 0.96 | 0.91 | 0.63 | 0.54 | 0.61 | 0.94 |
| 26 | 0.69 | 0.62 | 0.58 | 0.44 | 0.61 | 0.69 | 0.46 | 0.60 | 0.72 | 0.94 | 0.95 | 0.95 | 0.63 | 0.44 | 0.46 | 0.94 |
| 27 | 0.82 | 0.49 | 0.56 | 0.44 | 0.31 | 0.35 | 0.45 | 0.32 | 0.36 | 0.97 | 0.93 | 0.92 | 0.52 | 0.23 | 0.24 | 0.94 |
| 28 | 0.62 | 0.53 | 0.60 | 0.78 | 0.53 | 0.50 | 0.79 | 0.56 | 0.50 | 0.97 | 0.95 | 0.94 | 0.56 | 0.44 | 0.46 | 0.96 |
| 29 | 0.56 | 0.38 | 0.45 | 0.83 | 0.50 | 0.51 | 0.85 | 0.51 | 0.59 | 0.97 | 0.93 | 0.92 | 0.55 | 0.45 | 0.50 | 0.95 |
| 30 | 0.57 | 0.55 | 0.51 | 0.67 | 0.56 | 0.66 | 0.70 | 0.60 | 0.69 | 0.94 | 0.93 | 0.95 | 0.57 | 0.49 | 0.52 | 0.94 |

## A.3. 2D and 3D Shape Descriptors of Sand B

The values of the determined 2D and 3D shape descriptors of Sand B are presented in the following tables. The results are presented for all particle size ranges of the sample.

Table A.5. Determined 2D and 3D shape descriptors of Sand B grains retained on sieve #20, PR = 16.90, PSR = 0.850 – 2.00 mm.

| Part | $R_{2D}$ | | | $S_{2D}$ | | | $AR_{2D}$ | | | $CX_{2D}$ | | | | | | |
|---|---|---|---|---|---|---|---|---|---|---|---|---|---|---|---|---|
| No. | $F_D$ | $F_1$ | $F_2$ | $F_D$ | $F_1$ | $F_2$ | $F_D$ | $F_1$ | $F_2$ | $F_D$ | $F_1$ | $F_2$ | $R_{3D}$ | $S_{3D}$ | $AR_{3D}$ | $CX_{3D}$ |
| 1 | 0.49 | 0.58 | 0.66 | 0.74 | 0.42 | 0.47 | 0.87 | 0.42 | 0.47 | 0.98 | 0.97 | 0.98 | 0.64 | 0.40 | 0.41 | 0.98 |
| 2 | 0.42 | 0.46 | 0.51 | 0.63 | 0.71 | 0.62 | 0.67 | 0.75 | 0.66 | 0.95 | 0.96 | 0.97 | 0.46 | 0.61 | 0.65 | 0.96 |
| 3 | 0.41 | 0.42 | 0.42 | 0.67 | 0.73 | 0.76 | 0.71 | 0.76 | 0.79 | 0.97 | 0.97 | 0.98 | 0.43 | 0.61 | 0.63 | 0.97 |
| 4 | 0.38 | 0.53 | 0.52 | 0.50 | 0.73 | 0.47 | 0.57 | 0.81 | 0.48 | 0.92 | 0.97 | 0.94 | 0.50 | 0.44 | 0.47 | 0.94 |
| 5 | 0.47 | 0.53 | 0.49 | 0.60 | 0.50 | 0.52 | 0.67 | 0.52 | 0.53 | 0.95 | 0.96 | 0.97 | 0.55 | 0.45 | 0.47 | 0.96 |
| 6 | 0.41 | 0.46 | 0.49 | 0.71 | 0.55 | 0.47 | 0.74 | 0.58 | 0.49 | 0.97 | 0.95 | 0.96 | 0.54 | 0.42 | 0.45 | 0.96 |
| 7 | 0.42 | 0.48 | 0.51 | 0.73 | 0.60 | 0.69 | 0.77 | 0.63 | 0.75 | 0.97 | 0.97 | 0.97 | 0.50 | 0.56 | 0.61 | 0.97 |
| 8 | 0.50 | 0.57 | 0.58 | 0.55 | 0.42 | 0.41 | 0.69 | 0.44 | 0.42 | 0.92 | 0.94 | 0.94 | 0.59 | 0.34 | 0.36 | 0.93 |
| 9 | 0.41 | 0.44 | 0.61 | 0.53 | 0.55 | 0.38 | 0.58 | 0.57 | 0.40 | 0.95 | 0.96 | 0.93 | 0.48 | 0.35 | 0.37 | 0.95 |
| 10 | 0.53 | 0.67 | 0.50 | 0.63 | 0.65 | 0.54 | 0.71 | 0.67 | 0.55 | 0.95 | 0.98 | 0.97 | 0.58 | 0.49 | 0.50 | 0.97 |
| 11 | 0.48 | 0.65 | 0.39 | 0.59 | 0.51 | 0.58 | 0.59 | 0.52 | 0.58 | 0.98 | 0.97 | 0.96 | 0.54 | 0.49 | 0.49 | 0.97 |
| 12 | 0.47 | 0.37 | 0.52 | 0.77 | 0.57 | 0.58 | 0.84 | 0.58 | 0.63 | 0.97 | 0.96 | 0.96 | 0.51 | 0.52 | 0.54 | 0.97 |
| 13 | 0.43 | 0.51 | 0.51 | 0.66 | 0.53 | 0.70 | 0.69 | 0.55 | 0.72 | 0.96 | 0.97 | 0.96 | 0.48 | 0.52 | 0.54 | 0.96 |
| 14 | 0.36 | 0.42 | 0.47 | 0.54 | 0.53 | 0.64 | 0.58 | 0.59 | 0.65 | 0.92 | 0.94 | 0.97 | 0.43 | 0.51 | 0.55 | 0.94 |
| 15 | 0.44 | 0.64 | 0.57 | 0.75 | 0.51 | 0.49 | 0.78 | 0.53 | 0.53 | 0.99 | 0.95 | 0.94 | 0.58 | 0.44 | 0.46 | 0.96 |
| 16 | 0.47 | 0.51 | 0.72 | 0.72 | 0.48 | 0.44 | 0.84 | 0.49 | 0.45 | 0.97 | 0.96 | 0.97 | 0.62 | 0.40 | 0.43 | 0.97 |
| 17 | 0.34 | 0.57 | 0.49 | 0.60 | 0.46 | 0.51 | 0.71 | 0.50 | 0.53 | 0.95 | 0.94 | 0.95 | 0.52 | 0.41 | 0.45 | 0.95 |
| 18 | 0.36 | 0.68 | 0.42 | 0.58 | 0.48 | 0.59 | 0.70 | 0.50 | 0.67 | 0.90 | 0.97 | 0.95 | 0.52 | 0.48 | 0.50 | 0.93 |
| 19 | 0.46 | 0.63 | 0.62 | 0.77 | 0.53 | 0.52 | 0.82 | 0.56 | 0.53 | 0.96 | 0.95 | 0.98 | 0.61 | 0.48 | 0.51 | 0.96 |
| 20 | 0.51 | 0.47 | 0.49 | 0.62 | 0.56 | 0.57 | 0.65 | 0.60 | 0.60 | 0.96 | 0.94 | 0.96 | 0.51 | 0.50 | 0.54 | 0.96 |
| 21 | 0.53 | 0.44 | 0.43 | 0.70 | 0.51 | 0.60 | 0.79 | 0.52 | 0.60 | 0.97 | 0.97 | 0.97 | 0.55 | 0.48 | 0.49 | 0.97 |
| 22 | 0.54 | 0.54 | 0.58 | 0.53 | 0.53 | 0.56 | 0.55 | 0.55 | 0.56 | 0.97 | 0.97 | 0.98 | 0.57 | 0.42 | 0.44 | 0.97 |
| 23 | 0.43 | 0.55 | 0.44 | 0.60 | 0.46 | 0.32 | 0.68 | 0.47 | 0.32 | 0.94 | 0.95 | 0.95 | 0.56 | 0.32 | 0.32 | 0.94 |
| 24 | 0.48 | 0.46 | 0.48 | 0.66 | 0.42 | 0.52 | 0.71 | 0.43 | 0.53 | 0.97 | 0.97 | 0.96 | 0.51 | 0.41 | 0.43 | 0.97 |
| 25 | 0.32 | 0.62 | 0.58 | 0.69 | 0.67 | 0.57 | 0.73 | 0.69 | 0.59 | 0.92 | 0.97 | 0.97 | 0.54 | 0.56 | 0.58 | 0.95 |
| 26 | 0.56 | 0.55 | 0.53 | 0.49 | 0.44 | 0.52 | 0.50 | 0.45 | 0.57 | 0.96 | 0.93 | 0.96 | 0.59 | 0.36 | 0.38 | 0.95 |
| 27 | 0.47 | 0.55 | 0.68 | 0.63 | 0.49 | 0.61 | 0.71 | 0.49 | 0.61 | 0.92 | 0.98 | 0.98 | 0.58 | 0.46 | 0.47 | 0.95 |
| 28 | 0.60 | 0.45 | 0.58 | 0.55 | 0.58 | 0.57 | 0.55 | 0.62 | 0.58 | 0.97 | 0.91 | 0.97 | 0.46 | 0.47 | 0.52 | 0.96 |
| 29 | 0.62 | 0.49 | 0.57 | 0.61 | 0.69 | 0.62 | 0.63 | 0.78 | 0.64 | 0.97 | 0.97 | 0.98 | 0.53 | 0.51 | 0.56 | 0.97 |
| 30 | 0.53 | 0.26 | 0.59 | 0.73 | 0.72 | 0.68 | 0.74 | 0.78 | 0.82 | 0.98 | 0.97 | 0.97 | 0.48 | 0.67 | 0.72 | 0.97 |

Table A.6. Determined 2D and 3D shape descriptors of Sand B grains retained on sieve #40, PR = 35.42, PSR = 0.425 – 0.850 mm.

| Part | $R_{2D}$ | | | $S_{2D}$ | | | $AR_{2D}$ | | | $CX_{2D}$ | | | | | | |
|---|---|---|---|---|---|---|---|---|---|---|---|---|---|---|---|---|
| No. | $F_D$ | $F_1$ | $F_2$ | $F_D$ | $F_1$ | $F_2$ | $F_D$ | $F_1$ | $F_2$ | $F_D$ | $F_1$ | $F_2$ | $R_{3D}$ | $S_{3D}$ | $AR_{3D}$ | $CX_{3D}$ |
| 1 | 0.47 | 0.53 | 0.55 | 0.56 | 0.71 | 0.49 | 0.63 | 0.74 | 0.50 | 0.94 | 0.97 | 0.97 | 0.53 | 0.49 | 0.50 | 0.96 |
| 2 | 0.38 | 0.42 | 0.51 | 0.64 | 0.67 | 0.46 | 0.71 | 0.70 | 0.48 | 0.93 | 0.95 | 0.93 | 0.48 | 0.46 | 0.48 | 0.94 |
| 3 | 0.46 | 0.55 | 0.52 | 0.74 | 0.60 | 0.60 | 0.76 | 0.60 | 0.61 | 0.94 | 0.97 | 0.96 | 0.53 | 0.52 | 0.53 | 0.96 |
| 4 | 0.44 | 0.41 | 0.49 | 0.74 | 0.76 | 0.76 | 0.79 | 0.83 | 0.83 | 0.96 | 0.97 | 0.96 | 0.44 | 0.73 | 0.79 | 0.96 |
| 5 | 0.42 | 0.44 | 0.50 | 0.79 | 0.52 | 0.65 | 0.86 | 0.56 | 0.69 | 0.97 | 0.96 | 0.96 | 0.48 | 0.52 | 0.56 | 0.96 |
| 6 | 0.52 | 0.43 | 0.54 | 0.70 | 0.64 | 0.79 | 0.71 | 0.66 | 0.81 | 0.98 | 0.97 | 0.98 | 0.51 | 0.59 | 0.61 | 0.97 |
| 7 | 0.33 | 0.58 | 0.55 | 0.63 | 0.48 | 0.61 | 0.63 | 0.49 | 0.62 | 0.96 | 0.97 | 0.98 | 0.49 | 0.46 | 0.47 | 0.97 |
| 8 | 0.57 | 0.62 | 0.62 | 0.60 | 0.50 | 0.74 | 0.60 | 0.53 | 0.75 | 0.97 | 0.96 | 0.98 | 0.60 | 0.49 | 0.49 | 0.97 |
| 9 | 0.48 | 0.55 | 0.58 | 0.53 | 0.55 | 0.52 | 0.54 | 0.56 | 0.53 | 0.98 | 0.97 | 0.97 | 0.56 | 0.46 | 0.47 | 0.97 |
| 10 | 0.49 | 0.48 | 0.61 | 0.65 | 0.68 | 0.57 | 0.67 | 0.70 | 0.60 | 0.96 | 0.98 | 0.97 | 0.56 | 0.52 | 0.53 | 0.97 |
| 11 | 0.49 | 0.53 | 0.44 | 0.81 | 0.71 | 0.68 | 0.83 | 0.75 | 0.80 | 0.98 | 0.98 | 0.94 | 0.52 | 0.64 | 0.74 | 0.97 |
| 12 | 0.46 | 0.45 | 0.49 | 0.69 | 0.58 | 0.64 | 0.70 | 0.59 | 0.70 | 0.97 | 0.95 | 0.94 | 0.49 | 0.53 | 0.57 | 0.96 |
| 13 | 0.48 | 0.42 | 0.40 | 0.63 | 0.50 | 0.57 | 0.65 | 0.50 | 0.62 | 0.97 | 0.96 | 0.94 | 0.48 | 0.47 | 0.50 | 0.96 |
| 14 | 0.48 | 0.42 | 0.44 | 0.60 | 0.23 | 0.23 | 0.64 | 0.25 | 0.23 | 0.96 | 0.90 | 0.89 | 0.44 | 0.19 | 0.20 | 0.94 |
| 15 | 0.45 | 0.41 | 0.62 | 0.58 | 0.50 | 0.71 | 0.64 | 0.58 | 0.80 | 0.95 | 0.93 | 0.97 | 0.53 | 0.49 | 0.57 | 0.95 |
| 16 | 0.40 | 0.61 | 0.62 | 0.79 | 0.72 | 0.64 | 0.84 | 0.76 | 0.71 | 0.97 | 0.97 | 0.96 | 0.54 | 0.63 | 0.71 | 0.96 |
| 17 | 0.36 | 0.54 | 0.46 | 0.73 | 0.63 | 0.66 | 0.77 | 0.69 | 0.69 | 0.97 | 0.95 | 0.97 | 0.48 | 0.58 | 0.63 | 0.96 |
| 18 | 0.35 | 0.52 | 0.37 | 0.78 | 0.78 | 0.72 | 0.89 | 0.83 | 0.85 | 0.96 | 0.97 | 0.95 | 0.44 | 0.70 | 0.81 | 0.96 |
| 19 | 0.39 | 0.57 | 0.61 | 0.69 | 0.55 | 0.51 | 0.73 | 0.55 | 0.52 | 0.96 | 0.98 | 0.98 | 0.57 | 0.50 | 0.50 | 0.97 |
| 20 | 0.36 | 0.55 | 0.50 | 0.69 | 0.55 | 0.64 | 0.71 | 0.57 | 0.69 | 0.96 | 0.96 | 0.96 | 0.51 | 0.52 | 0.55 | 0.96 |
| 21 | 0.43 | 0.51 | 0.49 | 0.60 | 0.61 | 0.60 | 0.68 | 0.62 | 0.69 | 0.95 | 0.97 | 0.95 | 0.51 | 0.54 | 0.61 | 0.96 |
| 22 | 0.52 | 0.40 | 0.48 | 0.72 | 0.72 | 0.63 | 0.80 | 0.74 | 0.79 | 0.96 | 0.97 | 0.94 | 0.49 | 0.59 | 0.73 | 0.95 |
| 23 | 0.57 | 0.50 | 0.59 | 0.62 | 0.69 | 0.58 | 0.64 | 0.78 | 0.60 | 0.97 | 0.96 | 0.96 | 0.54 | 0.51 | 0.57 | 0.96 |
| 24 | 0.46 | 0.55 | 0.53 | 0.62 | 0.51 | 0.61 | 0.67 | 0.55 | 0.64 | 0.96 | 0.94 | 0.96 | 0.53 | 0.49 | 0.51 | 0.96 |
| 25 | 0.42 | 0.71 | 0.57 | 0.78 | 0.54 | 0.59 | 0.82 | 0.54 | 0.59 | 0.97 | 0.98 | 0.96 | 0.62 | 0.53 | 0.53 | 0.97 |
| 26 | 0.56 | 0.60 | 0.49 | 0.66 | 0.58 | 0.52 | 0.67 | 0.60 | 0.54 | 0.98 | 0.97 | 0.95 | 0.53 | 0.51 | 0.53 | 0.97 |
| 27 | 0.44 | 0.63 | 0.54 | 0.60 | 0.42 | 0.62 | 0.68 | 0.43 | 0.62 | 0.96 | 0.97 | 0.97 | 0.59 | 0.42 | 0.43 | 0.97 |
| 28 | 0.55 | 0.58 | 0.55 | 0.71 | 0.66 | 0.56 | 0.74 | 0.66 | 0.56 | 0.98 | 0.98 | 0.98 | 0.61 | 0.54 | 0.55 | 0.98 |
| 29 | 0.35 | 0.42 | 0.36 | 0.77 | 0.65 | 0.73 | 0.80 | 0.71 | 0.84 | 0.96 | 0.94 | 0.95 | 0.39 | 0.61 | 0.70 | 0.95 |
| 30 | 0.34 | 0.52 | 0.55 | 0.69 | 0.54 | 0.56 | 0.75 | 0.55 | 0.58 | 0.95 | 0.97 | 0.97 | 0.54 | 0.43 | 0.44 | 0.96 |

Table A.7. Determined 2D and 3D shape descriptors of Sand B grains retained on sieve #60, PR = 22.01, PSR = 0.250 – 0.425 mm.

| Part | $R_{2D}$ | | | $S_{2D}$ | | | $AR_{2D}$ | | | $CX_{2D}$ | | | | | | |
|---|---|---|---|---|---|---|---|---|---|---|---|---|---|---|---|---|
| No. | $F_D$ | $F_1$ | $F_2$ | $F_D$ | $F_1$ | $F_2$ | $F_D$ | $F_1$ | $F_2$ | $F_D$ | $F_1$ | $F_2$ | $R_{3D}$ | $S_{3D}$ | $AR_{3D}$ | $CX_{3D}$ |
| 1 | 0.54 | 0.65 | 0.55 | 0.74 | 0.67 | 0.78 | 0.75 | 0.68 | 0.84 | 0.97 | 0.97 | 0.96 | 0.57 | 0.63 | 0.66 | 0.97 |
| 2 | 0.56 | 0.50 | 0.50 | 0.69 | 0.57 | 0.46 | 0.75 | 0.59 | 0.47 | 0.95 | 0.95 | 0.96 | 0.52 | 0.46 | 0.47 | 0.95 |
| 3 | 0.34 | 0.56 | 0.52 | 0.67 | 0.64 | 0.53 | 0.71 | 0.64 | 0.55 | 0.93 | 0.96 | 0.94 | 0.50 | 0.52 | 0.55 | 0.94 |
| 4 | 0.53 | 0.57 | 0.49 | 0.80 | 0.73 | 0.71 | 0.83 | 0.74 | 0.78 | 0.96 | 0.97 | 0.96 | 0.54 | 0.70 | 0.70 | 0.96 |
| 5 | 0.34 | 0.56 | 0.66 | 0.62 | 0.32 | 0.31 | 0.69 | 0.34 | 0.33 | 0.92 | 0.92 | 0.95 | 0.56 | 0.27 | 0.29 | 0.92 |
| 6 | 0.43 | 0.46 | 0.47 | 0.72 | 0.69 | 0.77 | 0.74 | 0.81 | 0.90 | 0.97 | 0.93 | 0.97 | 0.45 | 0.69 | 0.71 | 0.96 |
| 7 | 0.41 | 0.57 | 0.61 | 0.65 | 0.70 | 0.62 | 0.84 | 0.70 | 0.73 | 0.92 | 0.96 | 0.93 | 0.58 | 0.54 | 0.65 | 0.94 |
| 8 | 0.45 | 0.64 | 0.57 | 0.80 | 0.70 | 0.48 | 0.80 | 0.72 | 0.54 | 0.97 | 0.96 | 0.92 | 0.63 | 0.48 | 0.54 | 0.95 |
| 9 | 0.47 | 0.44 | 0.38 | 0.71 | 0.70 | 0.62 | 0.85 | 0.75 | 0.71 | 0.96 | 0.95 | 0.92 | 0.48 | 0.58 | 0.70 | 0.95 |
| 10 | 0.38 | 0.47 | 0.54 | 0.75 | 0.60 | 0.49 | 0.79 | 0.61 | 0.50 | 0.95 | 0.96 | 0.96 | 0.52 | 0.49 | 0.50 | 0.96 |
| 11 | 0.47 | 0.44 | 0.68 | 0.80 | 0.57 | 0.51 | 0.90 | 0.58 | 0.55 | 0.97 | 0.95 | 0.94 | 0.58 | 0.48 | 0.55 | 0.96 |
| 12 | 0.54 | 0.54 | 0.62 | 0.62 | 0.52 | 0.50 | 0.66 | 0.55 | 0.51 | 0.95 | 0.94 | 0.93 | 0.61 | 0.42 | 0.44 | 0.94 |
| 13 | 0.57 | 0.60 | 0.56 | 0.57 | 0.51 | 0.38 | 0.62 | 0.54 | 0.40 | 0.96 | 0.95 | 0.94 | 0.63 | 0.37 | 0.39 | 0.95 |
| 14 | 0.41 | 0.49 | 0.64 | 0.66 | 0.66 | 0.44 | 0.74 | 0.66 | 0.53 | 0.94 | 0.96 | 0.87 | 0.62 | 0.39 | 0.49 | 0.92 |
| 15 | 0.68 | 0.69 | 0.65 | 0.55 | 0.58 | 0.46 | 0.55 | 0.58 | 0.47 | 0.96 | 0.96 | 0.96 | 0.65 | 0.37 | 0.38 | 0.96 |
| 16 | 0.42 | 0.58 | 0.49 | 0.74 | 0.55 | 0.49 | 0.81 | 0.56 | 0.50 | 0.96 | 0.95 | 0.95 | 0.56 | 0.48 | 0.49 | 0.95 |
| 17 | 0.61 | 0.59 | 0.45 | 0.73 | 0.57 | 0.54 | 0.84 | 0.58 | 0.56 | 0.96 | 0.96 | 0.95 | 0.56 | 0.49 | 0.50 | 0.96 |
| 18 | 0.62 | 0.59 | 0.46 | 0.70 | 0.49 | 0.57 | 0.72 | 0.51 | 0.57 | 0.97 | 0.96 | 0.96 | 0.62 | 0.47 | 0.49 | 0.97 |
| 19 | 0.51 | 0.49 | 0.44 | 0.69 | 0.54 | 0.67 | 0.73 | 0.55 | 0.67 | 0.97 | 0.96 | 0.96 | 0.48 | 0.50 | 0.52 | 0.96 |
| 20 | 0.54 | 0.46 | 0.56 | 0.80 | 0.78 | 0.81 | 0.84 | 0.82 | 0.86 | 0.97 | 0.96 | 0.97 | 0.51 | 0.71 | 0.75 | 0.97 |
| 21 | 0.49 | 0.57 | 0.43 | 0.72 | 0.45 | 0.42 | 0.74 | 0.46 | 0.43 | 0.96 | 0.95 | 0.96 | 0.59 | 0.39 | 0.40 | 0.96 |
| 22 | 0.53 | 0.52 | 0.56 | 0.81 | 0.52 | 0.57 | 0.84 | 0.52 | 0.58 | 0.96 | 0.95 | 0.94 | 0.56 | 0.47 | 0.49 | 0.95 |
| 23 | 0.39 | 0.45 | 0.63 | 0.81 | 0.50 | 0.50 | 0.84 | 0.50 | 0.52 | 0.96 | 0.94 | 0.94 | 0.58 | 0.44 | 0.45 | 0.95 |
| 24 | 0.52 | 0.68 | 0.55 | 0.60 | 0.45 | 0.70 | 0.64 | 0.46 | 0.71 | 0.96 | 0.93 | 0.97 | 0.64 | 0.44 | 0.45 | 0.95 |
| 25 | 0.45 | 0.63 | 0.55 | 0.63 | 0.54 | 0.58 | 0.66 | 0.55 | 0.60 | 0.97 | 0.97 | 0.97 | 0.56 | 0.50 | 0.53 | 0.97 |
| 26 | 0.52 | 0.71 | 0.50 | 0.67 | 0.48 | 0.41 | 0.74 | 0.48 | 0.42 | 0.96 | 0.96 | 0.96 | 0.65 | 0.36 | 0.36 | 0.96 |
| 27 | 0.44 | 0.57 | 0.35 | 0.70 | 0.61 | 0.63 | 0.73 | 0.61 | 0.69 | 0.97 | 0.96 | 0.94 | 0.49 | 0.49 | 0.54 | 0.96 |
| 28 | 0.53 | 0.54 | 0.71 | 0.62 | 0.55 | 0.49 | 0.62 | 0.55 | 0.50 | 0.97 | 0.96 | 0.95 | 0.62 | 0.42 | 0.44 | 0.96 |
| 29 | 0.45 | 0.49 | 0.38 | 0.86 | 0.43 | 0.38 | 0.92 | 0.44 | 0.41 | 0.97 | 0.91 | 0.88 | 0.62 | 0.36 | 0.40 | 0.94 |
| 30 | 0.56 | 0.54 | 0.37 | 0.61 | 0.61 | 0.60 | 0.62 | 0.68 | 0.70 | 0.97 | 0.93 | 0.96 | 0.54 | 0.48 | 0.54 | 0.96 |

Table A.8. Determined 2D and 3D shape descriptors of Sand B grains retained on sieve #100, PR = 20.07, PSR = 0.150 – 0.250 mm.

| Part | $R_{2D}$ | | | $S_{2D}$ | | | $AR_{2D}$ | | | $CX_{2D}$ | | | | | | |
|---|---|---|---|---|---|---|---|---|---|---|---|---|---|---|---|---|
| No. | $F_D$ | $F_1$ | $F_2$ | $F_D$ | $F_1$ | $F_2$ | $F_D$ | $F_1$ | $F_2$ | $F_D$ | $F_1$ | $F_2$ | $R_{3D}$ | $S_{3D}$ | $AR_{3D}$ | $CX_{3D}$ |
| 1 | 0.43 | 0.50 | 0.53 | 0.74 | 0.51 | 0.37 | 0.74 | 0.50 | 0.41 | 0.96 | 0.95 | 0.92 | 0.63 | 0.34 | 0.38 | 0.95 |
| 2 | 0.63 | 0.66 | 0.58 | 0.60 | 0.45 | 0.68 | 0.63 | 0.47 | 0.70 | 0.97 | 0.92 | 0.96 | 0.64 | 0.43 | 0.45 | 0.95 |
| 3 | 0.71 | 0.64 | 0.59 | 0.67 | 0.66 | 0.69 | 0.67 | 0.70 | 0.71 | 0.97 | 0.94 | 0.97 | 0.65 | 0.58 | 0.62 | 0.96 |
| 4 | 0.65 | 0.43 | 0.52 | 0.75 | 0.65 | 0.81 | 0.76 | 0.66 | 0.82 | 0.98 | 0.95 | 0.97 | 0.56 | 0.62 | 0.62 | 0.97 |
| 5 | 0.56 | 0.48 | 0.69 | 0.76 | 0.66 | 0.61 | 0.76 | 0.71 | 0.59 | 0.96 | 0.95 | 0.96 | 0.57 | 0.57 | 0.59 | 0.96 |
| 6 | 0.59 | 0.59 | 0.49 | 0.59 | 0.48 | 0.74 | 0.59 | 0.49 | 0.79 | 0.97 | 0.95 | 0.95 | 0.58 | 0.46 | 0.47 | 0.96 |
| 7 | 0.69 | 0.47 | 0.51 | 0.64 | 0.44 | 0.73 | 0.64 | 0.47 | 0.71 | 0.97 | 0.94 | 0.98 | 0.52 | 0.41 | 0.41 | 0.96 |
| 8 | 0.51 | 0.62 | 0.60 | 0.77 | 0.73 | 0.74 | 0.87 | 0.75 | 0.79 | 0.96 | 0.97 | 0.96 | 0.61 | 0.68 | 0.73 | 0.96 |
| 9 | 0.55 | 0.61 | 0.64 | 0.63 | 0.31 | 0.43 | 0.64 | 0.33 | 0.44 | 0.96 | 0.94 | 0.94 | 0.65 | 0.29 | 0.30 | 0.95 |
| 10 | 0.48 | 0.52 | 0.68 | 0.81 | 0.49 | 0.50 | 0.89 | 0.49 | 0.50 | 0.96 | 0.92 | 0.94 | 0.64 | 0.46 | 0.46 | 0.94 |
| 11 | 0.67 | 0.64 | 0.65 | 0.62 | 0.58 | 0.52 | 0.61 | 0.57 | 0.52 | 0.97 | 0.96 | 0.94 | 0.65 | 0.45 | 0.46 | 0.96 |
| 12 | 0.51 | 0.57 | 0.59 | 0.51 | 0.54 | 0.76 | 0.51 | 0.56 | 0.81 | 0.96 | 0.96 | 0.95 | 0.60 | 0.48 | 0.48 | 0.96 |
| 13 | 0.65 | 0.64 | 0.72 | 0.68 | 0.61 | 0.70 | 0.69 | 0.63 | 0.70 | 0.97 | 0.96 | 0.97 | 0.66 | 0.59 | 0.61 | 0.97 |
| 14 | 0.76 | 0.48 | 0.64 | 0.47 | 0.80 | 0.43 | 0.49 | 0.88 | 0.48 | 0.94 | 0.95 | 0.91 | 0.64 | 0.43 | 0.47 | 0.93 |
| 15 | 0.54 | 0.65 | 0.48 | 0.76 | 0.74 | 0.70 | 0.83 | 0.74 | 0.72 | 0.96 | 0.97 | 0.95 | 0.60 | 0.60 | 0.61 | 0.96 |
| 16 | 0.48 | 0.61 | 0.46 | 0.67 | 0.61 | 0.43 | 0.70 | 0.61 | 0.47 | 0.95 | 0.97 | 0.94 | 0.63 | 0.43 | 0.47 | 0.95 |
| 17 | 0.62 | 0.49 | 0.59 | 0.58 | 0.46 | 0.68 | 0.60 | 0.47 | 0.70 | 0.97 | 0.96 | 0.97 | 0.58 | 0.45 | 0.46 | 0.96 |
| 18 | 0.60 | 0.52 | 0.47 | 0.54 | 0.57 | 0.43 | 0.57 | 0.59 | 0.46 | 0.95 | 0.95 | 0.94 | 0.54 | 0.38 | 0.40 | 0.94 |
| 19 | 0.54 | 0.59 | 0.57 | 0.70 | 0.61 | 0.57 | 0.70 | 0.64 | 0.59 | 0.97 | 0.96 | 0.96 | 0.63 | 0.50 | 0.53 | 0.96 |
| 20 | 0.44 | 0.54 | 0.47 | 0.63 | 0.59 | 0.71 | 0.65 | 0.64 | 0.71 | 0.96 | 0.92 | 0.96 | 0.51 | 0.55 | 0.56 | 0.94 |
| 21 | 0.45 | 0.48 | 0.61 | 0.58 | 0.55 | 0.51 | 0.68 | 0.57 | 0.53 | 0.91 | 0.92 | 0.94 | 0.55 | 0.41 | 0.43 | 0.92 |
| 22 | 0.58 | 0.64 | 0.68 | 0.71 | 0.70 | 0.75 | 0.78 | 0.71 | 0.76 | 0.95 | 0.97 | 0.96 | 0.64 | 0.64 | 0.64 | 0.96 |
| 23 | 0.39 | 0.44 | 0.57 | 0.62 | 0.62 | 0.52 | 0.67 | 0.64 | 0.53 | 0.95 | 0.96 | 0.94 | 0.55 | 0.43 | 0.44 | 0.95 |
| 24 | 0.43 | 0.48 | 0.45 | 0.63 | 0.53 | 0.77 | 0.64 | 0.54 | 0.83 | 0.96 | 0.96 | 0.96 | 0.48 | 0.53 | 0.54 | 0.96 |
| 25 | 0.55 | 0.49 | 0.57 | 0.67 | 0.29 | 0.43 | 0.68 | 0.30 | 0.45 | 0.97 | 0.92 | 0.91 | 0.57 | 0.27 | 0.27 | 0.94 |
| 26 | 0.44 | 0.52 | 0.50 | 0.70 | 0.43 | 0.58 | 0.76 | 0.43 | 0.58 | 0.95 | 0.94 | 0.95 | 0.59 | 0.43 | 0.43 | 0.95 |
| 27 | 0.57 | 0.65 | 0.57 | 0.58 | 0.46 | 0.51 | 0.60 | 0.45 | 0.50 | 0.96 | 0.96 | 0.96 | 0.67 | 0.36 | 0.36 | 0.96 |
| 28 | 0.48 | 0.51 | 0.39 | 0.62 | 0.74 | 0.62 | 0.64 | 0.72 | 0.64 | 0.96 | 0.96 | 0.96 | 0.48 | 0.58 | 0.57 | 0.96 |
| 29 | 0.64 | 0.68 | 0.54 | 0.48 | 0.60 | 0.66 | 0.52 | 0.62 | 0.66 | 0.95 | 0.96 | 0.97 | 0.65 | 0.48 | 0.52 | 0.96 |
| 30 | 0.55 | 0.58 | 0.47 | 0.55 | 0.48 | 0.43 | 0.61 | 0.49 | 0.49 | 0.91 | 0.89 | 0.87 | 0.60 | 0.36 | 0.40 | 0.89 |

Table A.9. Determined 2D and 3D shape descriptors of Sand B grains retained on sieve #140, PR = 5.60, PSR = 0.106 – 0.150 mm.

| Part | $R_{2D}$ | | | $S_{2D}$ | | | $AR_{2D}$ | | | $CX_{2D}$ | | | | | | |
|---|---|---|---|---|---|---|---|---|---|---|---|---|---|---|---|---|
| No. | $F_D$ | $F_1$ | $F_2$ | $F_D$ | $F_1$ | $F_2$ | $F_D$ | $F_1$ | $F_2$ | $F_D$ | $F_1$ | $F_2$ | $R_{3D}$ | $S_{3D}$ | $AR_{3D}$ | $CX_{3D}$ |
| 1 | 0.71 | 0.60 | 0.66 | 0.62 | 0.69 | 0.67 | 0.61 | 0.66 | 0.69 | 0.95 | 0.95 | 0.96 | 0.67 | 0.46 | 0.44 | 0.95 |
| 2 | 0.52 | 0.69 | 0.64 | 0.75 | 0.85 | 0.61 | 0.79 | 0.83 | 0.59 | 0.95 | 0.95 | 0.96 | 0.65 | 0.61 | 0.59 | 0.95 |
| 3 | 0.71 | 0.68 | 0.63 | 0.70 | 0.72 | 0.72 | 0.67 | 0.69 | 0.72 | 0.96 | 0.96 | 0.96 | 0.68 | 0.68 | 0.65 | 0.96 |
| 4 | 0.37 | 0.29 | 0.60 | 0.73 | 0.30 | 0.34 | 0.79 | 0.30 | 0.35 | 0.95 | 0.90 | 0.91 | 0.56 | 0.28 | 0.28 | 0.93 |
| 5 | 0.60 | 0.50 | 0.56 | 0.78 | 0.62 | 0.53 | 0.79 | 0.69 | 0.54 | 0.95 | 0.90 | 0.94 | 0.70 | 0.34 | 0.38 | 0.93 |
| 6 | 0.59 | 0.66 | 0.63 | 0.49 | 0.55 | 0.60 | 0.49 | 0.56 | 0.60 | 0.93 | 0.94 | 0.95 | 0.65 | 0.46 | 0.46 | 0.94 |
| 7 | 0.41 | 0.68 | 0.72 | 0.77 | 0.45 | 0.61 | 0.76 | 0.45 | 0.60 | 0.96 | 0.94 | 0.94 | 0.74 | 0.42 | 0.42 | 0.95 |
| 8 | 0.64 | 0.68 | 0.44 | 0.68 | 0.81 | 0.49 | 0.74 | 0.79 | 0.52 | 0.94 | 0.96 | 0.92 | 0.66 | 0.48 | 0.52 | 0.94 |
| 9 | 0.61 | 0.67 | 0.53 | 0.58 | 0.61 | 0.66 | 0.59 | 0.63 | 0.66 | 0.95 | 0.95 | 0.94 | 0.58 | 0.49 | 0.51 | 0.94 |
| 10 | 0.58 | 0.69 | 0.60 | 0.78 | 0.66 | 0.84 | 0.80 | 0.66 | 0.87 | 0.96 | 0.96 | 0.96 | 0.64 | 0.64 | 0.66 | 0.96 |
| 11 | 0.66 | 0.56 | 0.53 | 0.76 | 0.62 | 0.63 | 0.76 | 0.63 | 0.67 | 0.96 | 0.95 | 0.96 | 0.66 | 0.51 | 0.56 | 0.95 |
| 12 | 0.46 | 0.62 | 0.64 | 0.59 | 0.53 | 0.80 | 0.61 | 0.53 | 0.76 | 0.96 | 0.95 | 0.95 | 0.62 | 0.51 | 0.49 | 0.95 |
| 13 | 0.60 | 0.58 | 0.59 | 0.78 | 0.45 | 0.59 | 0.81 | 0.47 | 0.58 | 0.96 | 0.93 | 0.94 | 0.65 | 0.42 | 0.42 | 0.95 |
| 14 | 0.48 | 0.60 | 0.69 | 0.64 | 0.57 | 0.62 | 0.68 | 0.55 | 0.63 | 0.92 | 0.95 | 0.95 | 0.62 | 0.57 | 0.55 | 0.94 |
| 15 | 0.69 | 0.68 | 0.68 | 0.70 | 0.80 | 0.89 | 0.70 | 0.76 | 0.89 | 0.95 | 0.97 | 0.96 | 0.71 | 0.70 | 0.70 | 0.96 |
| 16 | 0.57 | 0.60 | 0.55 | 0.72 | 0.62 | 0.65 | 0.72 | 0.61 | 0.63 | 0.96 | 0.96 | 0.96 | 0.57 | 0.53 | 0.52 | 0.96 |
| 17 | 0.61 | 0.49 | 0.64 | 0.75 | 0.48 | 0.72 | 0.77 | 0.49 | 0.71 | 0.96 | 0.95 | 0.96 | 0.63 | 0.48 | 0.49 | 0.95 |
| 18 | 0.70 | 0.58 | 0.59 | 0.79 | 0.81 | 0.74 | 0.79 | 0.82 | 0.74 | 0.95 | 0.96 | 0.95 | 0.62 | 0.69 | 0.70 | 0.95 |
| 19 | 0.71 | 0.63 | 0.58 | 0.60 | 0.59 | 0.46 | 0.60 | 0.60 | 0.45 | 0.96 | 0.95 | 0.95 | 0.67 | 0.46 | 0.45 | 0.95 |
| 20 | 0.59 | 0.49 | 0.62 | 0.68 | 0.80 | 0.61 | 0.74 | 0.80 | 0.60 | 0.96 | 0.95 | 0.95 | 0.57 | 0.52 | 0.54 | 0.95 |
| 21 | 0.45 | 0.74 | 0.63 | 0.57 | 0.67 | 0.82 | 0.59 | 0.68 | 0.83 | 0.94 | 0.96 | 0.96 | 0.65 | 0.51 | 0.53 | 0.95 |
| 22 | 0.74 | 0.70 | 0.67 | 0.54 | 0.80 | 0.55 | 0.54 | 0.80 | 0.54 | 0.95 | 0.95 | 0.95 | 0.71 | 0.51 | 0.51 | 0.95 |
| 23 | 0.80 | 0.48 | 0.66 | 0.57 | 0.55 | 0.55 | 0.56 | 0.56 | 0.55 | 0.95 | 0.95 | 0.94 | 0.66 | 0.42 | 0.43 | 0.95 |
| 24 | 0.72 | 0.33 | 0.49 | 0.60 | 0.38 | 0.44 | 0.61 | 0.36 | 0.45 | 0.96 | 0.90 | 0.93 | 0.54 | 0.31 | 0.29 | 0.94 |
| 25 | 0.65 | 0.57 | 0.34 | 0.57 | 0.59 | 0.40 | 0.59 | 0.61 | 0.40 | 0.94 | 0.94 | 0.92 | 0.44 | 0.36 | 0.37 | 0.93 |
| 26 | 0.55 | 0.44 | 0.54 | 0.78 | 0.69 | 0.77 | 0.82 | 0.67 | 0.78 | 0.95 | 0.94 | 0.96 | 0.55 | 0.69 | 0.67 | 0.95 |
| 27 | 0.56 | 0.41 | 0.57 | 0.71 | 0.47 | 0.42 | 0.78 | 0.48 | 0.45 | 0.93 | 0.91 | 0.89 | 0.58 | 0.40 | 0.42 | 0.91 |
| 28 | 0.65 | 0.32 | 0.70 | 0.66 | 0.36 | 0.49 | 0.67 | 0.37 | 0.52 | 0.96 | 0.94 | 0.93 | 0.62 | 0.34 | 0.36 | 0.95 |
| 29 | 0.56 | 0.38 | 0.72 | 0.70 | 0.50 | 0.60 | 0.71 | 0.49 | 0.58 | 0.95 | 0.92 | 0.95 | 0.67 | 0.49 | 0.49 | 0.94 |
| 30 | 0.67 | 0.51 | 0.54 | 0.81 | 0.50 | 0.56 | 0.82 | 0.54 | 0.54 | 0.96 | 0.92 | 0.93 | 0.56 | 0.45 | 0.49 | 0.94 |

## A.4. 2D and 3D Shape Descriptors of Sand C

The values of the determined 2D and 3D shape descriptors of Sand C are presented in the following tables. The results are presented for all particle size ranges of the sample.

Table A.10. Determined 2D and 3D shape descriptors of Sand.

| Part | $R_{2D}$ | | | $S_{2D}$ | | | $AR_{2D}$ | | | $CX_{2D}$ | | | | | | |
|---|---|---|---|---|---|---|---|---|---|---|---|---|---|---|---|---|
| No. | $F_D$ | $F_1$ | $F_2$ | $F_D$ | $F_1$ | $F_2$ | $F_D$ | $F_1$ | $F_2$ | $F_D$ | $F_1$ | $F_2$ | $R_{3D}$ | $S_{3D}$ | $AR_{3D}$ | $CX_{3D}$ |
| 1 | 0.67 | 0.81 | 0.80 | 0.55 | 0.50 | 0.46 | 0.55 | 0.53 | 0.47 | 0.99 | 0.99 | 0.97 | 0.76 | 0.38 | 0.40 | 0.99 |
| 2 | 0.65 | 0.55 | 0.59 | 0.78 | 0.59 | 0.58 | 0.89 | 0.60 | 0.58 | 0.99 | 0.98 | 0.99 | 0.56 | 0.52 | 0.56 | 0.99 |
| 3 | 0.50 | 0.63 | 0.45 | 0.77 | 0.57 | 0.52 | 0.81 | 0.58 | 0.53 | 0.98 | 0.99 | 0.99 | 0.58 | 0.47 | 0.49 | 0.99 |
| 4 | 0.74 | 0.63 | 0.68 | 0.59 | 0.27 | 0.25 | 0.59 | 0.27 | 0.26 | 0.99 | 0.99 | 0.99 | 0.65 | 0.22 | 0.22 | 0.99 |
| 5 | 0.40 | 0.49 | 0.44 | 0.70 | 0.33 | 0.27 | 0.75 | 0.33 | 0.27 | 0.96 | 0.96 | 0.96 | 0.51 | 0.26 | 0.26 | 0.96 |
| 6 | 0.67 | 0.79 | 0.66 | 0.67 | 0.48 | 0.37 | 0.70 | 0.48 | 0.37 | 0.99 | 0.99 | 0.99 | 0.69 | 0.35 | 0.35 | 0.99 |
| 7 | 0.61 | 0.47 | 0.57 | 0.64 | 0.29 | 0.26 | 0.66 | 0.29 | 0.26 | 0.98 | 0.99 | 0.99 | 0.55 | 0.23 | 0.23 | 0.98 |
| 8 | 0.45 | 0.53 | 0.53 | 0.58 | 0.39 | 0.45 | 0.60 | 0.40 | 0.45 | 0.96 | 0.98 | 0.98 | 0.55 | 0.33 | 0.33 | 0.97 |
| 9 | 0.75 | 0.66 | 0.66 | 0.67 | 0.30 | 0.29 | 0.68 | 0.30 | 0.30 | 0.99 | 0.96 | 0.97 | 0.65 | 0.25 | 0.25 | 0.98 |
| 10 | 0.78 | 0.66 | 0.67 | 0.81 | 0.52 | 0.52 | 0.84 | 0.52 | 0.52 | 1.00 | 1.00 | 1.00 | 0.65 | 0.48 | 0.49 | 1.00 |
| 11 | 0.51 | 0.40 | 0.36 | 0.58 | 0.40 | 0.49 | 0.67 | 0.43 | 0.50 | 0.93 | 0.95 | 0.94 | 0.48 | 0.38 | 0.39 | 0.94 |
| 12 | 0.53 | 0.57 | 0.36 | 0.51 | 0.49 | 0.38 | 0.52 | 0.49 | 0.38 | 0.98 | 0.99 | 0.98 | 0.52 | 0.35 | 0.35 | 0.98 |
| 13 | 0.48 | 0.40 | 0.40 | 0.83 | 0.69 | 0.65 | 0.87 | 0.77 | 0.72 | 0.99 | 0.98 | 0.95 | 0.45 | 0.63 | 0.71 | 0.98 |
| 14 | 0.54 | 0.55 | 0.56 | 0.71 | 0.23 | 0.23 | 0.86 | 0.23 | 0.23 | 0.97 | 0.98 | 0.96 | 0.57 | 0.20 | 0.21 | 0.97 |
| 15 | 0.40 | 0.53 | 0.46 | 0.72 | 0.40 | 0.37 | 0.91 | 0.40 | 0.38 | 0.96 | 0.98 | 0.96 | 0.55 | 0.34 | 0.37 | 0.97 |
| 16 | 0.52 | 0.58 | 0.54 | 0.50 | 0.36 | 0.37 | 0.52 | 0.37 | 0.38 | 0.96 | 0.98 | 0.97 | 0.60 | 0.33 | 0.33 | 0.97 |
| 17 | 0.63 | 0.60 | 0.49 | 0.67 | 0.53 | 0.55 | 0.67 | 0.53 | 0.55 | 0.99 | 0.99 | 0.98 | 0.54 | 0.46 | 0.46 | 0.98 |
| 18 | 0.42 | 0.39 | 0.54 | 0.75 | 0.60 | 0.55 | 0.84 | 0.60 | 0.61 | 0.97 | 0.98 | 0.97 | 0.51 | 0.51 | 0.58 | 0.97 |
| 19 | 0.40 | 0.39 | 0.42 | 0.60 | 0.49 | 0.47 | 0.69 | 0.49 | 0.50 | 0.92 | 0.95 | 0.96 | 0.44 | 0.42 | 0.42 | 0.94 |
| 20 | 0.60 | 0.37 | 0.49 | 0.55 | 0.51 | 0.49 | 0.59 | 0.54 | 0.51 | 0.96 | 0.96 | 0.95 | 0.44 | 0.41 | 0.44 | 0.96 |
| 21 | 0.47 | 0.41 | 0.41 | 0.70 | 0.66 | 0.74 | 0.88 | 0.72 | 0.76 | 0.98 | 0.96 | 0.98 | 0.43 | 0.64 | 0.72 | 0.97 |
| 22 | 0.48 | 0.47 | 0.60 | 0.81 | 0.46 | 0.45 | 0.84 | 0.46 | 0.48 | 0.98 | 0.99 | 0.97 | 0.56 | 0.40 | 0.42 | 0.98 |

Table A.10 Determined 2D and 3D shape descriptors of Sand. (cont.)

| Part | $R_{2D}$ | | | $S_{2D}$ | | | $AR_{2D}$ | | | $CX_{2D}$ | | | | | | |
|---|---|---|---|---|---|---|---|---|---|---|---|---|---|---|---|---|
| No. | $F_D$ | $F_1$ | $F_2$ | $F_D$ | $F_1$ | $F_2$ | $F_D$ | $F_1$ | $F_2$ | $F_D$ | $F_1$ | $F_2$ | $R_{3D}$ | $S_{3D}$ | $AR_{3D}$ | $CX_{3D}$ |
| 23 | 0.74 | 0.86 | 0.76 | 0.83 | 0.49 | 0.53 | 0.85 | 0.49 | 0.52 | 1.00 | 0.99 | 1.00 | 0.78 | 0.46 | 0.47 | 0.99 |
| 24 | 0.42 | 0.43 | 0.48 | 0.59 | 0.36 | 0.38 | 0.79 | 0.37 | 0.39 | 0.95 | 0.97 | 0.98 | 0.47 | 0.34 | 0.37 | 0.96 |
| 25 | 0.42 | 0.54 | 0.42 | 0.80 | 0.43 | 0.42 | 0.82 | 0.46 | 0.43 | 0.97 | 0.96 | 0.96 | 0.52 | 0.40 | 0.43 | 0.97 |
| 26 | 0.40 | 0.46 | 0.42 | 0.74 | 0.52 | 0.49 | 0.78 | 0.54 | 0.50 | 0.97 | 0.98 | 0.98 | 0.47 | 0.46 | 0.48 | 0.98 |
| 27 | 0.43 | 0.44 | 0.58 | 0.77 | 0.73 | 0.63 | 0.83 | 0.75 | 0.68 | 0.98 | 0.99 | 0.98 | 0.50 | 0.62 | 0.68 | 0.98 |
| 28 | 0.72 | 0.53 | 0.63 | 0.70 | 0.43 | 0.43 | 0.70 | 0.43 | 0.43 | 0.99 | 1.00 | 0.99 | 0.62 | 0.39 | 0.39 | 0.99 |
| 29 | 0.44 | 0.35 | 0.38 | 0.59 | 0.69 | 0.62 | 0.62 | 0.81 | 0.69 | 0.97 | 0.97 | 0.97 | 0.39 | 0.58 | 0.62 | 0.97 |
| 30 | 0.36 | 0.33 | 0.45 | 0.70 | 0.44 | 0.34 | 0.78 | 0.46 | 0.36 | 0.96 | 0.95 | 0.95 | 0.46 | 0.33 | 0.36 | 0.96 |
| 31 | 0.49 | 0.33 | 0.43 | 0.63 | 0.46 | 0.58 | 0.68 | 0.47 | 0.62 | 0.98 | 0.96 | 0.96 | 0.41 | 0.43 | 0.46 | 0.97 |
| 32 | 0.63 | 0.61 | 0.65 | 0.67 | 0.45 | 0.47 | 0.70 | 0.45 | 0.48 | 0.99 | 0.99 | 0.97 | 0.62 | 0.39 | 0.40 | 0.98 |
| 33 | 0.33 | 0.33 | 0.31 | 0.65 | 0.63 | 0.62 | 0.88 | 0.65 | 0.64 | 0.94 | 0.95 | 0.94 | 0.34 | 0.59 | 0.62 | 0.95 |
| 34 | 0.45 | 0.32 | 0.54 | 0.66 | 0.64 | 0.58 | 0.74 | 0.65 | 0.59 | 0.96 | 0.98 | 0.98 | 0.43 | 0.55 | 0.56 | 0.97 |
| 35 | 0.36 | 0.38 | 0.37 | 0.73 | 0.64 | 0.53 | 0.79 | 0.68 | 0.56 | 0.97 | 0.96 | 0.95 | 0.42 | 0.52 | 0.56 | 0.96 |
| 36 | 0.51 | 0.56 | 0.50 | 0.68 | 0.64 | 0.61 | 0.80 | 0.65 | 0.63 | 0.98 | 0.99 | 0.97 | 0.54 | 0.56 | 0.59 | 0.98 |
| 37 | 0.52 | 0.47 | 0.72 | 0.69 | 0.53 | 0.49 | 0.82 | 0.54 | 0.49 | 0.98 | 0.98 | 0.98 | 0.56 | 0.43 | 0.46 | 0.98 |
| 38 | 0.78 | 0.55 | 0.63 | 0.63 | 0.67 | 0.71 | 0.63 | 0.71 | 0.72 | 1.00 | 0.99 | 1.00 | 0.64 | 0.57 | 0.60 | 0.99 |
| 39 | 0.35 | 0.35 | 0.48 | 0.65 | 0.73 | 0.55 | 0.72 | 0.92 | 0.60 | 0.95 | 0.97 | 0.97 | 0.41 | 0.55 | 0.60 | 0.96 |
| 40 | 0.44 | 0.47 | 0.53 | 0.65 | 0.60 | 0.67 | 0.72 | 0.80 | 0.81 | 0.98 | 0.96 | 0.96 | 0.47 | 0.60 | 0.70 | 0.97 |
| 41 | 0.41 | 0.47 | 0.54 | 0.70 | 0.50 | 0.49 | 0.89 | 0.53 | 0.50 | 0.98 | 0.95 | 0.97 | 0.54 | 0.43 | 0.48 | 0.97 |
| 42 | 0.28 | 0.36 | 0.47 | 0.66 | 0.35 | 0.34 | 0.69 | 0.38 | 0.36 | 0.96 | 0.94 | 0.96 | 0.48 | 0.28 | 0.31 | 0.96 |
| 43 | 0.48 | 0.35 | 0.48 | 0.71 | 0.61 | 0.55 | 0.74 | 0.65 | 0.62 | 0.98 | 0.97 | 0.97 | 0.44 | 0.52 | 0.58 | 0.97 |
| 44 | 0.48 | 0.57 | 0.58 | 0.66 | 0.58 | 0.52 | 0.71 | 0.58 | 0.55 | 0.98 | 0.98 | 0.97 | 0.56 | 0.47 | 0.49 | 0.98 |
| 45 | 0.48 | 0.32 | 0.36 | 0.71 | 0.48 | 0.55 | 0.75 | 0.58 | 0.60 | 0.96 | 0.91 | 0.95 | 0.43 | 0.44 | 0.50 | 0.95 |
| 46 | 0.36 | 0.58 | 0.41 | 0.57 | 0.53 | 0.51 | 0.70 | 0.53 | 0.52 | 0.95 | 0.99 | 0.98 | 0.46 | 0.47 | 0.50 | 0.98 |
| 47 | 0.49 | 0.42 | 0.53 | 0.72 | 0.57 | 0.54 | 0.77 | 0.61 | 0.56 | 0.98 | 0.97 | 0.98 | 0.52 | 0.47 | 0.50 | 0.98 |
| 48 | 0.46 | 0.50 | 0.41 | 0.54 | 0.36 | 0.41 | 0.56 | 0.37 | 0.41 | 0.95 | 0.98 | 0.98 | 0.49 | 0.33 | 0.34 | 0.97 |
| 49 | 0.42 | 0.41 | 0.38 | 0.70 | 0.60 | 0.56 | 0.75 | 0.61 | 0.61 | 0.97 | 0.96 | 0.97 | 0.43 | 0.52 | 0.57 | 0.97 |
| 50 | 0.30 | 0.43 | 0.39 | 0.64 | 0.68 | 0.74 | 0.72 | 0.78 | 0.85 | 0.96 | 0.97 | 0.98 | 0.40 | 0.64 | 0.72 | 0.97 |

Table A.11. Determined 2D and 3D particle shape descriptors of Sand C retained on sieve #20, PR = 36.75, PSR = 0.850 – 2.00 mm.

| Part | $R_{2D}$ | | | $S_{2D}$ | | | $AR_{2D}$ | | | $CX_{2D}$ | | | | | | |
|---|---|---|---|---|---|---|---|---|---|---|---|---|---|---|---|---|
| No. | $F_D$ | $F_1$ | $F_2$ | $F_D$ | $F_1$ | $F_2$ | $F_D$ | $F_1$ | $F_2$ | $F_D$ | $F_1$ | $F_2$ | $R_{3D}$ | $S_{3D}$ | $AR_{3D}$ | $CX_{3D}$ |
| 1 | 0.47 | 0.55 | 0.52 | 0.46 | 0.39 | 0.52 | 0.60 | 0.44 | 0.55 | 0.90 | 0.92 | 0.93 | 0.52 | 0.37 | 0.42 | 0.91 |
| 2 | 0.56 | 0.42 | 0.57 | 0.53 | 0.57 | 0.48 | 0.55 | 0.62 | 0.55 | 0.95 | 0.96 | 0.94 | 0.56 | 0.46 | 0.52 | 0.95 |
| 3 | 0.42 | 0.45 | 0.47 | 0.69 | 0.58 | 0.53 | 0.80 | 0.62 | 0.61 | 0.98 | 0.94 | 0.95 | 0.49 | 0.51 | 0.59 | 0.96 |
| 4 | 0.53 | 0.37 | 0.52 | 0.50 | 0.45 | 0.38 | 0.59 | 0.52 | 0.40 | 0.95 | 0.96 | 0.97 | 0.57 | 0.34 | 0.40 | 0.96 |
| 5 | 0.42 | 0.53 | 0.47 | 0.43 | 0.42 | 0.35 | 0.46 | 0.43 | 0.36 | 0.92 | 0.97 | 0.96 | 0.47 | 0.32 | 0.32 | 0.95 |
| 6 | 0.57 | 0.32 | 0.52 | 0.62 | 0.49 | 0.47 | 0.65 | 0.50 | 0.47 | 0.98 | 0.98 | 0.97 | 0.52 | 0.41 | 0.41 | 0.98 |
| 7 | 0.57 | 0.60 | 0.60 | 0.72 | 0.54 | 0.65 | 0.74 | 0.55 | 0.69 | 0.98 | 0.99 | 0.98 | 0.64 | 0.54 | 0.54 | 0.98 |
| 8 | 0.51 | 0.45 | 0.50 | 0.77 | 0.56 | 0.60 | 0.79 | 0.59 | 0.60 | 0.98 | 0.98 | 0.98 | 0.54 | 0.49 | 0.52 | 0.98 |
| 9 | 0.48 | 0.51 | 0.43 | 0.62 | 0.65 | 0.56 | 0.63 | 0.66 | 0.57 | 0.98 | 0.99 | 0.97 | 0.45 | 0.50 | 0.51 | 0.98 |
| 10 | 0.45 | 0.51 | 0.65 | 0.65 | 0.65 | 0.46 | 0.66 | 0.68 | 0.48 | 0.97 | 0.97 | 0.97 | 0.58 | 0.45 | 0.46 | 0.97 |
| 11 | 0.51 | 0.44 | 0.37 | 0.61 | 0.55 | 0.64 | 0.67 | 0.58 | 0.66 | 0.96 | 0.97 | 0.97 | 0.44 | 0.50 | 0.53 | 0.96 |
| 12 | 0.58 | 0.36 | 0.47 | 0.59 | 0.67 | 0.61 | 0.60 | 0.69 | 0.70 | 0.99 | 0.99 | 0.98 | 0.48 | 0.54 | 0.60 | 0.98 |
| 13 | 0.39 | 0.36 | 0.44 | 0.62 | 0.50 | 0.61 | 0.67 | 0.57 | 0.63 | 0.95 | 0.94 | 0.94 | 0.47 | 0.45 | 0.51 | 0.95 |
| 14 | 0.49 | 0.56 | 0.51 | 0.71 | 0.48 | 0.51 | 0.73 | 0.49 | 0.51 | 0.98 | 0.96 | 0.97 | 0.57 | 0.45 | 0.45 | 0.97 |
| 15 | 0.59 | 0.47 | 0.43 | 0.76 | 0.73 | 0.72 | 0.78 | 0.84 | 0.75 | 0.99 | 0.96 | 0.98 | 0.47 | 0.64 | 0.70 | 0.98 |
| 16 | 0.30 | 0.34 | 0.25 | 0.71 | 0.33 | 0.40 | 0.80 | 0.37 | 0.41 | 0.94 | 0.90 | 0.97 | 0.44 | 0.32 | 0.36 | 0.94 |
| 17 | 0.57 | 0.50 | 0.45 | 0.60 | 0.43 | 0.35 | 0.62 | 0.45 | 0.36 | 0.97 | 0.96 | 0.96 | 0.55 | 0.32 | 0.33 | 0.96 |
| 18 | 0.55 | 0.52 | 0.41 | 0.58 | 0.36 | 0.33 | 0.63 | 0.36 | 0.34 | 0.95 | 0.98 | 0.97 | 0.51 | 0.31 | 0.32 | 0.96 |
| 19 | 0.53 | 0.45 | 0.56 | 0.65 | 0.60 | 0.65 | 0.68 | 0.62 | 0.67 | 0.98 | 0.98 | 0.98 | 0.53 | 0.60 | 0.62 | 0.98 |
| 20 | 0.45 | 0.42 | 0.60 | 0.72 | 0.67 | 0.83 | 0.72 | 0.74 | 0.88 | 0.98 | 0.95 | 0.96 | 0.48 | 0.67 | 0.67 | 0.96 |
| 21 | 0.73 | 0.51 | 0.59 | 0.64 | 0.68 | 0.68 | 0.67 | 0.72 | 0.90 | 0.98 | 0.98 | 0.98 | 0.60 | 0.57 | 0.67 | 0.98 |
| 22 | 0.55 | 0.45 | 0.41 | 0.74 | 0.60 | 0.73 | 0.75 | 0.75 | 0.79 | 0.98 | 0.98 | 0.97 | 0.51 | 0.60 | 0.66 | 0.98 |
| 23 | 0.38 | 0.52 | 0.47 | 0.67 | 0.67 | 0.58 | 0.73 | 0.68 | 0.59 | 0.97 | 0.98 | 0.96 | 0.49 | 0.52 | 0.53 | 0.97 |
| 24 | 0.53 | 0.49 | 0.33 | 0.70 | 0.50 | 0.43 | 0.73 | 0.51 | 0.50 | 0.98 | 0.98 | 0.96 | 0.47 | 0.39 | 0.44 | 0.98 |
| 25 | 0.48 | 0.48 | 0.48 | 0.77 | 0.50 | 0.56 | 0.85 | 0.54 | 0.57 | 0.98 | 0.97 | 0.98 | 0.49 | 0.50 | 0.53 | 0.98 |
| 26 | 0.58 | 0.38 | 0.51 | 0.77 | 0.73 | 0.68 | 0.80 | 0.82 | 0.71 | 0.99 | 0.99 | 0.98 | 0.50 | 0.62 | 0.69 | 0.99 |
| 27 | 0.66 | 0.58 | 0.59 | 0.57 | 0.60 | 0.45 | 0.57 | 0.62 | 0.46 | 0.99 | 0.98 | 0.97 | 0.58 | 0.42 | 0.44 | 0.98 |
| 28 | 0.51 | 0.46 | 0.55 | 0.66 | 0.55 | 0.45 | 0.75 | 0.56 | 0.46 | 0.98 | 0.98 | 0.97 | 0.54 | 0.45 | 0.46 | 0.98 |
| 29 | 0.51 | 0.65 | 0.51 | 0.74 | 0.50 | 0.50 | 0.84 | 0.51 | 0.50 | 0.97 | 0.98 | 0.98 | 0.56 | 0.46 | 0.48 | 0.97 |
| 30 | 0.50 | 0.41 | 0.50 | 0.51 | 0.44 | 0.52 | 0.53 | 0.45 | 0.55 | 0.96 | 0.96 | 0.96 | 0.50 | 0.41 | 0.43 | 0.96 |

Table A.12. Determined 2D and 3D shape descriptors of Sand C particles retained on sieve #40, PR = 21.17, PSR = 0.425 – 0.850 mm.

| Part | $R_{2D}$ | | | $S_{2D}$ | | | $AR_{2D}$ | | | $CX_{2D}$ | | | | | | |
|---|---|---|---|---|---|---|---|---|---|---|---|---|---|---|---|---|
| No. | $F_D$ | $F_1$ | $F_2$ | $F_D$ | $F_1$ | $F_2$ | $F_D$ | $F_1$ | $F_2$ | $F_D$ | $F_1$ | $F_2$ | $R_{3D}$ | $S_{3D}$ | $AR_{3D}$ | $CX_{3D}$ |
| 1 | 0.41 | 0.48 | 0.56 | 0.48 | 0.35 | 0.29 | 0.53 | 0.36 | 0.30 | 0.93 | 0.91 | 0.89 | 0.57 | 0.27 | 0.27 | 0.92 |
| 2 | 0.48 | 0.40 | 0.25 | 0.38 | 0.27 | 0.20 | 0.45 | 0.27 | 0.21 | 0.87 | 0.94 | 0.94 | 0.35 | 0.18 | 0.19 | 0.90 |
| 3 | 0.47 | 0.50 | 0.45 | 0.47 | 0.56 | 0.38 | 0.49 | 0.60 | 0.40 | 0.94 | 0.96 | 0.94 | 0.50 | 0.36 | 0.39 | 0.94 |
| 4 | 0.55 | 0.64 | 0.61 | 0.64 | 0.50 | 0.70 | 0.66 | 0.51 | 0.72 | 0.97 | 0.98 | 0.98 | 0.62 | 0.50 | 0.51 | 0.97 |
| 5 | 0.43 | 0.58 | 0.52 | 0.61 | 0.46 | 0.41 | 0.66 | 0.47 | 0.44 | 0.95 | 0.97 | 0.95 | 0.50 | 0.36 | 0.39 | 0.96 |
| 6 | 0.47 | 0.34 | 0.42 | 0.44 | 0.33 | 0.32 | 0.48 | 0.34 | 0.33 | 0.96 | 0.96 | 0.97 | 0.51 | 0.27 | 0.29 | 0.97 |
| 7 | 0.30 | 0.54 | 0.54 | 0.67 | 0.39 | 0.37 | 0.77 | 0.39 | 0.38 | 0.94 | 0.96 | 0.97 | 0.56 | 0.34 | 0.35 | 0.95 |
| 8 | 0.43 | 0.59 | 0.35 | 0.78 | 0.40 | 0.48 | 0.89 | 0.41 | 0.50 | 0.95 | 0.97 | 0.95 | 0.52 | 0.40 | 0.41 | 0.95 |
| 9 | 0.54 | 0.69 | 0.53 | 0.77 | 0.52 | 0.61 | 0.80 | 0.52 | 0.62 | 0.98 | 0.98 | 0.98 | 0.63 | 0.52 | 0.52 | 0.98 |
| 10 | 0.52 | 0.47 | 0.42 | 0.63 | 0.68 | 0.59 | 0.65 | 0.77 | 0.63 | 0.98 | 0.97 | 0.96 | 0.47 | 0.56 | 0.57 | 0.97 |
| 11 | 0.43 | 0.41 | 0.55 | 0.70 | 0.75 | 0.68 | 0.73 | 0.83 | 0.71 | 0.98 | 0.97 | 0.98 | 0.47 | 0.66 | 0.69 | 0.98 |
| 12 | 0.44 | 0.44 | 0.41 | 0.68 | 0.42 | 0.36 | 0.69 | 0.43 | 0.36 | 0.97 | 0.97 | 0.96 | 0.52 | 0.35 | 0.36 | 0.97 |
| 13 | 0.25 | 0.39 | 0.34 | 0.69 | 0.40 | 0.52 | 0.72 | 0.41 | 0.52 | 0.94 | 0.96 | 0.97 | 0.39 | 0.40 | 0.41 | 0.95 |
| 14 | 0.21 | 0.35 | 0.39 | 0.57 | 0.61 | 0.61 | 0.72 | 0.78 | 0.72 | 0.91 | 0.94 | 0.94 | 0.37 | 0.51 | 0.62 | 0.93 |
| 15 | 0.46 | 0.43 | 0.49 | 0.66 | 0.42 | 0.37 | 0.71 | 0.46 | 0.41 | 0.96 | 0.95 | 0.94 | 0.50 | 0.35 | 0.39 | 0.95 |
| 16 | 0.50 | 0.44 | 0.48 | 0.65 | 0.31 | 0.25 | 0.70 | 0.32 | 0.25 | 0.97 | 0.97 | 0.98 | 0.54 | 0.23 | 0.23 | 0.97 |
| 17 | 0.54 | 0.48 | 0.45 | 0.62 | 0.49 | 0.50 | 0.64 | 0.52 | 0.51 | 0.97 | 0.95 | 0.97 | 0.50 | 0.43 | 0.45 | 0.97 |
| 18 | 0.66 | 0.50 | 0.44 | 0.46 | 0.57 | 0.38 | 0.49 | 0.61 | 0.38 | 0.95 | 0.96 | 0.97 | 0.47 | 0.35 | 0.37 | 0.96 |
| 19 | 0.53 | 0.30 | 0.48 | 0.54 | 0.58 | 0.42 | 0.55 | 0.63 | 0.44 | 0.95 | 0.95 | 0.96 | 0.43 | 0.39 | 0.42 | 0.95 |
| 20 | 0.49 | 0.50 | 0.47 | 0.65 | 0.54 | 0.64 | 0.65 | 0.56 | 0.70 | 0.97 | 0.97 | 0.96 | 0.52 | 0.52 | 0.56 | 0.97 |
| 21 | 0.46 | 0.45 | 0.51 | 0.67 | 0.48 | 0.45 | 0.70 | 0.49 | 0.47 | 0.97 | 0.98 | 0.97 | 0.47 | 0.41 | 0.44 | 0.97 |
| 22 | 0.66 | 0.46 | 0.44 | 0.65 | 0.59 | 0.72 | 0.66 | 0.61 | 0.71 | 0.98 | 0.97 | 0.97 | 0.49 | 0.56 | 0.56 | 0.97 |
| 23 | 0.41 | 0.64 | 0.61 | 0.42 | 0.33 | 0.26 | 0.43 | 0.34 | 0.26 | 0.94 | 0.95 | 0.95 | 0.59 | 0.25 | 0.25 | 0.94 |
| 24 | 0.31 | 0.54 | 0.50 | 0.46 | 0.40 | 0.33 | 0.51 | 0.42 | 0.33 | 0.93 | 0.92 | 0.95 | 0.51 | 0.29 | 0.30 | 0.93 |
| 25 | 0.51 | 0.59 | 0.67 | 0.69 | 0.41 | 0.29 | 0.75 | 0.41 | 0.34 | 0.95 | 0.96 | 0.90 | 0.58 | 0.29 | 0.32 | 0.93 |
| 26 | 0.45 | 0.52 | 0.57 | 0.68 | 0.50 | 0.51 | 0.74 | 0.51 | 0.51 | 0.97 | 0.98 | 0.98 | 0.60 | 0.47 | 0.48 | 0.98 |
| 27 | 0.53 | 0.53 | 0.41 | 0.65 | 0.36 | 0.39 | 0.76 | 0.37 | 0.39 | 0.92 | 0.97 | 0.97 | 0.52 | 0.34 | 0.35 | 0.94 |
| 28 | 0.37 | 0.36 | 0.54 | 0.67 | 0.46 | 0.75 | 0.75 | 0.51 | 0.78 | 0.97 | 0.91 | 0.98 | 0.47 | 0.46 | 0.49 | 0.95 |
| 29 | 0.42 | 0.37 | 0.46 | 0.60 | 0.39 | 0.36 | 0.62 | 0.40 | 0.37 | 0.97 | 0.94 | 0.96 | 0.49 | 0.34 | 0.35 | 0.96 |
| 30 | 0.52 | 0.49 | 0.51 | 0.62 | 0.60 | 0.43 | 0.66 | 0.62 | 0.45 | 0.98 | 0.97 | 0.97 | 0.51 | 0.42 | 0.43 | 0.97 |

Table A.13. Determined 2D and 3D particle shape descriptors of Sand C retained on sieve #60, PR = 12.32, PSR = 0.250 – 0.425 mm.

| Part | $R_{2D}$ | | | $S_{2D}$ | | | $AR_{2D}$ | | | $CX_{2D}$ | | | | | | |
|---|---|---|---|---|---|---|---|---|---|---|---|---|---|---|---|---|
| No. | $F_D$ | $F_1$ | $F_2$ | $F_D$ | $F_1$ | $F_2$ | $F_D$ | $F_1$ | $F_2$ | $F_D$ | $F_1$ | $F_2$ | $R_{3D}$ | $S_{3D}$ | $AR_{3D}$ | $CX_{3D}$ |
| 1 | 0.48 | 0.41 | 0.40 | 0.63 | 0.63 | 0.48 | 0.66 | 0.68 | 0.52 | 0.97 | 0.95 | 0.94 | 0.45 | 0.44 | 0.47 | 0.96 |
| 2 | 0.40 | 0.61 | 0.57 | 0.59 | 0.39 | 0.43 | 0.63 | 0.41 | 0.44 | 0.96 | 0.92 | 0.96 | 0.60 | 0.35 | 0.37 | 0.95 |
| 3 | 0.41 | 0.38 | 0.58 | 0.72 | 0.54 | 0.46 | 0.79 | 0.55 | 0.47 | 0.97 | 0.95 | 0.98 | 0.52 | 0.44 | 0.45 | 0.97 |
| 4 | 0.38 | 0.55 | 0.47 | 0.69 | 0.28 | 0.40 | 0.75 | 0.29 | 0.40 | 0.96 | 0.96 | 0.96 | 0.59 | 0.28 | 0.29 | 0.96 |
| 5 | 0.43 | 0.57 | 0.42 | 0.69 | 0.50 | 0.54 | 0.75 | 0.51 | 0.54 | 0.94 | 0.97 | 0.98 | 0.50 | 0.50 | 0.51 | 0.96 |
| 6 | 0.52 | 0.68 | 0.36 | 0.57 | 0.47 | 0.55 | 0.57 | 0.48 | 0.58 | 0.98 | 0.98 | 0.98 | 0.59 | 0.46 | 0.48 | 0.98 |
| 7 | 0.49 | 0.47 | 0.34 | 0.51 | 0.53 | 0.41 | 0.55 | 0.55 | 0.42 | 0.94 | 0.97 | 0.97 | 0.46 | 0.38 | 0.40 | 0.96 |
| 8 | 0.46 | 0.35 | 0.37 | 0.49 | 0.44 | 0.45 | 0.53 | 0.44 | 0.46 | 0.95 | 0.94 | 0.98 | 0.44 | 0.36 | 0.36 | 0.95 |
| 9 | 0.52 | 0.59 | 0.48 | 0.80 | 0.40 | 0.47 | 0.81 | 0.43 | 0.48 | 0.98 | 0.95 | 0.96 | 0.58 | 0.38 | 0.40 | 0.97 |
| 10 | 0.31 | 0.46 | 0.45 | 0.74 | 0.47 | 0.41 | 0.84 | 0.49 | 0.43 | 0.95 | 0.95 | 0.96 | 0.51 | 0.40 | 0.42 | 0.95 |
| 11 | 0.49 | 0.59 | 0.44 | 0.74 | 0.58 | 0.65 | 0.75 | 0.59 | 0.70 | 0.98 | 0.97 | 0.97 | 0.55 | 0.58 | 0.59 | 0.97 |
| 12 | 0.63 | 0.47 | 0.47 | 0.62 | 0.67 | 0.64 | 0.66 | 0.90 | 0.68 | 0.94 | 0.96 | 0.97 | 0.48 | 0.52 | 0.63 | 0.96 |
| 13 | 0.58 | 0.48 | 0.61 | 0.71 | 0.70 | 0.76 | 0.72 | 0.76 | 0.80 | 0.98 | 0.98 | 0.98 | 0.55 | 0.64 | 0.69 | 0.98 |
| 14 | 0.46 | 0.41 | 0.43 | 0.55 | 0.54 | 0.40 | 0.58 | 0.56 | 0.40 | 0.95 | 0.97 | 0.97 | 0.47 | 0.37 | 0.38 | 0.96 |
| 15 | 0.42 | 0.46 | 0.50 | 0.48 | 0.39 | 0.43 | 0.49 | 0.41 | 0.44 | 0.95 | 0.93 | 0.95 | 0.52 | 0.34 | 0.36 | 0.94 |
| 16 | 0.49 | 0.69 | 0.65 | 0.63 | 0.56 | 0.45 | 0.66 | 0.57 | 0.46 | 0.96 | 0.97 | 0.95 | 0.64 | 0.41 | 0.42 | 0.96 |
| 17 | 0.41 | 0.44 | 0.72 | 0.62 | 0.40 | 0.57 | 0.76 | 0.41 | 0.58 | 0.90 | 0.96 | 0.97 | 0.53 | 0.40 | 0.41 | 0.94 |
| 18 | 0.75 | 0.53 | 0.51 | 0.52 | 0.66 | 0.46 | 0.52 | 0.76 | 0.47 | 0.99 | 0.97 | 0.96 | 0.60 | 0.39 | 0.44 | 0.97 |
| 19 | 0.45 | 0.74 | 0.69 | 0.68 | 0.54 | 0.48 | 0.71 | 0.54 | 0.49 | 0.97 | 0.97 | 0.97 | 0.67 | 0.45 | 0.45 | 0.97 |
| 20 | 0.56 | 0.62 | 0.52 | 0.72 | 0.35 | 0.33 | 0.73 | 0.36 | 0.33 | 0.98 | 0.97 | 0.95 | 0.56 | 0.29 | 0.30 | 0.97 |
| 21 | 0.52 | 0.55 | 0.69 | 0.62 | 0.58 | 0.45 | 0.64 | 0.59 | 0.45 | 0.98 | 0.98 | 0.95 | 0.58 | 0.43 | 0.44 | 0.97 |
| 22 | 0.45 | 0.62 | 0.41 | 0.62 | 0.66 | 0.66 | 0.72 | 0.68 | 0.71 | 0.93 | 0.98 | 0.97 | 0.49 | 0.60 | 0.63 | 0.96 |
| 23 | 0.32 | 0.66 | 0.59 | 0.72 | 0.38 | 0.41 | 0.80 | 0.39 | 0.42 | 0.96 | 0.92 | 0.94 | 0.59 | 0.38 | 0.39 | 0.95 |
| 24 | 0.62 | 0.50 | 0.59 | 0.69 | 0.66 | 0.57 | 0.73 | 0.69 | 0.57 | 0.97 | 0.97 | 0.96 | 0.57 | 0.52 | 0.55 | 0.96 |
| 25 | 0.45 | 0.56 | 0.59 | 0.75 | 0.43 | 0.46 | 0.83 | 0.44 | 0.47 | 0.95 | 0.97 | 0.96 | 0.59 | 0.43 | 0.44 | 0.96 |
| 26 | 0.67 | 0.49 | 0.47 | 0.40 | 0.47 | 0.34 | 0.44 | 0.48 | 0.35 | 0.95 | 0.94 | 0.95 | 0.55 | 0.29 | 0.30 | 0.95 |
| 27 | 0.62 | 0.52 | 0.52 | 0.56 | 0.51 | 0.58 | 0.58 | 0.52 | 0.59 | 0.98 | 0.97 | 0.98 | 0.56 | 0.48 | 0.49 | 0.98 |
| 28 | 0.49 | 0.33 | 0.35 | 0.78 | 0.32 | 0.38 | 0.83 | 0.41 | 0.54 | 0.96 | 0.83 | 0.87 | 0.39 | 0.32 | 0.41 | 0.91 |
| 29 | 0.43 | 0.63 | 0.58 | 0.49 | 0.56 | 0.60 | 0.58 | 0.60 | 0.64 | 0.91 | 0.97 | 0.97 | 0.55 | 0.49 | 0.54 | 0.95 |
| 30 | 0.49 | 0.61 | 0.55 | 0.70 | 0.35 | 0.40 | 0.71 | 0.35 | 0.40 | 0.96 | 0.95 | 0.97 | 0.60 | 0.32 | 0.33 | 0.96 |

Table A.14. Determined 2D and 3D particle shape descriptors of Sand C retained on sieve #100, PR = 11.00, PSR = 0.150 – 0.250 mm.

| Part | $R_{2D}$ | | | $S_{2D}$ | | | $AR_{2D}$ | | | $CX_{2D}$ | | | | | | |
|---|---|---|---|---|---|---|---|---|---|---|---|---|---|---|---|---|
| No. | $F_D$ | $F_1$ | $F_2$ | $F_D$ | $F_1$ | $F_2$ | $F_D$ | $F_1$ | $F_2$ | $F_D$ | $F_1$ | $F_2$ | $R_{3D}$ | $S_{3D}$ | $AR_{3D}$ | $CX_{3D}$ |
| 1 | 0.57 | 0.35 | 0.46 | 0.63 | 0.66 | 0.63 | 0.64 | 0.69 | 0.62 | 0.97 | 0.97 | 0.96 | 0.50 | 0.57 | 0.59 | 0.97 |
| 2 | 0.48 | 0.87 | 0.59 | 0.80 | 0.39 | 0.40 | 0.87 | 0.39 | 0.41 | 0.95 | 0.95 | 0.95 | 0.66 | 0.37 | 0.38 | 0.95 |
| 3 | 0.52 | 0.38 | 0.56 | 0.74 | 0.38 | 0.40 | 0.79 | 0.40 | 0.41 | 0.97 | 0.94 | 0.94 | 0.52 | 0.38 | 0.39 | 0.96 |
| 4 | 0.64 | 0.66 | 0.33 | 0.74 | 0.62 | 0.66 | 0.76 | 0.62 | 0.67 | 0.97 | 0.94 | 0.96 | 0.58 | 0.57 | 0.58 | 0.96 |
| 5 | 0.53 | 0.63 | 0.49 | 0.77 | 0.61 | 0.60 | 0.80 | 0.64 | 0.67 | 0.95 | 0.97 | 0.95 | 0.58 | 0.55 | 0.61 | 0.96 |
| 6 | 0.53 | 0.55 | 0.57 | 0.49 | 0.44 | 0.39 | 0.51 | 0.44 | 0.43 | 0.95 | 0.95 | 0.91 | 0.57 | 0.35 | 0.38 | 0.94 |
| 7 | 0.38 | 0.59 | 0.49 | 0.76 | 0.61 | 0.57 | 0.88 | 0.69 | 0.65 | 0.97 | 0.95 | 0.90 | 0.53 | 0.54 | 0.64 | 0.94 |
| 8 | 0.75 | 0.63 | 0.57 | 0.71 | 0.65 | 0.61 | 0.72 | 0.65 | 0.62 | 0.98 | 0.96 | 0.96 | 0.61 | 0.54 | 0.54 | 0.97 |
| 9 | 0.55 | 0.55 | 0.60 | 0.81 | 0.63 | 0.67 | 0.86 | 0.64 | 0.67 | 0.97 | 0.97 | 0.97 | 0.60 | 0.61 | 0.62 | 0.97 |
| 10 | 0.52 | 0.45 | 0.65 | 0.63 | 0.32 | 0.49 | 0.63 | 0.33 | 0.50 | 0.98 | 0.96 | 0.97 | 0.57 | 0.32 | 0.32 | 0.97 |
| 11 | 0.56 | 0.45 | 0.57 | 0.70 | 0.58 | 0.58 | 0.74 | 0.62 | 0.58 | 0.95 | 0.96 | 0.95 | 0.53 | 0.56 | 0.57 | 0.95 |
| 12 | 0.30 | 0.20 | 0.64 | 0.55 | 0.34 | 0.58 | 0.59 | 0.34 | 0.58 | 0.94 | 0.96 | 0.97 | 0.43 | 0.34 | 0.34 | 0.95 |
| 13 | 0.57 | 0.65 | 0.53 | 0.70 | 0.60 | 0.48 | 0.70 | 0.61 | 0.49 | 0.98 | 0.97 | 0.96 | 0.60 | 0.45 | 0.46 | 0.97 |
| 14 | 0.61 | 0.65 | 0.50 | 0.81 | 0.53 | 0.56 | 0.83 | 0.53 | 0.59 | 0.97 | 0.97 | 0.95 | 0.55 | 0.48 | 0.50 | 0.96 |
| 15 | 0.54 | 0.59 | 0.43 | 0.60 | 0.75 | 0.52 | 0.62 | 0.78 | 0.52 | 0.97 | 0.97 | 0.96 | 0.53 | 0.49 | 0.52 | 0.97 |
| 16 | 0.71 | 0.47 | 0.47 | 0.61 | 0.68 | 0.40 | 0.64 | 0.71 | 0.42 | 0.97 | 0.94 | 0.96 | 0.56 | 0.40 | 0.42 | 0.96 |
| 17 | 0.66 | 0.52 | 0.68 | 0.77 | 0.72 | 0.62 | 0.78 | 0.76 | 0.63 | 0.98 | 0.96 | 0.97 | 0.63 | 0.62 | 0.63 | 0.97 |
| 18 | 0.50 | 0.66 | 0.51 | 0.82 | 0.63 | 0.59 | 0.86 | 0.65 | 0.63 | 0.97 | 0.96 | 0.96 | 0.64 | 0.53 | 0.55 | 0.97 |
| 19 | 0.54 | 0.51 | 0.68 | 0.62 | 0.53 | 0.55 | 0.63 | 0.53 | 0.56 | 0.97 | 0.96 | 0.97 | 0.58 | 0.45 | 0.46 | 0.97 |
| 20 | 0.52 | 0.33 | 0.44 | 0.69 | 0.38 | 0.47 | 0.76 | 0.38 | 0.50 | 0.94 | 0.97 | 0.92 | 0.52 | 0.37 | 0.37 | 0.94 |
| 21 | 0.52 | 0.60 | 0.57 | 0.69 | 0.50 | 0.44 | 0.69 | 0.51 | 0.45 | 0.97 | 0.95 | 0.97 | 0.65 | 0.35 | 0.36 | 0.96 |
| 22 | 0.53 | 0.59 | 0.47 | 0.58 | 0.52 | 0.67 | 0.63 | 0.52 | 0.67 | 0.97 | 0.97 | 0.97 | 0.54 | 0.52 | 0.52 | 0.97 |
| 23 | 0.54 | 0.59 | 0.66 | 0.75 | 0.41 | 0.53 | 0.84 | 0.41 | 0.54 | 0.96 | 0.95 | 0.96 | 0.69 | 0.41 | 0.41 | 0.96 |
| 24 | 0.64 | 0.38 | 0.41 | 0.62 | 0.51 | 0.48 | 0.64 | 0.55 | 0.55 | 0.98 | 0.93 | 0.94 | 0.56 | 0.48 | 0.53 | 0.95 |
| 25 | 0.71 | 0.58 | 0.49 | 0.75 | 0.70 | 0.81 | 0.78 | 0.73 | 0.83 | 0.97 | 0.96 | 0.96 | 0.62 | 0.68 | 0.70 | 0.96 |
| 26 | 0.49 | 0.63 | 0.74 | 0.51 | 0.41 | 0.43 | 0.52 | 0.43 | 0.46 | 0.94 | 0.93 | 0.93 | 0.66 | 0.32 | 0.34 | 0.94 |
| 27 | 0.55 | 0.33 | 0.49 | 0.62 | 0.39 | 0.55 | 0.64 | 0.40 | 0.56 | 0.96 | 0.95 | 0.96 | 0.54 | 0.37 | 0.38 | 0.96 |
| 28 | 0.66 | 0.65 | 0.61 | 0.66 | 0.43 | 0.54 | 0.66 | 0.44 | 0.54 | 0.97 | 0.96 | 0.97 | 0.65 | 0.37 | 0.38 | 0.97 |
| 29 | 0.55 | 0.50 | 0.68 | 0.73 | 0.58 | 0.60 | 0.78 | 0.62 | 0.63 | 0.95 | 0.91 | 0.96 | 0.58 | 0.55 | 0.58 | 0.94 |
| 30 | 0.50 | 0.45 | 0.58 | 0.59 | 0.51 | 0.39 | 0.64 | 0.52 | 0.40 | 0.95 | 0.96 | 0.94 | 0.58 | 0.37 | 0.38 | 0.95 |

Table A.15. Determined 2D and 3D particle shape descriptors of Sand C retained on sieve #140, PR = 3.78, PSR = 0.106 – 0.150 mm.

| Part | $R_{2D}$ | | | $S_{2D}$ | | | $AR_{2D}$ | | | $CX_{2D}$ | | | | | | |
|---|---|---|---|---|---|---|---|---|---|---|---|---|---|---|---|---|
| No. | $F_D$ | $F_1$ | $F_2$ | $F_D$ | $F_1$ | $F_2$ | $F_D$ | $F_1$ | $F_2$ | $F_D$ | $F_1$ | $F_2$ | $R_{3D}$ | $S_{3D}$ | $AR_{3D}$ | $CX_{3D}$ |
| 1 | 0.64 | 0.52 | 0.55 | 0.57 | 0.33 | 0.58 | 0.58 | 0.33 | 0.60 | 0.96 | 0.94 | 0.95 | 0.65 | 0.33 | 0.33 | 0.95 |
| 2 | 0.76 | 0.58 | 0.56 | 0.54 | 0.72 | 0.67 | 0.54 | 0.72 | 0.70 | 0.97 | 0.95 | 0.96 | 0.64 | 0.53 | 0.54 | 0.96 |
| 3 | 0.25 | 0.49 | 0.45 | 0.30 | 0.74 | 0.55 | 0.31 | 0.89 | 0.59 | 0.95 | 0.95 | 0.96 | 0.58 | 0.30 | 0.31 | 0.95 |
| 4 | 0.41 | 0.51 | 0.55 | 0.81 | 0.54 | 0.65 | 0.81 | 0.59 | 0.69 | 0.95 | 0.93 | 0.94 | 0.51 | 0.51 | 0.54 | 0.94 |
| 5 | 0.42 | 0.56 | 0.59 | 0.82 | 0.54 | 0.55 | 0.93 | 0.55 | 0.57 | 0.95 | 0.95 | 0.95 | 0.56 | 0.52 | 0.54 | 0.95 |
| 6 | 0.66 | 0.52 | 0.50 | 0.53 | 0.53 | 0.64 | 0.53 | 0.53 | 0.64 | 0.95 | 0.95 | 0.95 | 0.58 | 0.47 | 0.47 | 0.95 |
| 7 | 0.59 | 0.44 | 0.35 | 0.61 | 0.28 | 0.37 | 0.65 | 0.31 | 0.37 | 0.96 | 0.91 | 0.90 | 0.48 | 0.25 | 0.27 | 0.93 |
| 8 | 0.55 | 0.52 | 0.63 | 0.68 | 0.59 | 0.52 | 0.76 | 0.64 | 0.53 | 0.94 | 0.95 | 0.95 | 0.57 | 0.48 | 0.53 | 0.95 |
| 9 | 0.73 | 0.56 | 0.41 | 0.56 | 0.45 | 0.41 | 0.58 | 0.48 | 0.49 | 0.92 | 0.91 | 0.85 | 0.56 | 0.40 | 0.45 | 0.90 |
| 10 | 0.46 | 0.61 | 0.54 | 0.58 | 0.73 | 0.76 | 0.62 | 0.79 | 0.78 | 0.94 | 0.95 | 0.96 | 0.58 | 0.58 | 0.62 | 0.95 |
| 11 | 0.57 | 0.54 | 0.37 | 0.52 | 0.50 | 0.45 | 0.52 | 0.57 | 0.45 | 0.94 | 0.86 | 0.95 | 0.55 | 0.33 | 0.38 | 0.93 |
| 12 | 0.55 | 0.35 | 0.58 | 0.57 | 0.56 | 0.69 | 0.57 | 0.66 | 0.81 | 0.96 | 0.90 | 0.93 | 0.57 | 0.44 | 0.53 | 0.93 |
| 13 | 0.52 | 0.56 | 0.64 | 0.67 | 0.49 | 0.48 | 0.73 | 0.49 | 0.49 | 0.95 | 0.94 | 0.95 | 0.70 | 0.42 | 0.43 | 0.95 |
| 14 | 0.46 | 0.75 | 0.62 | 0.48 | 0.52 | 0.51 | 0.56 | 0.51 | 0.64 | 0.92 | 0.96 | 0.88 | 0.63 | 0.33 | 0.42 | 0.93 |
| 15 | 0.84 | 0.66 | 0.42 | 0.45 | 0.67 | 0.67 | 0.45 | 0.67 | 0.68 | 0.96 | 0.95 | 0.96 | 0.65 | 0.45 | 0.45 | 0.96 |
| 16 | 0.60 | 0.55 | 0.49 | 0.42 | 0.49 | 0.49 | 0.43 | 0.51 | 0.50 | 0.95 | 0.93 | 0.95 | 0.59 | 0.32 | 0.33 | 0.94 |
| 17 | 0.67 | 0.53 | 0.64 | 0.79 | 0.81 | 0.77 | 0.81 | 0.79 | 0.78 | 0.97 | 0.96 | 0.96 | 0.62 | 0.74 | 0.73 | 0.96 |
| 18 | 0.62 | 0.54 | 0.50 | 0.64 | 0.62 | 0.58 | 0.68 | 0.63 | 0.58 | 0.94 | 0.95 | 0.96 | 0.57 | 0.48 | 0.50 | 0.95 |
| 19 | 0.50 | 0.51 | 0.61 | 0.79 | 0.51 | 0.58 | 0.80 | 0.53 | 0.60 | 0.95 | 0.95 | 0.95 | 0.53 | 0.45 | 0.48 | 0.95 |
| 20 | 0.60 | 0.65 | 0.65 | 0.59 | 0.60 | 0.55 | 0.65 | 0.61 | 0.55 | 0.94 | 0.96 | 0.96 | 0.67 | 0.46 | 0.47 | 0.95 |
| 21 | 0.59 | 0.76 | 0.51 | 0.47 | 0.38 | 0.68 | 0.48 | 0.38 | 0.68 | 0.96 | 0.94 | 0.96 | 0.50 | 0.33 | 0.33 | 0.95 |
| 22 | 0.49 | 0.56 | 0.58 | 0.67 | 0.67 | 0.79 | 0.74 | 0.76 | 0.79 | 0.93 | 0.94 | 0.94 | 0.58 | 0.59 | 0.67 | 0.94 |
| 23 | 0.57 | 0.53 | 0.61 | 0.54 | 0.75 | 0.49 | 0.53 | 0.78 | 0.49 | 0.96 | 0.95 | 0.94 | 0.57 | 0.49 | 0.49 | 0.95 |
| 24 | 0.31 | 0.62 | 0.70 | 0.32 | 0.69 | 0.65 | 0.33 | 0.72 | 0.69 | 0.93 | 0.93 | 0.93 | 0.67 | 0.32 | 0.33 | 0.93 |
| 25 | 0.50 | 0.59 | 0.65 | 0.79 | 0.33 | 0.54 | 0.82 | 0.36 | 0.55 | 0.95 | 0.90 | 0.94 | 0.66 | 0.33 | 0.36 | 0.93 |
| 26 | 0.50 | 0.58 | 0.66 | 0.63 | 0.63 | 0.68 | 0.67 | 0.65 | 0.68 | 0.93 | 0.96 | 0.95 | 0.62 | 0.56 | 0.58 | 0.95 |
| 27 | 0.53 | 0.57 | 0.57 | 0.65 | 0.72 | 0.51 | 0.64 | 0.74 | 0.67 | 0.95 | 0.96 | 0.84 | 0.65 | 0.43 | 0.55 | 0.92 |
| 28 | 0.48 | 0.52 | 0.65 | 0.61 | 0.76 | 0.67 | 0.76 | 0.82 | 0.69 | 0.89 | 0.94 | 0.93 | 0.61 | 0.59 | 0.69 | 0.92 |
| 29 | 0.69 | 0.61 | 0.63 | 0.53 | 0.70 | 0.44 | 0.54 | 0.74 | 0.48 | 0.96 | 0.94 | 0.90 | 0.62 | 0.41 | 0.45 | 0.94 |
| 30 | 0.57 | 0.67 | 0.73 | 0.86 | 0.77 | 0.58 | 0.89 | 0.81 | 0.57 | 0.97 | 0.94 | 0.96 | 0.70 | 0.58 | 0.57 | 0.96 |

## A.5. 2D and 3D Shape Descriptors of Sand D

The values of the determined 2D and 3D shape descriptors of Sand D are presented in the following tables. The results are presented for all particle size ranges of the sample.

Table A.16. Determined 2D and 3D particle shape descriptors of Sand D retained on sieve #10, PR = 36.61, PSR = 2.00 – 2.74 mm.

| Part | $R_{2D}$ | | | $S_{2D}$ | | | $AR_{2D}$ | | | $CX_{2D}$ | | | | | | |
|---|---|---|---|---|---|---|---|---|---|---|---|---|---|---|---|---|
| No. | $F_D$ | $F_1$ | $F_2$ | $F_D$ | $F_1$ | $F_2$ | $F_D$ | $F_1$ | $F_2$ | $F_D$ | $F_1$ | $F_2$ | $R_{3D}$ | $S_{3D}$ | $AR_{3D}$ | $CX_{3D}$ |
| 1 | 0.52 | 0.25 | 0.57 | 0.33 | 0.27 | 0.28 | 0.35 | 0.28 | 0.28 | 0.95 | 0.96 | 0.96 | 0.46 | 0.21 | 0.23 | 0.96 |
| 2 | 0.52 | 0.43 | 0.58 | 0.67 | 0.41 | 0.45 | 0.70 | 0.42 | 0.46 | 0.98 | 0.99 | 0.98 | 0.54 | 0.36 | 0.36 | 0.98 |
| 3 | 0.40 | 0.53 | 0.38 | 0.63 | 0.63 | 0.70 | 0.71 | 0.73 | 0.75 | 0.95 | 0.98 | 0.97 | 0.45 | 0.57 | 0.65 | 0.97 |
| 4 | 0.40 | 0.54 | 0.49 | 0.71 | 0.36 | 0.35 | 0.85 | 0.36 | 0.35 | 0.97 | 0.97 | 0.98 | 0.56 | 0.30 | 0.32 | 0.98 |
| 5 | 0.45 | 0.38 | 0.68 | 0.54 | 0.19 | 0.26 | 0.57 | 0.19 | 0.26 | 0.97 | 0.96 | 0.97 | 0.57 | 0.16 | 0.17 | 0.97 |
| 6 | 0.36 | 0.60 | 0.53 | 0.79 | 0.40 | 0.47 | 0.84 | 0.40 | 0.47 | 0.98 | 0.98 | 0.99 | 0.60 | 0.38 | 0.39 | 0.98 |
| 7 | 0.37 | 0.40 | 0.65 | 0.60 | 0.24 | 0.25 | 0.67 | 0.25 | 0.27 | 0.95 | 0.95 | 0.95 | 0.59 | 0.20 | 0.21 | 0.95 |
| 8 | 0.43 | 0.42 | 0.54 | 0.34 | 0.26 | 0.33 | 0.44 | 0.33 | 0.41 | 0.85 | 0.84 | 0.86 | 0.50 | 0.22 | 0.28 | 0.85 |
| 9 | 0.54 | 0.46 | 0.46 | 0.50 | 0.43 | 0.41 | 0.51 | 0.45 | 0.42 | 0.97 | 0.96 | 0.97 | 0.52 | 0.36 | 0.37 | 0.96 |
| 10 | 0.37 | 0.54 | 0.56 | 0.74 | 0.48 | 0.46 | 0.92 | 0.49 | 0.49 | 0.96 | 0.97 | 0.96 | 0.56 | 0.42 | 0.47 | 0.96 |
| 11 | 0.56 | 0.30 | 0.44 | 0.41 | 0.53 | 0.51 | 0.41 | 0.58 | 0.54 | 0.98 | 0.96 | 0.96 | 0.43 | 0.41 | 0.41 | 0.97 |
| 12 | 0.33 | 0.25 | 0.55 | 0.67 | 0.18 | 0.22 | 0.73 | 0.18 | 0.22 | 0.95 | 0.96 | 0.97 | 0.63 | 0.17 | 0.17 | 0.95 |
| 13 | 0.49 | 0.33 | 0.42 | 0.46 | 0.45 | 0.40 | 0.55 | 0.47 | 0.42 | 0.92 | 0.96 | 0.95 | 0.43 | 0.34 | 0.36 | 0.94 |
| 14 | 0.48 | 0.40 | 0.62 | 0.72 | 0.34 | 0.35 | 0.81 | 0.36 | 0.36 | 0.98 | 0.94 | 0.97 | 0.58 | 0.30 | 0.31 | 0.97 |
| 15 | 0.32 | 0.49 | 0.46 | 0.27 | 0.38 | 0.38 | 0.32 | 0.41 | 0.46 | 0.80 | 0.96 | 0.94 | 0.40 | 0.27 | 0.32 | 0.89 |
| 16 | 0.47 | 0.40 | 0.44 | 0.61 | 0.42 | 0.46 | 0.66 | 0.47 | 0.48 | 0.97 | 0.95 | 0.96 | 0.55 | 0.34 | 0.38 | 0.96 |
| 17 | 0.53 | 0.49 | 0.50 | 0.60 | 0.43 | 0.45 | 0.63 | 0.44 | 0.46 | 0.98 | 0.95 | 0.95 | 0.53 | 0.38 | 0.39 | 0.96 |
| 18 | 0.68 | 0.37 | 0.41 | 0.50 | 0.43 | 0.38 | 0.52 | 0.45 | 0.42 | 0.98 | 0.95 | 0.95 | 0.48 | 0.33 | 0.34 | 0.97 |
| 19 | 0.52 | 0.53 | 0.60 | 0.66 | 0.46 | 0.50 | 0.70 | 0.47 | 0.50 | 0.98 | 0.98 | 0.99 | 0.59 | 0.41 | 0.42 | 0.98 |
| 20 | 0.48 | 0.39 | 0.44 | 0.48 | 0.26 | 0.21 | 0.50 | 0.26 | 0.24 | 0.92 | 0.98 | 0.94 | 0.56 | 0.19 | 0.19 | 0.93 |
| 21 | 0.37 | 0.51 | 0.35 | 0.69 | 0.47 | 0.51 | 0.85 | 0.49 | 0.60 | 0.96 | 0.97 | 0.97 | 0.46 | 0.44 | 0.48 | 0.97 |
| 22 | 0.38 | 0.39 | 0.53 | 0.60 | 0.42 | 0.45 | 0.64 | 0.43 | 0.45 | 0.94 | 0.95 | 0.97 | 0.43 | 0.35 | 0.37 | 0.95 |
| 23 | 0.46 | 0.45 | 0.46 | 0.73 | 0.56 | 0.63 | 0.79 | 0.58 | 0.65 | 0.97 | 0.97 | 0.98 | 0.52 | 0.51 | 0.53 | 0.97 |
| 24 | 0.37 | 0.45 | 0.58 | 0.46 | 0.28 | 0.39 | 0.49 | 0.30 | 0.40 | 0.91 | 0.94 | 0.96 | 0.46 | 0.25 | 0.26 | 0.93 |
| 25 | 0.45 | 0.53 | 0.45 | 0.76 | 0.51 | 0.50 | 0.82 | 0.52 | 0.51 | 0.98 | 0.98 | 0.97 | 0.51 | 0.46 | 0.46 | 0.97 |
| 26 | 0.52 | 0.32 | 0.69 | 0.37 | 0.32 | 0.34 | 0.39 | 0.33 | 0.34 | 0.94 | 0.94 | 0.98 | 0.54 | 0.25 | 0.26 | 0.95 |
| 27 | 0.43 | 0.43 | 0.58 | 0.69 | 0.41 | 0.41 | 0.84 | 0.41 | 0.41 | 0.97 | 0.97 | 0.97 | 0.42 | 0.36 | 0.37 | 0.97 |
| 28 | 0.40 | 0.55 | 0.44 | 0.58 | 0.44 | 0.43 | 0.60 | 0.45 | 0.46 | 0.97 | 0.94 | 0.96 | 0.57 | 0.34 | 0.35 | 0.96 |
| 29 | 0.57 | 0.41 | 0.49 | 0.59 | 0.28 | 0.24 | 0.68 | 0.30 | 0.25 | 0.96 | 0.94 | 0.94 | 0.51 | 0.19 | 0.21 | 0.95 |
| 30 | 0.46 | 0.49 | 0.53 | 0.59 | 0.38 | 0.47 | 0.62 | 0.39 | 0.48 | 0.97 | 0.98 | 0.97 | 0.54 | 0.34 | 0.34 | 0.97 |

Table A.17. Determined 2D and 3D particle shape descriptors of Sand D retained on sieve #20, PR = 36.31, PSR = 0.850 – 2.00 mm.

| Part | $R_{2D}$ | | | $S_{2D}$ | | | $AR_{2D}$ | | | $CX_{2D}$ | | | | | | |
|---|---|---|---|---|---|---|---|---|---|---|---|---|---|---|---|---|
| No. | $F_D$ | $F_1$ | $F_2$ | $F_D$ | $F_1$ | $F_2$ | $F_D$ | $F_1$ | $F_2$ | $F_D$ | $F_1$ | $F_2$ | $R_{3D}$ | $S_{3D}$ | $AR_{3D}$ | $CX_{3D}$ |
| 1 | 0.46 | 0.58 | 0.39 | 0.64 | 0.62 | 0.59 | 0.70 | 0.68 | 0.69 | 0.95 | 0.97 | 0.96 | 0.49 | 0.54 | 0.60 | 0.96 |
| 2 | 0.46 | 0.41 | 0.42 | 0.71 | 0.59 | 0.61 | 0.81 | 0.61 | 0.64 | 0.95 | 0.97 | 0.95 | 0.43 | 0.54 | 0.56 | 0.96 |
| 3 | 0.61 | 0.58 | 0.45 | 0.38 | 0.42 | 0.24 | 0.40 | 0.42 | 0.24 | 0.96 | 0.98 | 0.98 | 0.62 | 0.22 | 0.23 | 0.97 |
| 4 | 0.47 | 0.59 | 0.63 | 0.67 | 0.42 | 0.34 | 0.72 | 0.42 | 0.35 | 0.97 | 0.98 | 0.97 | 0.62 | 0.32 | 0.33 | 0.97 |
| 5 | 0.34 | 0.17 | 0.69 | 0.67 | 0.35 | 0.31 | 0.83 | 0.36 | 0.32 | 0.94 | 0.95 | 0.85 | 0.52 | 0.29 | 0.30 | 0.93 |
| 6 | 0.52 | 0.36 | 0.46 | 0.75 | 0.59 | 0.51 | 0.76 | 0.60 | 0.51 | 0.99 | 0.97 | 0.98 | 0.46 | 0.50 | 0.51 | 0.98 |
| 7 | 0.53 | 0.52 | 0.40 | 0.57 | 0.60 | 0.58 | 0.65 | 0.61 | 0.66 | 0.95 | 0.97 | 0.94 | 0.47 | 0.49 | 0.55 | 0.95 |
| 8 | 0.57 | 0.34 | 0.57 | 0.61 | 0.31 | 0.24 | 0.62 | 0.33 | 0.26 | 0.97 | 0.95 | 0.94 | 0.48 | 0.23 | 0.25 | 0.96 |
| 9 | 0.53 | 0.53 | 0.50 | 0.59 | 0.39 | 0.32 | 0.63 | 0.40 | 0.33 | 0.97 | 0.94 | 0.97 | 0.53 | 0.30 | 0.31 | 0.96 |
| 10 | 0.31 | 0.32 | 0.36 | 0.47 | 0.42 | 0.39 | 0.50 | 0.42 | 0.40 | 0.94 | 0.94 | 0.94 | 0.36 | 0.34 | 0.35 | 0.94 |
| 11 | 0.37 | 0.34 | 0.53 | 0.57 | 0.35 | 0.30 | 0.67 | 0.36 | 0.31 | 0.96 | 0.96 | 0.93 | 0.47 | 0.29 | 0.30 | 0.95 |
| 12 | 0.40 | 0.66 | 0.50 | 0.48 | 0.20 | 0.15 | 0.55 | 0.20 | 0.16 | 0.92 | 0.89 | 0.88 | 0.62 | 0.15 | 0.16 | 0.90 |
| 13 | 0.45 | 0.43 | 0.54 | 0.64 | 0.35 | 0.50 | 0.67 | 0.37 | 0.52 | 0.96 | 0.94 | 0.95 | 0.53 | 0.35 | 0.37 | 0.95 |
| 14 | 0.43 | 0.28 | 0.40 | 0.59 | 0.29 | 0.30 | 0.60 | 0.31 | 0.33 | 0.97 | 0.87 | 0.91 | 0.54 | 0.25 | 0.29 | 0.93 |
| 15 | 0.40 | 0.50 | 0.37 | 0.67 | 0.41 | 0.49 | 0.74 | 0.42 | 0.51 | 0.94 | 0.96 | 0.96 | 0.45 | 0.40 | 0.42 | 0.95 |
| 16 | 0.47 | 0.37 | 0.46 | 0.48 | 0.70 | 0.50 | 0.48 | 0.78 | 0.52 | 0.97 | 0.95 | 0.96 | 0.44 | 0.47 | 0.47 | 0.96 |
| 17 | 0.45 | 0.26 | 0.22 | 0.65 | 0.52 | 0.45 | 0.74 | 0.58 | 0.53 | 0.92 | 0.90 | 0.88 | 0.35 | 0.44 | 0.52 | 0.91 |
| 18 | 0.46 | 0.64 | 0.52 | 0.54 | 0.29 | 0.21 | 0.55 | 0.29 | 0.22 | 0.96 | 0.94 | 0.91 | 0.61 | 0.20 | 0.21 | 0.94 |
| 19 | 0.44 | 0.51 | 0.36 | 0.76 | 0.44 | 0.48 | 0.81 | 0.47 | 0.49 | 0.97 | 0.96 | 0.96 | 0.50 | 0.43 | 0.45 | 0.96 |
| 20 | 0.44 | 0.51 | 0.52 | 0.60 | 0.37 | 0.26 | 0.60 | 0.37 | 0.26 | 0.98 | 0.97 | 0.96 | 0.54 | 0.26 | 0.26 | 0.97 |
| 21 | 0.48 | 0.39 | 0.47 | 0.64 | 0.57 | 0.45 | 0.67 | 0.59 | 0.47 | 0.95 | 0.97 | 0.96 | 0.47 | 0.42 | 0.44 | 0.96 |
| 22 | 0.45 | 0.35 | 0.42 | 0.67 | 0.57 | 0.55 | 0.71 | 0.63 | 0.59 | 0.97 | 0.95 | 0.97 | 0.44 | 0.54 | 0.59 | 0.97 |
| 23 | 0.46 | 0.61 | 0.53 | 0.47 | 0.24 | 0.21 | 0.51 | 0.25 | 0.21 | 0.95 | 0.95 | 0.96 | 0.59 | 0.20 | 0.20 | 0.95 |
| 24 | 0.47 | 0.40 | 0.34 | 0.52 | 0.33 | 0.35 | 0.57 | 0.33 | 0.36 | 0.96 | 0.97 | 0.95 | 0.41 | 0.30 | 0.31 | 0.96 |
| 25 | 0.33 | 0.36 | 0.36 | 0.58 | 0.35 | 0.25 | 0.71 | 0.35 | 0.27 | 0.89 | 0.93 | 0.89 | 0.41 | 0.25 | 0.27 | 0.90 |
| 26 | 0.47 | 0.34 | 0.37 | 0.46 | 0.35 | 0.33 | 0.50 | 0.37 | 0.35 | 0.94 | 0.91 | 0.90 | 0.42 | 0.27 | 0.29 | 0.92 |
| 27 | 0.42 | 0.47 | 0.49 | 0.65 | 0.31 | 0.26 | 0.85 | 0.33 | 0.28 | 0.97 | 0.91 | 0.90 | 0.59 | 0.24 | 0.28 | 0.94 |
| 28 | 0.36 | 0.53 | 0.46 | 0.60 | 0.34 | 0.37 | 0.72 | 0.36 | 0.38 | 0.95 | 0.95 | 0.92 | 0.55 | 0.29 | 0.30 | 0.94 |
| 29 | 0.60 | 0.64 | 0.46 | 0.51 | 0.41 | 0.33 | 0.52 | 0.47 | 0.36 | 0.97 | 0.94 | 0.93 | 0.57 | 0.30 | 0.34 | 0.95 |
| 30 | 0.37 | 0.37 | 0.56 | 0.44 | 0.23 | 0.22 | 0.58 | 0.24 | 0.23 | 0.84 | 0.92 | 0.95 | 0.43 | 0.19 | 0.21 | 0.88 |

Table A.18. Determined 2D and 3D particle shape descriptors of Sand D retained on sieve #60. PR=7.10, PSR=0.250-0.425 mm.

| Part | $R_{2D}$ | | | $S_{2D}$ | | | $AR_{2D}$ | | | $CX_{2D}$ | | | | | | |
|---|---|---|---|---|---|---|---|---|---|---|---|---|---|---|---|---|
| No. | $F_D$ | $F_1$ | $F_2$ | $F_D$ | $F_1$ | $F_2$ | $F_D$ | $F_1$ | $F_2$ | $F_D$ | $F_1$ | $F_2$ | $R_{3D}$ | $S_{3D}$ | $AR_{3D}$ | $CX_{3D}$ |
| 1 | 0.51 | 0.46 | 0.37 | 0.39 | 0.42 | 0.35 | 0.40 | 0.42 | 0.38 | 0.95 | 0.94 | 0.93 | 0.42 | 0.33 | 0.35 | 0.94 |
| 2 | 0.60 | 0.61 | 0.26 | 0.69 | 0.38 | 0.37 | 0.73 | 0.38 | 0.38 | 0.95 | 0.92 | 0.94 | 0.55 | 0.32 | 0.33 | 0.94 |
| 3 | 0.49 | 0.62 | 0.31 | 0.78 | 0.41 | 0.41 | 0.81 | 0.42 | 0.41 | 0.97 | 0.94 | 0.91 | 0.59 | 0.39 | 0.39 | 0.95 |
| 4 | 0.56 | 0.33 | 0.55 | 0.62 | 0.30 | 0.28 | 0.64 | 0.33 | 0.30 | 0.96 | 0.91 | 0.91 | 0.56 | 0.28 | 0.30 | 0.93 |
| 5 | 0.39 | 0.42 | 0.33 | 0.52 | 0.39 | 0.27 | 0.57 | 0.39 | 0.26 | 0.93 | 0.94 | 0.95 | 0.46 | 0.26 | 0.26 | 0.94 |
| 6 | 0.71 | 0.54 | 0.51 | 0.82 | 0.47 | 0.44 | 0.83 | 0.49 | 0.44 | 0.97 | 0.93 | 0.92 | 0.59 | 0.38 | 0.40 | 0.95 |
| 7 | 0.62 | 0.50 | 0.50 | 0.77 | 0.44 | 0.46 | 0.86 | 0.45 | 0.48 | 0.94 | 0.94 | 0.93 | 0.53 | 0.43 | 0.45 | 0.94 |
| 8 | 0.48 | 0.74 | 0.43 | 0.55 | 0.56 | 0.41 | 0.56 | 0.58 | 0.41 | 0.95 | 0.95 | 0.95 | 0.61 | 0.36 | 0.37 | 0.95 |
| 9 | 0.66 | 0.60 | 0.52 | 0.61 | 0.50 | 0.38 | 0.62 | 0.51 | 0.40 | 0.96 | 0.92 | 0.94 | 0.67 | 0.37 | 0.39 | 0.95 |
| 10 | 0.47 | 0.24 | 0.28 | 0.43 | 0.19 | 0.24 | 0.43 | 0.19 | 0.25 | 0.92 | 0.87 | 0.88 | 0.42 | 0.17 | 0.18 | 0.90 |
| 11 | 0.51 | 0.54 | 0.44 | 0.53 | 0.54 | 0.52 | 0.55 | 0.54 | 0.53 | 0.94 | 0.95 | 0.95 | 0.54 | 0.45 | 0.46 | 0.94 |
| 12 | 0.49 | 0.51 | 0.73 | 0.67 | 0.40 | 0.58 | 0.68 | 0.41 | 0.63 | 0.96 | 0.94 | 0.90 | 0.63 | 0.40 | 0.41 | 0.94 |
| 13 | 0.53 | 0.47 | 0.47 | 0.57 | 0.35 | 0.51 | 0.61 | 0.35 | 0.51 | 0.94 | 0.92 | 0.94 | 0.50 | 0.35 | 0.35 | 0.93 |
| 14 | 0.52 | 0.46 | 0.47 | 0.58 | 0.24 | 0.34 | 0.60 | 0.25 | 0.34 | 0.95 | 0.90 | 0.90 | 0.52 | 0.24 | 0.25 | 0.93 |
| 15 | 0.54 | 0.56 | 0.53 | 0.75 | 0.40 | 0.51 | 0.84 | 0.42 | 0.51 | 0.96 | 0.93 | 0.94 | 0.61 | 0.38 | 0.41 | 0.95 |
| 16 | 0.66 | 0.50 | 0.39 | 0.70 | 0.35 | 0.43 | 0.71 | 0.35 | 0.45 | 0.97 | 0.95 | 0.92 | 0.49 | 0.32 | 0.32 | 0.95 |
| 17 | 0.42 | 0.23 | 0.34 | 0.71 | 0.23 | 0.26 | 0.79 | 0.26 | 0.27 | 0.96 | 0.87 | 0.92 | 0.51 | 0.20 | 0.23 | 0.94 |
| 18 | 0.46 | 0.56 | 0.50 | 0.68 | 0.54 | 0.62 | 0.75 | 0.55 | 0.63 | 0.96 | 0.96 | 0.94 | 0.57 | 0.50 | 0.52 | 0.95 |
| 19 | 0.57 | 0.18 | 0.54 | 0.44 | 0.30 | 0.40 | 0.45 | 0.31 | 0.42 | 0.96 | 0.93 | 0.94 | 0.41 | 0.25 | 0.26 | 0.95 |
| 20 | 0.65 | 0.58 | 0.60 | 0.61 | 0.40 | 0.25 | 0.62 | 0.41 | 0.26 | 0.95 | 0.93 | 0.90 | 0.68 | 0.25 | 0.26 | 0.93 |
| 21 | 0.66 | 0.49 | 0.40 | 0.62 | 0.44 | 0.55 | 0.62 | 0.45 | 0.55 | 0.97 | 0.94 | 0.95 | 0.51 | 0.40 | 0.42 | 0.96 |
| 22 | 0.39 | 0.63 | 0.47 | 0.52 | 0.41 | 0.33 | 0.54 | 0.41 | 0.33 | 0.95 | 0.95 | 0.95 | 0.53 | 0.31 | 0.32 | 0.95 |
| 23 | 0.60 | 0.56 | 0.40 | 0.56 | 0.46 | 0.64 | 0.57 | 0.48 | 0.67 | 0.97 | 0.94 | 0.92 | 0.48 | 0.44 | 0.47 | 0.95 |
| 24 | 0.55 | 0.26 | 0.49 | 0.48 | 0.40 | 0.43 | 0.48 | 0.44 | 0.45 | 0.96 | 0.90 | 0.91 | 0.48 | 0.34 | 0.37 | 0.93 |
| 25 | 0.54 | 0.58 | 0.34 | 0.43 | 0.59 | 0.40 | 0.43 | 0.62 | 0.41 | 0.94 | 0.96 | 0.95 | 0.49 | 0.36 | 0.38 | 0.95 |
| 26 | 0.38 | 0.64 | 0.45 | 0.46 | 0.57 | 0.73 | 0.46 | 0.61 | 0.74 | 0.97 | 0.94 | 0.95 | 0.53 | 0.46 | 0.46 | 0.95 |
| 27 | 0.50 | 0.49 | 0.43 | 0.61 | 0.58 | 0.44 | 0.67 | 0.57 | 0.47 | 0.96 | 0.96 | 0.94 | 0.52 | 0.40 | 0.41 | 0.95 |
| 28 | 0.52 | 0.53 | 0.28 | 0.76 | 0.35 | 0.32 | 0.78 | 0.35 | 0.32 | 0.97 | 0.94 | 0.93 | 0.52 | 0.31 | 0.31 | 0.95 |
| 29 | 0.66 | 0.64 | 0.59 | 0.59 | 0.48 | 0.46 | 0.59 | 0.49 | 0.48 | 0.97 | 0.94 | 0.93 | 0.64 | 0.39 | 0.40 | 0.95 |
| 30 | 0.68 | 0.37 | 0.49 | 0.60 | 0.47 | 0.39 | 0.61 | 0.46 | 0.40 | 0.97 | 0.95 | 0.94 | 0.48 | 0.37 | 0.38 | 0.96 |

Table A.19. Determined 2D and 3D particle shape descriptors of Sand D retained on sieve #100, PR = 4.97, PSR = 0.150 – 0.250 mm.

| Part | $R_{2D}$ | | | $S_{2D}$ | | | $AR_{2D}$ | | | $CX_{2D}$ | | | | | | |
|---|---|---|---|---|---|---|---|---|---|---|---|---|---|---|---|---|
| No. | $F_D$ | $F_1$ | $F_2$ | $F_D$ | $F_1$ | $F_2$ | $F_D$ | $F_1$ | $F_2$ | $F_D$ | $F_1$ | $F_2$ | $R_{3D}$ | $S_{3D}$ | $AR_{3D}$ | $CX_{3D}$ |
| 1 | 0.30 | 0.44 | 0.35 | 0.65 | 0.24 | 0.33 | 0.74 | 0.24 | 0.33 | 0.91 | 0.92 | 0.91 | 0.51 | 0.24 | 0.24 | 0.91 |
| 2 | 0.43 | 0.48 | 0.55 | 0.49 | 0.38 | 0.49 | 0.49 | 0.39 | 0.49 | 0.95 | 0.94 | 0.94 | 0.52 | 0.28 | 0.29 | 0.94 |
| 3 | 0.49 | 0.61 | 0.51 | 0.51 | 0.44 | 0.50 | 0.55 | 0.49 | 0.52 | 0.93 | 0.91 | 0.92 | 0.56 | 0.42 | 0.47 | 0.92 |
| 4 | 0.44 | 0.60 | 0.69 | 0.79 | 0.40 | 0.47 | 0.84 | 0.41 | 0.47 | 0.94 | 0.91 | 0.91 | 0.67 | 0.40 | 0.40 | 0.92 |
| 5 | 0.62 | 0.60 | 0.42 | 0.73 | 0.58 | 0.62 | 0.74 | 0.60 | 0.62 | 0.96 | 0.95 | 0.93 | 0.48 | 0.54 | 0.56 | 0.95 |
| 6 | 0.63 | 0.51 | 0.67 | 0.67 | 0.62 | 0.47 | 0.67 | 0.62 | 0.48 | 0.96 | 0.94 | 0.94 | 0.58 | 0.41 | 0.43 | 0.95 |
| 7 | 0.59 | 0.57 | 0.54 | 0.81 | 0.48 | 0.40 | 0.81 | 0.46 | 0.38 | 0.95 | 0.93 | 0.94 | 0.58 | 0.40 | 0.38 | 0.94 |
| 8 | 0.62 | 0.72 | 0.54 | 0.66 | 0.33 | 0.60 | 0.67 | 0.38 | 0.57 | 0.95 | 0.91 | 0.95 | 0.70 | 0.33 | 0.38 | 0.94 |
| 9 | 0.62 | 0.56 | 0.49 | 0.64 | 0.54 | 0.65 | 0.67 | 0.54 | 0.64 | 0.95 | 0.95 | 0.94 | 0.62 | 0.50 | 0.51 | 0.95 |
| 10 | 0.56 | 0.60 | 0.25 | 0.69 | 0.44 | 0.52 | 0.69 | 0.44 | 0.51 | 0.96 | 0.94 | 0.94 | 0.52 | 0.34 | 0.34 | 0.95 |
| 11 | 0.59 | 0.49 | 0.40 | 0.73 | 0.61 | 0.50 | 0.74 | 0.58 | 0.49 | 0.95 | 0.95 | 0.93 | 0.53 | 0.45 | 0.44 | 0.95 |
| 12 | 0.54 | 0.62 | 0.55 | 0.63 | 0.49 | 0.41 | 0.65 | 0.49 | 0.43 | 0.95 | 0.93 | 0.92 | 0.62 | 0.37 | 0.39 | 0.93 |
| 13 | 0.60 | 0.64 | 0.57 | 0.63 | 0.28 | 0.37 | 0.62 | 0.30 | 0.39 | 0.97 | 0.86 | 0.93 | 0.63 | 0.26 | 0.28 | 0.93 |
| 14 | 0.62 | 0.62 | 0.67 | 0.56 | 0.52 | 0.48 | 0.63 | 0.56 | 0.50 | 0.92 | 0.94 | 0.94 | 0.72 | 0.41 | 0.45 | 0.93 |
| 15 | 0.54 | 0.51 | 0.53 | 0.78 | 0.66 | 0.68 | 0.76 | 0.67 | 0.69 | 0.96 | 0.93 | 0.94 | 0.64 | 0.50 | 0.51 | 0.95 |
| 16 | 0.57 | 0.68 | 0.31 | 0.82 | 0.30 | 0.36 | 0.83 | 0.30 | 0.38 | 0.96 | 0.88 | 0.92 | 0.45 | 0.30 | 0.30 | 0.93 |
| 17 | 0.64 | 0.43 | 0.68 | 0.78 | 0.48 | 0.61 | 0.82 | 0.51 | 0.61 | 0.96 | 0.94 | 0.95 | 0.66 | 0.46 | 0.49 | 0.95 |
| 18 | 0.58 | 0.56 | 0.62 | 0.70 | 0.55 | 0.60 | 0.70 | 0.59 | 0.62 | 0.95 | 0.89 | 0.94 | 0.65 | 0.47 | 0.51 | 0.93 |
| 19 | 0.50 | 0.48 | 0.80 | 0.71 | 0.53 | 0.52 | 0.80 | 0.56 | 0.56 | 0.95 | 0.93 | 0.93 | 0.64 | 0.45 | 0.49 | 0.94 |
| 20 | 0.63 | 0.61 | 0.53 | 0.60 | 0.54 | 0.67 | 0.60 | 0.56 | 0.72 | 0.93 | 0.93 | 0.93 | 0.62 | 0.53 | 0.55 | 0.93 |
| 21 | 0.58 | 0.67 | 0.36 | 0.69 | 0.37 | 0.46 | 0.71 | 0.38 | 0.46 | 0.96 | 0.90 | 0.94 | 0.61 | 0.33 | 0.33 | 0.94 |
| 22 | 0.63 | 0.48 | 0.65 | 0.71 | 0.75 | 0.54 | 0.73 | 0.77 | 0.54 | 0.95 | 0.92 | 0.94 | 0.59 | 0.52 | 0.54 | 0.94 |
| 23 | 0.57 | 0.61 | 0.66 | 0.76 | 0.58 | 0.48 | 0.78 | 0.58 | 0.49 | 0.96 | 0.94 | 0.94 | 0.69 | 0.48 | 0.48 | 0.95 |
| 24 | 0.54 | 0.51 | 0.41 | 0.68 | 0.48 | 0.67 | 0.69 | 0.50 | 0.70 | 0.96 | 0.92 | 0.94 | 0.54 | 0.43 | 0.46 | 0.94 |
| 25 | 0.61 | 0.50 | 0.61 | 0.65 | 0.38 | 0.45 | 0.65 | 0.38 | 0.46 | 0.96 | 0.93 | 0.94 | 0.59 | 0.31 | 0.32 | 0.95 |
| 26 | 0.66 | 0.65 | 0.57 | 0.60 | 0.51 | 0.54 | 0.58 | 0.50 | 0.56 | 0.96 | 0.95 | 0.94 | 0.64 | 0.41 | 0.43 | 0.95 |
| 27 | 0.76 | 0.55 | 0.59 | 0.61 | 0.41 | 0.38 | 0.61 | 0.43 | 0.39 | 0.96 | 0.93 | 0.94 | 0.57 | 0.38 | 0.39 | 0.95 |
| 28 | 0.72 | 0.62 | 0.63 | 0.56 | 0.61 | 0.76 | 0.57 | 0.61 | 0.77 | 0.96 | 0.95 | 0.94 | 0.77 | 0.47 | 0.48 | 0.95 |
| 29 | 0.72 | 0.32 | 0.68 | 0.54 | 0.34 | 0.68 | 0.54 | 0.36 | 0.72 | 0.95 | 0.90 | 0.90 | 0.52 | 0.32 | 0.34 | 0.93 |
| 30 | 0.70 | 0.62 | 0.57 | 0.68 | 0.46 | 0.34 | 0.70 | 0.45 | 0.34 | 0.94 | 0.91 | 0.91 | 0.58 | 0.32 | 0.32 | 0.92 |

Table A.20. Determined 2D and 3D particle shape descriptors of Sand D retained on sieve #140, PR = 2.22, PSR = 0.106 – 0.150 mm.

| Part | $R_{2D}$ | | | $S_{2D}$ | | | $AR_{2D}$ | | | $CX_{2D}$ | | | | | | |
|---|---|---|---|---|---|---|---|---|---|---|---|---|---|---|---|---|
| No. | $F_D$ | $F_1$ | $F_2$ | $F_D$ | $F_1$ | $F_2$ | $F_D$ | $F_1$ | $F_2$ | $F_D$ | $F_1$ | $F_2$ | $R_{3D}$ | $S_{3D}$ | $AR_{3D}$ | $CX_{3D}$ |
| 1 | 0.64 | 0.71 | 0.57 | 0.66 | 0.51 | 0.54 | 0.65 | 0.51 | 0.53 | 0.95 | 0.92 | 0.95 | 0.56 | 0.48 | 0.48 | 0.94 |
| 2 | 0.64 | 0.47 | 0.54 | 0.68 | 0.40 | 0.49 | 0.70 | 0.40 | 0.54 | 0.97 | 0.94 | 0.92 | 0.58 | 0.37 | 0.40 | 0.95 |
| 3 | 0.71 | 0.63 | 0.59 | 0.77 | 0.59 | 0.72 | 0.83 | 0.58 | 0.72 | 0.93 | 0.93 | 0.94 | 0.58 | 0.59 | 0.58 | 0.93 |
| 4 | 0.60 | 0.31 | 0.39 | 0.79 | 0.57 | 0.49 | 0.89 | 0.66 | 0.50 | 0.94 | 0.92 | 0.94 | 0.59 | 0.48 | 0.50 | 0.94 |
| 5 | 0.58 | 0.41 | 0.41 | 0.57 | 0.46 | 0.52 | 0.59 | 0.46 | 0.52 | 0.95 | 0.94 | 0.95 | 0.44 | 0.45 | 0.45 | 0.94 |
| 6 | 0.66 | 0.48 | 0.67 | 0.48 | 0.48 | 0.74 | 0.46 | 0.51 | 0.71 | 0.95 | 0.93 | 0.94 | 0.59 | 0.42 | 0.41 | 0.94 |
| 7 | 0.74 | 0.73 | 0.70 | 0.90 | 0.68 | 0.65 | 0.90 | 0.71 | 0.66 | 0.97 | 0.94 | 0.94 | 0.77 | 0.60 | 0.61 | 0.95 |
| 8 | 0.48 | 0.60 | 0.64 | 0.77 | 0.68 | 0.60 | 0.74 | 0.73 | 0.60 | 0.95 | 0.92 | 0.94 | 0.60 | 0.60 | 0.60 | 0.94 |
| 9 | 0.54 | 0.73 | 0.70 | 0.62 | 0.39 | 0.45 | 0.67 | 0.40 | 0.45 | 0.94 | 0.92 | 0.93 | 0.82 | 0.30 | 0.31 | 0.93 |
| 10 | 0.27 | 0.60 | 0.54 | 0.32 | 0.77 | 0.40 | 0.33 | 0.83 | 0.40 | 0.93 | 0.93 | 0.93 | 0.50 | 0.30 | 0.33 | 0.93 |
| 11 | 0.59 | 0.70 | 0.69 | 0.77 | 0.54 | 0.63 | 0.81 | 0.55 | 0.62 | 0.92 | 0.89 | 0.93 | 0.73 | 0.48 | 0.49 | 0.92 |
| 12 | 0.66 | 0.28 | 0.80 | 0.67 | 0.47 | 0.44 | 0.68 | 0.48 | 0.46 | 0.96 | 0.91 | 0.90 | 0.61 | 0.35 | 0.37 | 0.93 |
| 13 | 0.53 | 0.59 | 0.45 | 0.75 | 0.43 | 0.51 | 0.78 | 0.44 | 0.51 | 0.93 | 0.93 | 0.90 | 0.59 | 0.37 | 0.38 | 0.93 |
| 14 | 0.78 | 0.41 | 0.73 | 0.76 | 0.42 | 0.34 | 0.76 | 0.43 | 0.36 | 0.96 | 0.91 | 0.92 | 0.47 | 0.30 | 0.32 | 0.94 |
| 15 | 0.62 | 0.80 | 0.34 | 0.64 | 0.74 | 0.44 | 0.66 | 0.73 | 0.46 | 0.94 | 0.95 | 0.92 | 0.64 | 0.43 | 0.46 | 0.94 |
| 16 | 0.75 | 0.68 | 0.58 | 0.70 | 0.70 | 0.64 | 0.71 | 0.69 | 0.65 | 0.95 | 0.95 | 0.94 | 0.67 | 0.57 | 0.59 | 0.95 |
| 17 | 0.63 | 0.37 | 0.50 | 0.81 | 0.37 | 0.44 | 0.84 | 0.41 | 0.45 | 0.96 | 0.90 | 0.92 | 0.47 | 0.36 | 0.41 | 0.94 |
| 18 | 0.75 | 0.32 | 0.46 | 0.70 | 0.32 | 0.52 | 0.72 | 0.34 | 0.53 | 0.96 | 0.92 | 0.93 | 0.46 | 0.32 | 0.34 | 0.94 |
| 19 | 0.67 | 0.60 | 0.85 | 0.56 | 0.78 | 0.52 | 0.58 | 0.82 | 0.55 | 0.96 | 0.94 | 0.94 | 0.68 | 0.52 | 0.55 | 0.94 |
| 20 | 0.77 | 0.69 | 0.80 | 0.57 | 0.39 | 0.46 | 0.59 | 0.40 | 0.47 | 0.95 | 0.84 | 0.90 | 0.68 | 0.23 | 0.24 | 0.92 |
| 21 | 0.46 | 0.55 | 0.51 | 0.36 | 0.33 | 0.49 | 0.37 | 0.33 | 0.51 | 0.94 | 0.88 | 0.94 | 0.55 | 0.26 | 0.28 | 0.92 |
| 22 | 0.69 | 0.84 | 0.46 | 0.62 | 0.60 | 0.67 | 0.66 | 0.63 | 0.66 | 0.94 | 0.94 | 0.94 | 0.68 | 0.60 | 0.62 | 0.94 |
| 23 | 0.51 | 0.58 | 0.41 | 0.77 | 0.49 | 0.63 | 0.79 | 0.51 | 0.68 | 0.93 | 0.93 | 0.93 | 0.54 | 0.39 | 0.43 | 0.93 |
| 24 | 0.58 | 0.46 | 0.74 | 0.53 | 0.38 | 0.70 | 0.54 | 0.39 | 0.71 | 0.94 | 0.93 | 0.93 | 0.64 | 0.38 | 0.39 | 0.93 |
| 25 | 0.37 | 0.74 | 0.41 | 0.52 | 0.70 | 0.37 | 0.55 | 0.70 | 0.37 | 0.92 | 0.94 | 0.94 | 0.59 | 0.37 | 0.37 | 0.93 |
| 26 | 0.46 | 0.34 | 0.28 | 0.63 | 0.45 | 0.40 | 0.64 | 0.45 | 0.41 | 0.97 | 0.94 | 0.93 | 0.48 | 0.29 | 0.29 | 0.95 |
| 27 | 0.55 | 0.57 | 0.62 | 0.68 | 0.57 | 0.66 | 0.68 | 0.62 | 0.72 | 0.95 | 0.92 | 0.93 | 0.60 | 0.56 | 0.57 | 0.93 |
| 28 | 0.55 | 0.78 | 0.51 | 0.54 | 0.57 | 0.51 | 0.56 | 0.55 | 0.52 | 0.91 | 0.93 | 0.93 | 0.67 | 0.35 | 0.35 | 0.92 |
| 29 | 0.45 | 0.70 | 0.45 | 0.58 | 0.69 | 0.50 | 0.59 | 0.72 | 0.50 | 0.95 | 0.93 | 0.93 | 0.62 | 0.46 | 0.46 | 0.94 |
| 30 | 0.47 | 0.66 | 0.69 | 0.37 | 0.34 | 0.52 | 0.38 | 0.33 | 0.52 | 0.92 | 0.95 | 0.94 | 0.68 | 0.23 | 0.24 | 0.93 |

## A.6. 2D and 3D Shape Descriptors of Sand E

Table A.21. Determined 2D and 3D particle shape descriptors of Sand E retained on sieve #10, PR = 66.43, PSR = 2.00 - 4.75 mm.

| Part | $R_{2D}$ | | | $S_{2D}$ | | | $AR_{2D}$ | | | $CX_{2D}$ | | | | | | |
|---|---|---|---|---|---|---|---|---|---|---|---|---|---|---|---|---|
| No. | $F_D$ | $F_1$ | $F_2$ | $F_D$ | $F_1$ | $F_2$ | $F_D$ | $F_1$ | $F_2$ | $F_D$ | $F_1$ | $F_2$ | $R_{3D}$ | $S_{3D}$ | $AR_{3D}$ | $CX_{3D}$ |
| 1 | 0.72 | 0.58 | 0.67 | 0.53 | 0.43 | 0.41 | 0.53 | 0.44 | 0.41 | 0.99 | 0.98 | 0.99 | 0.67 | 0.34 | 0.35 | 0.99 |
| 2 | 0.63 | 0.39 | 0.50 | 0.65 | 0.45 | 0.38 | 0.66 | 0.46 | 0.38 | 0.99 | 0.98 | 0.98 | 0.57 | 0.33 | 0.34 | 0.98 |
| 3 | 0.38 | 0.43 | 0.42 | 0.74 | 0.41 | 0.41 | 0.83 | 0.42 | 0.42 | 0.95 | 0.97 | 0.97 | 0.50 | 0.37 | 0.39 | 0.96 |
| 4 | 0.49 | 0.56 | 0.51 | 0.64 | 0.51 | 0.58 | 0.71 | 0.52 | 0.60 | 0.97 | 0.98 | 0.97 | 0.56 | 0.45 | 0.46 | 0.97 |
| 5 | 0.50 | 0.38 | 0.54 | 0.45 | 0.42 | 0.38 | 0.50 | 0.47 | 0.39 | 0.94 | 0.96 | 0.97 | 0.50 | 0.33 | 0.36 | 0.96 |
| 6 | 0.49 | 0.47 | 0.40 | 0.66 | 0.67 | 0.67 | 0.67 | 0.69 | 0.77 | 0.97 | 0.98 | 0.96 | 0.48 | 0.57 | 0.64 | 0.97 |
| 7 | 0.44 | 0.45 | 0.49 | 0.60 | 0.21 | 0.24 | 0.68 | 0.22 | 0.24 | 0.95 | 0.93 | 0.96 | 0.53 | 0.18 | 0.19 | 0.95 |
| 8 | 0.44 | 0.45 | 0.52 | 0.67 | 0.79 | 0.66 | 0.76 | 0.81 | 0.77 | 0.96 | 0.98 | 0.99 | 0.49 | 0.58 | 0.67 | 0.97 |
| 9 | 0.46 | 0.46 | 0.52 | 0.61 | 0.65 | 0.73 | 0.65 | 0.75 | 0.77 | 0.95 | 0.97 | 0.98 | 0.46 | 0.60 | 0.65 | 0.97 |
| 10 | 0.41 | 0.43 | 0.41 | 0.68 | 0.54 | 0.60 | 0.73 | 0.55 | 0.63 | 0.96 | 0.97 | 0.98 | 0.44 | 0.49 | 0.51 | 0.97 |
| 11 | 0.59 | 0.63 | 0.67 | 0.72 | 0.65 | 0.61 | 0.82 | 0.67 | 0.62 | 0.99 | 0.99 | 0.99 | 0.64 | 0.58 | 0.60 | 0.99 |
| 12 | 0.53 | 0.72 | 0.54 | 0.57 | 0.58 | 0.72 | 0.59 | 0.58 | 0.81 | 0.96 | 0.99 | 0.98 | 0.61 | 0.50 | 0.56 | 0.98 |
| 13 | 0.53 | 0.68 | 0.61 | 0.69 | 0.44 | 0.47 | 0.70 | 0.45 | 0.48 | 0.97 | 0.98 | 0.99 | 0.65 | 0.39 | 0.39 | 0.98 |
| 14 | 0.61 | 0.50 | 0.49 | 0.49 | 0.52 | 0.52 | 0.51 | 0.53 | 0.56 | 0.98 | 0.98 | 0.98 | 0.51 | 0.41 | 0.42 | 0.98 |
| 15 | 0.40 | 0.39 | 0.46 | 0.68 | 0.60 | 0.70 | 0.73 | 0.62 | 0.72 | 0.97 | 0.97 | 0.97 | 0.45 | 0.55 | 0.57 | 0.97 |
| 16 | 0.56 | 0.54 | 0.55 | 0.58 | 0.51 | 0.47 | 0.67 | 0.53 | 0.48 | 0.93 | 0.97 | 0.97 | 0.57 | 0.44 | 0.44 | 0.95 |
| 17 | 0.48 | 0.62 | 0.62 | 0.50 | 0.46 | 0.41 | 0.53 | 0.47 | 0.42 | 0.96 | 0.98 | 0.98 | 0.60 | 0.36 | 0.37 | 0.97 |
| 18 | 0.61 | 0.54 | 0.46 | 0.81 | 0.41 | 0.36 | 0.82 | 0.41 | 0.38 | 0.99 | 0.94 | 0.97 | 0.56 | 0.33 | 0.34 | 0.97 |
| 19 | 0.57 | 0.58 | 0.64 | 0.75 | 0.42 | 0.47 | 0.76 | 0.45 | 0.47 | 0.99 | 0.97 | 0.99 | 0.69 | 0.40 | 0.41 | 0.98 |
| 20 | 0.51 | 0.54 | 0.52 | 0.81 | 0.63 | 0.63 | 0.84 | 0.66 | 0.67 | 0.99 | 0.98 | 0.98 | 0.57 | 0.60 | 0.64 | 0.98 |
| 21 | 0.50 | 0.41 | 0.58 | 0.70 | 0.55 | 0.55 | 0.81 | 0.57 | 0.56 | 0.96 | 0.98 | 0.98 | 0.53 | 0.46 | 0.48 | 0.97 |
| 22 | 0.54 | 0.35 | 0.45 | 0.55 | 0.42 | 0.49 | 0.57 | 0.43 | 0.51 | 0.98 | 0.97 | 0.98 | 0.47 | 0.35 | 0.36 | 0.98 |
| 23 | 0.49 | 0.50 | 0.56 | 0.39 | 0.50 | 0.36 | 0.43 | 0.55 | 0.50 | 0.95 | 0.88 | 0.85 | 0.56 | 0.29 | 0.40 | 0.90 |
| 24 | 0.47 | 0.41 | 0.58 | 0.60 | 0.72 | 0.62 | 0.67 | 0.77 | 0.65 | 0.96 | 0.97 | 0.97 | 0.50 | 0.57 | 0.61 | 0.97 |
| 25 | 0.58 | 0.52 | 0.60 | 0.60 | 0.60 | 0.63 | 0.66 | 0.65 | 0.64 | 0.97 | 0.97 | 0.98 | 0.58 | 0.54 | 0.59 | 0.97 |
| 26 | 0.65 | 0.67 | 0.75 | 0.44 | 0.43 | 0.43 | 0.45 | 0.43 | 0.44 | 0.98 | 0.97 | 0.97 | 0.71 | 0.34 | 0.35 | 0.97 |
| 27 | 0.32 | 0.54 | 0.34 | 0.62 | 0.29 | 0.24 | 0.68 | 0.30 | 0.24 | 0.95 | 0.96 | 0.94 | 0.53 | 0.20 | 0.20 | 0.95 |
| 28 | 0.61 | 0.47 | 0.46 | 0.48 | 0.57 | 0.62 | 0.53 | 0.59 | 0.67 | 0.97 | 0.97 | 0.98 | 0.52 | 0.48 | 0.51 | 0.97 |
| 29 | 0.46 | 0.55 | 0.49 | 0.54 | 0.57 | 0.38 | 0.58 | 0.58 | 0.40 | 0.97 | 0.98 | 0.97 | 0.51 | 0.37 | 0.38 | 0.97 |
| 30 | 0.42 | 0.55 | 0.49 | 0.68 | 0.57 | 0.66 | 0.74 | 0.57 | 0.69 | 0.98 | 0.98 | 0.97 | 0.47 | 0.54 | 0.57 | 0.98 |

Table A.22. Determined 2D and 3D particle shape descriptors of Sand E retained on sieve #20, PR = 33.57, PSR = 0.850 – 2.00 mm.

| Part | $R_{2D}$ | | | $S_{2D}$ | | | $AR_{2D}$ | | | $CX_{2D}$ | | | | | | |
|---|---|---|---|---|---|---|---|---|---|---|---|---|---|---|---|---|
| No. | $F_D$ | $F_1$ | $F_2$ | $F_D$ | $F_1$ | $F_2$ | $F_D$ | $F_1$ | $F_2$ | $F_D$ | $F_1$ | $F_2$ | $R_{3D}$ | $S_{3D}$ | $AR_{3D}$ | $CX_{3D}$ |
| 1 | 0.48 | 0.40 | 0.38 | 0.79 | 0.68 | 0.76 | 0.84 | 0.75 | 0.81 | 0.97 | 0.95 | 0.98 | 0.41 | 0.68 | 0.73 | 0.96 |
| 2 | 0.53 | 0.51 | 0.60 | 0.59 | 0.47 | 0.46 | 0.64 | 0.48 | 0.48 | 0.96 | 0.98 | 0.97 | 0.57 | 0.37 | 0.39 | 0.97 |
| 3 | 0.53 | 0.61 | 0.48 | 0.59 | 0.42 | 0.41 | 0.60 | 0.43 | 0.42 | 0.97 | 0.97 | 0.96 | 0.59 | 0.34 | 0.36 | 0.97 |
| 4 | 0.68 | 0.57 | 0.54 | 0.53 | 0.50 | 0.51 | 0.53 | 0.52 | 0.53 | 0.98 | 0.98 | 0.98 | 0.54 | 0.39 | 0.40 | 0.98 |
| 5 | 0.56 | 0.39 | 0.46 | 0.81 | 0.47 | 0.61 | 0.82 | 0.51 | 0.61 | 0.98 | 0.97 | 0.99 | 0.54 | 0.47 | 0.51 | 0.98 |
| 6 | 0.55 | 0.41 | 0.65 | 0.35 | 0.38 | 0.36 | 0.35 | 0.40 | 0.37 | 0.98 | 0.96 | 0.98 | 0.49 | 0.27 | 0.28 | 0.97 |
| 7 | 0.47 | 0.37 | 0.56 | 0.79 | 0.76 | 0.68 | 0.83 | 0.82 | 0.77 | 0.98 | 0.98 | 0.96 | 0.48 | 0.66 | 0.74 | 0.97 |
| 8 | 0.59 | 0.51 | 0.47 | 0.58 | 0.49 | 0.49 | 0.63 | 0.49 | 0.49 | 0.97 | 0.99 | 0.99 | 0.53 | 0.40 | 0.40 | 0.98 |
| 9 | 0.46 | 0.45 | 0.54 | 0.58 | 0.58 | 0.48 | 0.62 | 0.62 | 0.50 | 0.96 | 0.97 | 0.97 | 0.52 | 0.46 | 0.48 | 0.96 |
| 10 | 0.54 | 0.69 | 0.75 | 0.60 | 0.34 | 0.39 | 0.61 | 0.35 | 0.41 | 0.98 | 0.97 | 0.97 | 0.72 | 0.31 | 0.32 | 0.98 |
| 11 | 0.44 | 0.42 | 0.42 | 0.74 | 0.68 | 0.65 | 0.86 | 0.70 | 0.67 | 0.96 | 0.97 | 0.97 | 0.45 | 0.61 | 0.65 | 0.96 |
| 12 | 0.58 | 0.83 | 0.59 | 0.47 | 0.36 | 0.42 | 0.49 | 0.36 | 0.43 | 0.97 | 0.98 | 0.98 | 0.68 | 0.32 | 0.33 | 0.97 |
| 13 | 0.46 | 0.61 | 0.54 | 0.48 | 0.48 | 0.38 | 0.54 | 0.48 | 0.39 | 0.95 | 0.98 | 0.96 | 0.57 | 0.34 | 0.36 | 0.96 |
| 14 | 0.62 | 0.62 | 0.53 | 0.68 | 0.51 | 0.49 | 0.76 | 0.54 | 0.49 | 0.96 | 0.97 | 0.97 | 0.57 | 0.41 | 0.44 | 0.97 |
| 15 | 0.40 | 0.56 | 0.50 | 0.68 | 0.51 | 0.49 | 0.76 | 0.54 | 0.49 | 0.96 | 0.97 | 0.97 | 0.57 | 0.41 | 0.44 | 0.97 |
| 16 | 0.36 | 0.51 | 0.41 | 0.84 | 0.55 | 0.54 | 0.91 | 0.57 | 0.59 | 0.97 | 0.96 | 0.94 | 0.51 | 0.52 | 0.56 | 0.96 |
| 17 | 0.58 | 0.51 | 0.39 | 0.48 | 0.53 | 0.53 | 0.50 | 0.53 | 0.55 | 0.96 | 0.98 | 0.95 | 0.51 | 0.42 | 0.43 | 0.96 |
| 18 | 0.60 | 0.69 | 0.55 | 0.77 | 0.51 | 0.61 | 0.78 | 0.52 | 0.62 | 0.99 | 0.99 | 0.98 | 0.63 | 0.49 | 0.49 | 0.99 |
| 19 | 0.55 | 0.58 | 0.45 | 0.54 | 0.43 | 0.33 | 0.57 | 0.44 | 0.34 | 0.98 | 0.97 | 0.96 | 0.61 | 0.28 | 0.28 | 0.97 |
| 20 | 0.45 | 0.43 | 0.47 | 0.70 | 0.54 | 0.70 | 0.77 | 0.59 | 0.78 | 0.97 | 0.97 | 0.97 | 0.49 | 0.52 | 0.59 | 0.97 |
| 21 | 0.56 | 0.73 | 0.65 | 0.57 | 0.43 | 0.41 | 0.63 | 0.44 | 0.42 | 0.95 | 0.98 | 0.98 | 0.59 | 0.37 | 0.37 | 0.96 |
| 22 | 0.57 | 0.56 | 0.49 | 0.46 | 0.49 | 0.60 | 0.48 | 0.51 | 0.71 | 0.96 | 0.97 | 0.96 | 0.54 | 0.45 | 0.46 | 0.96 |
| 23 | 0.40 | 0.48 | 0.56 | 0.76 | 0.70 | 0.73 | 0.81 | 0.75 | 0.74 | 0.97 | 0.97 | 0.98 | 0.51 | 0.61 | 0.64 | 0.97 |
| 24 | 0.55 | 0.56 | 0.61 | 0.72 | 0.44 | 0.52 | 0.82 | 0.45 | 0.53 | 0.98 | 0.99 | 0.98 | 0.59 | 0.42 | 0.43 | 0.98 |
| 25 | 0.69 | 0.60 | 0.54 | 0.53 | 0.41 | 0.43 | 0.55 | 0.44 | 0.44 | 0.97 | 0.96 | 0.97 | 0.60 | 0.32 | 0.35 | 0.97 |
| 26 | 0.53 | 0.58 | 0.67 | 0.61 | 0.65 | 0.55 | 0.67 | 0.71 | 0.56 | 0.95 | 0.97 | 0.97 | 0.63 | 0.52 | 0.54 | 0.96 |
| 27 | 0.69 | 0.64 | 0.66 | 0.72 | 0.57 | 0.56 | 0.85 | 0.62 | 0.57 | 0.97 | 0.96 | 0.97 | 0.65 | 0.51 | 0.54 | 0.97 |
| 28 | 0.59 | 0.59 | 0.61 | 0.66 | 0.52 | 0.63 | 0.67 | 0.52 | 0.63 | 0.98 | 0.98 | 0.98 | 0.58 | 0.52 | 0.52 | 0.98 |
| 29 | 0.53 | 0.65 | 0.60 | 0.56 | 0.36 | 0.41 | 0.60 | 0.36 | 0.41 | 0.98 | 0.98 | 0.99 | 0.63 | 0.32 | 0.32 | 0.98 |
| 30 | 0.61 | 0.54 | 0.57 | 0.59 | 0.55 | 0.66 | 0.65 | 0.56 | 0.71 | 0.97 | 0.98 | 0.97 | 0.57 | 0.48 | 0.51 | 0.97 |

## A.7. 2D and 3D Shape Descriptors of Sand F

Table A.23. Determined 2D and 3D particle shape descriptors of Sand F retained on sieve #10, PR = 90.70, PSR = 2.00 - 4.75 mm.

| Part | $R_{2D}$ | | | $S_{2D}$ | | | $AR_{2D}$ | | | $CX_{2D}$ | | | | | | |
|---|---|---|---|---|---|---|---|---|---|---|---|---|---|---|---|---|
| No. | $F_D$ | $F_1$ | $F_2$ | $F_D$ | $F_1$ | $F_2$ | $F_D$ | $F_1$ | $F_2$ | $F_D$ | $F_1$ | $F_2$ | $R_{3D}$ | $S_{3D}$ | $AR_{3D}$ | $CX_{3D}$ |
| 1 | 0.57 | 0.53 | 0.60 | 0.65 | 0.50 | 0.48 | 0.68 | 0.50 | 0.49 | 0.99 | 0.98 | 0.99 | 0.57 | 0.42 | 0.43 | 0.98 |
| 2 | 0.53 | 0.57 | 0.47 | 0.80 | 0.59 | 0.59 | 0.82 | 0.61 | 0.64 | 0.99 | 0.98 | 0.95 | 0.56 | 0.56 | 0.60 | 0.98 |
| 3 | 0.63 | 0.61 | 0.64 | 0.65 | 0.55 | 0.54 | 0.65 | 0.56 | 0.54 | 0.99 | 0.99 | 0.99 | 0.66 | 0.46 | 0.46 | 0.99 |
| 4 | 0.60 | 0.59 | 0.66 | 0.66 | 0.70 | 0.51 | 0.70 | 0.72 | 0.52 | 0.97 | 0.98 | 0.99 | 0.64 | 0.50 | 0.51 | 0.98 |
| 5 | 0.61 | 0.49 | 0.58 | 0.77 | 0.76 | 0.71 | 0.82 | 0.82 | 0.73 | 0.99 | 0.99 | 0.99 | 0.58 | 0.69 | 0.70 | 0.99 |
| 6 | 0.72 | 0.56 | 0.57 | 0.77 | 0.76 | 0.76 | 0.82 | 0.82 | 0.78 | 0.99 | 0.99 | 0.99 | 0.62 | 0.74 | 0.75 | 0.99 |
| 7 | 0.44 | 0.42 | 0.54 | 0.75 | 0.57 | 0.68 | 0.76 | 0.61 | 0.77 | 0.98 | 0.97 | 0.97 | 0.51 | 0.54 | 0.60 | 0.97 |
| 8 | 0.45 | 0.61 | 0.56 | 0.65 | 0.72 | 0.51 | 0.66 | 0.74 | 0.51 | 0.98 | 0.99 | 0.97 | 0.55 | 0.49 | 0.50 | 0.98 |
| 9 | 0.47 | 0.54 | 0.46 | 0.84 | 0.57 | 0.55 | 0.93 | 0.96 | 0.94 | 1.00 | 1.00 | 1.00 | 0.50 | 0.54 | 0.64 | 1.00 |
| 10 | 0.38 | 0.46 | 0.46 | 0.70 | 0.53 | 0.52 | 0.82 | 0.54 | 0.56 | 0.96 | 0.96 | 0.94 | 0.47 | 0.43 | 0.47 | 0.96 |
| 11 | 0.45 | 0.49 | 0.40 | 0.79 | 0.71 | 0.71 | 0.82 | 0.74 | 0.73 | 0.97 | 0.98 | 0.98 | 0.46 | 0.67 | 0.69 | 0.98 |
| 12 | 0.43 | 0.48 | 0.53 | 0.81 | 0.63 | 0.61 | 0.85 | 0.65 | 0.63 | 0.97 | 0.98 | 0.98 | 0.50 | 0.61 | 0.63 | 0.97 |
| 13 | 0.48 | 0.63 | 0.51 | 0.76 | 0.60 | 0.53 | 0.80 | 0.61 | 0.54 | 0.97 | 0.98 | 0.98 | 0.57 | 0.52 | 0.53 | 0.97 |
| 14 | 0.38 | 0.41 | 0.66 | 0.57 | 0.52 | 0.41 | 0.65 | 0.52 | 0.42 | 0.97 | 0.99 | 0.98 | 0.51 | 0.40 | 0.41 | 0.98 |
| 15 | 0.47 | 0.46 | 0.55 | 0.65 | 0.54 | 0.48 | 0.66 | 0.55 | 0.48 | 0.98 | 0.99 | 0.98 | 0.51 | 0.44 | 0.44 | 0.98 |
| 16 | 0.46 | 0.62 | 0.53 | 0.65 | 0.49 | 0.53 | 0.67 | 0.49 | 0.54 | 0.97 | 0.97 | 0.98 | 0.59 | 0.44 | 0.45 | 0.98 |
| 17 | 0.50 | 0.47 | 0.51 | 0.54 | 0.67 | 0.60 | 0.61 | 0.73 | 0.64 | 0.96 | 0.95 | 0.96 | 0.50 | 0.53 | 0.57 | 0.96 |
| 18 | 0.54 | 0.53 | 0.43 | 0.54 | 0.56 | 0.44 | 0.59 | 0.56 | 0.44 | 0.93 | 0.99 | 0.99 | 0.55 | 0.37 | 0.38 | 0.96 |
| 19 | 0.42 | 0.60 | 0.59 | 0.57 | 0.58 | 0.54 | 0.62 | 0.60 | 0.54 | 0.96 | 0.98 | 0.98 | 0.57 | 0.45 | 0.45 | 0.97 |
| 20 | 0.63 | 0.47 | 0.65 | 0.58 | 0.57 | 0.50 | 0.63 | 0.59 | 0.51 | 0.97 | 0.97 | 0.98 | 0.60 | 0.47 | 0.48 | 0.97 |
| 21 | 0.63 | 0.65 | 0.65 | 0.67 | 0.82 | 0.70 | 0.65 | 0.70 | 0.66 | 0.99 | 1.00 | 1.00 | 0.64 | 0.62 | 0.61 | 0.99 |
| 22 | 0.32 | 0.47 | 0.45 | 0.69 | 0.28 | 0.30 | 0.72 | 0.28 | 0.31 | 0.96 | 0.91 | 0.98 | 0.50 | 0.24 | 0.25 | 0.96 |
| 23 | 0.64 | 0.63 | 0.64 | 0.75 | 0.66 | 0.64 | 0.76 | 0.67 | 0.64 | 0.99 | 0.99 | 0.99 | 0.63 | 0.58 | 0.59 | 0.99 |
| 24 | 0.55 | 0.67 | 0.54 | 0.80 | 0.55 | 0.46 | 0.81 | 0.55 | 0.46 | 0.99 | 0.99 | 0.99 | 0.61 | 0.46 | 0.46 | 0.99 |
| 25 | 0.62 | 0.59 | 0.61 | 0.81 | 0.57 | 0.54 | 0.84 | 0.57 | 0.54 | 0.99 | 0.98 | 0.99 | 0.59 | 0.50 | 0.51 | 0.99 |
| 26 | 0.44 | 0.45 | 0.50 | 0.69 | 0.50 | 0.63 | 0.73 | 0.55 | 0.64 | 0.98 | 0.94 | 0.98 | 0.49 | 0.49 | 0.53 | 0.97 |
| 27 | 0.61 | 0.73 | 0.60 | 0.74 | 0.54 | 0.56 | 0.74 | 0.55 | 0.58 | 0.99 | 0.99 | 0.99 | 0.68 | 0.47 | 0.48 | 0.99 |
| 28 | 0.50 | 0.52 | 0.49 | 0.74 | 0.54 | 0.50 | 0.78 | 0.54 | 0.51 | 0.97 | 0.98 | 0.99 | 0.52 | 0.50 | 0.51 | 0.98 |
| 29 | 0.49 | 0.61 | 0.63 | 0.61 | 0.69 | 0.56 | 0.64 | 0.72 | 0.59 | 0.98 | 0.99 | 0.97 | 0.56 | 0.52 | 0.55 | 0.98 |
| 30 | 0.63 | 0.66 | 0.50 | 0.77 | 0.69 | 0.70 | 0.78 | 0.70 | 0.72 | 0.99 | 0.99 | 0.98 | 0.56 | 0.62 | 0.63 | 0.99 |

Table A.24. Determined 2D and 3D shape descriptors of Sand F grains retained on sieve #20, PR = 8.20, PSR = 0.850 – 2.00 mm.

| Part | $R_{2D}$ | | | $S_{2D}$ | | | $AR_{2D}$ | | | $CX_{2D}$ | | | | | | |
|---|---|---|---|---|---|---|---|---|---|---|---|---|---|---|---|---|
| No. | $F_D$ | $F_1$ | $F_2$ | $F_D$ | $F_1$ | $F_2$ | $F_D$ | $F_1$ | $F_2$ | $F_D$ | $F_1$ | $F_2$ | $R_{3D}$ | $S_{3D}$ | $AR_{3D}$ | $CX_{3D}$ |
| 1 | 0.67 | 0.62 | 0.61 | 0.71 | 0.60 | 0.71 | 0.79 | 0.60 | 0.76 | 0.98 | 0.99 | 0.99 | 0.62 | 0.58 | 0.60 | 0.98 |
| 2 | 0.57 | 0.42 | 0.54 | 0.59 | 0.64 | 0.43 | 0.62 | 0.66 | 0.43 | 0.97 | 0.97 | 0.95 | 0.55 | 0.43 | 0.43 | 0.96 |
| 3 | 0.43 | 0.55 | 0.60 | 0.53 | 0.57 | 0.48 | 0.54 | 0.58 | 0.49 | 0.97 | 0.98 | 0.97 | 0.54 | 0.41 | 0.42 | 0.97 |
| 4 | 0.46 | 0.48 | 0.30 | 0.69 | 0.68 | 0.65 | 0.75 | 0.71 | 0.69 | 0.96 | 0.97 | 0.95 | 0.44 | 0.59 | 0.63 | 0.96 |
| 5 | 0.57 | 0.59 | 0.51 | 0.42 | 0.34 | 0.35 | 0.42 | 0.35 | 0.35 | 0.96 | 0.97 | 0.97 | 0.56 | 0.27 | 0.28 | 0.96 |
| 6 | 0.49 | 0.53 | 0.41 | 0.65 | 0.63 | 0.76 | 0.72 | 0.66 | 0.79 | 0.96 | 0.97 | 0.98 | 0.49 | 0.61 | 0.66 | 0.97 |
| 7 | 0.48 | 0.55 | 0.50 | 0.64 | 0.56 | 0.72 | 0.66 | 0.56 | 0.76 | 0.97 | 0.98 | 0.97 | 0.52 | 0.53 | 0.56 | 0.97 |
| 8 | 0.40 | 0.45 | 0.44 | 0.72 | 0.79 | 0.75 | 0.74 | 0.85 | 0.78 | 0.97 | 0.98 | 0.98 | 0.44 | 0.69 | 0.74 | 0.97 |
| 9 | 0.49 | 0.61 | 0.52 | 0.78 | 0.77 | 0.74 | 0.83 | 0.85 | 0.76 | 0.98 | 0.98 | 0.98 | 0.55 | 0.67 | 0.72 | 0.98 |
| 10 | 0.45 | 0.46 | 0.63 | 0.81 | 0.60 | 0.53 | 0.89 | 0.62 | 0.53 | 0.97 | 0.97 | 0.98 | 0.57 | 0.51 | 0.52 | 0.97 |
| 11 | 0.36 | 0.51 | 0.51 | 0.65 | 0.49 | 0.60 | 0.67 | 0.50 | 0.65 | 0.96 | 0.96 | 0.94 | 0.50 | 0.48 | 0.49 | 0.96 |
| 12 | 0.62 | 0.72 | 0.67 | 0.70 | 0.68 | 0.50 | 0.72 | 0.69 | 0.56 | 0.98 | 0.99 | 0.95 | 0.70 | 0.50 | 0.54 | 0.97 |
| 13 | 0.46 | 0.46 | 0.42 | 0.68 | 0.54 | 0.61 | 0.74 | 0.56 | 0.64 | 0.95 | 0.96 | 0.97 | 0.46 | 0.54 | 0.56 | 0.96 |
| 14 | 0.49 | 0.42 | 0.50 | 0.59 | 0.78 | 0.57 | 0.60 | 0.79 | 0.58 | 0.97 | 0.98 | 0.97 | 0.49 | 0.55 | 0.55 | 0.97 |
| 15 | 0.63 | 0.60 | 0.63 | 0.80 | 0.65 | 0.68 | 0.86 | 0.66 | 0.70 | 0.98 | 0.99 | 0.99 | 0.59 | 0.63 | 0.65 | 0.98 |
| 16 | 0.61 | 0.55 | 0.63 | 0.50 | 0.63 | 0.50 | 0.52 | 0.66 | 0.54 | 0.97 | 0.98 | 0.97 | 0.60 | 0.46 | 0.50 | 0.97 |
| 17 | 0.36 | 0.47 | 0.50 | 0.56 | 0.79 | 0.54 | 0.67 | 0.79 | 0.55 | 0.93 | 0.98 | 0.97 | 0.44 | 0.54 | 0.55 | 0.96 |
| 18 | 0.51 | 0.47 | 0.61 | 0.66 | 0.79 | 0.58 | 0.66 | 0.83 | 0.66 | 0.98 | 0.98 | 0.96 | 0.50 | 0.56 | 0.62 | 0.97 |
| 19 | 0.48 | 0.48 | 0.55 | 0.83 | 0.54 | 0.60 | 0.86 | 0.54 | 0.61 | 0.97 | 0.98 | 0.99 | 0.55 | 0.52 | 0.53 | 0.98 |
| 20 | 0.62 | 0.56 | 0.61 | 0.76 | 0.67 | 0.65 | 0.78 | 0.68 | 0.67 | 0.98 | 0.98 | 0.97 | 0.61 | 0.61 | 0.64 | 0.98 |
| 21 | 0.60 | 0.43 | 0.67 | 0.68 | 0.75 | 0.61 | 0.73 | 0.82 | 0.63 | 0.97 | 0.98 | 0.99 | 0.58 | 0.58 | 0.59 | 0.98 |
| 22 | 0.74 | 0.47 | 0.45 | 0.68 | 0.63 | 0.75 | 0.68 | 0.67 | 0.79 | 0.99 | 0.97 | 0.98 | 0.54 | 0.62 | 0.67 | 0.98 |
| 23 | 0.55 | 0.76 | 0.56 | 0.71 | 0.52 | 0.57 | 0.78 | 0.54 | 0.59 | 0.98 | 0.98 | 0.97 | 0.62 | 0.47 | 0.50 | 0.97 |
| 24 | 0.55 | 0.56 | 0.43 | 0.70 | 0.64 | 0.66 | 0.75 | 0.68 | 0.69 | 0.98 | 0.97 | 0.98 | 0.52 | 0.62 | 0.67 | 0.98 |
| 25 | 0.65 | 0.53 | 0.55 | 0.51 | 0.67 | 0.50 | 0.52 | 0.68 | 0.56 | 0.96 | 0.99 | 0.94 | 0.60 | 0.45 | 0.51 | 0.96 |
| 26 | 0.61 | 0.43 | 0.55 | 0.67 | 0.65 | 0.65 | 0.69 | 0.66 | 0.67 | 0.98 | 0.98 | 0.98 | 0.53 | 0.59 | 0.60 | 0.98 |
| 27 | 0.48 | 0.55 | 0.45 | 0.71 | 0.78 | 0.67 | 0.74 | 0.86 | 0.68 | 0.98 | 0.98 | 0.98 | 0.50 | 0.65 | 0.68 | 0.98 |
| 28 | 0.48 | 0.62 | 0.56 | 0.74 | 0.54 | 0.60 | 0.80 | 0.55 | 0.60 | 0.97 | 0.99 | 0.98 | 0.56 | 0.53 | 0.54 | 0.98 |
| 29 | 0.52 | 0.61 | 0.58 | 0.59 | 0.59 | 0.50 | 0.67 | 0.66 | 0.50 | 0.94 | 0.97 | 0.99 | 0.58 | 0.44 | 0.49 | 0.96 |
| 30 | 0.49 | 0.55 | 0.62 | 0.79 | 0.72 | 0.74 | 0.86 | 0.73 | 0.76 | 0.98 | 0.98 | 0.99 | 0.57 | 0.71 | 0.73 | 0.98 |

Table A.25. Determined 2D and 3D particle shape descriptors of Sand F retained on sieve #40, PR = 0.34, PSR = 0.425 – 0.850 mm.

| Part | $R_{2D}$ | | | $S_{2D}$ | | | $AR_{2D}$ | | | $CX_{2D}$ | | | | | | |
|---|---|---|---|---|---|---|---|---|---|---|---|---|---|---|---|---|
| No. | $F_D$ | $F_1$ | $F_2$ | $F_D$ | $F_1$ | $F_2$ | $F_D$ | $F_1$ | $F_2$ | $F_D$ | $F_1$ | $F_2$ | $R_{3D}$ | $S_{3D}$ | $AR_{3D}$ | $CX_{3D}$ |
| 1 | 0.54 | 0.38 | 0.41 | 0.60 | 0.64 | 0.60 | 0.65 | 0.69 | 0.68 | 0.95 | 0.95 | 0.94 | 0.46 | 0.55 | 0.60 | 0.95 |
| 2 | 0.54 | 0.56 | 0.36 | 0.52 | 0.52 | 0.40 | 0.52 | 0.54 | 0.40 | 0.98 | 0.95 | 0.97 | 0.46 | 0.36 | 0.37 | 0.97 |
| 3 | 0.53 | 0.40 | 0.52 | 0.69 | 0.63 | 0.63 | 0.83 | 0.67 | 0.69 | 0.94 | 0.96 | 0.96 | 0.53 | 0.57 | 0.61 | 0.95 |
| 4 | 0.37 | 0.55 | 0.55 | 0.64 | 0.59 | 0.51 | 0.75 | 0.60 | 0.51 | 0.94 | 0.97 | 0.97 | 0.52 | 0.49 | 0.50 | 0.96 |
| 5 | 0.38 | 0.41 | 0.41 | 0.68 | 0.84 | 0.74 | 0.81 | 0.90 | 0.83 | 0.93 | 0.96 | 0.94 | 0.43 | 0.66 | 0.78 | 0.94 |
| 6 | 0.37 | 0.60 | 0.46 | 0.56 | 0.71 | 0.56 | 0.66 | 0.74 | 0.58 | 0.94 | 0.97 | 0.96 | 0.49 | 0.52 | 0.55 | 0.95 |
| 7 | 0.59 | 0.41 | 0.46 | 0.65 | 0.66 | 0.72 | 0.69 | 0.67 | 0.74 | 0.96 | 0.97 | 0.96 | 0.48 | 0.64 | 0.66 | 0.96 |
| 8 | 0.48 | 0.53 | 0.41 | 0.75 | 0.77 | 0.69 | 0.87 | 0.79 | 0.74 | 0.96 | 0.96 | 0.93 | 0.46 | 0.65 | 0.71 | 0.95 |
| 9 | 0.49 | 0.57 | 0.56 | 0.72 | 0.65 | 0.73 | 0.75 | 0.67 | 0.76 | 0.96 | 0.98 | 0.97 | 0.54 | 0.60 | 0.62 | 0.97 |
| 10 | 0.33 | 0.61 | 0.59 | 0.53 | 0.37 | 0.34 | 0.59 | 0.38 | 0.35 | 0.95 | 0.93 | 0.95 | 0.56 | 0.30 | 0.32 | 0.95 |
| 11 | 0.65 | 0.58 | 0.62 | 0.60 | 0.55 | 0.64 | 0.61 | 0.57 | 0.65 | 0.98 | 0.94 | 0.97 | 0.57 | 0.48 | 0.50 | 0.97 |
| 12 | 0.46 | 0.46 | 0.48 | 0.61 | 0.52 | 0.74 | 0.63 | 0.56 | 0.81 | 0.96 | 0.96 | 0.96 | 0.49 | 0.52 | 0.56 | 0.96 |
| 13 | 0.47 | 0.62 | 0.40 | 0.71 | 0.61 | 0.67 | 0.73 | 0.64 | 0.70 | 0.97 | 0.94 | 0.97 | 0.52 | 0.59 | 0.63 | 0.96 |
| 14 | 0.53 | 0.53 | 0.42 | 0.70 | 0.76 | 0.60 | 0.79 | 0.77 | 0.60 | 0.96 | 0.96 | 0.96 | 0.52 | 0.60 | 0.60 | 0.96 |
| 15 | 0.46 | 0.74 | 0.67 | 0.64 | 0.64 | 0.44 | 0.67 | 0.65 | 0.44 | 0.98 | 0.98 | 0.96 | 0.69 | 0.44 | 0.44 | 0.97 |
| 16 | 0.37 | 0.49 | 0.53 | 0.75 | 0.48 | 0.48 | 0.90 | 0.58 | 0.53 | 0.93 | 0.92 | 0.95 | 0.52 | 0.46 | 0.53 | 0.93 |
| 17 | 0.42 | 0.38 | 0.39 | 0.83 | 0.70 | 0.74 | 0.85 | 0.72 | 0.79 | 0.96 | 0.96 | 0.96 | 0.42 | 0.70 | 0.72 | 0.96 |
| 18 | 0.44 | 0.46 | 0.45 | 0.70 | 0.67 | 0.60 | 0.75 | 0.74 | 0.67 | 0.96 | 0.94 | 0.94 | 0.47 | 0.60 | 0.67 | 0.94 |
| 19 | 0.48 | 0.51 | 0.57 | 0.62 | 0.64 | 0.68 | 0.69 | 0.67 | 0.69 | 0.96 | 0.96 | 0.96 | 0.50 | 0.61 | 0.63 | 0.96 |
| 20 | 0.43 | 0.43 | 0.47 | 0.60 | 0.71 | 0.69 | 0.62 | 0.74 | 0.71 | 0.95 | 0.97 | 0.97 | 0.44 | 0.60 | 0.62 | 0.96 |
| 21 | 0.37 | 0.61 | 0.32 | 0.83 | 0.77 | 0.72 | 0.86 | 0.80 | 0.79 | 0.97 | 0.96 | 0.94 | 0.47 | 0.72 | 0.79 | 0.95 |
| 22 | 0.38 | 0.50 | 0.35 | 0.69 | 0.55 | 0.41 | 0.77 | 0.59 | 0.46 | 0.95 | 0.94 | 0.92 | 0.46 | 0.41 | 0.46 | 0.94 |
| 23 | 0.47 | 0.54 | 0.38 | 0.51 | 0.57 | 0.43 | 0.55 | 0.60 | 0.44 | 0.96 | 0.97 | 0.97 | 0.50 | 0.41 | 0.44 | 0.96 |
| 24 | 0.46 | 0.60 | 0.49 | 0.56 | 0.63 | 0.45 | 0.59 | 0.66 | 0.46 | 0.95 | 0.96 | 0.96 | 0.52 | 0.43 | 0.44 | 0.95 |
| 25 | 0.50 | 0.54 | 0.60 | 0.60 | 0.60 | 0.43 | 0.63 | 0.61 | 0.43 | 0.96 | 0.97 | 0.97 | 0.56 | 0.43 | 0.43 | 0.96 |
| 26 | 0.39 | 0.56 | 0.65 | 0.69 | 0.51 | 0.69 | 0.90 | 0.94 | 0.95 | 1.00 | 1.00 | 1.00 | 0.58 | 0.51 | 0.74 | 1.00 |
| 27 | 0.50 | 0.52 | 0.46 | 0.67 | 0.62 | 0.65 | 0.84 | 0.66 | 0.66 | 0.97 | 0.96 | 0.97 | 0.51 | 0.57 | 0.65 | 0.97 |
| 28 | 0.53 | 0.59 | 0.49 | 0.53 | 0.66 | 0.74 | 0.56 | 0.66 | 0.78 | 0.93 | 0.97 | 0.97 | 0.58 | 0.53 | 0.56 | 0.96 |
| 29 | 0.38 | 0.49 | 0.28 | 0.69 | 0.57 | 0.57 | 0.76 | 0.61 | 0.62 | 0.95 | 0.94 | 0.94 | 0.43 | 0.53 | 0.57 | 0.94 |
| 30 | 0.30 | 0.58 | 0.54 | 0.68 | 0.40 | 0.43 | 0.79 | 0.42 | 0.46 | 0.94 | 0.95 | 0.94 | 0.51 | 0.36 | 0.38 | 0.94 |

Table A.26. Determined 2D and 3D particle shape descriptors of Sand F retained on sieve #60, PR = 0.70, PSR = 0.250 – 0.425 mm.

| Part | $R_{2D}$ | | | $S_{2D}$ | | | $AR_{2D}$ | | | $CX_{2D}$ | | | | | | |
|---|---|---|---|---|---|---|---|---|---|---|---|---|---|---|---|---|
| No. | $F_D$ | $F_1$ | $F_2$ | $F_D$ | $F_1$ | $F_2$ | $F_D$ | $F_1$ | $F_2$ | $F_D$ | $F_1$ | $F_2$ | $R_{3D}$ | $S_{3D}$ | $AR_{3D}$ | $CX_{3D}$ |
| 1 | 0.58 | 0.46 | 0.49 | 0.58 | 0.58 | 0.78 | 0.64 | 0.62 | 0.84 | 0.92 | 0.95 | 0.97 | 0.51 | 0.57 | 0.61 | 0.94 |
| 2 | 0.47 | 0.49 | 0.57 | 0.81 | 0.68 | 0.78 | 0.82 | 0.69 | 0.80 | 0.96 | 0.97 | 0.96 | 0.52 | 0.62 | 0.64 | 0.96 |
| 3 | 0.49 | 0.63 | 0.56 | 0.78 | 0.47 | 0.59 | 0.79 | 0.52 | 0.60 | 0.97 | 0.91 | 0.97 | 0.61 | 0.47 | 0.52 | 0.95 |
| 4 | 0.42 | 0.48 | 0.52 | 0.69 | 0.53 | 0.58 | 0.71 | 0.53 | 0.63 | 0.94 | 0.95 | 0.94 | 0.50 | 0.50 | 0.53 | 0.94 |
| 5 | 0.53 | 0.39 | 0.34 | 0.67 | 0.55 | 0.65 | 0.68 | 0.56 | 0.79 | 0.97 | 0.96 | 0.94 | 0.48 | 0.46 | 0.55 | 0.96 |
| 6 | 0.35 | 0.34 | 0.36 | 0.67 | 0.63 | 0.60 | 0.78 | 0.66 | 0.63 | 0.94 | 0.95 | 0.93 | 0.37 | 0.56 | 0.59 | 0.94 |
| 7 | 0.51 | 0.38 | 0.43 | 0.58 | 0.57 | 0.79 | 0.62 | 0.64 | 0.89 | 0.95 | 0.95 | 0.96 | 0.45 | 0.54 | 0.58 | 0.95 |
| 8 | 0.41 | 0.59 | 0.54 | 0.54 | 0.80 | 0.60 | 0.58 | 0.87 | 0.61 | 0.94 | 0.98 | 0.96 | 0.48 | 0.54 | 0.58 | 0.96 |
| 9 | 0.62 | 0.48 | 0.47 | 0.55 | 0.80 | 0.61 | 0.62 | 0.86 | 0.65 | 0.95 | 0.97 | 0.95 | 0.51 | 0.55 | 0.61 | 0.95 |
| 10 | 0.29 | 0.43 | 0.53 | 0.63 | 0.44 | 0.57 | 0.71 | 0.47 | 0.58 | 0.92 | 0.94 | 0.93 | 0.46 | 0.44 | 0.46 | 0.93 |
| 11 | 0.51 | 0.47 | 0.47 | 0.68 | 0.70 | 0.65 | 0.72 | 0.77 | 0.68 | 0.96 | 0.95 | 0.96 | 0.50 | 0.60 | 0.65 | 0.96 |
| 12 | 0.56 | 0.55 | 0.48 | 0.73 | 0.62 | 0.75 | 0.74 | 0.64 | 0.76 | 0.97 | 0.96 | 0.95 | 0.56 | 0.58 | 0.60 | 0.96 |
| 13 | 0.58 | 0.49 | 0.39 | 0.70 | 0.73 | 0.67 | 0.75 | 0.84 | 0.75 | 0.96 | 0.95 | 0.94 | 0.52 | 0.64 | 0.73 | 0.95 |
| 14 | 0.42 | 0.66 | 0.42 | 0.66 | 0.53 | 0.64 | 0.72 | 0.56 | 0.64 | 0.95 | 0.98 | 0.96 | 0.54 | 0.51 | 0.52 | 0.96 |
| 15 | 0.47 | 0.54 | 0.50 | 0.64 | 0.68 | 0.59 | 0.66 | 0.69 | 0.60 | 0.97 | 0.97 | 0.97 | 0.51 | 0.52 | 0.53 | 0.97 |
| 16 | 0.58 | 0.51 | 0.50 | 0.67 | 0.82 | 0.56 | 0.72 | 0.86 | 0.68 | 0.96 | 0.97 | 0.90 | 0.57 | 0.56 | 0.63 | 0.94 |
| 17 | 0.56 | 0.49 | 0.50 | 0.54 | 0.45 | 0.75 | 0.56 | 0.48 | 0.78 | 0.96 | 0.95 | 0.96 | 0.54 | 0.45 | 0.47 | 0.96 |
| 18 | 0.53 | 0.38 | 0.47 | 0.64 | 0.46 | 0.36 | 0.66 | 0.46 | 0.37 | 0.97 | 0.96 | 0.96 | 0.49 | 0.32 | 0.32 | 0.97 |
| 19 | 0.44 | 0.57 | 0.57 | 0.70 | 0.51 | 0.61 | 0.73 | 0.52 | 0.66 | 0.96 | 0.97 | 0.94 | 0.52 | 0.46 | 0.49 | 0.96 |
| 20 | 0.43 | 0.47 | 0.54 | 0.58 | 0.50 | 0.66 | 0.66 | 0.51 | 0.66 | 0.94 | 0.97 | 0.97 | 0.50 | 0.49 | 0.49 | 0.96 |
| 21 | 0.49 | 0.51 | 0.52 | 0.58 | 0.68 | 0.62 | 0.65 | 0.72 | 0.65 | 0.94 | 0.95 | 0.95 | 0.57 | 0.50 | 0.52 | 0.95 |
| 22 | 0.53 | 0.49 | 0.19 | 0.82 | 0.59 | 0.52 | 0.83 | 0.60 | 0.57 | 0.97 | 0.97 | 0.94 | 0.47 | 0.52 | 0.56 | 0.96 |
| 23 | 0.37 | 0.48 | 0.39 | 0.72 | 0.58 | 0.63 | 0.80 | 0.76 | 0.80 | 0.94 | 0.93 | 0.92 | 0.46 | 0.54 | 0.72 | 0.93 |
| 24 | 0.71 | 0.56 | 0.61 | 0.59 | 0.54 | 0.75 | 0.60 | 0.55 | 0.81 | 0.97 | 0.96 | 0.97 | 0.56 | 0.53 | 0.55 | 0.97 |
| 25 | 0.30 | 0.60 | 0.61 | 0.67 | 0.61 | 0.47 | 0.76 | 0.64 | 0.48 | 0.91 | 0.96 | 0.92 | 0.52 | 0.46 | 0.48 | 0.92 |
| 26 | 0.52 | 0.59 | 0.46 | 0.70 | 0.63 | 0.73 | 0.74 | 0.66 | 0.75 | 0.95 | 0.95 | 0.95 | 0.55 | 0.61 | 0.64 | 0.95 |
| 27 | 0.52 | 0.61 | 0.58 | 0.63 | 0.60 | 0.43 | 0.67 | 0.61 | 0.48 | 0.95 | 0.96 | 0.93 | 0.56 | 0.42 | 0.47 | 0.95 |
| 28 | 0.46 | 0.54 | 0.56 | 0.54 | 0.60 | 0.74 | 0.57 | 0.62 | 0.75 | 0.95 | 0.95 | 0.97 | 0.52 | 0.53 | 0.54 | 0.95 |
| 29 | 0.61 | 0.45 | 0.53 | 0.66 | 0.68 | 0.71 | 0.68 | 0.76 | 0.77 | 0.96 | 0.92 | 0.97 | 0.54 | 0.62 | 0.68 | 0.95 |
| 30 | 0.50 | 0.50 | 0.57 | 0.55 | 0.67 | 0.73 | 0.59 | 0.69 | 0.87 | 0.93 | 0.96 | 0.97 | 0.57 | 0.55 | 0.59 | 0.95 |

Table A.27. Determined 2D and 3D particle shape descriptors of Sand F retained on sieve #100, PR = 0.06, PSR = 0.150 – 0.250 mm.

| Part | $R_{2D}$ | | | $S_{2D}$ | | | $AR_{2D}$ | | | $CX_{2D}$ | | | | | | |
|---|---|---|---|---|---|---|---|---|---|---|---|---|---|---|---|---|
| No. | $F_D$ | $F_1$ | $F_2$ | $F_D$ | $F_1$ | $F_2$ | $F_D$ | $F_1$ | $F_2$ | $F_D$ | $F_1$ | $F_2$ | $R_{3D}$ | $S_{3D}$ | $AR_{3D}$ | $CX_{3D}$ |
| 1 | 0.55 | 0.42 | 0.58 | 0.56 | 0.50 | 0.54 | 0.66 | 0.51 | 0.55 | 0.92 | 0.94 | 0.97 | 0.57 | 0.46 | 0.47 | 0.94 |
| 2 | 0.57 | 0.50 | 0.45 | 0.72 | 0.55 | 0.54 | 0.73 | 0.55 | 0.55 | 0.96 | 0.96 | 0.94 | 0.53 | 0.51 | 0.51 | 0.95 |
| 3 | 0.52 | 0.40 | 0.49 | 0.68 | 0.72 | 0.68 | 0.69 | 0.75 | 0.73 | 0.95 | 0.95 | 0.95 | 0.49 | 0.60 | 0.65 | 0.95 |
| 4 | 0.44 | 0.47 | 0.53 | 0.56 | 0.54 | 0.67 | 0.58 | 0.58 | 0.69 | 0.95 | 0.95 | 0.95 | 0.50 | 0.51 | 0.52 | 0.95 |
| 5 | 0.57 | 0.50 | 0.48 | 0.67 | 0.41 | 0.54 | 0.68 | 0.44 | 0.57 | 0.96 | 0.93 | 0.94 | 0.55 | 0.38 | 0.40 | 0.95 |
| 6 | 0.54 | 0.55 | 0.63 | 0.66 | 0.56 | 0.70 | 0.68 | 0.56 | 0.77 | 0.97 | 0.97 | 0.95 | 0.59 | 0.50 | 0.53 | 0.96 |
| 7 | 0.45 | 0.61 | 0.63 | 0.69 | 0.47 | 0.52 | 0.81 | 0.48 | 0.54 | 0.92 | 0.96 | 0.95 | 0.58 | 0.42 | 0.45 | 0.94 |
| 8 | 0.48 | 0.61 | 0.63 | 0.65 | 0.73 | 0.56 | 0.68 | 0.78 | 0.61 | 0.94 | 0.94 | 0.94 | 0.60 | 0.55 | 0.59 | 0.94 |
| 9 | 0.42 | 0.60 | 0.59 | 0.63 | 0.56 | 0.51 | 0.66 | 0.56 | 0.51 | 0.95 | 0.96 | 0.96 | 0.59 | 0.46 | 0.47 | 0.95 |
| 10 | 0.57 | 0.48 | 0.55 | 0.85 | 0.78 | 0.85 | 0.85 | 0.81 | 0.90 | 0.96 | 0.96 | 0.96 | 0.54 | 0.78 | 0.81 | 0.96 |
| 11 | 0.55 | 0.19 | 0.65 | 0.46 | 0.35 | 0.40 | 0.50 | 0.36 | 0.40 | 0.94 | 0.93 | 0.95 | 0.55 | 0.31 | 0.32 | 0.94 |
| 12 | 0.61 | 0.54 | 0.48 | 0.72 | 0.70 | 0.78 | 0.76 | 0.75 | 0.82 | 0.94 | 0.95 | 0.95 | 0.58 | 0.69 | 0.75 | 0.94 |
| 13 | 0.48 | 0.51 | 0.51 | 0.59 | 0.62 | 0.42 | 0.65 | 0.62 | 0.44 | 0.91 | 0.94 | 0.84 | 0.57 | 0.42 | 0.44 | 0.90 |
| 14 | 0.57 | 0.46 | 0.59 | 0.66 | 0.68 | 0.62 | 0.76 | 0.70 | 0.63 | 0.92 | 0.94 | 0.95 | 0.64 | 0.53 | 0.54 | 0.94 |
| 15 | 0.46 | 0.52 | 0.49 | 0.76 | 0.70 | 0.72 | 0.81 | 0.79 | 0.73 | 0.94 | 0.94 | 0.96 | 0.50 | 0.69 | 0.71 | 0.94 |
| 16 | 0.32 | 0.40 | 0.59 | 0.63 | 0.62 | 0.72 | 0.64 | 0.66 | 0.74 | 0.95 | 0.92 | 0.94 | 0.46 | 0.55 | 0.57 | 0.94 |
| 17 | 0.56 | 0.64 | 0.64 | 0.64 | 0.64 | 0.70 | 0.66 | 0.66 | 0.72 | 0.94 | 0.95 | 0.94 | 0.66 | 0.57 | 0.59 | 0.94 |
| 18 | 0.70 | 0.57 | 0.60 | 0.36 | 0.35 | 0.33 | 0.38 | 0.36 | 0.36 | 0.88 | 0.92 | 0.90 | 0.65 | 0.26 | 0.28 | 0.90 |
| 19 | 0.53 | 0.52 | 0.51 | 0.68 | 0.58 | 0.66 | 0.68 | 0.63 | 0.76 | 0.95 | 0.93 | 0.93 | 0.53 | 0.54 | 0.63 | 0.94 |
| 20 | 0.53 | 0.56 | 0.53 | 0.83 | 0.81 | 0.82 | 0.92 | 0.84 | 0.87 | 0.97 | 0.96 | 0.95 | 0.55 | 0.78 | 0.82 | 0.96 |
| 21 | 0.48 | 0.36 | 0.57 | 0.59 | 0.65 | 0.57 | 0.74 | 0.70 | 0.62 | 0.89 | 0.93 | 0.96 | 0.50 | 0.51 | 0.56 | 0.92 |
| 22 | 0.57 | 0.63 | 0.53 | 0.51 | 0.44 | 0.33 | 0.54 | 0.44 | 0.34 | 0.94 | 0.94 | 0.94 | 0.60 | 0.29 | 0.30 | 0.94 |
| 23 | 0.49 | 0.73 | 0.52 | 0.76 | 0.49 | 0.52 | 0.81 | 0.50 | 0.53 | 0.95 | 0.95 | 0.94 | 0.61 | 0.47 | 0.48 | 0.95 |
| 24 | 0.60 | 0.52 | 0.43 | 0.64 | 0.63 | 0.57 | 0.67 | 0.64 | 0.58 | 0.94 | 0.95 | 0.95 | 0.57 | 0.49 | 0.51 | 0.94 |
| 25 | 0.48 | 0.68 | 0.66 | 0.57 | 0.44 | 0.48 | 0.58 | 0.46 | 0.50 | 0.96 | 0.94 | 0.91 | 0.64 | 0.35 | 0.37 | 0.94 |
| 26 | 0.67 | 0.63 | 0.53 | 0.78 | 0.71 | 0.67 | 0.81 | 0.73 | 0.71 | 0.97 | 0.97 | 0.96 | 0.65 | 0.64 | 0.68 | 0.97 |
| 27 | 0.46 | 0.66 | 0.64 | 0.72 | 0.53 | 0.49 | 0.80 | 0.51 | 0.49 | 0.94 | 0.96 | 0.94 | 0.69 | 0.47 | 0.47 | 0.94 |
| 28 | 0.65 | 0.55 | 0.64 | 0.73 | 0.65 | 0.78 | 0.72 | 0.68 | 0.80 | 0.97 | 0.95 | 0.96 | 0.59 | 0.63 | 0.65 | 0.96 |
| 29 | 0.59 | 0.30 | 0.59 | 0.73 | 0.61 | 0.69 | 0.89 | 0.75 | 0.70 | 0.94 | 0.95 | 0.95 | 0.60 | 0.56 | 0.66 | 0.95 |
| 30 | 0.51 | 0.48 | 0.41 | 0.46 | 0.65 | 0.48 | 0.47 | 0.79 | 0.49 | 0.97 | 0.93 | 0.96 | 0.49 | 0.41 | 0.44 | 0.96 |

## A.8. Copyright Details

The images that emerged within the scope of this thesis work and whose copyrights were transferred to the publishing house were used in this thesis in accordance with the "valid publishing policy for the reuse of the text and graphics produced by the author" on the website of the publisher. Figure 2.1 was utilized under a copyright license agreement with the publisher, facilitated by the Copyright Clearance Center, Inc. ("CCC"), under license ID 1493369-1 on behalf of the identified Rightsholder. The author generated all remaining figures, tables, and sketches.